



MINISTÉRIO DA CIÊNCIA, TECNOLOGIA E INOVAÇÃO
INSTITUTO NACIONAL DE PESQUISAS ESPACIAIS

sid.inpe.br/mtc-m21b/2014/05.30.00.36-TDI

**MULTI-SCALE FIRE MODELING IN THE
NEOTROPICS: COUPLING A LAND SURFACE MODEL
TO A HIGH RESOLUTION FIRE SPREAD MODEL,
CONSIDERING LAND COVER HETEROGENEITY**

Etienne Tourigny

Doctorate Thesis Course Graduate
in Meteorology, guided by Dr. Carlos Afonso Nobre, approved in may
05, 2014.

URL of the original document:

<<http://urlib.net/8JMKD3MGP5W34M/3GD37Q2>>

INPE
São José dos Campos
2014

PUBLISHED BY:

Instituto Nacional de Pesquisas Espaciais - INPE

Gabinete do Diretor (GB)

Serviço de Informação e Documentação (SID)

Caixa Postal 515 - CEP 12.245-970

São José dos Campos - SP - Brasil

Tel.:(012) 3208-6923/6921

Fax: (012) 3208-6919

E-mail: pubtc@sid.inpe.br

BOARD OF PUBLISHING AND PRESERVATION OF INPE INTELLECTUAL PRODUCTION (RE/DIR-204):**Chairperson:**

Marciana Leite Ribeiro - Serviço de Informação e Documentação (SID)

Members:

Dr. Gerald Jean Francis Banon - Coordenação Observação da Terra (OBT)

Dr. Amauri Silva Montes - Coordenação Engenharia e Tecnologia Espaciais (ETE)

Dr. André de Castro Milone - Coordenação Ciências Espaciais e Atmosféricas (CEA)

Dr. Joaquim José Barroso de Castro - Centro de Tecnologias Espaciais (CTE)

Dr. Manoel Alonso Gan - Centro de Previsão de Tempo e Estudos Climáticos (CPT)

Dr^a Maria do Carmo de Andrade Nono - Conselho de Pós-Graduação

Dr. Plínio Carlos Alvalá - Centro de Ciência do Sistema Terrestre (CST)

DIGITAL LIBRARY:

Dr. Gerald Jean Francis Banon - Coordenação de Observação da Terra (OBT)

DOCUMENT REVIEW:

Maria Tereza Smith de Brito - Serviço de Informação e Documentação (SID)

Yolanda Ribeiro da Silva Souza - Serviço de Informação e Documentação (SID)

ELECTRONIC EDITING:

Maria Tereza Smith de Brito - Serviço de Informação e Documentação (SID)

André Luis Dias Fernandes - Serviço de Informação e Documentação (SID)



MINISTÉRIO DA CIÊNCIA, TECNOLOGIA E INOVAÇÃO
INSTITUTO NACIONAL DE PESQUISAS ESPACIAIS

sid.inpe.br/mtc-m21b/2014/05.30.00.36-TDI

**MULTI-SCALE FIRE MODELING IN THE
NEOTROPICS: COUPLING A LAND SURFACE MODEL
TO A HIGH RESOLUTION FIRE SPREAD MODEL,
CONSIDERING LAND COVER HETEROGENEITY**

Etienne Tourigny

Doctorate Thesis Course Graduate
in Meteorology, guided by Dr. Car-
los Afonso Nobre, approved in may
05, 2014.

URL of the original document:

<<http://urlib.net/8JMKD3MGP5W34M/3GD37Q2>>

INPE
São José dos Campos
2014

Cataloging in Publication Data

Tourigny, Etienne.

T645m Multi-scale fire modeling in the neotropics: coupling a land surface model to a high resolution fire spread model, considering land cover heterogeneity / Etienne Tourigny. – São José dos Campos : INPE, 2014.

xxv + 153 p. ; (sid.inpe.br/mtc-m21b/2014/05.30.00.36-TDI)

Thesis (Doctorate in Meteorology) – Instituto Nacional de Pesquisas Espaciais, São José dos Campos, 2014.

Guiding : Dr. Carlos Afonso Nobre.

1. Fire. 2. Neotropics. 3. Multi-scale. 4. Burned area products validation. 5. Arc of deforestation. I.Título.

CDU 551.588.6:630*4



Esta obra foi licenciada sob uma Licença [Creative Commons Atribuição-NãoComercial 3.0 Não Adaptada](https://creativecommons.org/licenses/by-nc/3.0/).

This work is licensed under a [Creative Commons Attribution-NonCommercial 3.0 Unported License](https://creativecommons.org/licenses/by-nc/3.0/).

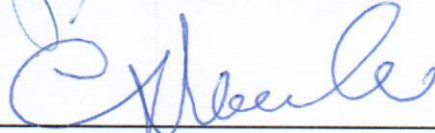
Aprovado (a) pela Banca Examinadora
em cumprimento ao requisito exigido para
obtenção do Título de **Doutor(a)** em
Meteorologia

Dr. Gilvan Sampaio de Oliveira



Presidente / CCST/INPE / Cachoeira Paulista - SP

Dr. Carlos Afonso Nobre



Orientador(a) / INPE / Cachoeira Paulista - SP

Dr. Manoel Ferreira Cardoso



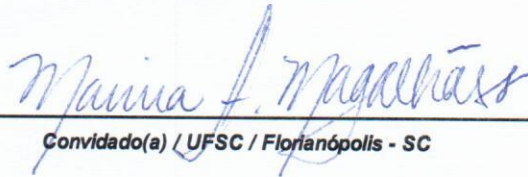
Convidado(a) / INPE / São José dos Campos - SP

Dr. Paulo Monteiro Brando



Convidado(a) / IPAM / Santarém - PA

Dra. Marina Hirota Magalhães



Convidado(a) / UFSC / Florianópolis - SC

Este trabalho foi aprovado por:

() maioria simples

unanimidade

Aluno (a): **Etienne Tourigny**

São José dos Campos, 26 de Maio de 2014

“No Guts, No Glory”.

MAJOR GENERAL FREDERICK C. “BOOTS” BLESSE
in *“No Guts, No Glory”*,
U.S. Air Force fighter tactics book, 1955

*To my parents Hélène Tourigny and John Manning, my
friends and loved ones.*

ACKNOWLEDGEMENTS

I thank Rede CLIMA – Rede Brasileira de Pesquisas sobre Mudanças Climáticas Globais and Le Fonds de recherche du Québec – Nature et technologies (FQRNT) for their financial support. This work is part of the development of the *Componente Interações Biosfera-Atmosfera* of *Instituto Nacional de Ciência e Tecnologia (INCT) para Mudanças Climáticas* (CNPq Processo 573797/2008-0 and FAPESP Processo 2008/57719-9). Many thanks go to my colleagues and collaborators; without this work would not be possible : my advisor Dr. Carlos Nobre, my colleagues Manoel Cardoso, Gilvan Sampaio, Raphael Pousa, Carlos Augusto, Marcos Sanches, André Lima and Aline Castro, and collaborators and acquaintances Sam Rabin, Marina Hirota, Thijs van Leeuwen, João Andrade de Carvalho Junior, José Carlos Santos, Helena França, and Ernesto Alvarado. I also thank my friends, family and loved ones for their support.

ABSTRACT

Land-Use and Land-Cover Change (LUCC) is a major cause of biomass burning in neotropical ecosystems, through logging and slash-and-burn clearing of forests for agriculture and subsequent pasture burning. Current Dynamic Vegetation Models (DGVMs), the land surface components of Earth System Models (ESMs), are incapable of modeling fire processes in tropical rainforests, and do not represent the local-scale land surface properties and processes associated with LUCC and fire spread. The modeling of the complex interactions between LUCC, climate change, droughts and fire in the tropics requires a framework to simulate these components and their interactions across multiple scales. A new modeling framework is proposed, in order to better represent fire in the neotropics within DGVMs, by simulating fire spread and its interactions with LUCC and the global Earth System. This study consists of three parts: the implementation of *subgrid tiling* in the INLAND DGVM and a multi-scale framework to down-scale the model to a finer scale; the implementation of a simple fire spread model and one-way coupling (downscaling) with the INLAND model ; the validation of global burned area products in the “arc of deforestation” for model calibration and validation. The implementation of *subgrid tiling* in the INLAND DGVM has made it possible to represent different land surface types (natural or modified by human activities) inside a given model grid cell. However further work is needed in order to parametrize landscapes influenced by human activities. The custom fire spread model, coupled to the INLAND model, has demonstrated the ability to simulate realistic fire spread patterns and sensitivity to various parameters such as land cover type, deforestation patterns, the presence of roads, and wind speed and direction. Further work is needed in order to improve the parametrizations and consider air and fuel moisture and fuel content, as well as up-scaling the results to the coupled DGVM. The validation of global burned area products in the “arc of deforestation” brings sufficient confidence in using these products for the calibration and validation of the fire components of DGVMs and ESMs in this region. This study has demonstrated the potential of the multi-scale modeling framework for studying the synergies between climate change, LUCC and fire in the neotropics.

MODELAGEM MULTI-ESCALA DO FOGO NOS NEOTRÓPICOS: ACOPLAMENTO DE UM MODELO DE SUPERFÍCIE COM UM MODELO DE ALTA RESOLUÇÃO DE PROPAGAÇÃO DO FOGO, CONSIDERANDO A HETEROGENEIDADE DA COBERTURA DO SOLO

RESUMO

A mudança do uso e cobertura da terra (LUCC; *Land-Use and Land-Cover Change*) é uma das principais causas de incêndios nas florestas neotropicais, principalmente pelo desmatamento e queima da floresta primária para usos agrícolas e subsequente queima de pasto. Os atuais Modelos Globais de Vegetação Dinâmica (DGVMs; *Dynamic Vegetation Models*), os quais são o componente superficial de Modelos do Sistema Terrestre (ESMs; *Earth System Models*), são incapazes de representar os processos do fogo em florestas tropicais úmidas e não representam em escala local as propriedades da superfície terrestre e os processos associados com o LUCC e a propagação do fogo. A modelagem das interações complexas entre LUCC, mudanças climáticas, secas e as queimadas nos trópicos requer um quadro para simular os diferentes componentes e suas interações em múltiplas escalas. Propõe-se um novo ambiente de modelagem para melhor representar o fogo nos ecossistemas neotropicais dentro dos DGVMs, simulando a propagação do fogo e as relações com LUCC e o sistema terrestre global. Este projeto de pesquisa consiste em três partes: implementação de *subgrid tiling* no modelo INLAND e de um ambiente de modelagem multi-escala para fazer o *downscaling* do modelo para a escala mais fina; implementação de um modelo simples de propagação do fogo e acoplamento unidirecional (*downscaling*) com o modelo INLAND; e validação de produtos globais de área queimada no “arco do desmatamento” para calibração e validação de modelos. A implementação de *subgrid tiling* no modelo INLAND tornou possível a representação de diferentes tipos de superfície (naturais ou modificados por atividades humanas) dentro de uma determinada célula de grade do modelo. Ainda assim mais estudos são necessários a fim de parametrizar paisagens influenciadas pelas atividades humanas. O modelo de propagação do fogo, acoplado ao modelo INLAND, demonstrou a habilidade em simular padrões realistas de propagação do fogo e sensibilidade à mudança de vários parâmetros, como o tipo de cobertura do solo, os padrões de desmatamento, a presença de estradas, e as velocidade e direção do vento. Em estudos futuros são necessários melhorias nas parametrizações e inclusão da umidade do ar e dos combustíveis, e a quantidade de combustível, bem como o *upscaling* dos resultados para a DGVM acoplado. A validação de produtos globais de área queimada no “arco do desmatamento” traz confiança suficiente para o uso desses produtos na calibração e validação dos componentes de fogo dos DGVMs e ESMs nessa área. Este estudo demonstrou o potencial deste ambiente de modelagem multi-escala para estudar as sinergias entre mudanças climáticas, LUCC e fogo nos neotrópicos.

LIST OF FIGURES

	<u>Page</u>
1.1 Illustration of subgrid-scale fragmentation in eastern Pará state, showing “fishbone” deforestation pattern with fragmentation much smaller than a 50x50km grid cell.	3
1.2 Overview of the multi-scale LSM/fire spread modeling framework, linking the multi-scale LSM (MS-LSM) to the atmospheric model and LUC and fire spread models.	4
2.1 The key elements represented in LSMs.	8
2.2 The evolution of LSMs	9
2.3 Schematic of the IBIS DGVM. The characteristic timescales of the processes are indicated at the bottom of the figure.	13
2.4 IBIS state description. The basic state description shown here is carried through the entire integrated biosphere model.	13
2.5 Global potential vegetation map resulting from the IBIS model.	14
2.6 Schematic of the INLAND model and its components, with new or planned components in grey.	15
2.7 Subgrid variability representations implemented in various LSMs.	17
2.8 Subgrid tile structure and transitions in the LM3V model. At each timestep the processes of deforestation and land use change modify the natural and anthropic tiles.	18
2.9 Overview of the multi-scale LSM (MS-LSM) modeling approach, linking high- and medium-resolution land cover maps (HRLC/MRLC).	19
2.10 Relationship between the high-resolution map and the model subgrid tiling in the multi-scale LSM modeling approach.	26
2.11 Time series of yearly <i>aet</i> and <i>totbiou</i> in the “natural vegetation” experiment	29
2.12 Time series of average yearly <i>aet</i> and <i>totbiou/totalit</i> in the “modified vegetation” experiment	30
2.13 Vegetation tile maps for the “tropical deforestation” experiment, where both tiles have a proportion of 50% for all grid points.	32
2.14 Maps of <i>aet</i> and <i>totbiou</i> at end of simulation in the “tropical deforestation” experiment, showing most of the Amazônia biome.	33
2.15 PROVEG land cover map for Brazil, overlaid on the IBIS base map for coverage of the rest of the continent. Shown here are <i>vegtype</i> (top) and <i>tilefrac</i> (bottom) of the first two tiles.	36

2.16	Maps of aet and totbiou at end of simulation of most of the Amazônia biome, when model is initialized with base IBIS vegtype map and using tiles with the PROVEG land cover map.	37
2.17	Location of the AMZ, NMT and EPA regions analysed	37
3.1	The extended “fire triangle”.	40
3.2	The extended “fire triangle” and fire modeling at various spatio-temporal scales.	40
3.3	Schematic representation of a flame front in the Rothermel model and the effects of wind and slope.	42
3.4	Example of near-identical fire growth patterns using the MTT algorithm and Huygens’s wavelet principal.	44
3.5	Input layers used by the FARSITE and FLAMMAP fire spread simulators.	44
3.6	Illustration of the Cellular Automata concept applied to fire spread modeling.	46
3.7	IBGE-TC land use map in eastern Pará state, at 250m (left) suffers from loss of detail when resampled to 1km (right).	51
3.8	Land use maps overlayed on GLS2010 Landsat imagery (WRS 226/63 acquired on 2010/07/24) showing a displacement of ~2km of the PROVEG map and perfect alignment of the IBGE-TC map.	51
3.9	State diagram of the Cellular Automata in the fire spread model. Dotted lines show stationary states and the dashed line shows interactions between adjacent cells.	53
3.10	Principal components of the main loophour() fire spread subroutine. Dashed line shows interactions with adjacent cells.	53
3.11	Map of the “highly deforested” domain test area in Southeastern Pará, showing <i>vegtype</i> and roads.	58
3.12	Map of the “fishbone pattern” test area, showing <i>vegtype</i> and roads.	59
3.13	Fire spread state at 3 day intervals (from top to bottom) with and without roads acting as fire breaks. Yellow cells are ignited, dark red are spreading, red are burning and grey are burned.	61
3.14	Fire spread state (3 ignitions) at 5 day intervals (from top to bottom) showing sensitivity to firespread parameters (spread rate and probability). Yellow cells are ignited, dark red are spreading, red are burning and grey are burned.	62
3.15	Fire spread state in a “fishbone” deforested landscape (3 ignitions) at 3 day intervals (from top to bottom) with and without roads acting as fire breaks. Yellow cells are ignited, dark red are spreading, red are burning and grey are burned.	64

3.16	Fire spread state in a “fishbone” deforested landscape (3 ignitions) at 7 day intervals (from top to bottom) with fire breaks and high forest spread probability (0.5). Yellow cells are ignited, dark red are spreading, red are burning and grey are burned.	65
3.17	Fire spread states at 3 day intervals (top to bottom) in a pasture landscape with varying northerly wind speeds. Yellow cells are ignited, dark red are spreading, red are burning and grey are burned.	67
3.18	As in Figure 3.17 but in a forested landscape, using fire spread parameters for pasture. Yellow cells are ignited, dark red are spreading, red are burning and grey are burned.	67
3.19	Fire spread states at 2 day intervals in the “deforested landscape” study area with varying northerly wind speeds. Yellow cells are ignited, dark red are spreading, red are burning and grey are burned.	68
3.20	Fire spread states at 3 day intervals (from top to bottom) in the “fishbone pattern” study area with varying wind direction. Yellow cells are ignited, dark red are spreading, red are burning and grey are burned.	69
3.21	Various fire-related variables downscaled from the INLAND model with tiles to the high-resolution land cover map, the “high deforested” area. Yellow cells are ignited, dark red are spreading, red are burning and grey are burned.	71
3.22	As in Figure 3.21 but for the “fishbone pattern” area.	72
3.23	Annual cycle of moisture-related variables in the “highly deforested” area, representing a “normal” and “dry” year.	74
3.24	As in Figure 3.23, but for the “fishbone pattern” area.	75
3.25	Fire spread states at 7 day intervals when 750 Pa VPD threshold is used for determining fire spread in forest. Contours identify the land use map (pasture vs. forest). Yellow cells are ignited, dark red are spreading, red are burning and grey are burned.	76
4.1	Location of Landsat scenes used, overlaid with burned area from MCD45 during the 2010 dry season.	80
4.2	Burned fraction by scene (at 500m resolution) of Landsat, MCD45 and MCD64 products.	85
4.3	500m and 5km maps for scene 224/067.	93
4.4	Burned fraction maps at 0.25° resolution for all products, scene 224/067.	94
B.1	Complete INLAND flowchart.	144
C.1	GlobCover 2009 Land Cover Map	148

C.2	MCD12Q1 2009 Land Cover Map, using the INLAND classification (see Table C.1)	149
C.3	IBIS Land Cover Map, using the INLAND classification	150
C.4	MCD12Q1 2009 and IBIS Land Cover Maps - South America only	151
C.5	Land Cover Maps for Brazil, using the INLAND classification. a) PROVEG and b) IBGE2006/TERRACCLASS.	152
C.6	PROVEG, IBGE-TC and MCD12Q1 land cover maps, <i>vegtype</i> of tiles 1 and 2 of the Amazon region. Legend is the same as in Figure C.5.	153

LIST OF TABLES

	<u>Page</u>
2.1 Yearly output variables for the “natural vegetation” experiment at end of simulation, individual tile and average values.	28
2.2 Yearly output variables for the “modified vegetation” experiment at end of simulation, individual tile and average values.	31
2.3 Yearly output variables for the “tropical deforestation” experiment at end of simulation, individual tile and tile average values of Amazônia biome spatial average.	34
2.4 Yearly output values, regional spatial average, of simulations using high-resolution land cover maps	38
3.1 Examples of ROS adjusted for wind speed.	55
4.1 UTM zone, mapping method, and dates for both images from each scene of the products used in this study. Dates are given in MM/DD format for Landsat 5 imagery and Julian day of year for the MODIS products.	79
4.2 Scene-wide burned fraction estimates from MCD45 and MCD64 products at native 500m resolution, compared with the resampled 500m Landsat burned area product, for each Landsat scene. Negative values of relative error indicate underestimates by the MODIS products. Also shown are average values across all scenes and for scenes with high Landsat-mapped burned fraction (“High BF”, defined as > 10%) and those with low burned fraction (“Low BF”).	84
4.3 As in Table 4.2, but for spatial performance instead of scene-wide burned fraction estimates.	86
4.4 Performance of the 5km MODIS products relative to the Landsat product.	87
4.5 Burned fraction and spatial correlation of MODIS and GFED4 products at 0.25°	89
B.1 climate and land surface input files	138
B.2 yearly output file variables	140
C.1 IGBP and INLAND land cover class equivalences	145
C.2 Mapping between PROVEG and INLAND land cover classes	145
C.3 Mapping between IBGE1992 and INLAND land cover classes	146
C.4 Mapping between TERRACLASS and INLAND land cover classes	147

LIST OF ABBREVIATIONS

AVHRR	–	Advanced Very High Resolution Radiometer
BATS	–	Biosphere Atmosphere Transfer Scheme
BESM	–	Brazilian Earth System Model
CFFDRS	–	Canadian Forest Fire Danger Rating System
CA	–	cellular automata
CPTEC	–	Centro de Previsão de Tempo e Estudos Climáticos
CRU	–	Climatic Research Unit
CTEM	–	Canadian Terrestrial Ecosystem Model
DEM	–	Digital Elevation Model
DGVM	–	Dynamic Global Vegetation Model
ESM	–	Earth System Model
FCCS	–	Fuel Characteristic Classification System
FDI	–	Fire Danger Index
FDRS	–	Fire Danger Rating Systems
FLSM	–	Forest Landscape Simulation Model
FMC	–	Fuel Moisture Content
FMS	–	Flexible Modeling System
GFDL	–	Geophysical Fluid Dynamics Laboratory
GFED	–	Global Fire Emissions Database
GIS	–	Geographic Information System
HRLC	–	high resolution land cover map
IBGE	–	Instituto Brasileiro de Geografia e Estatística
IBIS	–	Integrated Biosphere Simulator
INLAND	–	Integrated Model of Land Surface Processes
IPCC	–	Intergovernmental Panel on Climate Change
LAI	–	Leaf Area Index
LPJ	–	Lund-Potsdam-Jena
LSM	–	Land surface model
LUCC	–	Land Use and Cover Change
MMA	–	Ministério do Meio Ambiente
MODIS	–	Moderate Resolution Imaging Spectroradiometer
MRLC	–	medium resolution land cover map
MTT	–	minimum travel time
NFDRS	–	National Fire-Danger Rating System
PFT	–	Plant Function Type
PMDBBS	–	Projeto de Monitoramento do Desmatamento dos Biomás Brasileiros por Satélite
PROBIO	–	Projeto de Conservação e Utilização Sustentável da Diversidade Biológica
PRODES	–	Projeto de Monitoramento do Desmatamento na

		Amazônia Legal por Satélite
PVM	–	Potential Vegetation Model
ROS	–	Rate of Spread
SAV	–	surface-area-to-volume
SiB	–	Simple Biosphere Model
SVAT	–	Soil-Vegetation-Atmosphere-Transfer
SM2007	–	Scheller and Mladenoff (2007)
THMB	–	Terrestrial Hydrology Model with Biogeochemistry
VPD	–	Vapor Pressure Deficit
WFDSS	–	Wildland Fire Decision Support System

CONTENTS

	<u>Page</u>
1 INTRODUCTION	1
2 REPRESENTING SUBGRID-SCALE HETEROGENEITY IN THE INLAND DGVM	7
2.1 A review of Land Surface Models	7
2.1.1 The evolution of Land Surface Models	7
2.1.2 Dynamic Global Vegetation Models	10
2.1.3 Fire modeling within DGVMs	10
2.1.4 Forest Landscape Simulation Models	11
2.1.5 IBIS and INLAND Dynamic Global Vegetation Models	12
2.1.6 Representing subgrid-scale heterogeneity with subgrid tiling	16
2.2 Methodology	18
2.2.1 Overview	18
2.2.2 Subgrid tiling in the INLAND model	20
2.2.3 Changes to the vegetation dynamics module	22
2.2.4 Global and regional high-resolution land cover maps	23
2.2.5 Linking high-resolution maps to subgrid tile modeling	25
2.2.6 Experimental setup	26
2.3 Results	27
2.3.1 Natural vegetation, single point	27
2.3.2 Modified vegetation, single point	27
2.3.3 Tropical deforestation: modified vegetation, South America domain	32
2.3.4 Using high-resolution land cover maps	33
3 FIRE SPREAD MODELING WITHIN THE INLAND DGVM	39
3.1 A review of fire spread modeling	39
3.1.1 Overview of fire modeling	39
3.1.2 Empirical and semi-empirical fire behavior models	39
3.1.3 Fire spread simulation models	43
3.1.4 Fire in the Brazilian tropics	47
3.2 Methodology	49
3.2.1 Overview	49
3.2.2 Land cover map and other supporting data	50

3.2.3	Basic fire spread model structure and workflow	52
3.2.4	Influence of wind and topography	54
3.2.5	Influence of surface and air moisture	56
3.2.6	Experimental setup	57
3.3	Results	59
3.3.1	Sensitivity study of basic fire spread model	59
3.3.2	Sensitivity to wind speed and direction	66
3.3.3	Sensitivity to surface and air moisture	70
3.4	Discussion	72
4	EVALUATION OF GLOBAL BURNED AREA PRODUCTS IN THE BRAZILIAN ARC OF DEFORESTATION	77
4.1	Introduction	77
4.2	Data	78
4.2.1	Landsat TM burned area maps	78
4.2.2	MODIS daily burned area products (500m) MCD45 and MCD64	80
4.2.3	GFED4 daily burned area product (0.25°)	81
4.3	Methods	82
4.3.1	MODIS burned area products at native (500m) resolution	82
4.3.2	MODIS and GFED4 at coarser resolutions (5km and 0.25°)	83
4.4	Results	83
4.4.1	MODIS burned area products at native (500m) resolution	83
4.4.2	MODIS and GFED4 at coarser resolutions (5km and 0.25°)	87
4.4.3	Spatial analysis	90
4.5	Discussion	91
5	CONCLUSION	95
	REFERENCES	97
	APPENDIX A - PUBLICATIONS RELATED TO THESIS	121
A.1	Evaluation of global burned area products in the Brazilian Arc of Defor- estation	121
A.1.1	ABSTRACT	121
A.1.2	SUPPLEMENTARY MATERIAL	121
A.2	Comparação de dados de área queimada obtidos por sensores remotos TM e MODIS no Parque Nacional Serra da Canastra, MG	127

APPENDIX B - INLAND MODEL VARIABLES, DEFINITIONS AND SUPPORTING INFORMATION.	131
B.1 Important variables	131
B.1.1 Variables that pertain to the simulation parameters	131
B.1.2 Variables that pertain to each model grid point	131
B.2 Input files	131
B.2.1 PFT, <i>vegtype</i> , and <i>landusetype</i> parameters	131
B.2.2 Fire spread parameters	133
B.2.3 simulation and domain configuration files	135
B.2.4 climate and land surface input files	138
B.3 Output files	139
B.3.1 Output file variables	139
B.3.2 Example yearly output file	141
B.3.3 Example yearly PFT output file	142
B.4 INLAND model diagrams	143
APPENDIX C - LAND COVER MAPS	145

1 INTRODUCTION

Deforestation of tropical forests for agriculture, cattle ranching, deforestation and associated fires are main contributors of CO₂ emissions (MALHI et al., 2009; FEARN-SIDE, 2005), both immediate from biomass burning and future due to the elimination of a potential CO₂ sink. Moreover, climate change in the Amazon during the 21st century is projected to decrease the resilience of the Amazon forest, and could contribute to the conversion of large parts of tropical forests to savannas (COX et al., 2004), adding to the direct anthropogenic deforestation. Potential feedbacks between LUCC (Land-Use and Land-Cover Change) and climate change could further increase the loss of tropical forests and increase the rate of CO₂ emissions to the atmosphere. The mechanisms involved are land and soil degradation, land fragmentation and the increase in wildfire occurrence and severity (LAURANCE, 2004). However, current understanding of fire processes (including ignition, spread and consequences) in tropical biomes and their feedbacks with climate are not well understood and fire modeling needs further research (COCHRANE, 2003). In tropical forests such as the Amazon rainforest, natural fires are very rare thus trees are not adapted to frequent fires, and fires are almost exclusively associated with human activities (FEARNSIDE, 2005; NOBRE; BORMA, 2009). In contrast, within savannas such as the Brazilian *cerrado*, natural fires are frequent and play an important role in the distribution of vegetation (BOND; KEELEY, 2005).

The Amazonian basin encompasses 30% of the world’s tropical forests and is one of the areas of highest tropical biodiversity (PERES et al., 2010). However, past deforestation rates in the Amazon are by far the highest of all tropical regions (HANSEN et al., 2008), with an average rate of almost 20,000 km²/year from 1996–2005, although a decline has been observed since 2005 (NEPSTAD et al., 2009). Deforestation and associated fires have direct effects on the hydrological cycle, surface energy balance and carbon cycle (FEARNSIDE, 2005) as well as tree species composition and resilience (BARLOW; PERES, 2008). Moreover, forest fragmentation due to deforestation can lead to further forest damage through the spread of pasture maintenance fires to adjacent forests, direct edge effects (such as wind disturbance), and feedbacks involving recurrent fires, droughts, and the “vegetation breeze” effect (BRANDO et al., 2014; LAURANCE, 2004). Nobre and Borma (2009) identified a number of key “tipping points” in the Amazon forest, from which recuperation of primary forest could be compromised. These include deforestation and other LUCC processes, global warming, climate extremes (droughts) and forest fires and are interconnected through feedback mechanisms. Studies have linked climate change to a “die-back” of

the Amazon within the next century (e.g. Cox et al. (2004)), which could be exacerbated by deforestation and associated forest fires (ARAGÃO et al., 2007; CARDOSO et al., 2009; MALHI et al., 2009). However, recent models do not show evidence for this “die-back” effect.

Another neo-tropical ecosystem, the Brazilian *cerrado* is a rich and diverse savanna ecosystem, composed of a wide array of physiognomic forms which can be grouped into 3 categories (FURLEY, 1999): grasslands, savanna formations and savanna woodlands. Although the main controls on physiognomic forms are controversial, they are basically: climatic seasonality (marked dry season), soil fertility and drainage, and fire regimes (OLIVEIRA-FILHO; RATTER, 2002). A more comprehensive classification of the *cerrado* physiognomies (another controversial subject) is that of RIBEIRO and WALTER (1998), which separates the various physiognomic forms with greater detail (e.g. *campo limpo*, *campo sujo*, *mata ciliar*, *cerradão*). In the Brazilian *cerrado*, as well as other savanna ecosystems, natural and pre-historic anthropogenic fires played an important role in shaping the landscape, favoring more fire-resistant herbaceous plants over trees (HOFFMANN et al., 2003). Savanna ecosystems suffer from a dry season, and natural forest fires are initiated by lightning at the beginning of the rainy season, when vegetation is driest (BOND; KEELEY, 2005). However, there is evidence that large-scale anthropogenic deforestation and recurrent burning occurring since the arrival of the Europeans –or perhaps even before– (MIRANDA et al., 2009) modified the natural cycle by causing more fires during the dry season when vegetation is most vulnerable, threatening native ecosystems (RAMOS-NETO; PIVELLO, 2000; MISTRY; BERARDI, 2005). The original *cerrado* biome covers nearly 25% of Brazil’s land surface, of which today only 60.5% is composed of natural vegetation, with cultivated pasture and agriculture occupying 26.5% and 10.5% respectively (SANO et al., 2008).

Earth System Models represent the atmospheric, oceanic, cryogenic and land surface components of the Earth system. Land Surface Models (LSMs) and Dynamic Global Vegetation Models (DGVMS) used at the global scale represent the land surface properties and biosphere-atmosphere interactions at a coarse resolution. Fire processes are usually represented in a manner which does not consider the local-scale features of landscapes and the physical processes of fire spread and the effects of biomass burning. Figure 1.1 shows a typical “fishbone” deforestation pattern, where fragmentation is much smaller than a typical LSM grid-scale (0.5° or more). LSMs are not designed to represent local-scale fragmentation resulting from LUCC processes and other fine-scale features and processes. As the processes of LUCC

and associated fires (as well as natural fires) occur at local scale in a fragmented landscape (LAURANCE, 2004), linking them to large-scale atmospheric processes requires a means of up-scaling higher resolution processes to lower resolutions for use in Earth System Models.

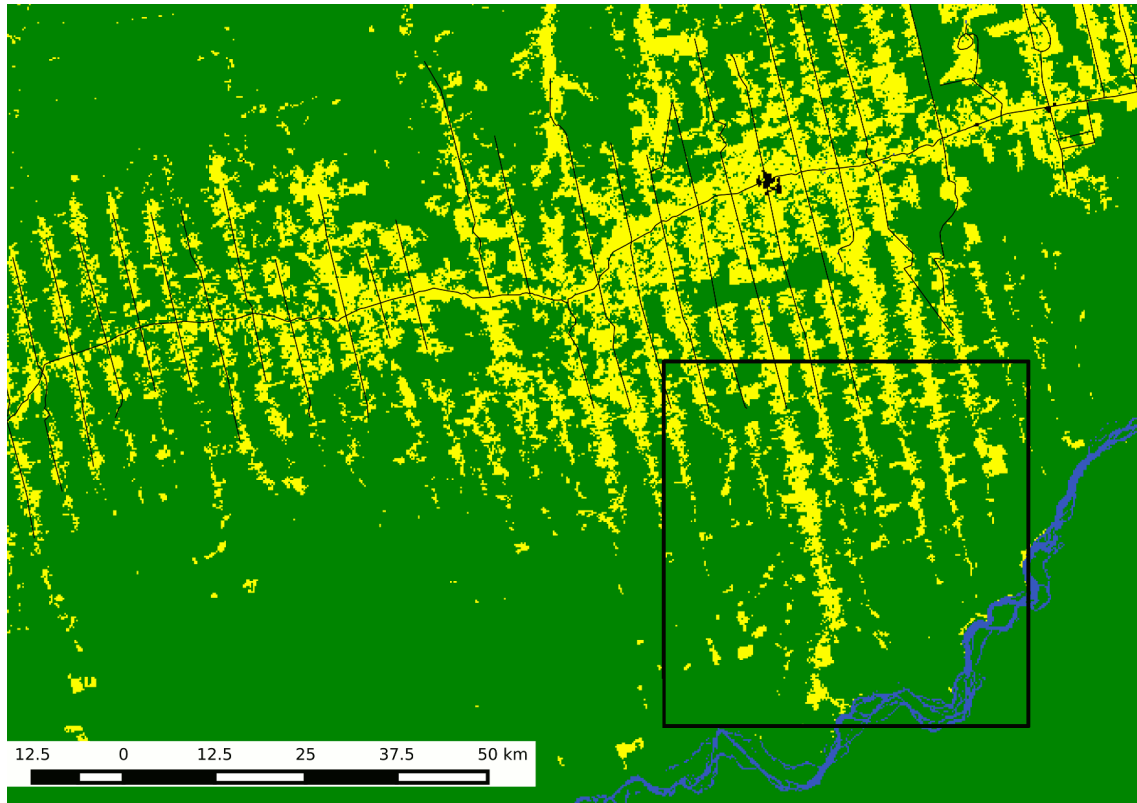


Figure 1.1 - Illustration of subgrid-scale fragmentation in eastern Pará state, showing “fishbone” deforestation pattern with fragmentation much smaller than a 50x50km grid cell.

A novel approach to solve the scale mismatch of these processes is to explicitly model and couple the processes which operate at various spatial and temporal scales: large-scale atmospheric processes, regional surface/land processes and human-related LUCC processes such as deforestation and proscribed burning, as well as natural fires. This model framework, depicted in Figure 1.2, has the potential to link a Global Climate Model (GCM), DGVM, regional-scale LUCC model and high-resolution fire spread model. The climate model resolves larger scale atmospheric processes and forcings, which impact surface DGVM and are fed-back to the climate. Higher-resolution processes such as deforestation, land use management and associated fires, as well as natural fires, are resolved at the local level.

Anthropogenic LUCC is modeled using spatially-explicit models operating within a Geographical Information System (GIS). Fire behavior is modeled at the local scale (~250m) to represent the detailed landscape using a simple empirical fire spread model. Modifications to the land surface are imposed on the land model, which has a potential feedback on the land surface properties through processes resolved by the atmospheric and land models. More details are given in Sections 2.2.1 and 3.2.1. The nested multi-scale and multi-model framework allows for detailed studies of the complex feedbacks between climate, land surface, LUCC and fires in tropical biomes. This framework will allow for a better understanding and evaluation of ecosystem resilience and CO₂ emissions from LUCC and feed-backs with climate change.

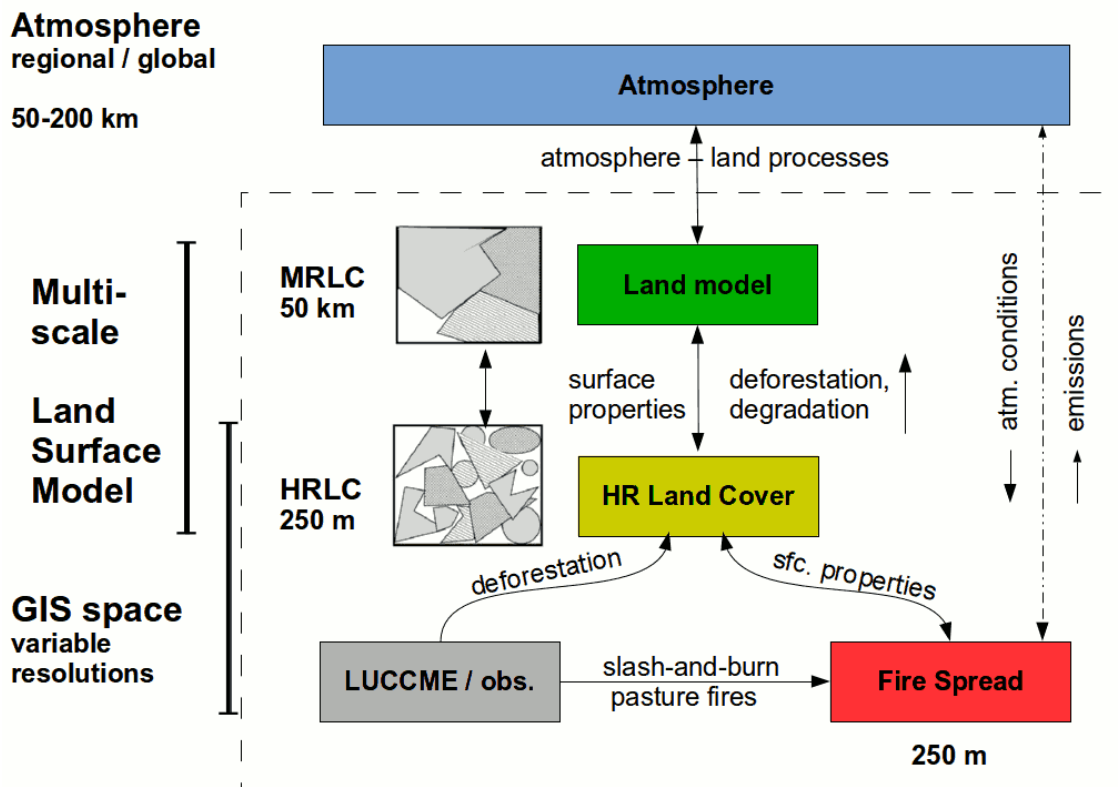


Figure 1.2 - Overview of the multi-scale LSM/fire spread modeling framework, linking the multi-scale LSM (MS-LSM) to the atmospheric model and LUCC and fire spread models.

The components of this framework which have been implemented for this study are:

- a) *subgrid tiling* within the INLAND DGVM, in order to represent different land cover types inside a single model grid cell

- b) representation of modified landscapes as new land cover types (pasture, croplands) and modified vegetation dynamics module within the INLAND DGVM, requires calibration
- c) basic custom fire spread model coupled to the INLAND DGVM, *via* one-way coupling (downscaling)

The scientific questions that could be addressed in studies employing this multi-scale Earth System Model framework are (but not limited to):

- a) what are the consequences of climate change on fire frequency and extent in the neotropics?
- b) what is the impact of different fire use scenarios and policies (e.g. *business as usual*, conservation) on fire activity?
- c) what are the synergies between climate change, LUCC and fire activity in the neotropics, and to which extent do they act?
- d) can local-scale fire spread processes be up-scaled to DGVMs with parametrizations using simple equations and rules?

Incidentally, the calibration and validation of any fire model require a reliable burned area dataset of sufficient spatio-temporal coverage – ideally global-scale for various years, with daily or monthly resolution. There have been several advances in fire activity monitoring on the global scale in recent years. Several products are available and give estimates of active fires (commonly referred to as “hot pixels” or “*focos de calor*”) and burned area (also known as “burn scars”, not to be confounded with actual burn scars left on trees after a fire) at various temporal and spatial scales. MODIS (Moderate Resolution Imaging Spectroradiometer) sensors provide 4 daily values of active fire data at 1 km resolution (GIGLIO *et al.*, 2006). Many other products are available from other sensors, with various spatial and temporal resolutions (GIGLIO *et al.*, 2009, and references therein). Brazil’s CPTEC produces real-time active fire data for South America from various data sources (SCHROEDER *et al.*, 2008). With the advent of high temporal frequency of the MODIS data, burned area products have become increasingly useful in monitoring fire activity and estimating burned area with greater detail. The recent work of Giglio *et al.* (2009) and Giglio *et al.* (2010) has led to a 500m resolution daily burned area product (MCD64A1) based on MODIS 500m reflectance bands and 1km active fire detection product. This data

is available publicly in lower-resolution global grids, at monthly and daily timescales and 0.25° resolutions, as part of the GFEDv4 database (WERF et al., 2010; GIGLIO et al., 2013) for use in climate modeling studies. Another product (MCD45A1), using slightly different techniques (ROY et al., 2008) is also available at 500m and daily frequency.

This study is divided into three sections, each representing distinct goals. This first goal is to implement *subgrid tiling* in the INLAND DGVM and will be discussed in Chapter 2. Implementation of the simple fire spread within this framework is the subject of Chapter 3. Finally, the validation of MCD45A1 and MCD64A1 global burned area products in the “arc of deforestation”, which has been submitted to *Remote Sensing of Environment* for review, is included in Chapter 4. These three parts are inter-connected in the following manner: the implementation of *subgrid tiling* in the INLAND model is a necessary pre-requisite for coupling to a fire spread model and the validation of existing burned area products is necessary in order to use these products for the fire spread model calibration and validation.

2 REPRESENTING SUBGRID-SCALE HETEROGENEITY IN THE INLAND DGVM

2.1 A review of Land Surface Models

2.1.1 The evolution of Land Surface Models

Earth System Models (ESMs) are widely used in climate studies and are designed to simulate the various abiotic and biotic components of the Earth System (including but not limited to: the atmosphere, biosphere, hydrosphere, cryosphere and anthroposphere) and their interactions (CLAUSSEN *et al.*, 2002). Also known as climate models, ESMs evolve continuously, by incorporating an increasing number of models which simulate aspects of the Earth System. Climate models initially consisted only of atmospheric models, but were eventually coupled to land surface and ocean models. The most recent additions to climate models are models that represent the carbon cycle, dynamic (or interactive) vegetation and atmospheric chemistry. The new generation of ESMs used in the last IPCC (Intergovernmental Panel on Climate Change) assessment report AR5 contain LUCC (Land Use and Cover Change) models (MOSS *et al.*, 2010). There is an ongoing modeling effort at the Brazilian national level to develop a fully-coupled global Earth System Model with a greater focus on South America named BESM (Brazilian Earth System Model). BESM will be composed of CPTEC 2.0 atmospheric model, MOM4 ocean model and INLAND, a land surface model based on IBIS, configured at different resolutions and coupled with GFDL's FMS flux coupler.

Land surface models (LSMs), also known as Soil-Vegetation-Atmosphere-Transfer (SVAT) models, are designed to represent the Earth's surface cover (including vegetation), characteristics and interactions with the lower atmosphere. Specifically, land surface models must represent the surface-atmosphere fluxes of energy, carbon, water and momentum. In a steady-state the balance of incoming and outgoing radiation (R_n) must equal the sum of sensible (H), latent (λE) and ground (G) heat fluxes (and in some models the chemical energy (F) stored in plants through photosynthesis). The nature of the land cover influences exchanges with the atmosphere through surface albedo, roughness length (which controls turbulent fluxes with the atmospheric boundary layer), partitioning of heat fluxes (i.e. latent vs. sensible), precipitation runoff and evapo-transpiration (PITMAN, 2003).

The key processes considered by most LSMs are shown in Figure 2.1, and the evolution of LSMs is outlined in Figure 2.2. The first generation of land surface models

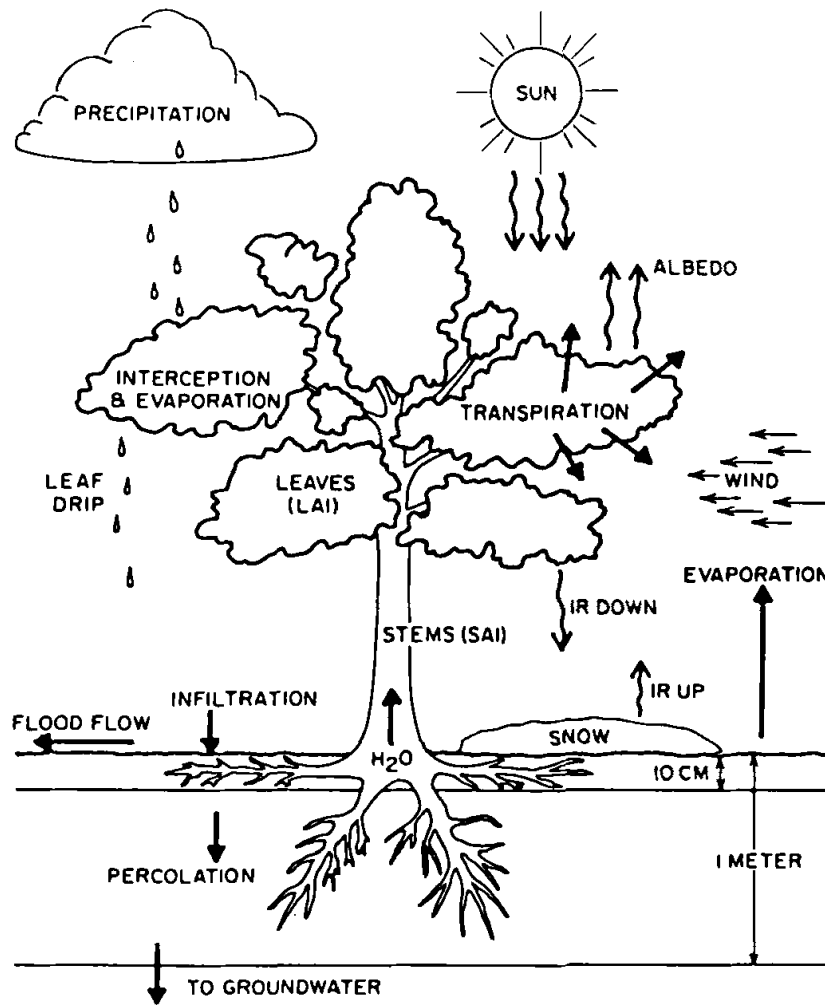


Figure 2.1 - The key elements represented in LSMs.

SOURCE: Dickinson (1984).

(i.e. Manabe, 1969) solved the surface energy budget, treated the land surface uniformly in space and time and used a simple “bucket” hydrology model with a single soil layer for calculating surface runoff. The development of the “force-restore” two-layer soil scheme and the inclusion of a vegetation layer (DEARDORFF, 1978) lead to the development of the so-called second-generation models, such as the Biosphere Atmosphere Transfer Scheme (BATS) (DICKINSON et al., 1986) and the Simple Biosphere Model (SiB) (SELLERS et al., 1986). The fundamental biophysical principles of these models are still commonly used in modern LSMs (PITMAN, 2003). The inclusion of plant layers (canopy, ground and roots) allowed for plants to influence the surface through radiation absorption, momentum transfer, evapo-transpiration

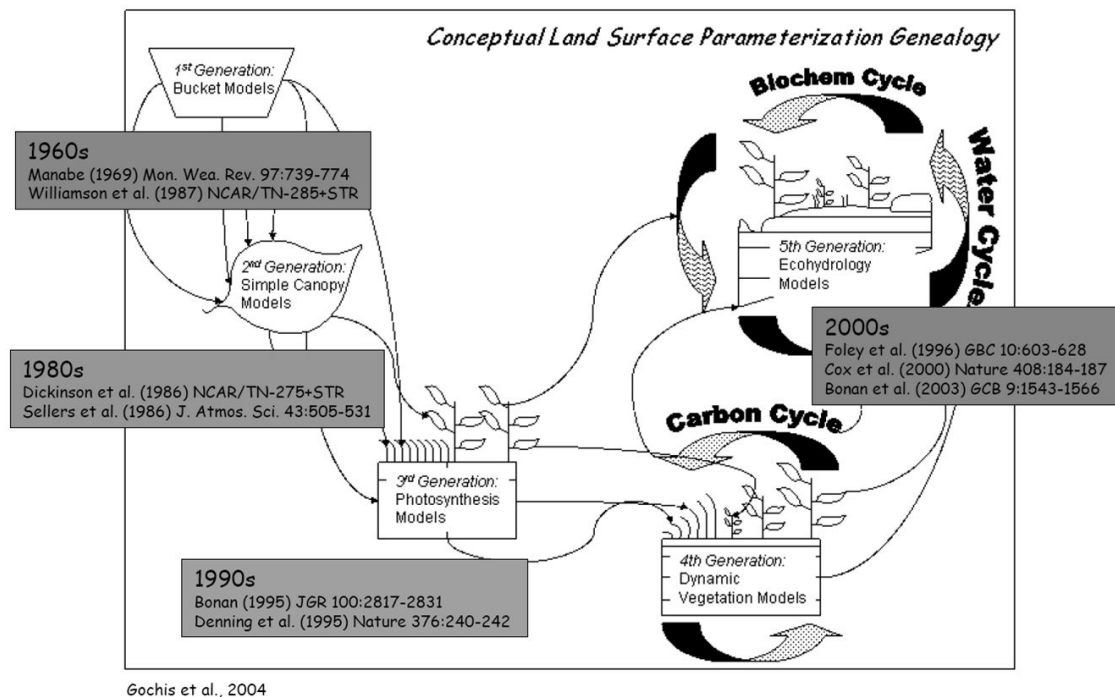


Figure 2.2 - The evolution of LSMs

SOURCE: Adapted from Gochis (2004).

and precipitation interception. Moreover, the classification of vegetation types with different physiological parameters allowed for a much more realistic representation of surface processes. The differences in surface parameters of, for example, forest and pasture, have important implications for the surface energy budget and hydrological cycle, especially in tropical climates (NOBRE et al., 1991, many others).

Third-generation LSMs incorporated knowledge on plant physiology, biology and biochemistry, such as the biochemical model of Farquhar et al. (1980). The explicit modeling of photosynthesis and respiration processes and integration of the biogeochemical cycles of carbon and nitrogen allows plants to allocate and consume resources such as carbon and nitrogen and grow (die) under favorable (unfavorable) environmental conditions (DICKINSON et al., 1998). The static vegetation types of second-generation models are replaced by Plant Function Types (PFTs) which respond differently to environmental conditions. PFTs represent a single vegetation type, and a biome can be represented by a variable mixture of different PFTs (such as grass, shrubs and trees for savanna biomes). Fourth- and fifth-generation models are discussed in the following section.

2.1.2 Dynamic Global Vegetation Models

The incorporation of the carbon cycle and long-term ecological processes led to the creation of the first DGVMs (Dynamic Global Vegetation Models), such as IBIS (Integrated Biosphere Simulator) (FOLEY et al., 1996), TRIFFID (COX, 2001) and LPJ (Lund-Potsdam-Jena) (SITCH et al., 2003). DGVMs include the higher frequency processes of second- and third-generation LSMs and slower frequency processes of vegetation dynamics. Simpler models called Potential Vegetation Models (PVMs), such as the CPTEC-PVM (OYAMA; NOBRE, 2003) can be coupled to a second-generation LSM and compute “equilibrium” vegetation cover based on climatic constraints. A simple DGVM can be obtained by updating the vegetation of the LSM after one or a few years of integration and repeating the process until equilibrium is reached, a technique known as asynchronous coupling. The updated CPTEC-PVM2 of Lapola et al. (2009) simulates photosynthesis and the carbon cycle, but does not represent vegetation phenology and competition among plant types, as do many DGVMs.

2.1.3 Fire modeling within DGVMs

Fire in DGVMs is frequently simulated at broad scales, using to a variable degree average observed fire occurrence and observed burned area. Subgrid variability and spatial distribution of PFTs are usually not considered by DGVMs. According to Arora and Boer (2005), many DGVMs such as TRIFFID, BIOME-BGC and IBIS model fire in a simple manner, or not at all. More realistic DGVM fire models simulate the occurrence, behavior and effects of fire. For example, in the MC1 model of Lenihan et al. (2008) fire occurs when fuel moisture and atmospheric conditions reach a certain threshold, considers that ignition events are always available, and computes burned fire area from observed fire return intervals. The fire component of the CTEM (Canadian Terrestrial Ecosystem Model) model (ARORA; BOER, 2005) simulates fire at the daily timescale (instead of the yearly timescale of earlier models) by computing the probability of fire occurrence which is based on biomass availability, flammability and ignition source (using observed lighting frequency). Burned area is modeled as an ellipse of dimensions determined by wind and fuel conditions.

The fire components of the LPJ models simulate fire in a more mechanistic way (SITCH et al., 2003). The empirical models Glob-FIRM (THONICKE et al., 2001) and Reg-FIRM (VENEVSKY et al., 2002) were improved to create the process-based SPIT-FIRE model (THONICKE et al., 2010; LEHSTEN et al., 2009), in which daily fire occurrence is a function of a Fire Danger Index (FDI) and the Rothermel model (ROTHERMEL, 1972) is used to estimate Rate of Spread (ROS) and average area

burnt. Surface and crown mortality and area burned are based on the availability and moisture of live and dead 1-h to 1000-h fuels.

The impact of anthropogenic fire is scarcely considered in DGVMs, which have traditionally focused on natural wildfires. The fire model of CTEM uses an arbitrary anthropogenic fire probability which is summed to the natural ignition probability. In the Brazilian cerrado, the highest month of fire occurrence simulated by CTEM is different than observed because of the lack of correct inclusion of anthropogenic sources of ignitions, which vary seasonally. In the LPJ fire models (SPITFIRE and Reg-FIRM), anthropogenic fire probability is a function of population density and observed human-caused fire occurrence. [Cardoso et al. \(2003\)](#) found that distance-to-roads is a good predictor for fire occurrence in the Brazilian Amazon. The characteristics and timing of natural and anthropogenic fires are different, as explained in the study of [Ramos-Neto and Pivello \(2000\)](#) in the *cerrado*. This suggests that anthropogenic and natural fires should be modeled using different approaches in these tropical areas (the Amazon and *cerrado*).

2.1.4 Forest Landscape Simulation Models

While DGVMs are designed to study long-term changes in vegetation and feedback with climate over large spatial scales (regional-global), there is another category of models whose goal is to study with great detail vegetation disturbance and succession processes at the regional scale. Forest Landscape Simulation Models (FLSMs) are used to study long-term, regional effects of disturbances, both natural (such as fire, wind, insects) and anthropogenic (such as fire and logging) and the effects of landscape management practices ([SCHELLER; MLADENOFF, 2007, SM2007](#)). SM2007 classify different FLSMs according to the following criteria: spatial interactions (processes which operate spatially such as seed dispersal), static or dynamic communities (variability within the plant communities) and ecosystems processes (dynamic vegetation, decomposition). FLSMs which include spatial interactions typically represent the landscape with a Geographic Information System (GIS) of relatively high resolution (10-500m). FLSMs operate across one or more of the following scales: landscape (103-106 ha) ; site (regions of similar topography, soils, weather and potential vegetation) ; stand (regions of different vegetation composition, 10-100 ha) ; gap (individual or group of trees, area < 10 ha). The complexity of computations and the high spatial resolution of FLSMs, as well as their regional approach and need for detailed GIS data, has traditionally limited their use to landscape (regional) spatial scales and annual time scales, making them unsuited for studies at the global scale. On the

other hand, most DGVMs, including IBIS, represent ecosystem processes but exclude spatial interactions, therefore are not mentioned in the strict FLSM classification of He (2008). Those that do include spatial interactions and operate at multiple scales are MC1 (BACHELET et al., 2001), FIRE-BGC (KEANE et al., 1996) and LANDIS-II (SCHELLER et al., 2007). Although they are considered “global” models, they have been used only in studies at the regional scale. Particularly, FIRE-BGC is a multi-scale model, combining a gap-replacement model and a mechanistic biogeochemical model, and simulates processes at the landscape, site, stand and plot levels, each with their representative spatial data. Ecosystem processes such as plant growth and biogeochemical cycling are modeled at the plot level and values are aggregated annually at the stand level. Fire occurrence is modeled using a site-level stochastic fire occurrence model based on observed fire return intervals, and fire extent and effects are modeled across the landscape using a spatially-explicit fire spread model.

2.1.5 IBIS and INLAND Dynamic Global Vegetation Models

The IBIS model (FOLEY et al., 1996; FOLEY et al., 1998; KUCHARIK et al., 2000) is composed of a land surface module (including canopy and soil physics and plant physiology), a vegetation dynamics module and a vegetation phenology module (Figure 2.3). The land surface module is taken from the second-generation LSX model (POLLARD; THOMPSON, 1995) and includes an upper and lower canopy (for trees and shrubs and grasses, respectively) and 6 soil layers (see Figure 2.4) and operates at timescales comparable to atmospheric models. Plants are represented by 12 PFTs, divided into evergreen trees, deciduous trees, shrubs and herbaceous plants, each with distinct carbon pools of leaves, stems and roots. The processes of photosynthesis and respiration are simulated in a mechanistic manner (details in Foley et al. (1996)). The vegetation phenology module (for processes such as budding and senescence) is based on simple empirically-based temperature thresholds for each PFT. The yearly dynamic vegetation module computes the following for each PFT : gross and net primary productivity (GPP and NPP), changes in biomass pools, simple mortality disturbance processes and resultant Leaf Area Index (LAI), thus allowing vegetation type and cover to change through time.

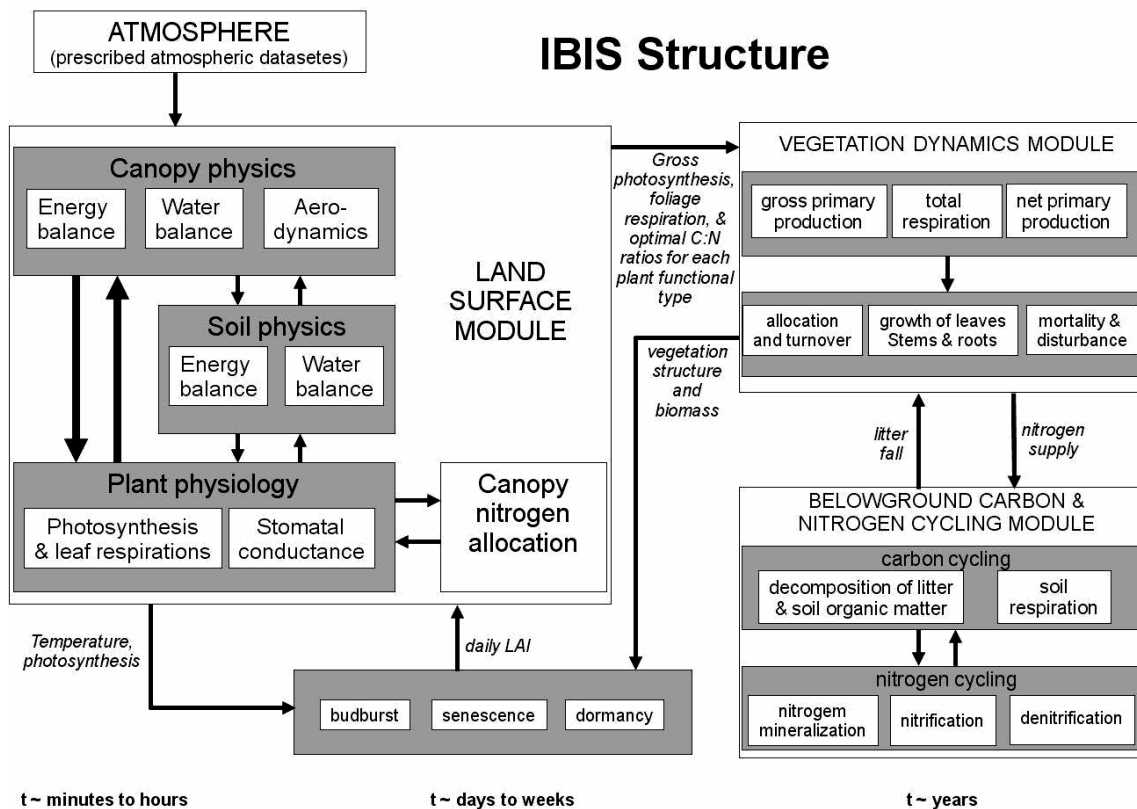


Figure 2.3 - Schematic of the IBIS DGVM. The characteristic timescales of the processes are indicated at the bottom of the figure.

SOURCE: Adapted from Kucharik et al. (2000).

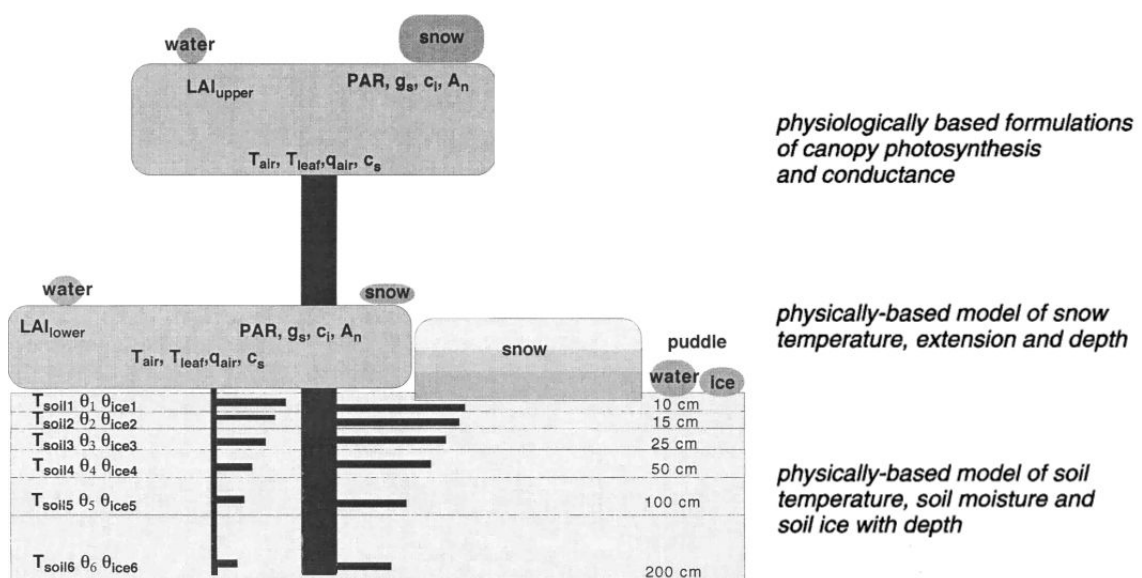


Figure 2.4 - IBIS state description. The basic state description shown here is carried through the entire integrated biosphere model.

SOURCE: Adapted from Kucharik et al. (2000).

The IBIS model has been used to generate a global potential vegetation map, shown in Figure 2.5 and available in 0.5° and 5min resolutions (SAGE, 2014). This data, as well as climatic data from the Climatic Research Unit (CRU ; monthly averages from 1961-1990) and soil texture data at 0.5° resolution, are used as input for the offline version of the IBIS model. Source code of the last release of IBIS (2.6b4) and supporting data can be downloaded from <http://www.sage.wisc.edu/download/IBIS/ibis.html>. Various studies using the IBIS model have been made on the potential impacts of deforestation and climate change the Amazon and cerrado (COSTA; PIRES, 2010; COE et al., 2009; SENNA et al., 2009; BOTTA et al., 2002; COSTA; FOLEY, 2000). There are no known fire modeling studies using IBIS as the fire module is a simple, fixed-value disturbance.

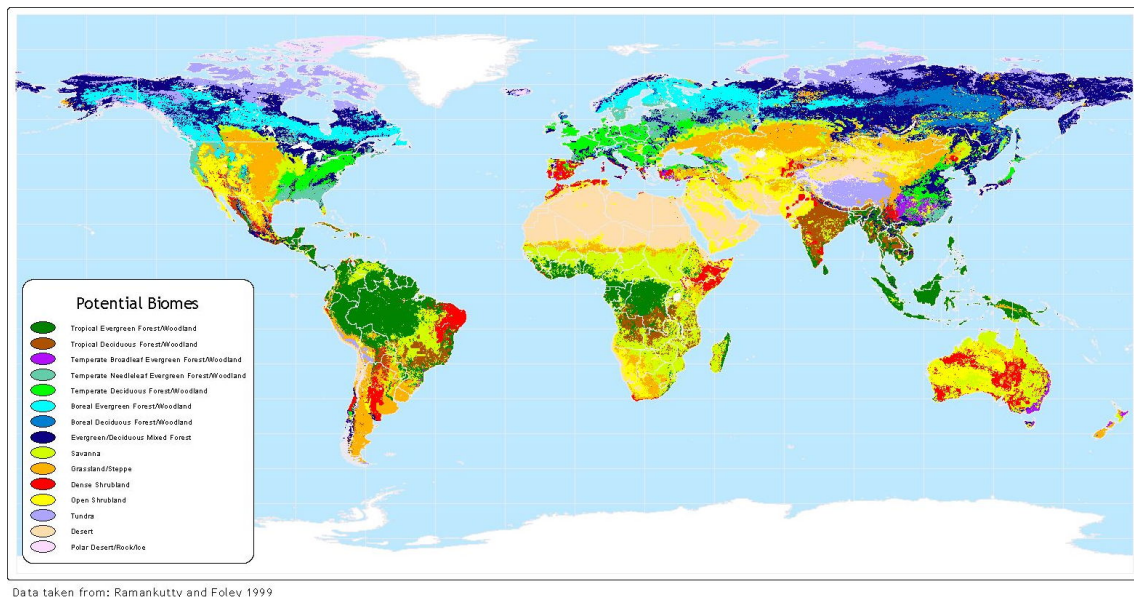


Figure 2.5 - Global potential vegetation map resulting from the IBIS model.

SOURCE: Ramankutty and Foley (1999) and SAGE (2002).

The Brazilian scientific community is actively involved in the development of INLAND (unpublished; Integrated Model of Land Surface Processes), the main land surface component of the BESM Earth System Model. INLAND is based on IBIS and focuses on issues important for biosphere-atmosphere interactions in South America. These issues, such as seasonally-flooded areas, deforestation and other LUCC practices, biomass burning, and soy and sugar cane crops, are outlined in Figure 2.6. The first public release of INLAND (version 1.0) can be obtained at

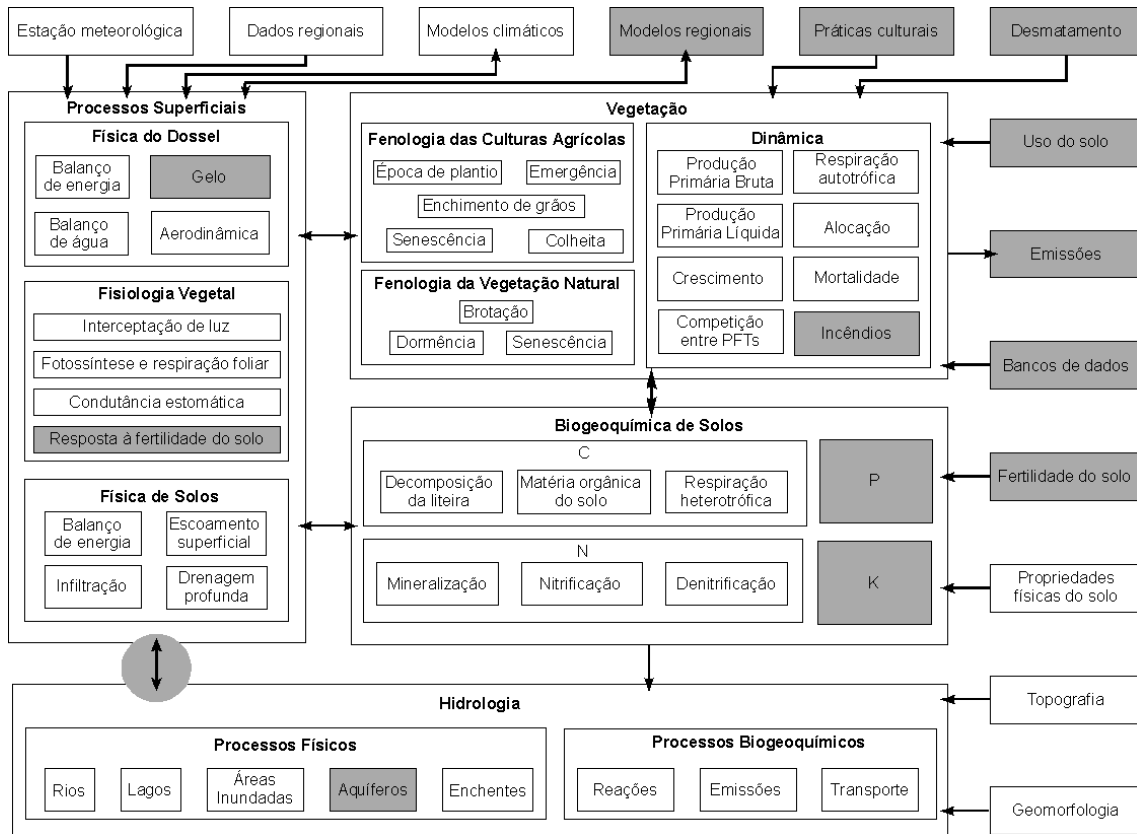


Figure 2.6 - Schematic of the INLAND model and its components, with new or planned components in grey.

SOURCE: Marcos Costa.

<http://www.ccst.inpe.br/inland/>. The following improvements have been made to the development version of the INLAND model relative to IBIS at the time of writing:

- software improvements: upgrade to Fortran 90, dynamic memory allocation of variables, parallel processing with OpenMP, incorporation of the single-point model from Costa et al. (2009)
- subgrid tiling (the subject of section 2.2.2)
- an improved natural fire module based on CTEM (ARORA; BOER, 2005)
- changes in land use and atmospheric CO₂
- improvements to the soil infiltration module and vegetation parameters

- incorporation of the Agro-Ecosystem Model Agro-IBIS (KUCHARIK, 2003) to simulate soybean, maize, wheat and sugar cane crops
- coupling with the THMB hydrologic model (COE et al., 2008) – not yet integrated
- preliminary coupling with the atmospheric model (CPTEC) – not yet complete

2.1.6 Representing subgrid-scale heterogeneity with subgrid tiling

An inherent limitation of land surface models used with global atmospheric models is that their coarse resolution does not allow to represent spatial heterogeneity at the subgrid scale (BONAN et al., 2002; MOLOD; SALMUN, 2002). Figure 2.7 illustrates a hypothetical grid square with different land cover types and the various strategies used by LSMs. First- and second-generation LSMs use the “dominant” approach, which assigns the most common cover type to the entire grid cell, thus ignoring a potentially high portion of the land surface. The “composite” approach (used in the IBIS model, discussed later) considers a homogeneous blend of the relative portions of the cover types. Most parameters are aggregated linearly, except for roughness length which is aggregated logarithmically. This technique does not allow to differentiate the physical properties (such as soil temperature and humidity) of different land cover types present in each grid cell.

The last technique is that of “mosaics”, which uses a mosaic of subgrid tiles which aggregate the different PFTs present in the grid cell (BONAN et al., 2002; MOLOD; SALMUN, 2002). The advantage over the composite approach is a better discrimination of the state of the different land cover types and a better representation of the heat and turbulent fluxes with the atmosphere, but it does not well represent competition among PFTs for finite resources, as they occupy separate spaces. For instance, GFDL’s LM3V (SHEVLIAKOVA et al., 2009) was designed with anthropogenic changes in land cover in mind and considers human-caused landscape fragmentation. Rather than using a high-resolution land surface grid, LM3V divides a gridbox into a mosaic of subgrid tiles, as shown in Figure 2.8. As land is cleared for agriculture or logged, a new grid tile is created to accommodate for the new land type. To avoid an exponential growth in subgrid tiles, similar tiles are merged into a single tile when needed.

As most DGVMs do not represent detailed land information within a model grid,

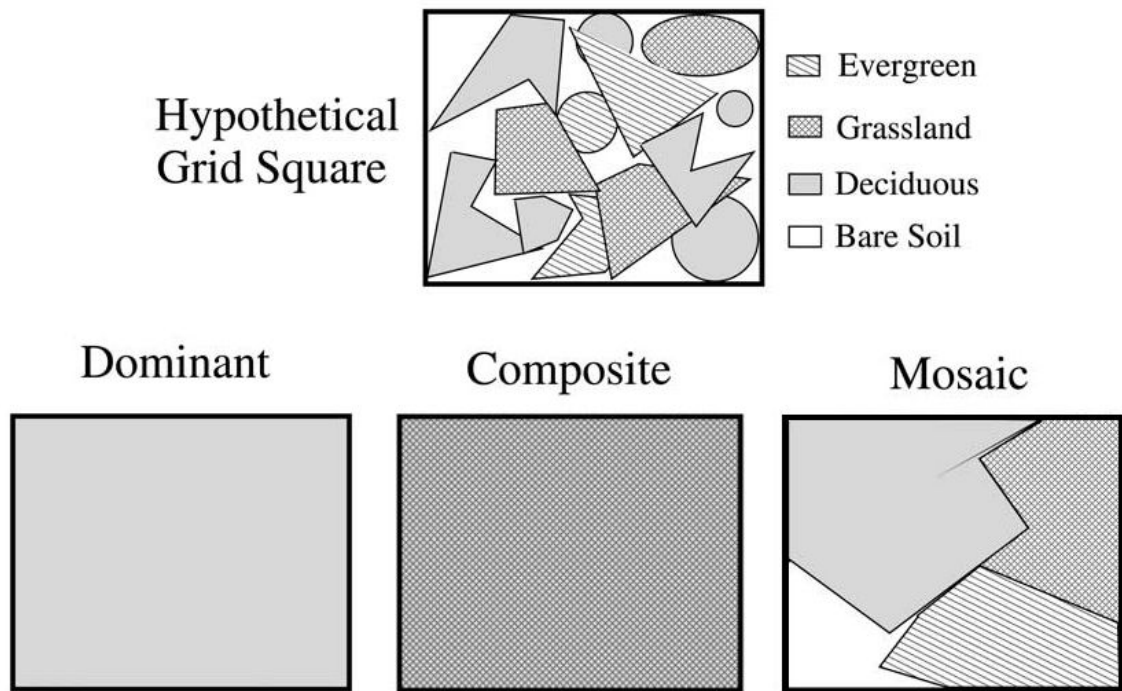


Figure 2.7 - Subgrid variability representations implemented in various LSMs.

SOURCE: Adapted from Molod and Salmun (2002).

fire simulations are usually not spatially aware. A spatially-explicit fire spread modeling approach requires one of the following: a high resolution land surface model which represents real land fragmentation (which would be prohibitive in a global simulation), or a mosaic of subgrid tiles (more efficient but not as accurate).

The IBIS model uses the composite approach to handle subgrid scale heterogeneity. For a given model cell, different PFTs are allowed to co-exist in the two plant layers and competition between different co-existing PFTs is allowed through contention of available light and water (i.e. trees can capture more light, and grasses more water). While this approach represents the natural environment to a certain extent, it is not suitable to represent anthropogenic disturbances which are responsible for heterogeneous fragmentation at the subgrid scale.

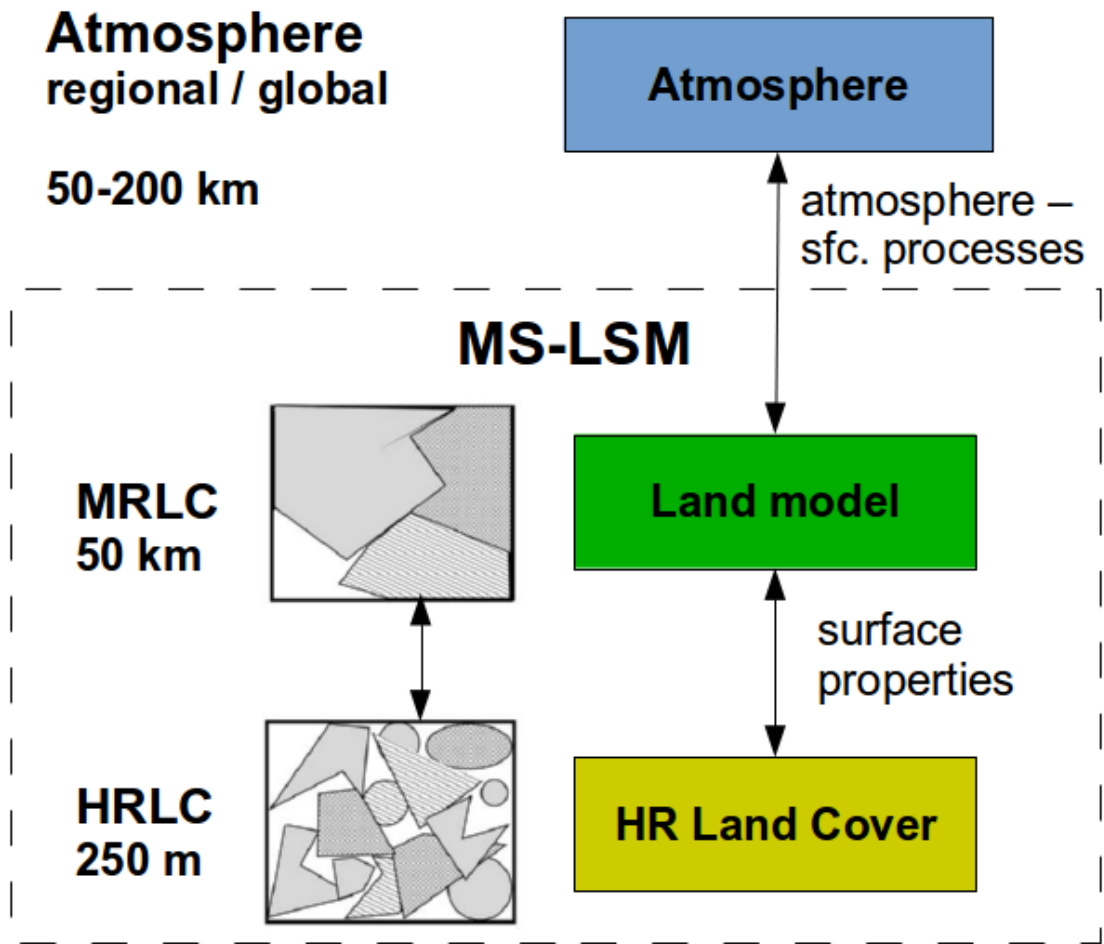


Figure 2.9 - Overview of the multi-scale LSM (MS-LSM) modeling approach, linking high- and medium-resolution land cover maps (HRLC/MRLC).

- a) a means to simulate the different land surface types independently (section 2.2.2)
- b) a high-resolution land surface map (section 2.2.4)
- c) a link between the high-resolution map and the coarse-scale LSM (section 2.2.5)

This is illustrated in Figure 2.9, which shows the link between low- or medium-resolution atmospheric processes (or model) and the multi-scale LSM (MS-LSM) to represent atmosphere-land interactions. The MS-LSM model itself is composed of a medium resolution LSM with subgrid tiles (MRLC), linked to a high resolution land cover map (HRLC).

2.2.2 Subgrid tiling in the INLAND model

This section explains how the “mosaics” or subgrid tiling approach has been implemented in the INLAND model, as part of this work. The execution flow of the INLAND model (shown in detail in Figure B.1) can be summarized as such:

- a) The simulation configuration (e.g. simulation duration in years, domain configuration, options such as dynamic vs. static vegetation, fire module, etc.) and vegetation parameters are read.
- b) The number of model grid points (n_{poi}) and their position is determined based on a land/sea mask and the rectangular domain configuration (global or regional).
- c) All grid-point variables (e.g. npp, soil temperature, etc.) are allocated as vectors with length n_{poi} .
- d) The initial existence and LAI of each PFT ($plai$) is determined from input vegetation type (see section B.2.1).
- e) The hourly, daily and monthly loops are executed on each grid point (with no spatial interactions), until the end of each year.
- f) At the beginning of each month the monthly CRU data is used as an external forcing (precipitation, temperature, etc.).
- g) Important variables are saved to output files at the end of each hourly, daily, monthly and yearly loop (if requested in the model configuration).
- h) The dynamic vegetation module is executed at the end of each model year (if requested in the model configuration).
- i) Execution stops at the end of the last model year.

The implementation of subgrid tiling was challenging from a computer engineering point of view. The data structure of the model (each variable stored in an array of n_{poi} length) is a dated and inflexible data structure (understandably caused by the limitation of the Fortran 77 language). Ideally, each grid cell could be represented by a structure or object (derived data type in Fortran 90) with a set of attributes (e.g. npp, soil temperature). It would then be simple to implement subgrid tiling by adding a number of “child” cells to each “primary” grid cell, as has been done in

the LM3V model of Shevliakova et al. (2009). However, it was decided to keep the basic structure intact, in order to avoid long development time and code conflicts with other modules (e.g. Agro-IBIS and THMB).

The strategy employed was to consider each subgrid tile as an independent grid model point, considering the “real” number of model grid points ($npoi$) multiplied by the number of subgrid tiles $mlpt$ (i.e. $npoi = mlpt * npoi1$). For example, if a simulation is configured with 2 tiles ($mlpt=2$), there are twice as many land points for the model to simulate as a simulation without tiles. Variables that are spatially dependent (longitude and latitude values for solar forcings, input climate and surface data) are replicated to all tiles. Therefore, if a given point has 2 subgrid tiles of the same *vegtype* (vegetation type), the tiles will have the same values during the simulation. However, if *vegtype* or soil properties are different (but external forcings are identical), the tile values will diverge with time.

The following modifications were incorporated into the offline INLAND model in order to implement basic subgrid tiling:

- a) Implementation of dynamic allocation of grid point variables, to simplify model execution.
- b) Implementation of parallel processing of the hourly loop using OpenMP (OpenMP architecture review board, 2011), to improve performance and offset performance losses due to the inclusion of subgrid tiling.
- c) Modification of the input routine and input files to specify *vegtype* and *tilefrac* (tile fraction) of each grid point and each tile.
- d) Modification of the climate and surface properties input routine to replicate values to all tiles.
- e) Inclusion of new *vegtype* definitions and modification of the dynamic vegetation routine to account for human influence on vegetation cover.
- f) Modification of the daily, monthly and yearly output routines to account for the new *tile* dimension.

The input and output of grid-point variables uses the NetCDF format, which allows to store multi-dimensional data and variable metadata. The dimensions used in output files are *latitude*, *longitude*, *time* and *pft* (without subgrid tiling) (see examples in section B.3). For example, some yearly output file variables (e.g. biomass)

have 2D (*latitude/longitude*) values for each day (*time* dimension) and pft (*pft* dimension). The implementation of subgrid tiling added the necessity to include an additional dimension (*tile*) in input and output NetCDF files. In addition to storing the values for each tile at each grid point, an additional *tile* layer is used (a total of $mlpt+1$ layers are stored) to store the grid-point average, which would be passed to a coupled atmospheric model at each timestep (soon to be done). It is thus possible to analyze results by tile, but also by grid-point average.

2.2.3 Changes to the vegetation dynamics module

One of the motivations to implement subgrid tiling in the INLAND model was to be able to separate natural vegetation from managed landscapes (e.g. pasture) within a given grid cell. For reasons that will become more apparent in the results section, modifications were required to the dynamic vegetation routine and *vegtype* definitions. In a nutshell, without these modifications non-natural tiles and natural tiles would both converge to the same *potential vegetation* state) after a certain stabilization time. This is because the vegetation dynamics module was driven solely by climate, and the tiles of a given point share the same climate forcings.

The following key elements were introduced as part of this work:

- a) Inclusion of new *vegtype* definitions (cropland, pasture, urban; see section B.2.1)
- b) Addition of a *landusetype* variable, dependent on *vegtype*, with the following possible values: natural, cropland, pasture, urban.
- c) Modification of the dynamic vegetation routine: if the *landusetype* of a given tile is not natural, climatic rules do not apply and only a certain number of PFTs are allowed to grow (more below).

In order to account for human influence on vegetation cover, only C4 (warm) grasses are allowed to grow in non-natural tiles. This represents human influence on the landscape by vegetation removal and control. This implementation is very basic and not meant for production, but it allows to separate non-natural tiles from natural tiles. It should be improved based on further research and parametrization studies. Ideally, pasture should be represented by a new PFT or a carefully chosen PFT mixture; cropland should be managed by the Agro module (provided the crop type is known and supported); and urban areas should be parametrized. Each of these topics could be the focus of a separate thesis.

2.2.4 Global and regional high-resolution land cover maps

Some land surface schemes, such as SSiB (Simplified Simple Biosphere Model; Xue et al. (1991)) used in CPTEC’s global atmospheric model, use simple “natural” vegetation maps for land cover (DORMAN; SELLERS, 1989; OLIVEIRA, 2008). Several global satellite-based land surface classification products have been produced in recent years. The 1 km-resolution map (HANSEN et al., 2000) based on 1992–1993 data from the Advanced Very High Resolution Radiometer (AVHRR) was the first satellite-based land cover map. With the advent of better and finer instruments, several datasets have been made available: GLC2000 based on SPOT VEGETATION data from 2000 at 1 km (BARTHOLOMÉ; BELWARD, 2005); MCD12Q1 using data from the MODIS (Moderate Resolution Imaging Spectroradiometer) sensor, available for all years from 2001–2012 at 500m resolution (FRIEDL et al., 2010); and the GlobCover product using 2005 and 2009 data from the MERIS sensor at 300m resolution (ARINO et al., 2008; BONTEMPS et al., 2011). The last two products are the most recent and of highest resolution. The MCD12Q1 product (see Figure C.2) is the most reliable, with a reported overall accuracy of 75%, but less reliable in areas of savanna, mixed forests, wetlands, and agriculture/natural mosaic (FRIEDL et al., 2010). The GlobCover product (see Figure C.1) has a higher resolution but a lower overall accuracy of 58% (BONTEMPS et al., 2011). The MCD12Q1 was considered for this study for the following reasons: better overall accuracy, resolution compatible with two MODIS-based global burned area products (see Chapter 4), subjectively deemed more reliable for separating forest from deforested areas in the Amazon (not shown), and classification scheme (IGBP) more compatible with the INLAND *vegtype* definitions.

The great geographical extent and biodiversity of Brazil pose a challenge to the monitoring of its land cover and land use/cover changes (LUCC) through human intervention. The most comprehensive national land cover dataset is from the PROBIO (Projeto de Conservação e Utilização Sustentável da Diversidade Biológica) project, from Brazil’s MMA (Ministério do Meio Ambiente). PROBIO is based on Landsat ETM+ data from 2002 at 30m resolution and field validation, and maps are available for each of Brazil’s biomes (Amazônia, Cerrado, Caatinga, Mata Atlântica, Pantanal, Pampas) at <http://mapas.mma.gov.br/mapas/aplic/probio/datadownload.htm>. The classification system used is IBGE’s “Sistema Brasileiro de Classificação da Vegetação Brasileira” (IBGE1992) of IBGE (1992), IBGE (2012). It uses a physiognomic-ecological classification system (*Sistema de Classificação Fisionômico-Ecológica*) to identify the various vegetation cover types present in

Brazil, with much more detail than considered in the climate modeling context.

Brazil has been very active in the development of operational methodologies for LUCC mapping through the use of remote sensing data. This has led to the creation by INPE of the PRODES (Projeto de Monitoramento do Desmatamento na Amazônia Legal por Satélite) DIGITAL dataset, consisting of yearly maps and areal values of deforestation estimated from high resolution Landsat and CBERS imagery since 2003. Recent data, available at <http://www.obt.inpe.br/prodes/> shows that deforestation rates has been diminishing since the peak of over 25000 km^2 in 2004 and reached a record low of 4571 km^2 in 2012. Annual totals of deforestation per state since 1988 are also available, generated by the previous PRODES analog methodology. Deforestation in the *cerrado* has been recently gathering attention from the Brazilian government, research institutions and environmental groups. The SIAD-cerrado (Sistema Integrado de Alertas de Desmatamentos) project (FERREIRA et al., 2007) of UFG/LAPIG available from at <http://www.lapig.iesa.ufg.br/lapig/> produces yearly maps of deforestation since 2002, using 250m MODIS data. A project from IBAMA - PMDBBS (Projeto de Monitoramento do Desmatamento dos Biomas Brasileiros por Satélite) produces deforestation datasets for various biomas of Brazil with greater detail, using 30m Landsat imagery, and is available from <http://siscom.ibama.gov.br/monitorabiomas/>. The deforestation estimates from PMDBBS are over twice as high as those of SIAD-cerrado as they use a higher-resolution dataset (unpublished study), but they are only available for certain years.

The PROVEG dataset (VIEIRA et al., 2013) is based on PROBIO data, deforestation up to 2009 from INPE's PRODES, and more recent mapping using Landsat imagery. Its vegetation classes are compatible with SSiB and resolution has been downgraded to 1 km resolution for use in global climate modeling studies. A certain number of issues have been identified in this dataset : misalignment of data relative to any ground-based imagery (including PRODES) shown in section 3.2.2; relative low resolution causing the absence of key fine-scale features (deforestation structure water bodies, etc.); lack of clear pasture vs. cropland distinction; missing PRODES deforestation since 2002. It is nevertheless a valid dataset when fine-scale structure is not important.

To overcome some of the limitations of the PROVEG dataset, a high-resolution (250m) dataset was compiled for the Legal Amazon of Brazil. This dataset, hereby named IBGE-TC, was compiled from two sources. Natural vegetation cover is de-

rived from the vegetation cover map from IBGE’s “Sistematização das Informações sobre Recursos Naturais” project (IBGE, 2006, IBGE2006). The IBGE2006 vegetation map is based on 2003 Landsat imagery and vegetation cover is classified using the IBGE1992 system. Secondary vegetation data from TERRACCLASS (ALMEIDA et al., 2009) is used to refine this map with more recent and more detailed land-use cover data. TERRACCLASS is a detailed classification of actual land-use over locations where the PRODES project has identified deforested areas in the Amazônia biome. Both products were rasterized (converted from shapes to pixels) at a resolution of 250m and their classes converted to the INLAND classification scheme (using the mapping between land cover classes shown in Tables C.3 and C.4), with TERRACCLASS data overriding the IBGE2006 data where available. This map is shown in Figure C.5, along with the PROVEG map, using the INLAND classification scheme.

2.2.5 Linking high-resolution maps to subgrid tile modeling

In its basic form, subgrid tiling is non-spatial, meaning that there is no information on the subgrid spatial structure of the different land cover types. A second configuration, activated by using the *hrmap* option in the main configuration file (see section B.2), allows to initialize the tiles from a high-resolution land cover map. The many-to-1 relationship between high-resolution land surface pixels and their parent tile is shown in Figure 2.10. The number of tiles is defined in the simulation parameters, with four tiles being largely sufficient for most applications. During model initialization the high-resolution *vegtype* map is read (it may be of any resolution, provided it fits within the model domain). For each model grid point, *vegtype* and *tilefrac* are determined for each model tile, based on the occurrence of the high-resolution pixels present in the relative area of high-resolution map. If there are more unique land cover types in the high-resolution map than tiles, the dominant land cover type is assigned to the excendent high-resolution pixels. Areas not covered by this map are assigned a single tile as defined in the base IBIS *vegtype* map. For a simulation over South America using the MCD12Q1 dataset, the vast majority of high-resolution pixels are represented when using a configuration of 4 tiles. Once the tile information is read, the pixel-to-tile relationship (*ihrtileparent* variable) is saved to disk for further use as it is discarded during the simulation. It is thus possible to create high-resolution maps of each of the output variables, using the per-tile output combined with the original high-resolution *vegtype* map and the *ihrtileparent* map. This is illustrated in Section 3.3.3.

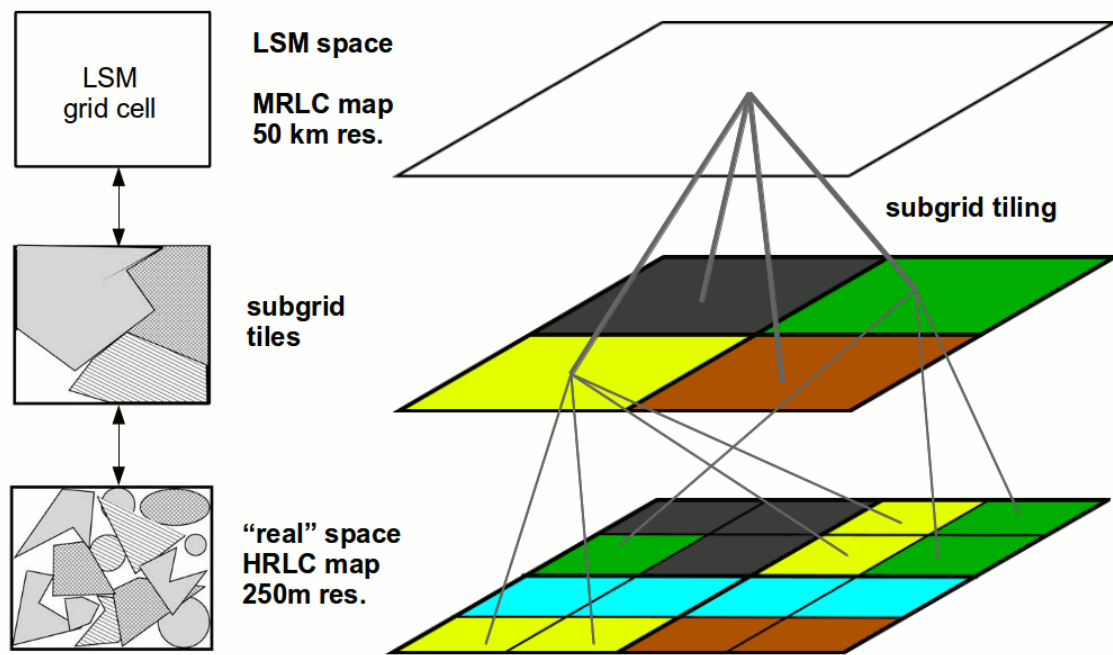


Figure 2.10 - Relationship between the high-resolution map and the model subgrid tiling in the multi-scale LSM modeling approach.

2.2.6 Experimental setup

In order to test and illustrate the subgrid tiling implementation in INLAND, a series of simple synthetic experiments was designed. Firstly, a simulation was done with 2 identical tiles using the original IBIS *vegtype* map, global domain, for a period of 20 years in both static and dynamic vegetation modes. Results (not shown) were identical to the INLAND model without the subgrid tiling implementation. A simple experiment was done to test the changes in the vegetation dynamic module to account for managed landscapes (natural vs. modified vegetation). A “tropical deforestation” experiment was designed in order to test the sensibility of the model to large-scale deforestation in the tropics. Finally land cover maps for Brazil (see section 2.2.4) were used to evaluate the sensitivity of the model when initialized with realistic land cover.

2.3 Results

2.3.1 Natural vegetation, single point

The first experiment uses a single grid point in the Amazon forest (at 57.75°W 14.75°S) with a simulation time of 100 years in both static and dynamic vegetation modes, using three tiles of *vegtype* 1 (Evergreen Forest), 9 (Savanna) and 10 (Grassland) of equal *tilefrac* (0.33). This period is sufficient to allow a stabilization of most variables when running in dynamic vegetation mode, the exception being soil carbon and nitrogen, which require centuries to stabilize (not shown). Figure 2.11 shows time series for two variables (*aet* - evapotranspiration and *totbiou* - upper canopy biomass) in both static and dynamic vegetation modes. In static vegetation, *aet* is very similar among different *vegtypes* although slightly lower for grass, but *totbiou* shows different values and the tile average is about half that of forest. In dynamic vegetation mode, we see that *aet* rapidly converges for all tiles, associated to a rapid convergence of upper-story LAI (not shown), which is an important factor for determining insolation and evaporation. On the other hand, *totbiou* takes around 70 years to converge, which is more “realistic” than the rapid changes in LAI and *aet*. Table 2.1 gives the values of all output variables at the end of the 100 year simulation. In the static simulation results, *wsoi* values are almost identical, which is a peculiar behavior of the model, as one would expect different soil moisture values due to very different upper canopy coverage. However, *aet* is lower and drainage is higher in the case of grassland *vegtype*, which is expected. In the dynamic vegetation case, we can see that all values are almost identical, as the various tiles have reached the same potential vegetation state (due to identical climate input for all tiles), after a sufficient stabilization period. This shows us the limited use of subgrid tiling in dynamic vegetation mode when considering natural vegetation.

2.3.2 Modified vegetation, single point

The second experiment uses a similar configuration as the previous one, but makes use of the new *vegtype* definitions for managed landscapes (described in Section B.2.1). In this case, there are two natural tiles with *vegtype* 1 (Evergreen Forest) and 10 (Grassland) and two tiles with *vegtype* 18 (Pasture), all of equal *tilefrac* (0.25). The two Pasture tiles differ in their initial LAI configuration: Pasture1 is equal to natural Grassland (all PFTs are initially present), while Pasture2 is equal to Desert (only Grass PFT is present). For exact LAI values refer to section B.2.1. In Figure 2.12 one can note that in static vegetation mode, the *aet* and *totbiou* values for Pasture2 are different from Pasture1 (which is nearly identical to Grassland), due

Table 2.1 - Yearly output variables for the “natural vegetation” experiment at end of simulation, individual tile and average values.

variable	Static vegetation				Dynamic vegetation			
	forest	savanna	grass	avg.	forest	savanna	grass	avg.
aet	1386	1385	1315	1362	1384	1384	1384	1384
anpptot	0.00	0.00	0.00	0.00	0.73	0.73	0.73	0.73
awc	8.78	7.05	7.02	7.63	8.90	8.90	8.90	8.90
caccount	0.00	0.00	0.00	0.00	0.00	0.00	0.00	0.00
co2mic	0.00	0.00	0.00	0.00	0.77	0.77	0.77	0.77
co2root	0.26	0.19	0.18	0.21	0.34	0.34	0.34	0.34
co2soi	0.26	0.19	0.18	0.21	1.12	1.11	1.11	1.11
drainage	2.80	0.53	28	10	3.43	3.42	3.42	3.42
fl	0.50	0.98	0.98	0.81	0.25	0.25	0.25	0.25
fu	0.98	0.92	0.57	0.82	0.98	0.98	0.98	0.98
neetot	0.96	1.16	1.56	1.22	0.14	0.14	0.14	0.14
nmintot	0.00	0.00	0.00	0.00	0.01	0.01	0.01	0.01
npptot	0.96	1.16	1.56	1.22	0.91	0.91	0.91	0.91
rootbio	0.13	0.10	0.09	0.11	0.17	0.17	0.17	0.17
srunoff	76	77	78	77	76	76	76	76
tilefrac	0.34	0.33	0.33	0.00	0.34	0.33	0.33	0.00
totalit	0.00	0.00	0.00	0.00	0.52	0.52	0.52	0.52
totanlit	0.00	0.00	0.00	0.00	0.00	0.00	0.00	0.00
totbiol	0.04	0.20	0.23	0.16	0.00	0.00	0.00	0.00
totbiou	10	2.59	0.86	4.66	9.18	9.14	9.12	9.15
totcmic	0.00	0.00	0.00	0.00	0.12	0.12	0.12	0.12
totcsoi	0.00	0.00	0.00	0.00	4.66	4.59	4.57	4.61
totfall	0.00	0.00	0.00	0.00	0.78	0.78	0.78	0.78
totlail	0.50	2.50	3.00	1.99	0.04	0.04	0.04	0.04
totlaiu	6.00	1.50	0.50	2.70	6.75	6.73	6.74	6.74
totnsoi	0.00	0.00	0.00	0.00	0.45	0.44	0.44	0.45
totrlit	0.00	0.00	0.00	0.00	0.05	0.05	0.05	0.05
totrnlit	0.00	0.00	0.00	0.00	0.00	0.00	0.00	0.00
trunoff	79	78	106	88	80	80	80	80
tsoi	26	27	27	27	27	27	27	27
vwc	0.24	0.22	0.22	0.22	0.24	0.24	0.24	0.24
wisoi	0.00	0.00	0.00	0.00	0.00	0.00	0.00	0.00
wsoi	0.59	0.55	0.55	0.56	0.60	0.60	0.60	0.60

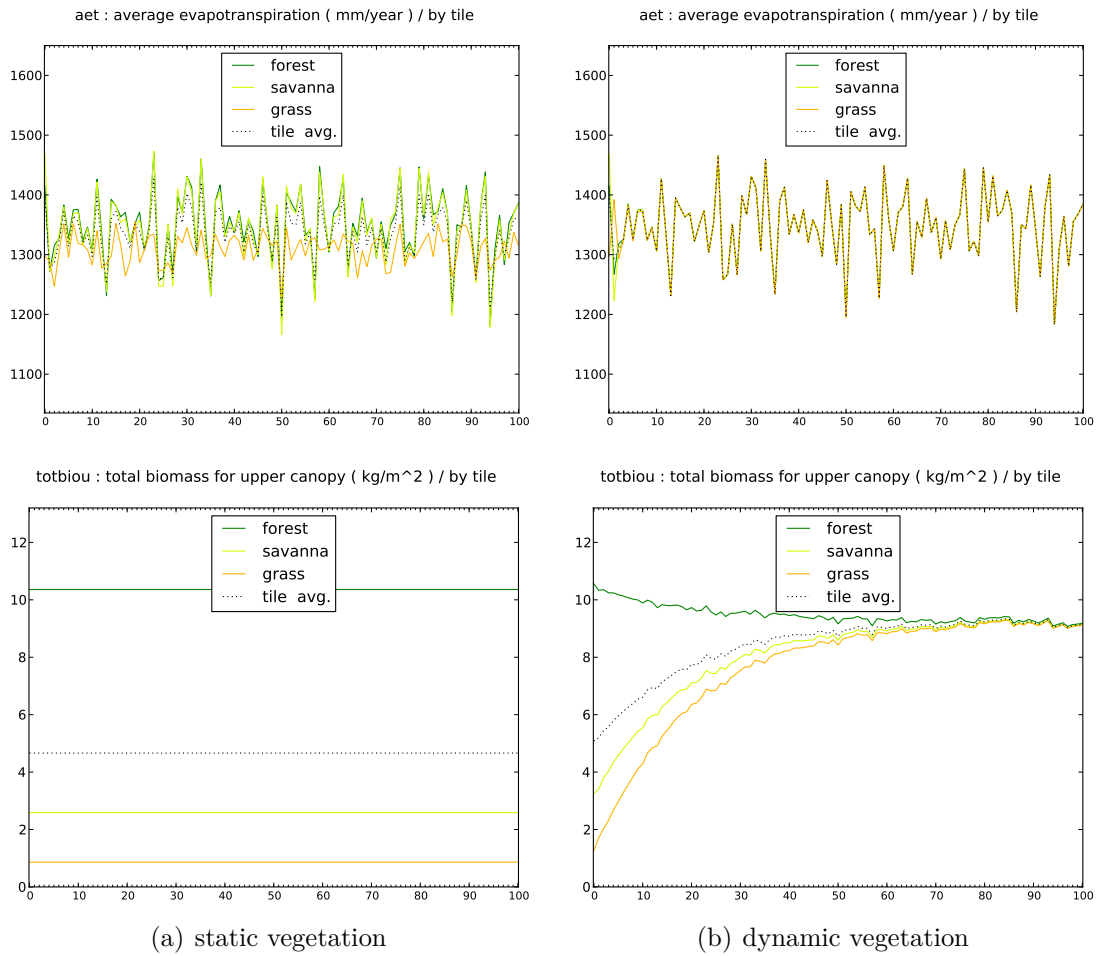


Figure 2.11 - Time series of yearly aet and totbiou in the “natural vegetation” experiment

to initial LAI which is persisted throughout the simulation. In the case of dynamic vegetation, the natural tiles converge to “natural equilibrium”, while the Pasture tiles converge to “natural potential equilibrium” (identical for both Pasture tiles). Table 2.2 shows that in dynamic vegetation mode, but without land use rules, all values converge to those of the natural tiles, just as in the “natural vegetation” experiment, but when land use rules are applied they converge to a same, modified state. In the dynamic vegetation column, *totalit* is shown instead of *totbiou* because the latter values are zero in the case of modified vegetation. Note that *aet* values for Pasture tiles are much (especially for Pasture2 in static vegetation), which may be due to lack of parameterization and should be investigated in further work. The key points are as follows: in static vegetation mode, initial LAI configuration is important as it is persistent and has an important influence on model results; in dynamic vegetation mode the initial LAI state is lost and the land use rules take

precedence ; land use rules are necessary to avoid that modified vegetation tiles drift to “natural potential equilibrium” state. This shows that land use rules are essential for representing subgrid-scale fragmentation through LUC processes.

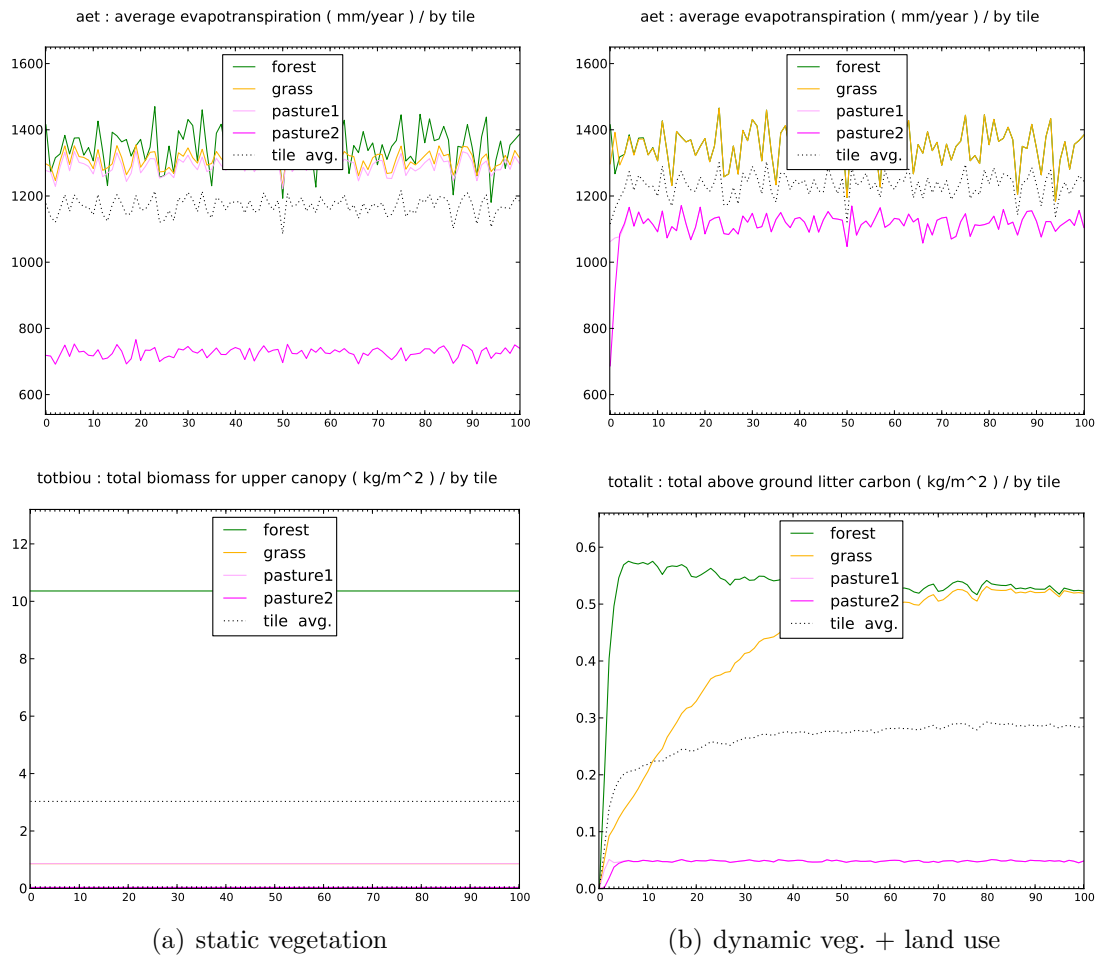


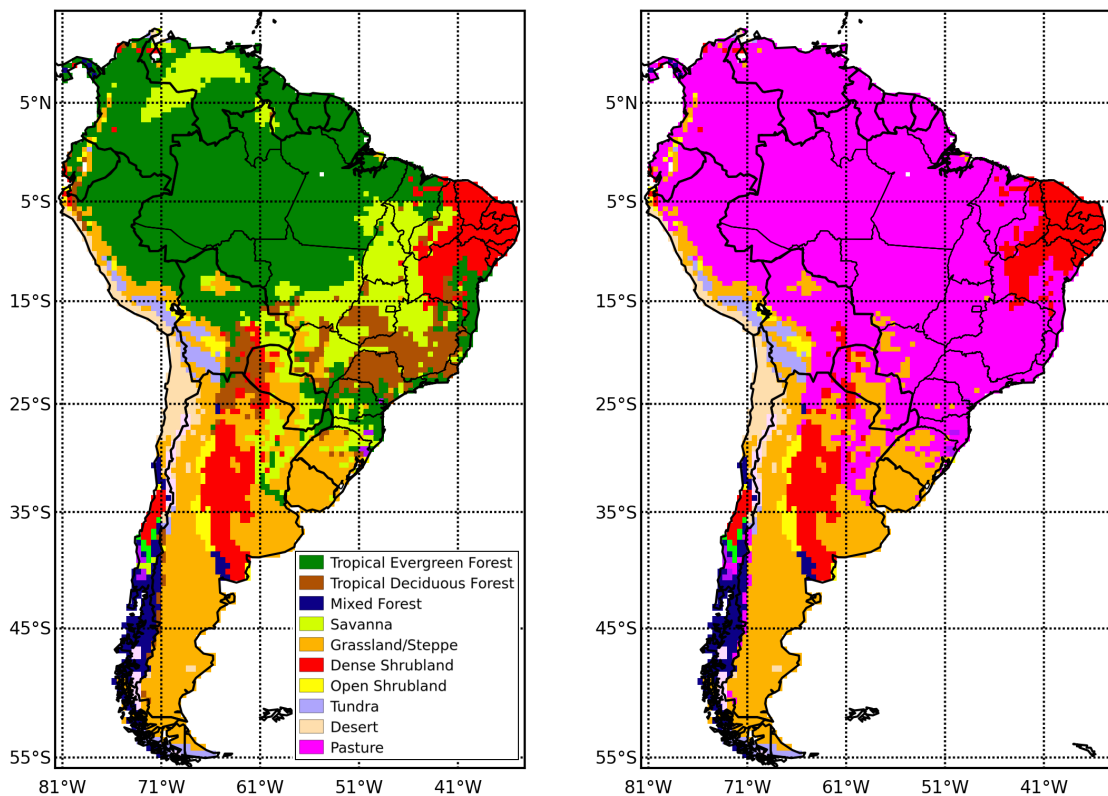
Figure 2.12 - Time series of average yearly *aet* and *totbiou/totalit* in the “modified vegetation” experiment

Table 2.2 - Yearly output variables for the “modified vegetation” experiment at end of simulation, individual tile and average values.

variable	Static vegetation						Dynamic vegetation						
	Natural			No Land use			Natural			No Land use			
	forest	savanna	pasture1	pasture2	avg.	pasture1	pasture2	avg.	forest	savanna	pasture1	pasture2	avg.
aet	1386	1315	1298	740	1185	1384	1384	1384	1384	1384	1105	1105	1244
anpptot	0.00	0.00	0.00	0.00	0.00	0.73	0.73	0.73	0.73	0.73	0.32	0.32	0.53
awc	8.78	7.02	7.27	11	8.40	8.90	8.90	8.90	8.90	8.90	6.64	6.64	7.77
caccount	0.00	0.00	0.00	0.00	0.00	0.00	0.00	0.00	0.00	0.00	0.00	0.00	0.00
co2mic	0.00	0.00	0.00	0.00	0.00	0.77	0.77	0.77	0.77	0.77	0.82	0.82	0.80
co2root	0.26	0.18	0.18	0.01	0.16	0.34	0.34	0.34	0.34	0.34	1.06	1.06	0.70
co2soi	0.26	0.18	0.18	0.01	0.16	1.12	1.11	1.11	1.11	1.11	1.88	1.88	1.50
drainage	2.80	28	56	635	180	3.43	3.42	3.42	3.42	3.42	251	251	127
fl	0.50	0.98	0.98	0.25	0.68	0.25	0.25	0.25	0.25	0.25	0.98	0.98	0.61
fu	0.98	0.57	0.57	0.25	0.59	0.98	0.98	0.98	0.98	0.98	0.25	0.25	0.61
neetot	0.96	1.56	1.38	0.13	1.01	0.14	0.14	0.14	0.14	0.14	0.10	0.10	0.02
nmintot	0.00	0.00	0.00	0.00	0.00	0.01	0.01	0.01	0.01	0.01	0.02	0.02	0.01
npptot	0.96	1.56	1.38	0.13	1.01	0.91	0.91	0.91	0.91	0.91	0.72	0.72	0.81
rootbio	0.13	0.09	0.09	0.00	0.08	0.17	0.17	0.17	0.17	0.17	0.50	0.50	0.34
srunoff	76	78	78	83	79	76	76	76	76	76	78	78	77
tilefrac	0.25	0.25	0.25	0.25	0.00	0.25	0.25	0.25	0.25	0.25	0.25	0.25	0.00
totalit	0.00	0.00	0.00	0.00	0.00	0.52	0.52	0.52	0.52	0.52	0.05	0.05	0.28
totamlit	0.00	0.00	0.00	0.00	0.00	0.00	0.00	0.00	0.00	0.00	0.00	0.00	0.00
totbiol	0.04	0.23	0.23	0.01	0.13	0.00	0.00	0.00	0.00	0.00	0.87	0.87	0.44
totbiou	10	0.86	0.86	0.03	3.03	9.18	9.12	9.12	9.12	9.12	0.00	0.00	4.58
totcnic	0.00	0.00	0.00	0.00	0.00	0.12	0.12	0.12	0.12	0.12	0.12	0.12	0.12
totcsoi	0.00	0.00	0.00	0.00	0.00	4.66	4.57	4.57	4.57	4.57	4.76	4.76	4.69
totfall	0.00	0.00	0.00	0.00	0.00	0.78	0.78	0.78	0.78	0.78	0.85	0.85	0.81
totlail	0.50	3.00	3.00	0.10	1.65	0.04	0.04	0.04	0.04	0.04	8.90	8.90	4.47
totlailu	6.00	0.50	0.50	0.02	1.75	6.74	6.74	6.74	6.74	6.74	0.00	0.00	3.37
totnsoi	0.00	0.00	0.00	0.00	0.00	0.45	0.44	0.44	0.44	0.44	0.46	0.46	0.45
totrlit	0.00	0.00	0.00	0.00	0.00	0.05	0.05	0.05	0.05	0.05	0.13	0.13	0.09
totrnlit	0.00	0.00	0.00	0.00	0.00	0.00	0.00	0.00	0.00	0.00	0.00	0.00	0.00
trunoff	79	106	134	718	259	80	80	80	80	80	329	329	204
tsoi	26	27	27	32	28	27	27	27	27	27	28	28	27
vwc	0.24	0.22	0.22	0.25	0.23	0.24	0.24	0.24	0.24	0.24	0.21	0.21	0.23
wisoi	0.00	0.00	0.00	0.00	0.00	0.00	0.00	0.00	0.00	0.00	0.00	0.00	0.00
wsoi	0.59	0.55	0.55	0.64	0.58	0.60	0.60	0.60	0.60	0.60	0.54	0.54	0.57

2.3.3 Tropical deforestation: modified vegetation, South America domain

The goal of this experiment is to test and demonstrate subgrid tiling over a large domain. It uses a synthetic scenario where 50% of all tropical forest and savanna is converted to pasture. Figure 2.13 shows the two *vegtype* tile maps used, based on the standard IBIS potential *vegtype* map. The simulation is over the South American continent for a duration of 100 years in dynamic vegetation mode. In Figure 2.14 we can see that average *aet* is somewhat lower in the tile average than in the natural tile, and *totbiou* is much lower (around 50%). Table 2.3 shows spatial averages over the Amazônia biome that are very different in the case of some variables (e.g. *totalit*, *totlaiu*) while some variables are almost unchanged (e.g. *npptot*, *tsoi*, *wsoi*).



(a) Tile 1 - IBIS natural potential vegetation map, as in SAGE (2014).

(b) Tile 2 - as in (a), but all tropical forest and savanna replaced with pasture.

Figure 2.13 - Vegetation tile maps for the “tropical deforestation” experiment, where both tiles have a proportion of 50% for all grid points.

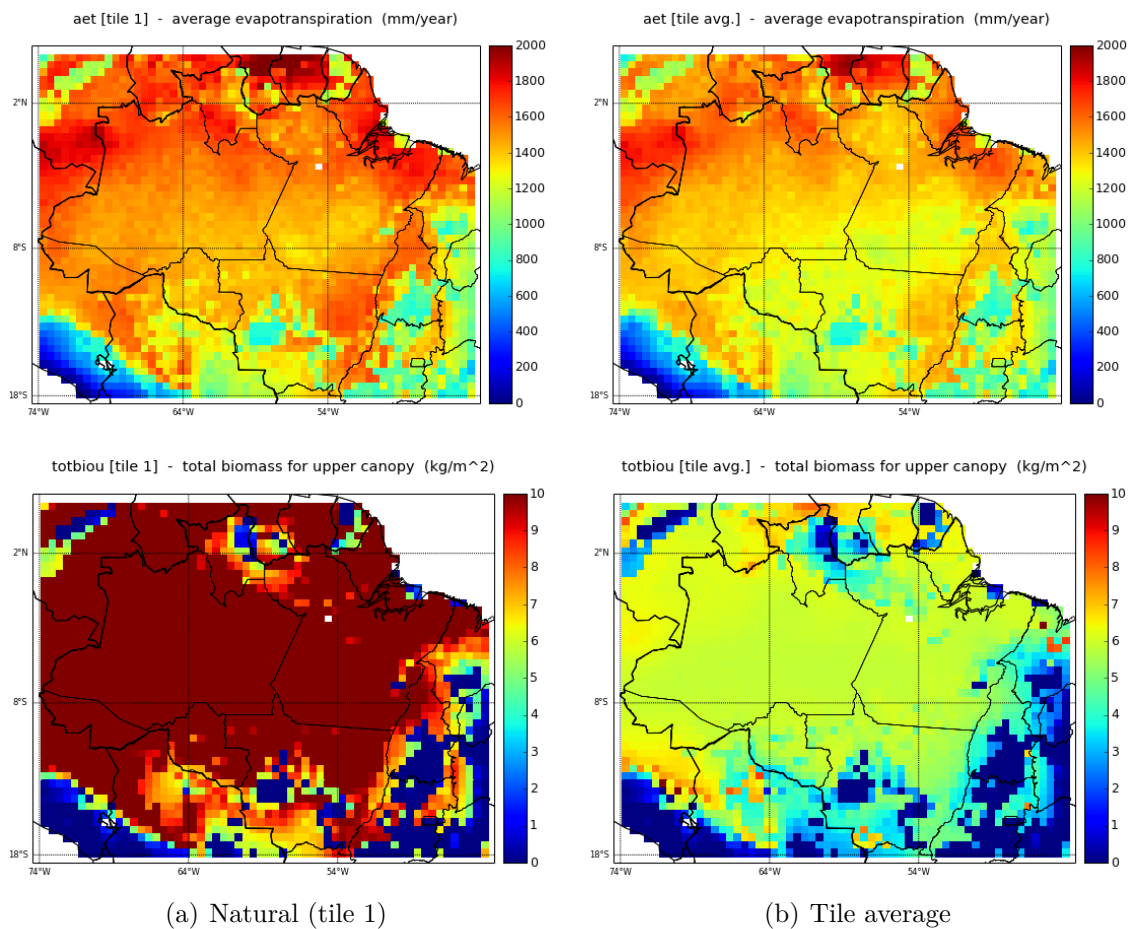


Figure 2.14 - Maps of *aet* and *totbiou* at end of simulation in the “tropical deforestation” experiment, showing most of the Amazônia biome.

2.3.4 Using high-resolution land cover maps

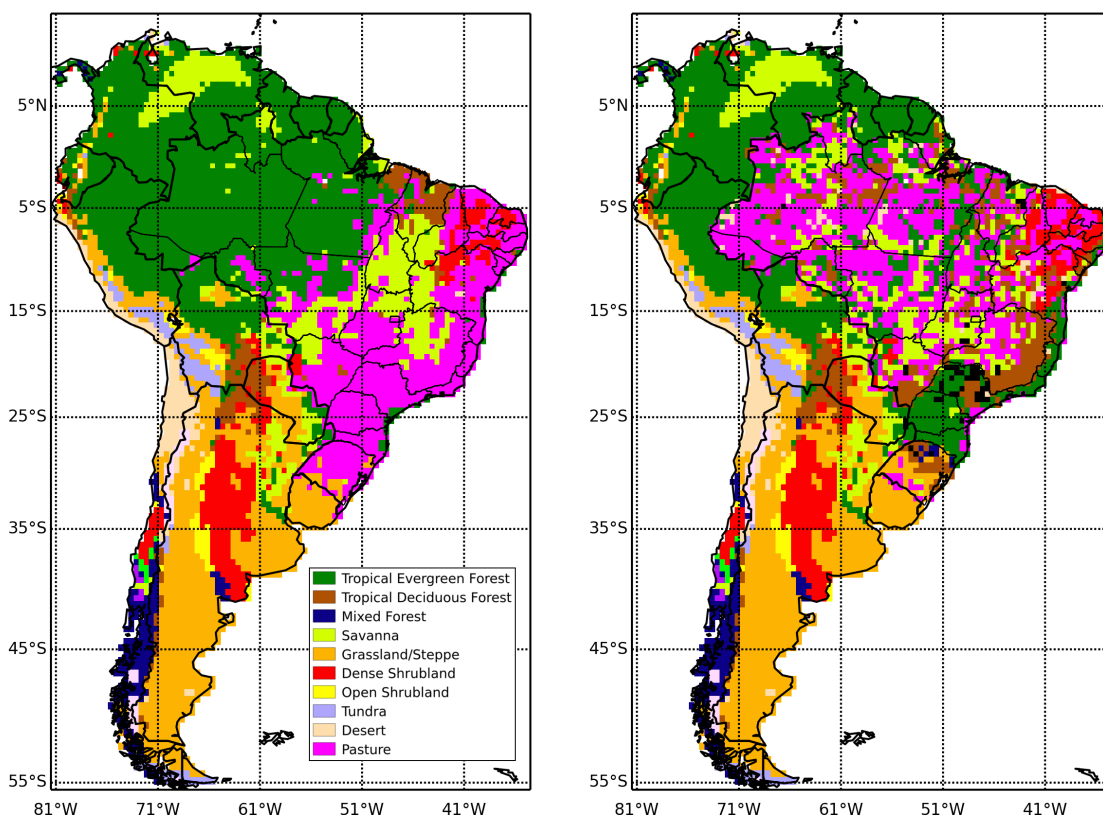
This experiment uses the land cover maps for Brazil (PROVEG and IBGE-TC), as well as the global land cover map MCD12Q1, described in section 2.2.4. The high resolution of these maps allows them to be used to initialize the INLAND model with a number of tiles (determined by the modeler), in a manner much more realistic than when using the IBIS *vegtype* maps. This experiment, similar to the “tropical deforestation” experiment, was run over the South American continent for 100 years with four tiles, initialized from these three land cover maps. Figure 2.15 shows the configuration of the first two tiles when using the PROVEG map. The *vegtype* and *tilefrac* values are determined from the high-resolution input map, as described in Section 2.2.5. For reference, the other maps are shown in Figure C.6 (Amazon only). Results are compared to a simulation without tiles, initialized with the base IBIS *vegtype* map.

Table 2.3 - Yearly output variables for the “tropical deforestation” experiment at end of simulation, individual tile and tile average values of Amazônia biome spatial average.

<u>variable</u>	<u>IBIS</u>	<u>defor.</u>	<u>avg.</u>	<u>variable</u>	<u>IBIS</u>	<u>defor.</u>	<u>avg.</u>
aet	1522	1269	1396	totalit	0.85	0.07	0.46
anpptot	0.86	0.50	0.68	totanlit	0.00	0.00	0.00
awc	15	12	13	totbiol	0.01	1.22	0.62
caccount	0.00	0.00	0.00	totbiou	11	0.02	5.60
co2mic	0.95	1.09	1.02	totcmic	0.18	0.17	0.17
co2root	0.45	1.30	0.88	totcsoi	7.53	6.92	7.22
co2soi	1.40	2.39	1.90	totfall	0.96	1.10	1.03
csoipas	0.28	0.31	0.30	totlail	0.16	12	6.25
csoislo	0.00	0.00	0.00	totlailu	8.03	0.02	4.02
drainage	253	470	361	totnsoi	0.73	0.67	0.70
fl	0.26	0.97	0.62	totrlit	0.08	0.19	0.13
fu	0.96	0.25	0.61	totrnlit	0.00	0.00	0.00
neetot	0.13	0.02	0.08	trunoff	690	942	816
nmintot	0.01	0.02	0.02	tsoi	28	28	28
npptot	1.08	1.11	1.10	vegtype	1	18	
rootbio	0.22	0.60	0.41	vwc	0.37	0.35	0.36
srunoff	437	472	454	wisoi	0.00	0.00	0.00
tilefrac	0.50	0.50	0.00	wsoi	0.81	0.75	0.78

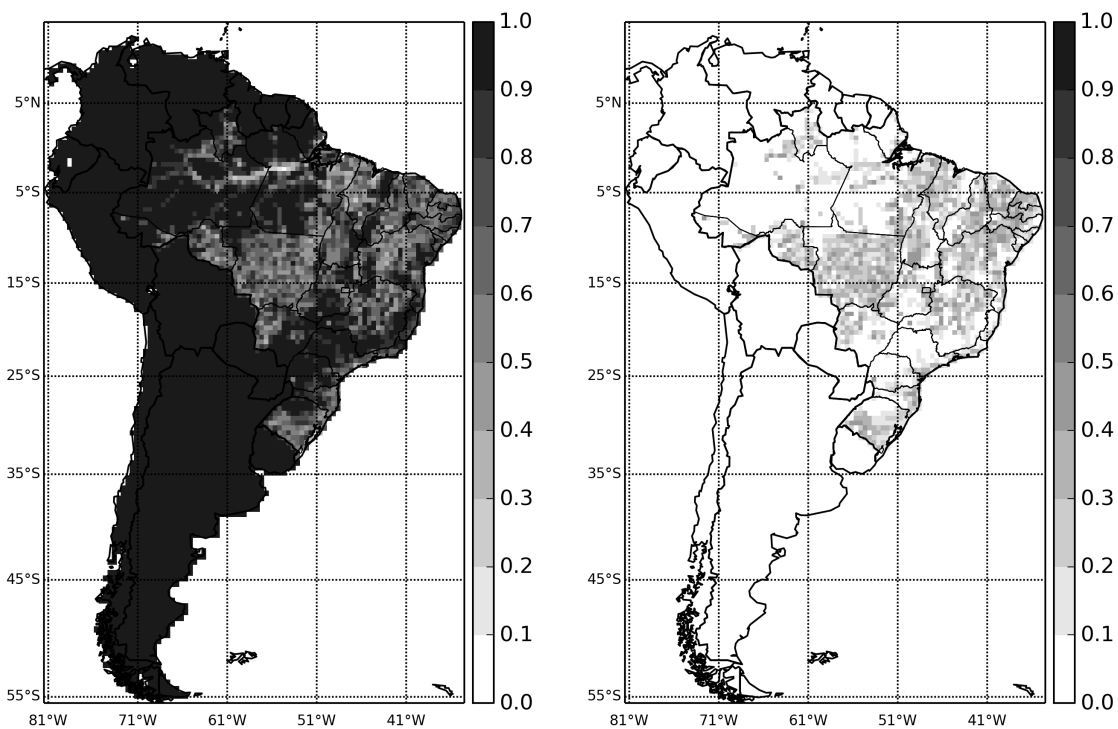
Shown in Figure 2.16 are *aet* and *totbioul* at the end of simulation, comparing the results with base IBIS map configuration to results using the PROVEG land cover map in tiled mode. Values of *aet* are not very different (as in other experiments), but the values are slightly lower in the “arc of deforestation” and eastern Pará state (where the dominant tile is pasture). Values of *totbiou* are more notably different, and highlight areas of deforestation outside of “the arc of deforestation” (e.g. central Pará). These results show the usefulness of the subgrid tiling approach in simulating the effects of deforestation at subgrid-scale. Spatial averages were computed for the following three areas (illustrated in Figure 2.17) : AMZ (the Amazônia biome), NMT (Northern Mato Grosso state, 60°W – 55.5°W and 9°S – 11°S) and EPA (Eastern Pará state, 50°W – 48.5°W and 4°S – 8°S) and are shown in Table 2.4. Spatial average results for the AMZ region show little difference compared to the base IBIS simulation. This is due to the high ratio of natural vs. modified vegetation (agro, pasture) when considering the entire Amazônia biome, as the average *tilefrac* values of Pasture and Cropland combined are 17%, 12% and 10% for IBGE-TC, PROVEG and MCD12Q1 experiments respectively (bottom row of Table 2.4). In the NMT area, differences are higher, consistent with modified vegetation *tilefrac*

averages of 30%, 20% and 15%, respectively. Finally, the results for the EPA area show greater differences, with of *totlaiu* and *totbiou* values ~ 4 times lower when compared to the IBIS configuration, except for MCD12Q1. Most notable are the differences in *drainage*, especially with the IBGE-TC and PROVEG input maps, which is explained by the fact that areas with less vegetation do not retain water as well as heavily vegetated areas. These large differences are consistent with higher modified vegetation *tilefrac* averages of 36%, 29% and 17%, respectively, than in other regions analyzed. Even though large-scale results are similar using any of the datasets (IBIS, PROVEG, IBGE-TC and MCD12Q1), regional results can be quite different due to regional and local-scale differences in land cover types between these maps.



(a) tile 1 *vegtype*

(b) tile 2 *vegtype*



(c) tile 1 *tilefrac*

(d) tile 2 *tilefrac*

Figure 2.15 - PROVEG land cover map for Brazil, overlaid on the IBIS base map for coverage of the rest of the continent. Shown here are *vegtype* (top) and *tilefrac* (bottom) of the first two tiles.

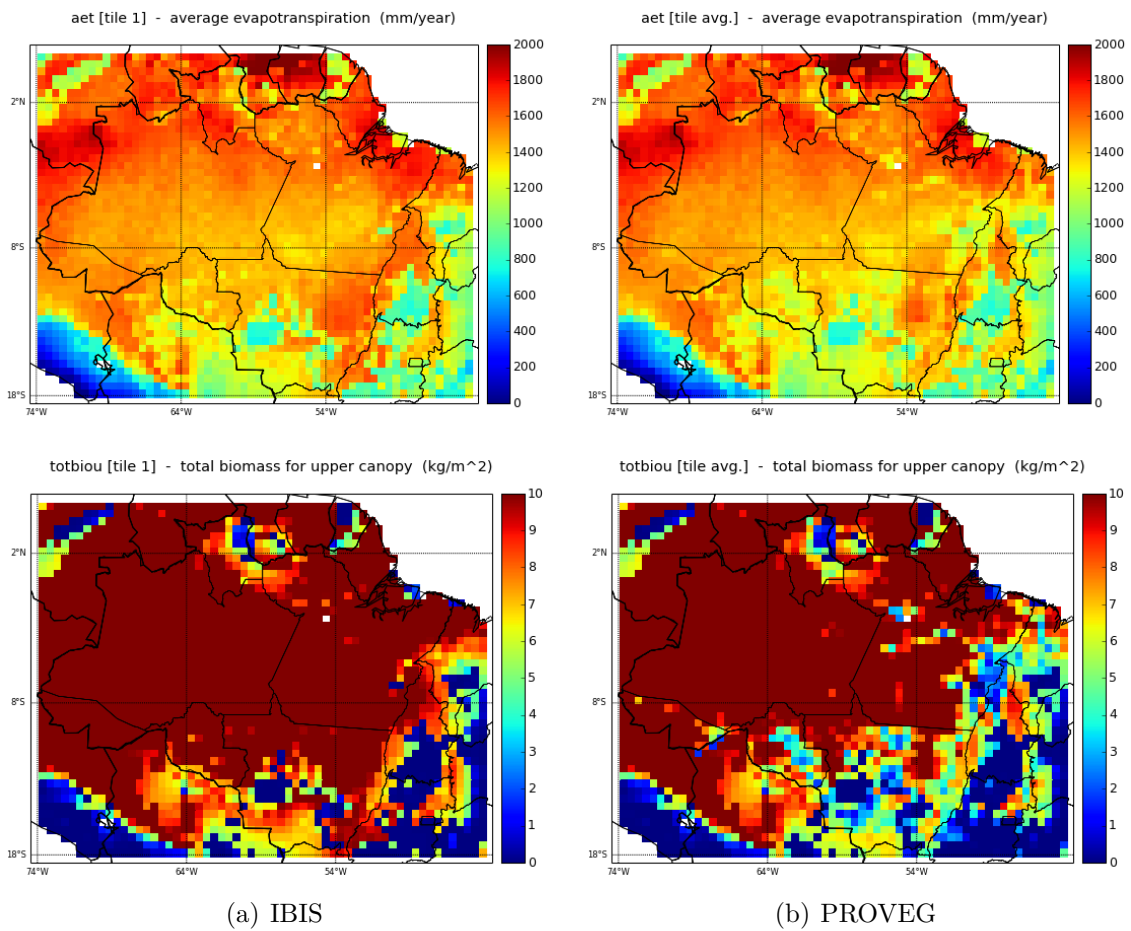


Figure 2.16 - Maps of aet and totbiou at end of simulation of most of the Amazônia biome, when model is initialized with base IBIS vegtype map and using tiles with the PROVEG land cover map.

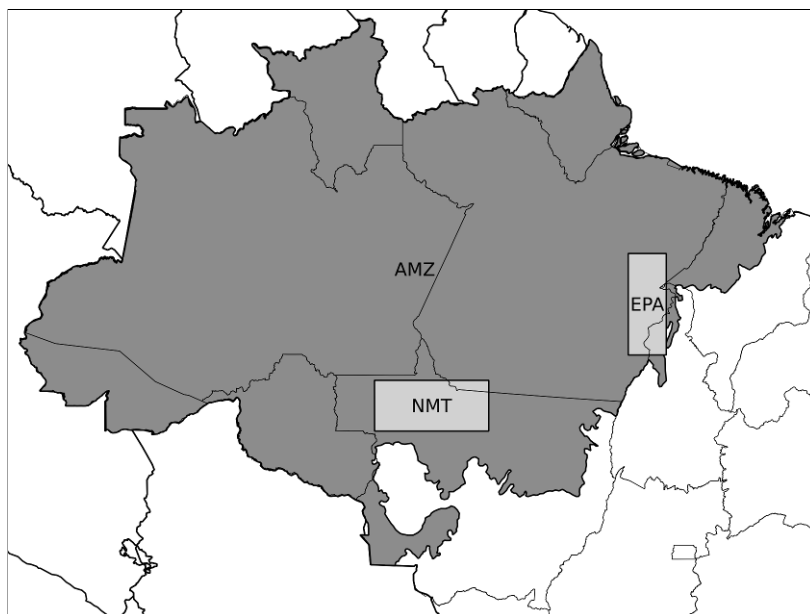


Figure 2.17 - Location of the AMZ, NMT and EPA regions analysed

Table 2.4 - Yearly output values, regional spatial average, of simulations using high-resolution land cover maps

variable	AMZ			NMT			EPA					
	IBIS	IBGE	PVG	MCD	IBIS	IBGE	PVG	MCD	IBIS	IBGE	PVG	MCD
aet	1522	1476	1486	1503	1421	1316	1338	1372	1533	1266	1280	1478
anpptot	0.86	0.81	0.82	0.84	0.87	0.74	0.77	0.81	0.74	0.49	0.51	0.69
awc	15	14	14	15	12	12	12	12	11	9.11	9.22	11
caccount	0.00	0.00	0.00	0.00	0.00	0.00	0.00	0.00	0.00	0.00	0.00	0.00
co2mic	0.95	0.96	0.96	0.96	0.96	0.95	0.95	0.96	0.83	0.87	0.87	0.84
co2root	0.45	0.56	0.54	0.50	0.43	0.62	0.58	0.52	0.40	0.92	0.89	0.53
co2soi	1.40	1.52	1.50	1.46	1.39	1.57	1.53	1.48	1.23	1.79	1.75	1.37
csoipas	0.28	0.28	0.28	0.28	0.29	0.28	0.28	0.28	0.25	0.26	0.26	0.25
csoislo	0.00	0.00	0.00	0.00	0.00	0.00	0.00	0.00	0.00	0.00	0.00	0.00
drainage	253	296	287	269	284	390	367	337	103	364	350	156
fl	0.26	0.37	0.35	0.31	0.25	0.47	0.42	0.36	0.28	0.81	0.78	0.41
fu	0.96	0.86	0.88	0.92	0.98	0.75	0.80	0.87	0.94	0.41	0.44	0.82
neetot	0.13	0.11	0.12	0.12	0.13	0.10	0.11	0.12	0.12	0.05	0.06	0.11
nmintot	0.01	0.01	0.01	0.01	0.01	0.02	0.02	0.01	0.01	0.02	0.02	0.01
npptot	1.08	1.08	1.08	1.08	1.09	1.06	1.06	1.07	0.94	0.93	0.93	0.95
rootbio	0.22	0.26	0.26	0.24	0.21	0.30	0.28	0.26	0.19	0.42	0.40	0.25
srunoff	437	440	439	439	493	494	495	492	336	343	343	339
tilefrac	0.50	0.04	0.04	0.03	0.50	0.01	0.01	0.01	0.50	0.04	0.05	0.04
totalit	0.85	0.76	0.77	0.81	0.83	0.59	0.65	0.71	0.61	0.19	0.21	0.51
totanlit	0.00	0.00	0.00	0.00	0.00	0.00	0.00	0.00	0.00	0.00	0.00	0.00
totbiol	0.01	0.17	0.14	0.08	0.00	0.32	0.25	0.16	0.04	0.77	0.73	0.21
totbiou	11	9.64	9.94	10	11	7.88	8.66	9.68	9.52	2.26	2.65	7.84
totcmic	0.18	0.18	0.18	0.18	0.18	0.17	0.17	0.17	0.14	0.13	0.13	0.14
totcsoi	7.53	7.42	7.44	7.47	7.29	6.83	6.93	7.03	5.52	5.25	5.26	5.41
totfall	0.96	0.97	0.97	0.97	0.97	0.96	0.96	0.96	0.84	0.87	0.87	0.85
totlail	0.16	1.73	1.42	0.87	0.04	3.29	2.57	1.62	0.38	7.78	7.38	2.17
totlailu	8.03	6.92	7.14	7.53	8.15	5.64	6.20	6.94	6.80	1.63	1.90	5.62
totnsoi	0.73	0.72	0.72	0.72	0.71	0.66	0.67	0.68	0.53	0.51	0.51	0.52
totrlit	0.08	0.09	0.09	0.08	0.07	0.10	0.09	0.09	0.06	0.12	0.11	0.07
totrnlit	0.00	0.00	0.00	0.00	0.00	0.00	0.00	0.00	0.00	0.00	0.00	0.00
trunoff	690	736	726	708	778	885	862	828	439	708	694	495
tsoi	28	28	28	28	27	27	27	27	28	29	29	28
vvc	0.37	0.37	0.37	0.37	0.34	0.33	0.34	0.34	0.32	0.30	0.30	0.32
wisoi	0.00	0.00	0.00	0.00	0.00	0.00	0.00	0.00	0.00	0.00	0.00	0.00
wsoi	0.81	0.80	0.80	0.81	0.77	0.75	0.75	0.76	0.72	0.68	0.68	0.71
mod. tilefrac	0	0.17	0.12	0.10	0	0.31	0.20	0.15	0	0.36	0.29	0.17

3 FIRE SPREAD MODELING WITHIN THE INLAND DGVM

3.1 A review of fire spread modeling

3.1.1 Overview of fire modeling

Fire and its controls can be viewed at different temporal and spatial scales, following the extended “fire triangle” concept of (MORITZ et al., 2005) : a flame (fuel, oxygen, heat), a wildfire lasting hours or days (fuel, weather, topography) and a fire regime at decadal and landscape/regional scales (vegetation, climate, ignitions). Figure 3.1 show the important processes across various spatio-temporal scales and Figure 3.2 illustrates the modeling strategies used at these scales. Physical-based models represent the chemical and physical reactions of combustion and heat transfer through convection and radiation with great detail. They are used for higher levels of process understanding, but are computationally expensive and unsuited for large-scale simulations (SULLIVAN, 2009a). Fire behavior models, ranging from the empirical to semi-empirical, are used to predict and understand the basic behavior of fire under certain fuel loadings and moisture and environmental conditions (SULLIVAN, 2009b). Spatially-explicit fire spread simulation models are designed to simulate the spread of fire across a landscape, relying on a varying degree level of sophistication for simulating fire behavior (SULLIVAN, 2009c). DGVMs and climate models typically consider fire regimes for their fire models.

3.1.2 Empirical and semi-empirical fire behavior models

Fire behavior models, used in national operational fire prediction systems, predict the Rate of Spread (ROS) of the heading flaming front of a fire, as well as other characteristics such as flame height, depth and angle and energy released by the combustion process. The Canadian Forest Fire Danger Rating System (CFFDRS) (FORESTRY CANADA FIRE DANGER GROUP, 1992) is an empirical model resulting from over 60 years of extensive observational studies and research on fuel moisture and content and fire behavior and has been implemented by several countries around the globe. Australia’s empirical Fire Danger Rating Systems (FDRS) are based on McArthur’s studies in experimental and natural grassland and forest fires, relating fire behavior to surface fuel and environmental conditions (McArthur, 1966; McArthur, 1967). These experiments, along with earlier laboratory experiments of Byram and others, inspired the pioneering works of Rothermel (1972) and others in the United States. Rothermel’s mathematical model, refined by Albini (1976), is based on empirical data and physical principles and equations. It computes fire ROS

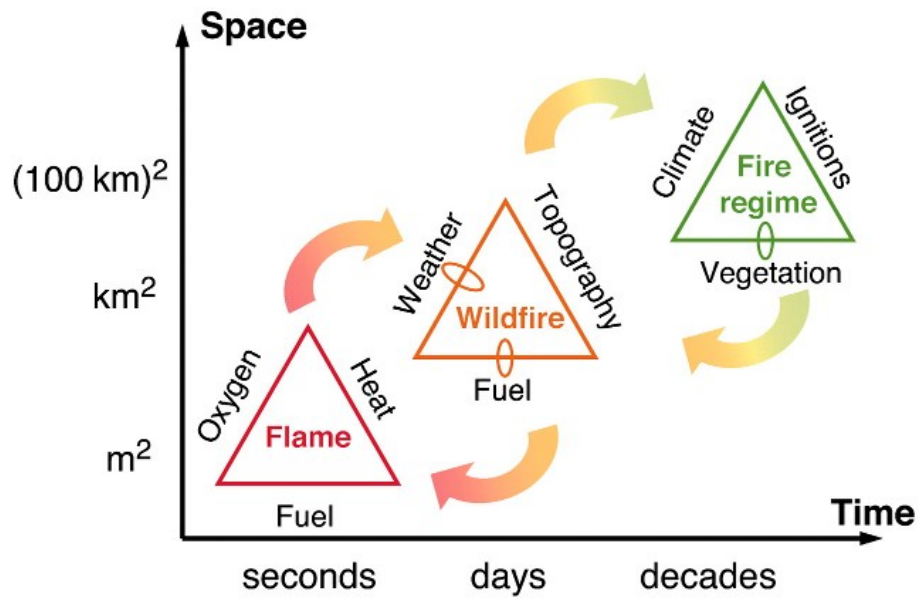


Figure 3.1 - The extended “fire triangle”.

SOURCE: Moritz et al. (2005).

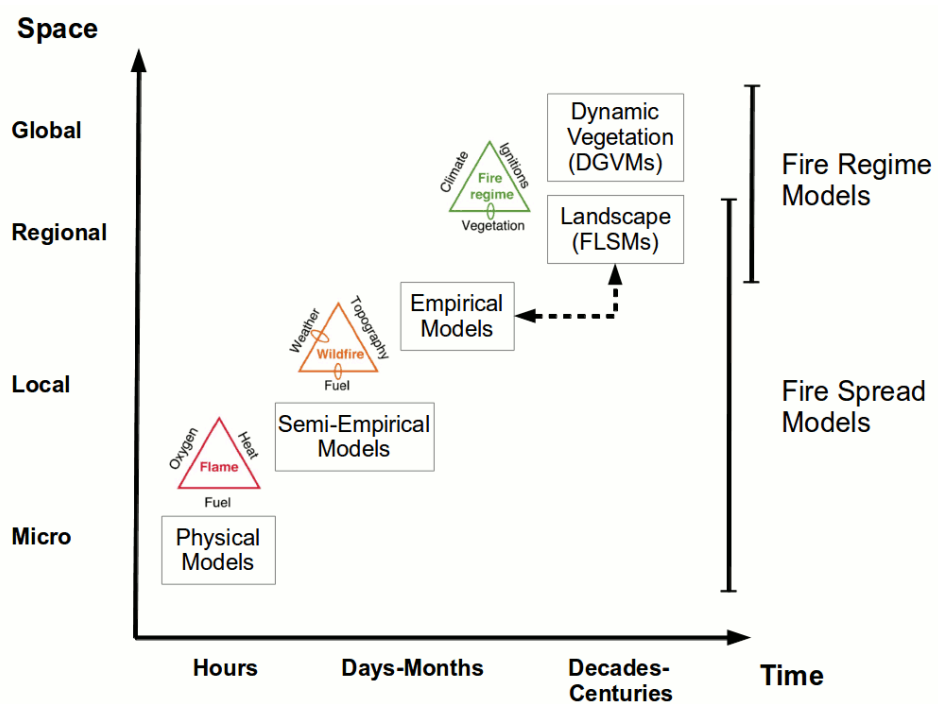


Figure 3.2 - The extended “fire triangle” and fire modeling at various spatio-temporal scales.

SOURCE: Adapted from Moritz et al. (2005).

in a homogeneous fuel bed and is summarized by Equation 3.1:

$$R = \frac{I_R \xi}{\rho_b \varepsilon Q_{ig}} (1 + \varphi_W + \varphi_S) \quad (3.1)$$

where R is the rate of spread ($m \text{ min}^{-1}$), I_R is the reaction intensity ($kJ \text{ m}^{-2} \text{ s}^{-1}$), ξ is the propagating flux ratio – the proportion of I_R transferred to unburned fuels (dimensionless), ρ_b is the oven-dry bulk density ($kg \text{ m}^{-3}$), ε is the effective heating number – the proportion of fuel that is heated (dimensionless) before ignition occurs, Q_{ig} is the heat of preignition – a function of fuel moisture content, specific heat, and assumed temperature at ignition ($kJ \text{ kg}^{-1}$), and $(1 + \varphi_W + \varphi_S)$ is the multiplication factor for slope and wind speed (dimensionless).

In simple terms, the nominator of equation 3.1 represents heat released by the combustion process, and the denominator represents the heat necessary to raise unburned combustible to the temperature necessary for ignition. When the computed reaction intensity (I_R) is null, fire does not spread. Figure 3.3 illustrates the main processes at work and the effects of wind and slope. Rothermel’s fire behavior model requires “fuel models” that describe the characteristics of different vegetation types. Fuel models separate biomass pools by category (live and dead), component (dead and live herbaceous and woody) and dead fuel size classes. Timelag is defined as the time required for a fuel particle to reach 63% of the difference between an initial moisture content and its equilibrium moisture content. Dead fuels are grouped into timelag categories of 1-h (less than 1/4 in. diameter / leaves, needles and twigs), 10-h (1/4 – 1 in. diameter / small branches), 100-h (1 – 3 in. diameter / large branches) and 1000-h (more than 3 in. diameter / trunks). The so-called “original 13 fuel models” of [Albini \(1976\)](#) describe various fuel beds and their characteristics in their driest and most fire-prone state. [Scott and Burgan \(2005\)](#) added fuel models for other vegetation types of the United States and introduced the concept of dynamic fuel models (to account for partly dry fuels), which are called the “standard fuel models”. The characteristics of each fuel model are: fuel load by live component (herbaceous and woody) and dead fuel size class (1-h, 10-h and 100-h) ; surface-area-to-volume (SAV) ratio by component and dead fuel size class ; fuel bed depth ; dead fuel moisture of extinction ; and heat content of dead and live fuels. The model also requires information on fuel moisture for the live and dead fuels, as well as wind speed and slope. The dead fuel moisture of extinction conceptually represents the moisture threshold at which fire can spread, but needs considerable adjustments in order to generate realistic output.

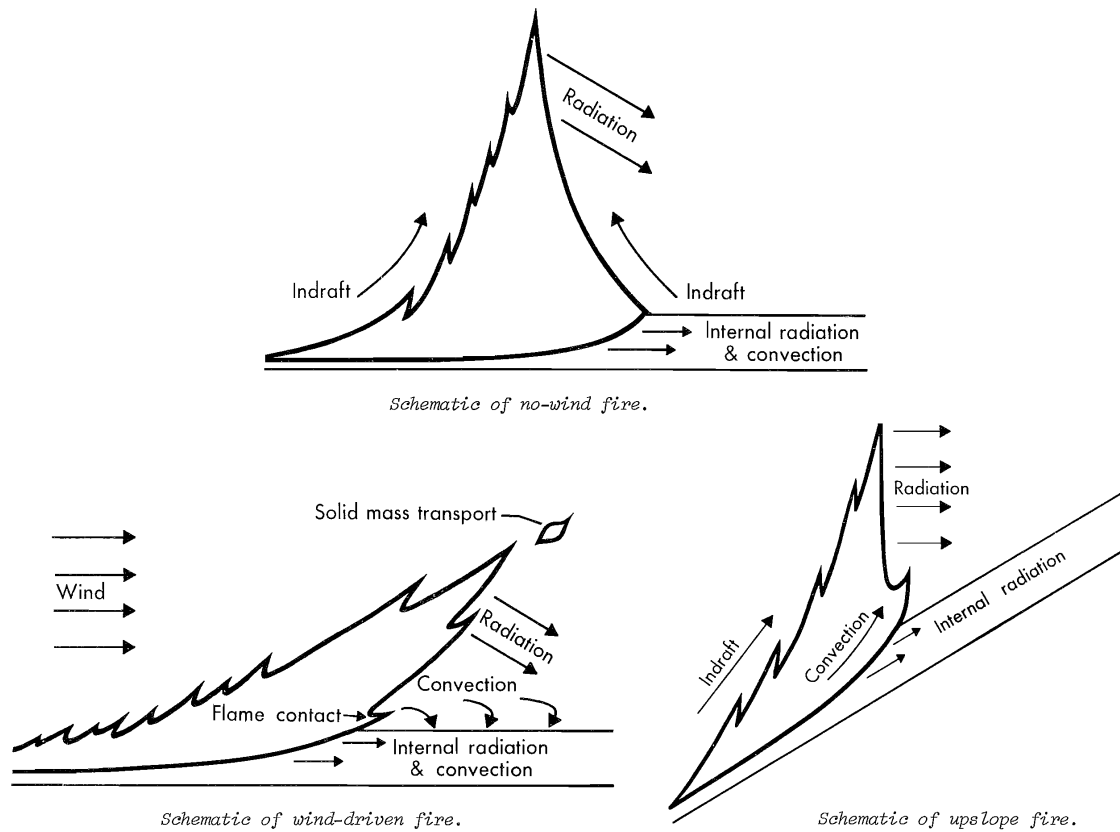


Figure 3.3 - Schematic representation of a flame front in the Rothermel model and the effects of wind and slope.

SOURCE: Adapted from [Rothermel \(1972\)](#).

Many operational semi-empirical fire behavior models used in the United States are based on Rothermel's equations, such as BEHAVE ([ANDREWS, 1986](#)) and the National Fire-Danger Rating System (NFDRS) ([BURGAN, 1988](#)). BEHAVE and its successor BehavePlus ([HEINSCH; ANDREWS, 2010](#)) are simple PC applications which implement Rothermel's fire behavior equations. BehavePlus is used to rapidly assess fire behavior from fuel and environmental conditions. It can be used as a tool to calibrate custom fuel models for fuel beds which do not fall into one of the pre-defined fuel models, comparing predicted behavior to that which is observed. Recent research has led to more realistic representation of fuel beds and overcome the limiting premise of homogeneous fuel beds of the original Rothermel model. The Fuel Characteristic Classification System (FCCS) ([OTTMAR et al., 2007](#)) allows to represent actual fuel beds as a combination of different fuel bed stratum (ground fuels, litter, woody fuels, nonwoody vegetation, shrubs and canopy) and specify with greater granularity the characteristics of the actual fuel bed components. The FCCS is often

used in conjunction with the various “Natural Fuel Photo Series” which consist of detailed fuelbed and standing biomass measurements for various natural settings in the United States, Mexico and the cerrado of Central Brazil (OTTMAR *et al.*, 2001). Modified Rothermel equations (SANDBERG *et al.*, 2007) represent fire behavior in greater detail and realism by including the actual fuel components involved in the combustion process. The FCCS is currently being used operationally in the United States to study the possible effects of fuel treatments in potentially hazardous sites, evaluation of first order fire effects such as smoke emissions and tree mortality. This system has been adopted by Mexico and Portugal, and it is being considered as a viable alternative in other countries.

3.1.3 Fire spread simulation models

Fire spread simulation models are used to simulated the spread of fire across a landscape, usually represented by discreet cells within a Geographic Information System (GIS). The most realistic method is to couple a physical fire propagation model to a high-resolution atmospheric model, thus representing the complex feedbacks between the atmosphere and fire processes. HIGRAD/FIRETEC from Linn *et al.* (2005) is such a model and respects conservation of mass, momentum and energy for both gas and solid phases. However, these models cannot be executed in real time due to the complexity of the resolved processes, and require detailed knowledge of both combustion and atmospheric processes. A more efficient approach is to couple an atmospheric model to a semi-empirical fire behavior model, such as that of Clark *et al.* (2004) and more recently the WRF-Fire (COEN *et al.*, 2012) and WRF-SFire models (MANDEL *et al.*, 2011), coupled to the WRF numeric weather prediction model. Less computationally demanding fire models are build using semi-empirical or empirical fire behavior models and modeling the fire spread on the landscape using a number of numerical techniques using vector- or raster-based approaches, driven by atmospheric observations or uncoupled simulations. The most efficient models use empirical models with a Cellular Automata (CA) approach or other mathematical analogues, with simple transitions rules.

Fire propagation has been modeled in an elliptic shape for quite some time (SULLIVAN, 2009b). Huygens’ wavelet principle (a dated theory to explain the propagation of light waves) was applied to model an elliptically-shaped fire perimeter propagation –analogous to a propagating wave– by Anderson *et al.* (1982). It was subsequently implemented into operational fire spread models such as FARSITE in the United States (FINNEY, 2004), Prometheus in Canada and SiroFIRE in Australia

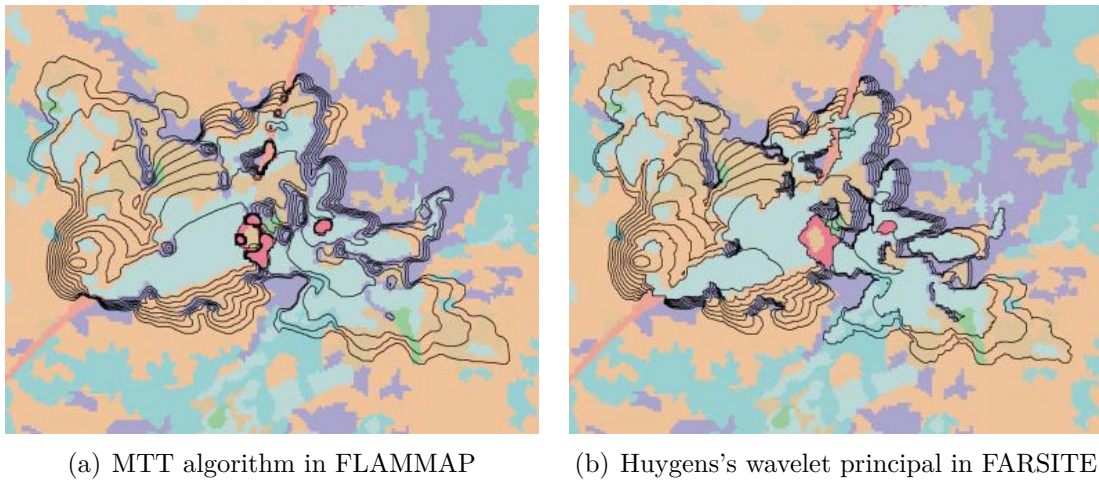


Figure 3.4 - Example of near-identical fire growth patterns using the MTT algorithm and Huygens's wavelet principal.

SOURCE: Finney (2002).

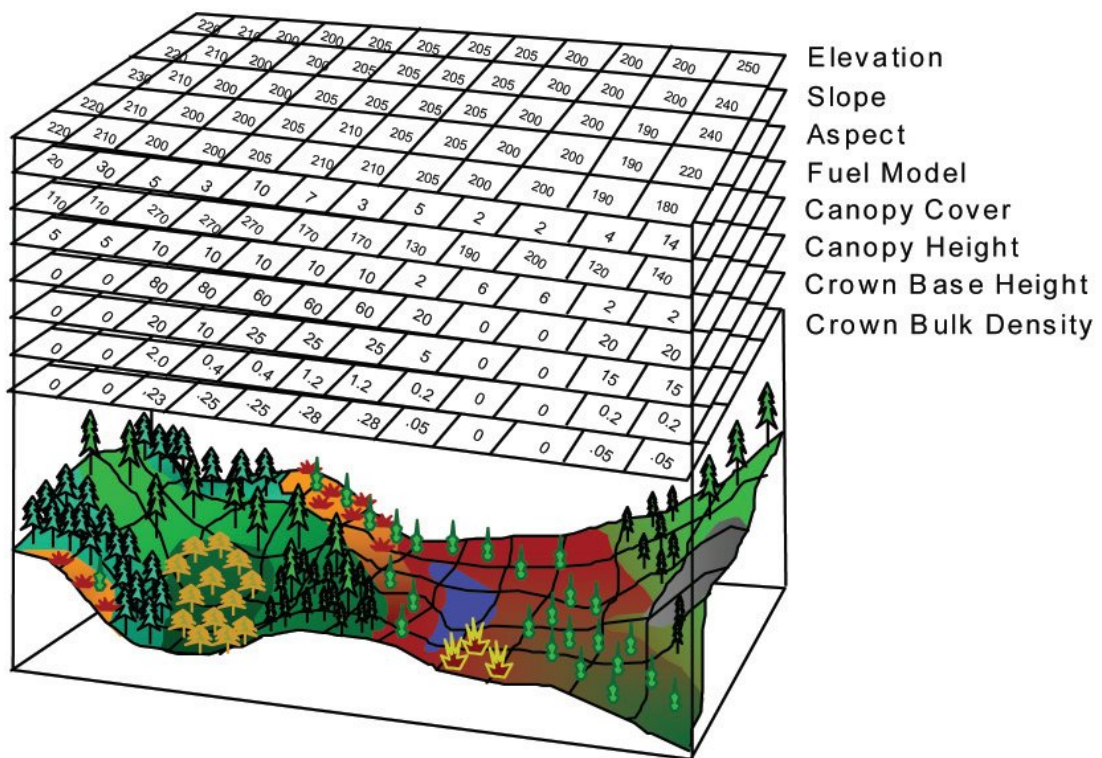


Figure 3.5 - Input layers used by the FARSITE and FLAMMAP fire spread simulators.

SOURCE: Finney (2004).

(SULLIVAN, 2009b), using these nations' respective fire behavior models. However, Huygen's wavelet principle is computationally expensive and has problems with the merging of convergent fire fronts. A technique using a "minimum travel time" (MTT) method in raster space (FINNEY, 2002) implemented into the FLAMMAP software, considerably speeds up the calculations of fire spread under constant atmospheric conditions and generates similar results to FARSITE (see Figure 3.4). MTT is based on Fermat's principle in which a wave will follow the path of minimum travel time, and by analogy the fire line follows the "path of least resistance", or highest rate of spread. FARSITE and FLAMMAP are both used operationally by the USDA Forest Service and use Rothermel's fire behavior equations. They take as input the terrain elevation, slope and aspect (from a Digital Elevation Model; DEM), fuel model and canopy characteristics of the landscape, as well as weather data such as temperature, relative humidity, wind and precipitation (see Figure 3.5). Optional information on the canopy cover and height is useful for computing canopy shading and wind reduction at ground level as well as crown scorching. FARSITE and FLAMMAP use the Rothermel fire behavior equations and fuel models to generate fireline intensity, flame length, ROS, heat/area, reaction intensity, crown fire type and spread direction. The forest landscape simulation model Fire-BGC (KEANE et al., 1996) initially used FARSITE for the fire behavior and spread calculations, but an updated version uses a simple CA spread algorithm to decrease computation time. An ensemble technique using FLAMMAP and the MTT algorithm has been developed by Finney et al. (2010) for use in an operational wildfire management system, the Wildland Fire Decision Support System (WFDSS). In the study, ensemble of weather forecasts were used to generate burn probability maps from fire spread simulations.

Empirical fire models are commonly implemented using Cellular Automata (WOLFRAM, 1983), a concept introduced by von Neumann in the 1940s. In the context of fire spread modeling, cells in GIS raster space can have a state of "unburned", "burning" or "burned", set of rules defines the possible transitions from said states, and fire can spread from burning cells to their neighbors, as illustrated in Figure 3.6. In percolation models, such as EMBYR of Hargrove et al. (2000), the probabilities of fire "contagion" are calibrated from empirical studies. The disadvantages of empirical fire spread models is that they must be calibrated for different regions, which can limit their application over extensive regions. Another mathematical analog, known as fuzzy logic theory, has been applied to fire spread modeling by Mraz et al. (1999) and Vakalis et al. (2004). Simply put, fuzzy logic *fuzzifies* input data (so-called crisp information) into discrete categories, and with simple rules based on expert knowledge generates stochastic output which is then *defuzzified* and in-

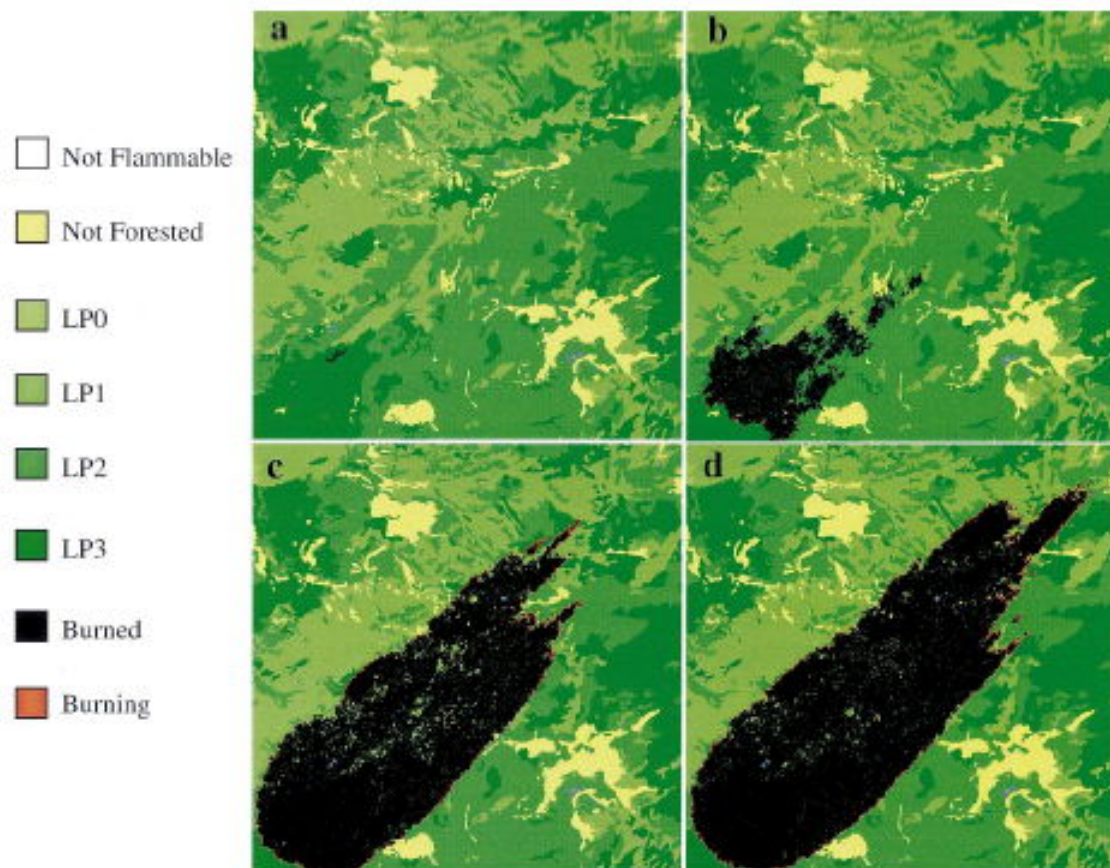


Figure 3.6 - Illustration of the Cellular Automata concept applied to fire spread modeling.
 SOURCE: Hargrove et al. (2000).

terpreted. This approach is interesting when detailed information on fuel and local conditions is scarce and fire spread behavior is not well known in exact numeric terms. Cellular Automata have also been used in conjunction with Rothermel's semi-empirical model. Berjak and Hearne (2002) improved upon the empirical CA model of Karafyllidis and Thanailakis (1997) by including Rothermel's equations in the fire propagation rules and applied their model to a heterogeneous savanna landscape in South Africa. Peterson et al. (2009) used HFIRE, a relatively simple fire spread algorithm, for simulating fire spread in synthetic landscapes and chapparal shrublands. HFIRE uses rate and directions of spread calculated using Rothermel's equations, and a raster method using adaptative timesteps for fire spread. The program uses the same input as FARSITE, and while requiring less computational time generate similar results, thus providing a potentially useful alternative to FARSITE.

3.1.4 Fire in the Brazilian tropics

Fire spread modeling in moist tropical forests such as the Amazon is a considerably challenging task. [Cochrane \(2009\)](#) identifies the major challenges as high species diversity, the complexity of processes controlling surface fuel moisture, high variability of organic decay rates and lack of fuel models despite many studies on fuel composition. Modern human activities are a significant source of ignitions and disturbance, but climate and weather are the dominant controls on fire spread and intensity, as seen in the extreme fire seasons during the 1997-1998 El Niño event ([ALENCAR et al., 2006](#)) and the Amazon drought of 2005 ([ARAGÃO et al., 2007](#); [MARENGO et al., 2008](#)). Fire return intervals in moist tropical forests have been historically low, which has led to the establishment of fire-prone species. The high evapo-transpiration rates combined with deep roots make moist tropical forests inherently resistant to moderate drought. Ecologists have long sought to explain the mechanisms by which drought can lead to fire vulnerability, despite natural resistance to drought, as prolonged droughts can render even undisturbed primary forests vulnerable to fire ([RAY et al., 2010](#)). Possible mechanisms identified are: 1) drought-induced leaf shedding which decreases LAI, increases incident solar heating and lowers litter moisture and raises litter content ; 2) low surface soil moisture and 3) high vapor pressure deficit (VPD) which both have a drying effect ([RAY et al., 2010](#)). There has not been so far a satisfactory model which predicts fuel moisture content (FMC) and a “magical” value at which fire can spread. However, anecdotal evidence points to a threshold value of 12% ([HOLDSWORTH; UHL, 1997](#)) and [Ray et al. \(2005\)](#) identified threshold values of 0.75 kPa VPD and 23% FMC for understory fire spread in the Amazon rainforest. Various studies of under-story fire report generally slow (~20-40 cm/min), low-intensity and low flame height (<50 cm) flaming fronts ([CARVALHO et al., 2010](#); [CARVALHO et al., 2003](#); [COCHRANE et al., 1999](#), personal experience). Despite low intensity and height flames, tree mortality due to understory fires is surprisingly high, due to low resilience to fire and high flame residence times. There is evidence of feed-backs of slash-and-burn and understory fires on tree mortality and increased vulnerability to fire ([LAURANCE, 2004](#); [BARLOW; PERES, 2008](#)). A few ground-based experimental data exists supporting these claims ([BALCH et al., 2008](#); [BALCH et al., 2009](#); [BALCH et al., 2011](#); [BRANDO et al., 2012](#); [BRANDO et al., 2014](#); [CARVALHO et al., 2010](#)).

Fires in the Amazon are usually small and limited to the understory, which makes them difficult to detect by conventional global burned area mapping methods ([ROY et al., 2008](#); [MORTON et al., 2011](#)), making model validation over large areas difficult

if not impossible. Silvestrini et al. (2011), Silvestrini et al. (2009), Silvestrini (2008) made a first attempt to model understory fire spread using Cellular Automata, with spread rules based on understory VPD, simulated by the CARLUC carbon cycle model. Fire occurrence was modeled using fire risk maps derived from anthropogenic and climatic factors (SILVESTRINI et al., 2011), and simulated fire spread was compared to a local burned area map from high-resolution LANDSAT imagery (ALENCAR et al., 2004). Although simulated burned area values were similar to those observed, spatial match was rather poor. The spatial discrepancies could be caused by the accuracy of the spatial locations of the simulated fire ignitions, errors in the simulation of understory VPD and the arbitrary VPD threshold used in the propagation rules. To the author's knowledge, there have been no published studies to date using the Rothermel model in the Amazon forest, and very few in other tropical forests. Carapiá (2006) cited the lack of proper fuel models for tropical forests in a fire propagating study using FARSITE in the Parque Nacional da Floresta da Tijuca near Rio de Janeiro. Cochrane (2009) elaborated on the need for a new suite of fuel models for the moist tropical forest and better science to explain and predict the processes controlling soil and understory fuel moisture. The Rothermel model may not be suited for heterogeneous moist tropical forests due to the model's design, which assumes fuel homogeneity and cylindrical fuel particles (i.e. needles, which are not present in tropical forests), and relies heavily on convective heat transfer, which is low in the usually windless, closed-canopy tropical forest (Ernesto Alvarado, personal communication). While this assumption may be considered exaggerated, there is no proof that the Rothermel is indeed adequate for tropical forests.

Fire in savanna ecosystems such as the Brazilian cerrado is comparatively simple to model, due to the prevalence of grasses as fire-carrying fuels and a clearly-defined fire season (at the end of the dry season). Observed fire behavior data, although scarce compared to that in temperate areas, have been published by Kauffman et al. (1994), Miranda et al. (1996), Castro and Kauffman (1998), with rates of spread near 0.5m/s. Fuel load is variable (with a dependence on physiognomy, species composition and time since last fire), fuel consumption is highest where the biomass density is lowest (nearly 100% in the grasslands) and woody species mortality is surprisingly low, due to the rapid rate of spread, low flame height and fire tolerance of the dominating species (MIRANDA et al., 2002; MIRANDA et al., 2009, and references therein). The percolation model of (HARGROVE et al., 2000) was used by (ALMEIDA, 2012) to study fire spread in cerrado vegetation within the Parque Nacional das Emas (PNE) – GO. Propagation probabilities were estimated from observed burn intervals (as a proxy for accumulated fuel), obtained from high-resolution remote

sensing imagery (FRANÇA et al., 2007), and adjusted for wind speed and direction. The standard fuel models of (SCOTT; BURGAN, 2005) contain various grass models which may be applied directly to the grassy physiognomies of the cerrado (such as campo limpo and campo sujo). The “stereo photo series” of Ottmar et al. (2001) contain detailed biomass measurements from various sites in the cerrado, which can be used to create custom fuel models. Mistry and Berardi (2005) conducted field and modeling experiments in the Reserva Ecológica do Roncador (RECOR) - DF, creating custom fuel models for the various vegetation types found in the cerrado and using them as input for FARSITE in the RECOR ecological reserve. They created the custom fuel models with information from various field experiments and published biomass inventories and used the BEHAVE program as a calibration tool. The authors commented on the difficulties of accurately simulating fire spread in natural areas of the cerrado, due to the natural patchiness of these landscapes. Fernandes (2003) used FARSITE for a study of fire-fighting strategies in the Parque Estadual Serra do Rola-Moça – MG. Simulated burned area was similar in size to observed through satellite imagery, but spatial pattern was somewhat different, which the author attributed to limited knowledge on actual fuel composition and a dated land cover map. Mbow et al. (2004) used FARSITE simulations as an input to their fire risk model for a National Park in Senegal, and found that simulated area correlated well with observations. They concluded on the importance of accurate detailed spatial information on fuel composition and moisture to properly simulate the spatial patterns of fire spread.

3.2 Methodology

3.2.1 Overview

This study lays the founding blocks of a much larger multi-scale modeling framework, as depicted in Figure 1.2. The core of the proposed framework is the multi-scale LSM model (MS-LSM) presented in Chapter 2. The lower-resolution interactions between the land surface and the atmosphere can be either one-way (as in the offline INLAND model) or two-way, when coupled to an atmospheric model (as in the BESM framework). A LUC model or historic observations (250m – 50km resolution) drive two changes to the high-resolution land cover map: one directly through deforestation and other LUC processes (land cover changes, land abandonment, etc.), and the other indirectly through deforestation and pastures fires. These ignition sources, as well as natural processes such as lightning, are used to initiate the high-resolution (250m) fire spread model. This model in turn interacts with the MS-LSM model

in two ways: land surface properties are received from the LSM and land cover is allowed to change through the combustion process. Atmospheric conditions are received from the atmospheric module and emissions through combustion processes is injected into the atmosphere (if applicable).

The fire spread model uses the Cellular Automata approach, with a simple fire spread algorithm that spreads by percolation (using the von Neumann neighborhood) and simple empirical fire spread rules. The model is implemented in Fortran90 for easy integration with the main INLAND model. The main components of the model are:

- multi-scale framework (MS-LSM) for downscaling LSM properties to the fine scale of the fire spread model (as described in section 2.2)
- high resolution land use map and other supporting data such as roads, rivers (and eventually topography) to act as fire spread barriers
- custom fire spread/behavior module – determine if and when fire spreads from a cell to adjacent cell and if a given cell can burn given land surface and atmospheric conditions

3.2.2 Land cover map and other supporting data

The spatial scale at which the model is configured depends on these major factors: computational resources, spatial detail of available land cover maps, and the knowledge on fire behavior at such scale. The combination of these factors leads to a subjectively determined ideal scale of 250m. Smaller scales such as 30 or 60m are not desirable because it would be computationally expensive, and knowledge on fire behavior in the Amazon and *cerrado* is not yet sufficient to warrant such a fine scale. On the other hand, using a coarser scale removes the fine-scale structure of landscape fragmentation and forest edges, particularly in regions of “fishbone pattern” deforestation, as shown in Figure 3.7. The PROVEG map suffers from a resolution that is slightly too low (1km) and in its current form presents displacement which is unacceptable at the scale considered – up to 2km as shown in Figure 3.8. Therefore the map of choice for this work is the IBGE-TC map described in section 2.2.4. This high-resolution map is used as an input for the subgrid tiling scheme in the INLAND model (as described in section 2.2.5). The fire spread and behavior routines operate at this same resolution.

The roads dataset from IBGE (ST_RODOVIA.shp) is used as a firebreak, effectively limiting fire spread. Currently fine-scale rivers and other hydrological features are

ignored if they are not represented in the 250m land cover map. Topography is not currently considered, but it could be used as a fire break and also as a parameter in the fire behavior and spread routines. The absence of consideration of topography in the model implies modelling errors in areas of moderate or high slope angles.

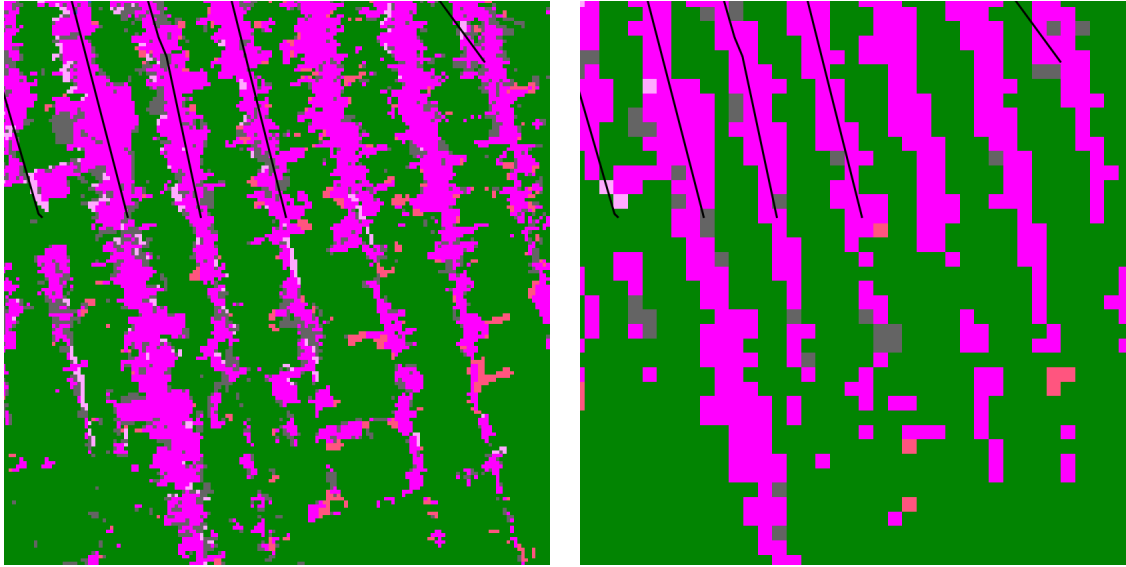


Figure 3.7 - IBGE-TC land use map in eastern Pará state, at 250m (left) suffers from loss of detail when resampled to 1km (right).

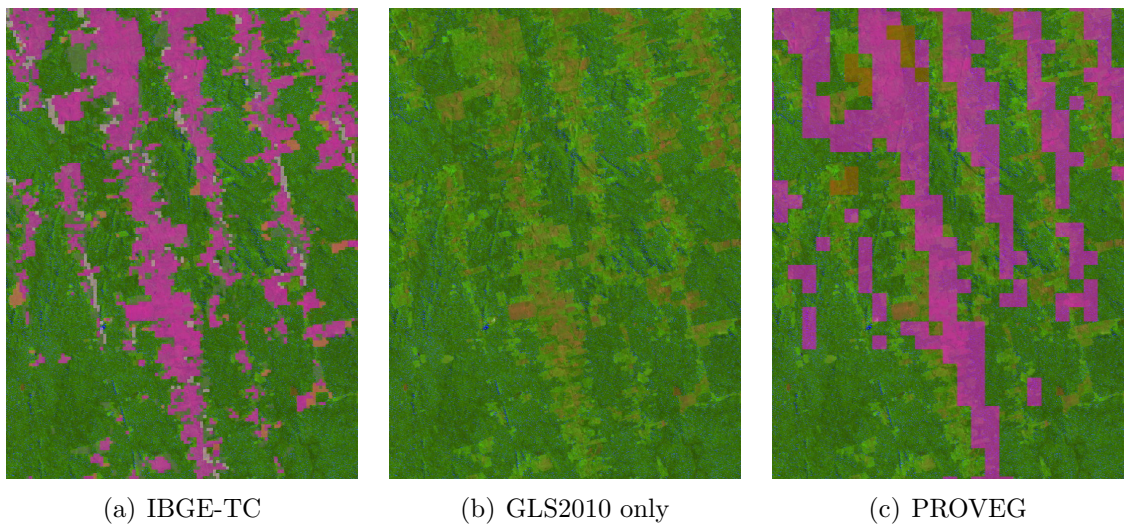


Figure 3.8 - Land use maps overlaid on GLS2010 Landsat imagery (WRS 226/63 acquired on 2010/07/24) showing a displacement of ~2km of the PROVEG map and perfect alignment of the IBGE-TC map.

3.2.3 Basic fire spread model structure and workflow

Firstly the main INLAND model is initialized, provided it is run in “high-resolution map” mode (see section 2.2.5). The many-to-one relationship between high-resolution grid cells and low-resolution tiles (see Figure 2.10) is kept in memory for usage throughout the simulation, so that any property of the tile parent can be accessed at any time. The firespread model is initialized and loads *vegtype*-dependent firespread parameters, as well as an ignitions list, containing the day and time as well as longitude/latitude position of fire ignitions. Next the Cellular Automata structure is created, with a *firecell* object created for each of the high-resolution points in the simulation. Note that this entire structure is taxing on memory usage due to the high resolution of the *firecell* grid, which consumes an extra ~1.25 MB of memory for each INLAND grid cell (for example, a simulation covering the entire Legal Amazon region with 2630 grid points and 2 tiles would require approximately 6.25 GB of memory, which is a large amount for desktop computers). This implies that the fire spread model should only be used with a small number of low-resolution INLAND grid cells when using a typical desktop computer. Processing time is not so much a limiting factor, as CPU resources are only necessary when simulating the fire spread and the model complexity is rather low. The *firecell* properties are:

burnstate	Burn state, one of {unburned, ignited, spreading (burning and spreading), burning (burning only), burned}
vegtype	The <i>vegtype</i> of the parent tile
firebreaktype	Fire break type (1 if a road passes through the grid cell, else 0)
spreadrate	Fire spread rate in m/s
burntime	Time cell has been burning in seconds

The *burnstate* property is common in all Cellular Automata models (as that of Hargrove et al. (2000) shown in Figure 3.6). The IBGE roads dataset, previously converted from shapefile format to a 250m raster map, is used to determine the *firebreaktype* of each *firecell*. This could be extended for other fire breaks such as riverbeds or breaks in topography. *Spreadrate* is determined when the cell is ignited and *burntime* is constantly updated.

The states of the firecell grid cells are allowed to change as illustrated in Figure 3.9. The main `loophour()` subroutine, summarized in a workflow diagram in Figure 3.10, is called at the end of each INLAND timestep loop (currently each hour). First the ignitions list is consulted and if an ignition entry matches the current timestep and location lies within the model domain, the corresponding cell state is set to

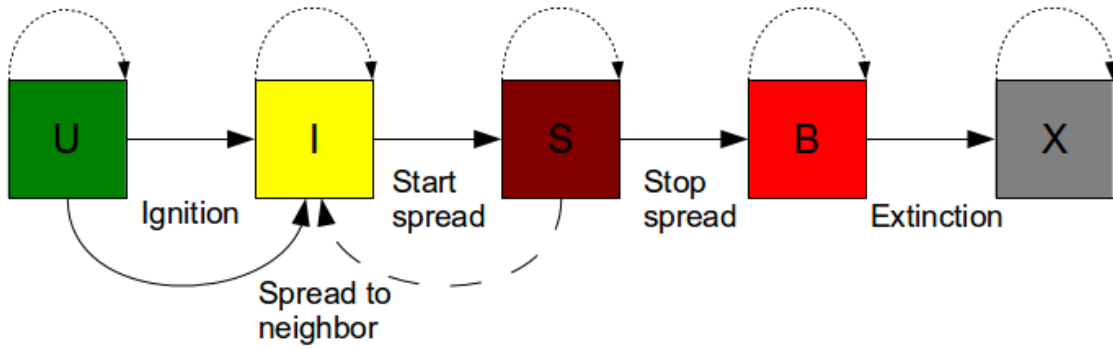


Figure 3.9 - State diagram of the Cellular Automata in the fire spread model. Dotted lines show stationary states and the dashed line shows interactions between adjacent cells.

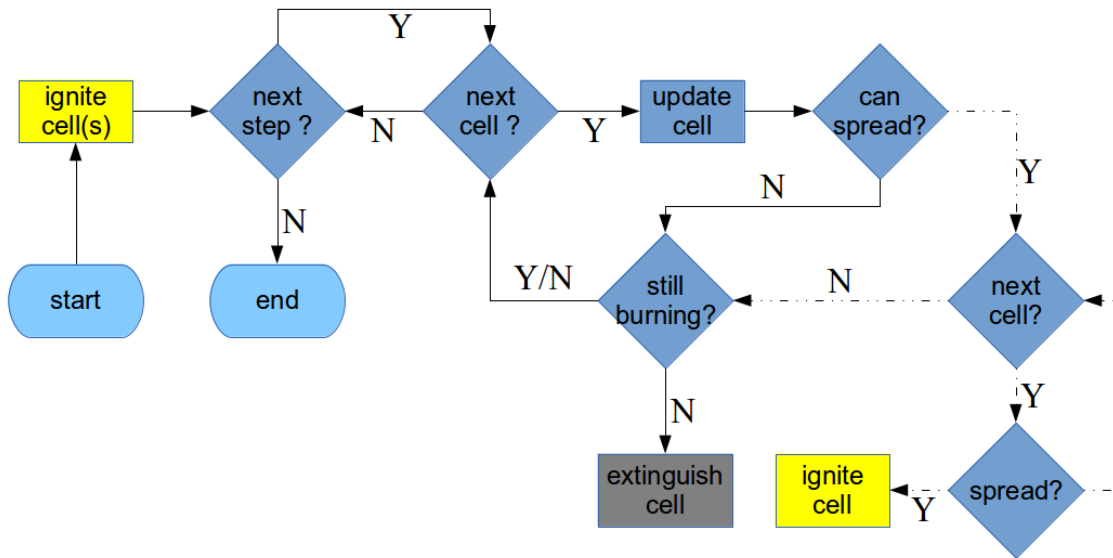


Figure 3.10 - Principal components of the main loophour() fire spread subroutine. Dashed line shows interactions with adjacent cells.

ignited. A fast internal loop, currently executed 10 times for each hour loop, allows to simulate fire spread and extinction on timescales shorter than the INLAND model hourly loop. For each cell in the list of burning cells the following steps are executed, simulating the typical rapid advance of a fireline, which is followed by longer burning and smoldering phases and finally extinction:

- a) burntime is updated
- b) if the cell is in *ignited* state, set it to *spreading*
- c) if the cell is in *spreading* state and the fireline has reached adjacent cells

(based on the cell's *spreadrate* and size), its state is set to *burning* and the `tryspread()` subroutine is called for each of the four adjacent cells

- d) if the cell has been burning for a sufficient time (spread time + burn time) the fire burns out and the cell's state is set to *burned*.

The `tryspread()` subroutine determines spread from a cell to its neighbors and can be summarized by these simple rules:

- a) do not spread to cells of certain *vegtype*
- b) do not spread from cells with fire breaks
- c) stochastically determine fire spread occurrence
- d) set fire spread rate from *vegtype* parameters

The `tryspread()` subroutine determines if fire can spread from one cell to another. Certain cells cannot burn based on their *vegtype* value (e.g. water). As real firebreak size is typically much smaller than the 250m grid cell and their path within a grid cell is not considered, any cell that contains a fire break may burn, but fire is not allowed to spread from it to adjacent cells. This is rather simple but works well in the case of linear fire breaks such as roads (shown in next section). Fire spread is determined stochastically, based on the *vegtype* dependent fire spread probabilities of the destination cell, which require calibration. For example, pasture has a much higher chance of burning than evergreen tropical forest. The fire spread rate of each cell is also dependent on *vegtype*, using average values from scientific literature and remote sensing data. These and other parameters are given in section B.2.2. Further development of the model, based on modeled bio-physical parameters, are discussed in section 3.3.3.

3.2.4 Influence of wind and topography

Fire rate of spread is heavily dependent on wind direction and speed, as well as topography. Figure 3.3 illustrates the effect of wind and slope on a flame front, and the Rothermel equation (Equation 3.1) includes factors for both wind and slope. A strong wind tilts the flame in the wind's direction, increasing radiative heat transfer to surface fuels and rate of spread in the wind's direction, whereas it lowers ROS in the opposite direction. This principle has been used in the Cellular Automata model of Berjak and Hearne (2002), which considers the flame angle between the

surface and the flame front. Equation 3.2 (BERJAK; HEARNE, 2002) and Equation 3.3 (WEISE; BIGING, 1996) account for the effect of wind and Equation 3.4 (BERJAK; HEARNE, 2002) accounts for slope effect:

$$R_w = R_0 \exp(\beta_1 \theta_f) \quad (3.2)$$

$$\theta_f = \arctan(\beta_2 (U^2 / gH)^{\beta_3}) \quad (3.3)$$

$$R_s = R_0 \exp(\alpha \theta_s) \quad (3.4)$$

where R_w is the ROS adjusted for wind, R_s is the ROS adjusted for slope, R_0 is the basic rate of spread (without wind or slope), θ_f is the “flame angle” (angle between the flame and the fuel, without slope), θ_s is the “slope angle”, U is wind speed, g is the gravity constant, H is flame height, and α , β_1 , β_2 and β_3 are empirical constants. The U^2/gH value is dimensionless and is called the Froude number. The effect of wind and slope is to alter the flame angle, which is considered to have an exponential effect on rate of spread.

In Berjak and Hearne (2002), the following empirical values are used for a South African savanna landscape: $g = 9.8m/s^2$, $H = 2.8m$, $alpha = 0.0693$, $\beta_1 = 0.0576$, $\beta_2 = 2.35$ and $\beta_3 = 0.57$. In a preliminary study, we use these values as they are adequate for representing fire spread in savanna and pasture, present in our study area. Table 3.1 shows examples of flame angle (θ_f), forward ROS (R_f), backward ROS (R_b) in function of wind (U) and base ROS (R_0), using these empirical values. For example, with a flame-height wind of 10km/h, forward ROS is 16.56 times stronger than basic ROS, and backward ROS is almost nil.

Table 3.1 - Examples of ROS adjusted for wind speed.

U (km/h)	θ_f (°)	ROS (m/s)		
		R_0	R_f	R_b
0	0.00	1.00	1.00	1.00
1	4.72	1.00	1.31	0.76
5	27.34	1.00	4.83	0.21
10	48.73	1.00	16.56	0.06
20	68.29	1.00	51.08	0.02

As the INLAND model only considers wind speed (using climatological wind speed from the CRU dataset), this study considers fixed wind directions. For further stud-

ies wind speed and direction from re-analyses (such as the ERA40 dataset) can be used, using monthly values of the 1961–1990 period to compute monthly climatological averages, interpolated to the model resolution (0.5°) using nearest neighbor resampling. Equation 3.2 and 3.3 were used to compute the northward (Rn), southward (Rs), westward (Rw) and eastward (Re) ROS, in function of the meridional (north-south) and zonal (west-east) wind components at flame height. As the model uses the von Neuman neighborhood, only wind from the main cardinal directions is considered. In order to represent arbitrary wind directions, the 8-cell Moore neighborhood must be used. For simplicity the $u2$ variable (wind speed at level $z2$ – effective bottom of the upper canopy) at each timestep was considered, as this height is fairly constant across land cover types (2.5–3m). Note that daily and hourly wind magnitude vary (due to the use of an internal weather generator), which introduces a stochastic element in the ROS. When a cell is ignited, the Rn, Rs, Rw and Re values are calculated and for each neighbor the “time to spread” value is calculated, based on current rate of spread (in the proper direction) and distance to the edge center of said neighbor. This simplified approach neglects changes in ROS during the period which fire spreads to the next cell.

3.2.5 Influence of surface and air moisture

An important factor in fire spread is the presence of surface litter and its moisture. LAI and VPD (Vapor Pressure Deficit) play an important role in determining surface Fuel Moisture Content (FMC), as sunlight can decrease soil moisture during the day and high VPD values (or low relative humidity) can dry surface fuels more quickly (RAY et al., 2010). VPD can be computed from INLAND model variables using Equation 3.5:

$$VPD = \left(1 - \frac{Q}{qsat(esat(T), P)}\right) * esat(t) \quad (3.5)$$

where VPD is in Pa, Q is actual specific humidity, T is temperature in K, P is surface pressure in Pa, $esat$ is saturation vapor density in Pa and $qsat$ is saturation specific humidity; T and Q are available in the model at various levels and $esat$ and $qsat$ are computed from the other values.

VPD can be computed at hourly intervals, accounting for changes in relative humidity, temperature and the drying effects related to LAI and solar heating. It can also be obtained at various heights: middle of the lower canopy, middle of the upper

canopy, 2m above the surface and in the free atmosphere above the upper canopy. All but this last height are function of actual land cover, therefore values may be different amongst tiles with different land cover type. The level chosen is 2m as it does not vary in height and is close to the height that most VPD measurements are taken in the field. VPD at 2m can be used as a condition for fire spread when above a certain threshold. FMC is not available in the INLAND model and should be estimated from surface soil moisture, litter content and VPD. Both litter content and moisture are not considered directly at this point.

3.2.6 Experimental setup

Two small areas (2x2 INLAND model grid points) have been selected to implement and test the fire spread model. The first, shown in Figure 3.11, is largely deforested and is located at the eastern border of Pará and Mato Grosso states. The second is less deforested and is typical of “fishbone” deforestation patterns, located in eastern Pará state and shown in Figure 3.12. In both cases, a previous model run has been executed for a duration of 100 years using the IBGE-TC high resolution map and 4 tiles, with the fire spread model disabled. This allows for most INLAND model values to stabilize to their potential or modified vegetation state (for natural/modified tiles respectively), as explained in section 2.2. The execution of the fire spread model is as follows: the INLAND model is executed in restart mode with the firespread model enabled, taking off where the previous 100 years model run stopped. A number of predefined ignitions (time and location are defined by the modeller) is used in order to start actual fire spread, all located in areas of pasture in order to ensure that the fire lines do in fact spread. The model is run for an entire year and daily values of *burnstate* are saved to a high resolution map for analysis.

vegtype - vegetation type - static

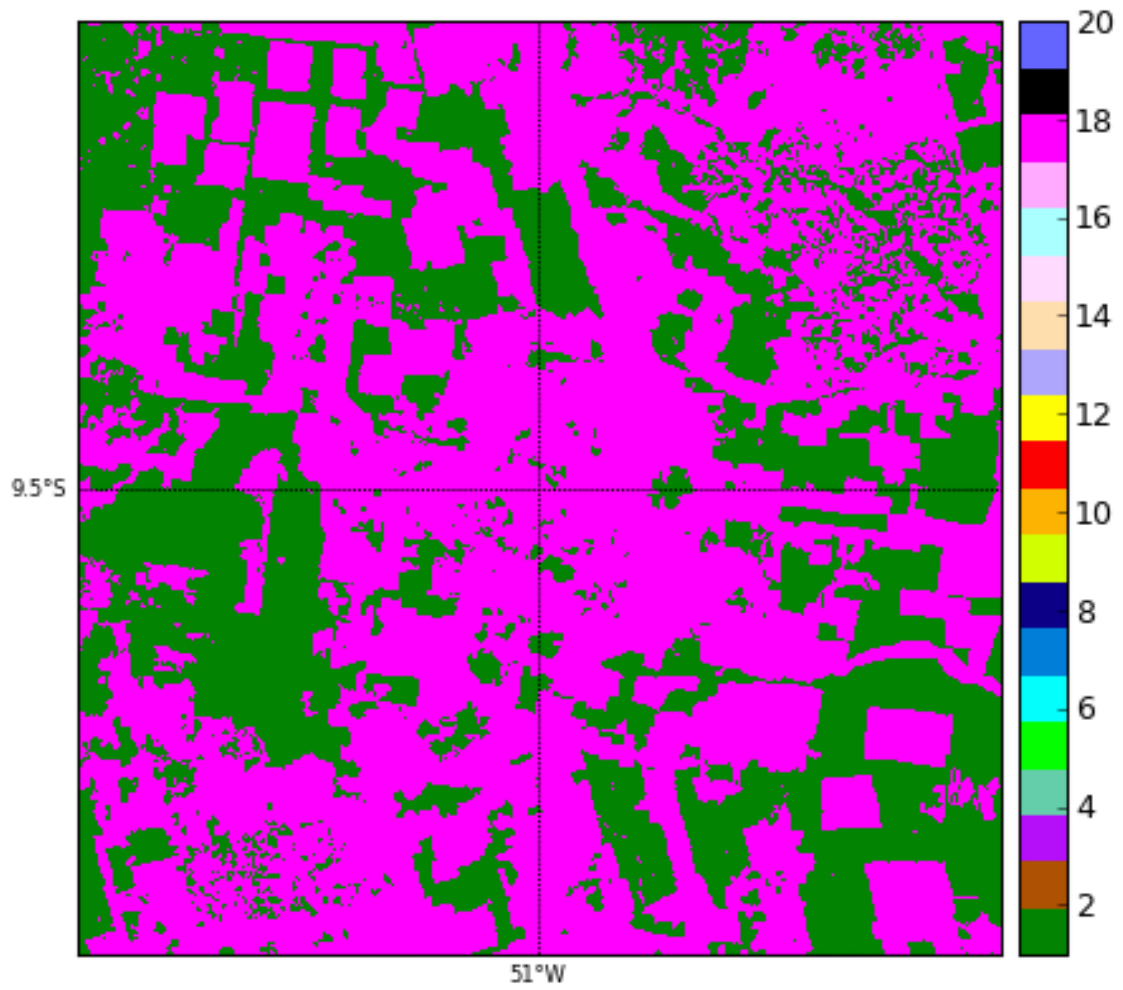


Figure 3.11 - Map of the “highly deforested” domain test area in Southeastern Pará, showing *vegtype* and roads.

vegtype - vegetation type - static

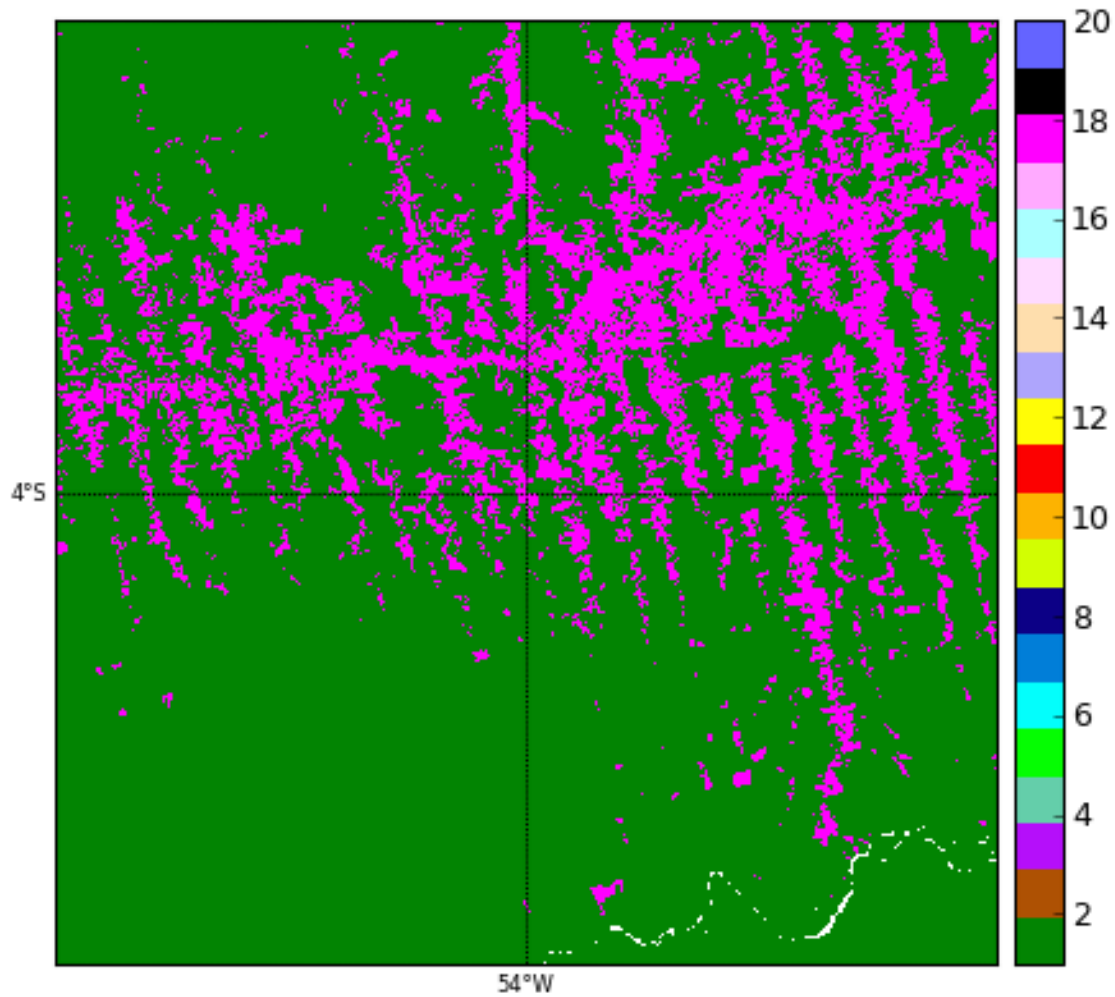


Figure 3.12 - Map of the “fishbone pattern” test area, showing *vegtype* and roads.

3.3 Results

3.3.1 Sensitivity study of basic fire spread model

In this section the basic fire spread model and its parameter sensitivity is illustrated. First are shown results for the “highly deforested” test case. Figure 3.13 shows fire model sensitivity to the use of roads acting as fire breaks. In the case without fire breaks, fire spreads to most of the area in a few days after a single ignition in the middle of the model domain, as the landscape consists mainly of pasture, with few obstacles to stop fire spread. Forested areas are largely intact as the basic fire spread parameters inhibit fire spread to forest. The shape of the fire line is almost

–but not quite– concentric due to the simplicity of the fire spread algorithm employed. Changing the fire spread velocity depending on spread direction (lateral vs. straight) would allow to make spread more circular. Adding more ignitions does not significantly change the final outcome (not shown). The introduction of roads allows to contain the spread to a much smaller area, even when additional ignitions are included. This more closely resembles real-life fires which tend to be more isolated. The sensitivity to model parameters, without fire breaks, is illustrated in Figure 3.14. The left column shows a decrease in fire spread rate in pasture (from 0.2 to 0.05 m/s). After 15 days the fire line has spread to a far smaller extension than in the control case. In the right column we see the effect of an increase in fire spread probability in forest (from 0.005 to 0.5): almost the entire landscape is burned, but at a relatively slow pace, due to a slow fire spread rate in forest.

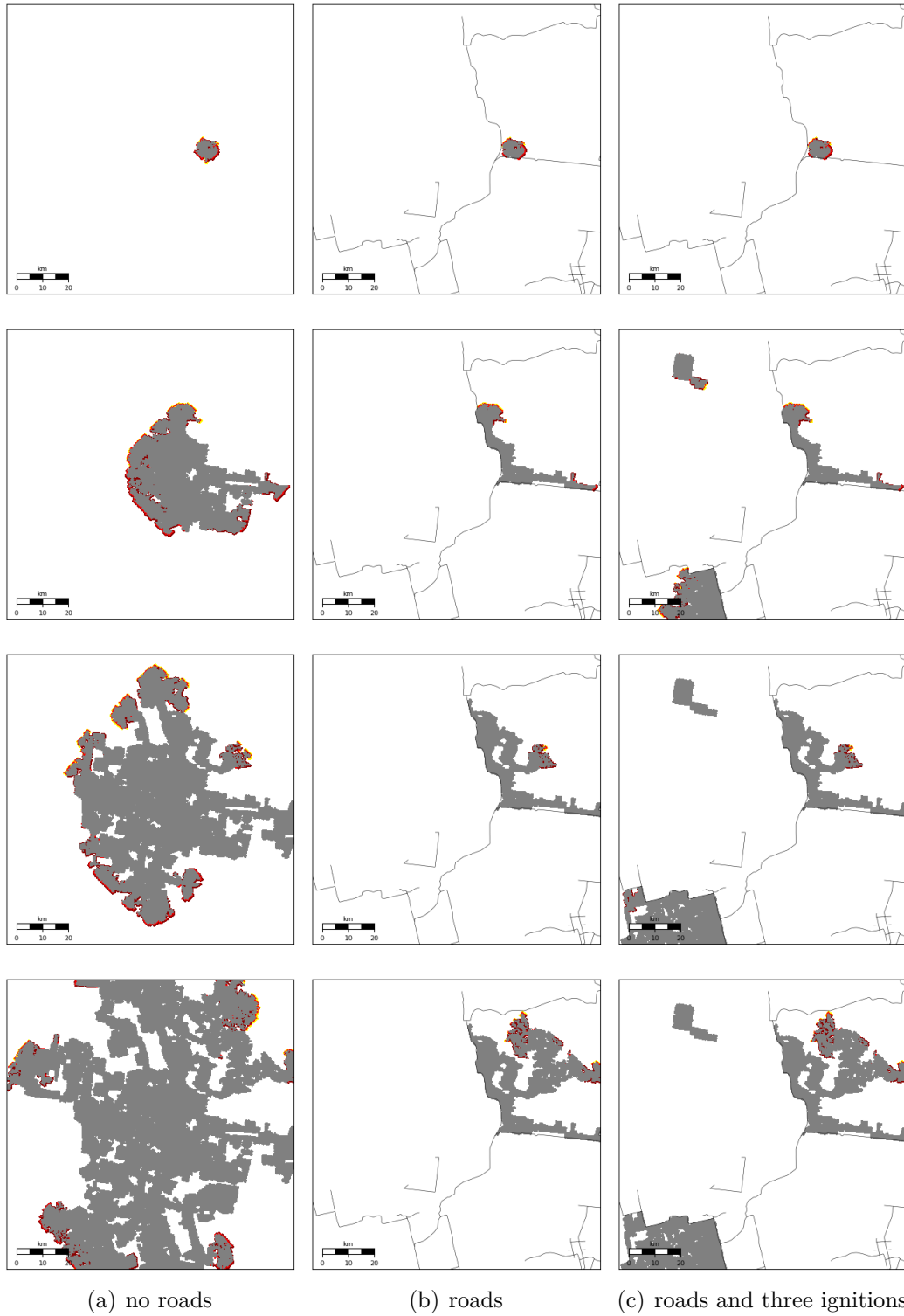
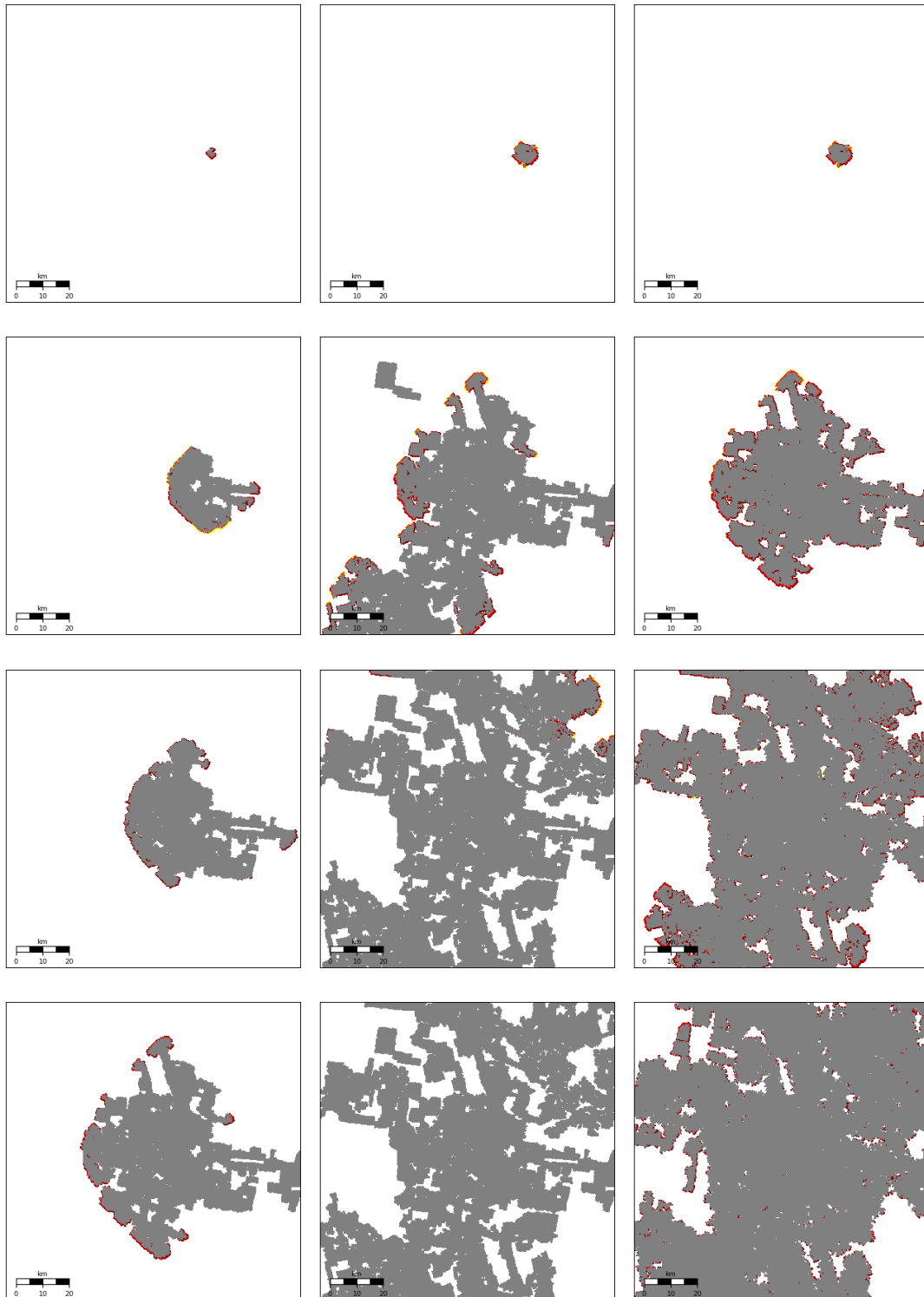


Figure 3.13 - Fire spread state at 3 day intervals (from top to bottom) with and without roads acting as fire breaks. Yellow cells are ignited, dark red are spreading, red are burning and grey are burned.



(a) lower pasture spread rate (0.05m/s)

(b) normal

(c) higher forest spread probability(0.5)

Figure 3.14 - Fire spread state (3 ignitions) at 5 day intervals (from top to bottom) showing sensitivity to firespread parameters (spread rate and probability). Yellow cells are ignited, dark red are spreading, red are burning and grey are burned.

Here are shown results from simulations done with three ignitions in the “fishbone pattern” test area. Figure 3.15 shows results with and without fire breaks. Without fire breaks the fire line spreads to most pasture areas surrounding the ignition points but does not spread to all pasture areas, contrary to the previous area, because the deforestation is not as extensive. The inclusion of fire breaks isolates the burned area patches further, as the roads generally cross the deforested areas in this “fishbone” pattern, limiting fire spread to one side of the road and confining spread at crossroads. Figure 3.16 shows a hypothetical “apocalyptic” scenario with high fire spread probability in forest (0.5), similar to fire patterns observed in years of extreme drought. Fire initially spreads through the deforested areas, but soon creeps through forest and reaches other deforested areas.

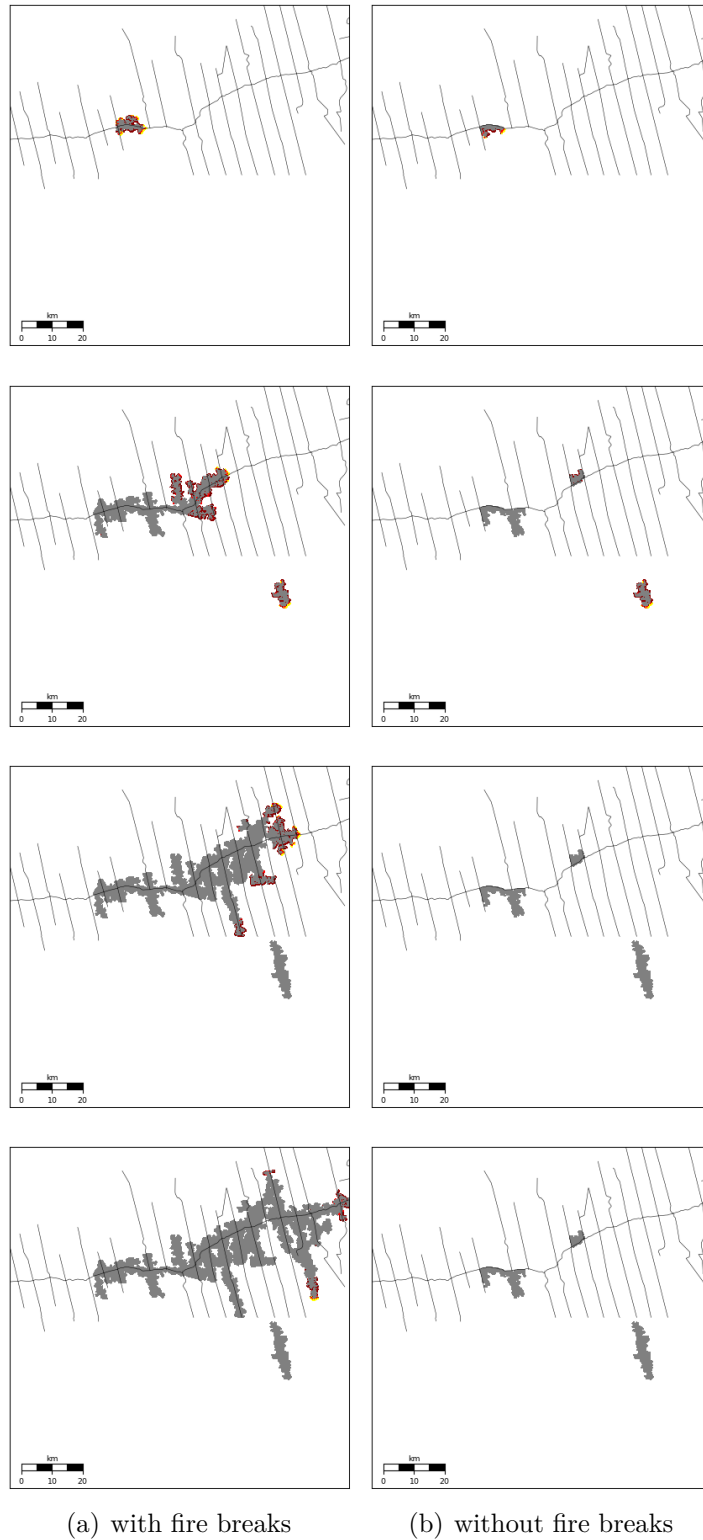


Figure 3.15 - Fire spread state in a “fishbone” deforested landscape (3 ignitions) at 3 day intervals (from top to bottom) with and without roads acting as fire breaks. Yellow cells are ignited, dark red are spreading, red are burning and grey are burned.

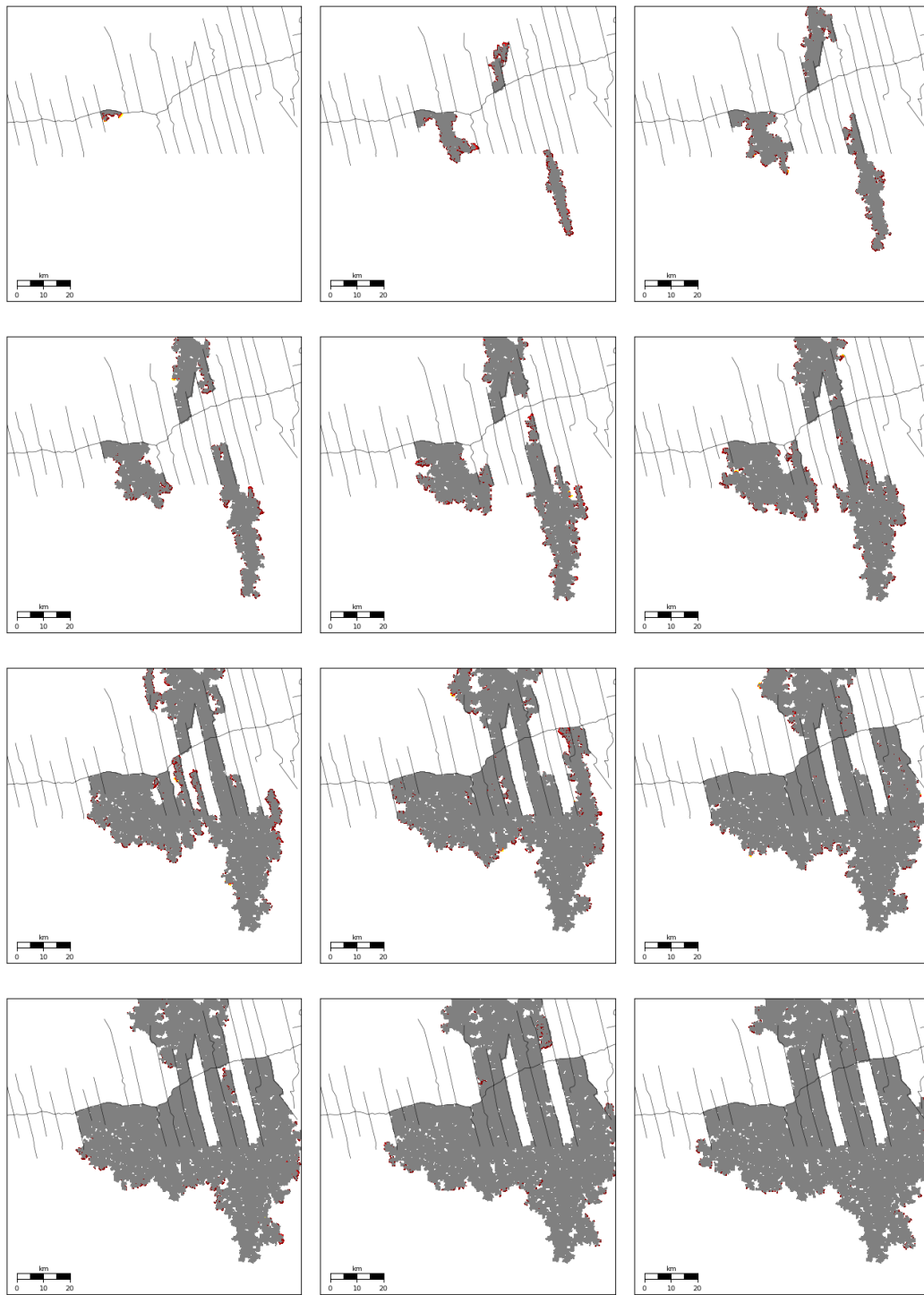


Figure 3.16 - Fire spread state in a “fishbone” deforested landscape (3 ignitions) at 7 day intervals (from top to bottom) with fire breaks and high forest spread probability (0.5). Yellow cells are ignited, dark red are spreading, red are burning and grey are burned.

3.3.2 Sensitivity to wind speed and direction

Sensitivity to wind speed is demonstrated in an experiment located in the “highly deforested” area, but with land cover consisting entirely of pasture and base ROS of 0.1 m/s and fire spread probability of 0.75. Figure 3.17 shows burn states after a single ignition in the center of the domain, with northerly wind speeds of 0, 2.5 and 10 m/s (at 10m height, and no stochastic daily/hourly variations in wind speed). In the case of no wind (left column), fire spread shape is circular, as expected, while in the case of low and high wind speeds (center and right column, respectively) the shape is roughly elliptical, with higher ROS in the southern direction. Note that the fire does not spread much against high winds, consistent with a $u2$ wind of 2 m/s and low backward ROS of 0.1 m/s, versus a high forward ROS of 1 m/s (approximately). Figure 3.18 shows results in a landscape consisting of tropical forest, with the same fire spread parameters as in the previous case, to evaluate the effect of sub-canopy wind speed only. In this case the effect of wind is minimal but slightly noticeable in the case of high winds. This is due to the fact that sub-canopy wind is much lower than 10m input wind speed in a dense forest (because of a high roughness length) – in this case 0.34 m/s, compared to 2 m/s in pasture.

Similar sensitivity experiments were done using the IBGE-TC land cover map used in section 3.3. First are shown results for “highly deforested” area, a landscape dominated by pasture, with some isolated forest patches. Figure 3.19 shows results similar to the pasture-only scenario, but with unburned patches in the forested areas: circular fire perimeter in the absence of winds and a roughly elliptical shape in the presence of low and high northerly winds. In the “fishbone pattern” study area, the configuration chosen was 3 ignitions, no fire breaks and 3 wind cases: no winds and strong northerly and westerly winds. Figure 3.20 shows fire spread states at 3 day intervals. In the northerly wind case, fire spreads slightly more to the south and less far north compared to the no winds case. In the westerly wind case, fire spreads more rapidly to the east and more slowly to the west. This illustrates the potential for more realistic fire spread representations in fragmented landscapes, in which wind direction and spatial structure are important in determining which areas are burned.

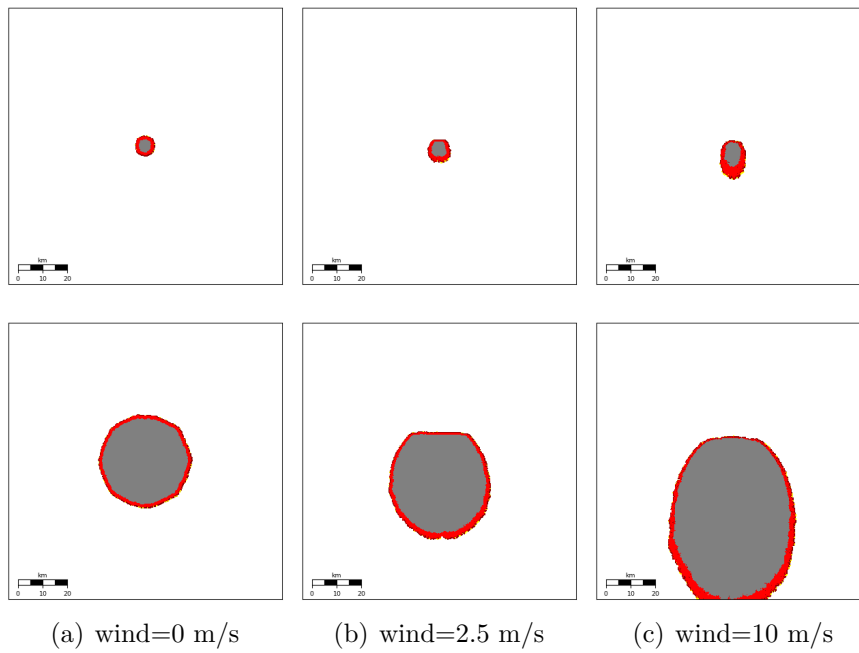


Figure 3.17 - Fire spread states at 3 day intervals (top to bottom) in a pasture landscape with varying northerly wind speeds. Yellow cells are ignited, dark red are spreading, red are burning and grey are burned.

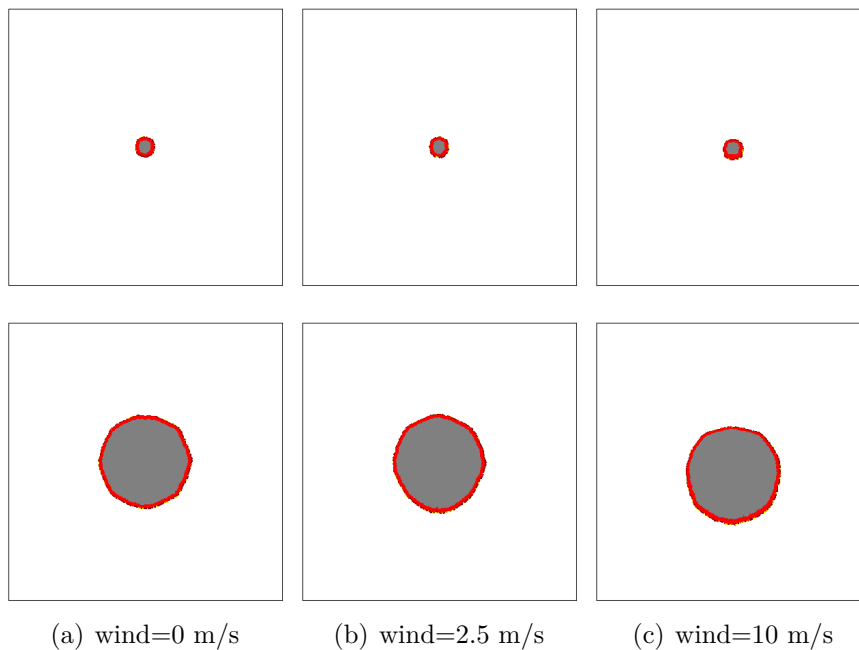


Figure 3.18 - As in Figure 3.17 but in a forested landscape, using fire spread parameters for pasture. Yellow cells are ignited, dark red are spreading, red are burning and grey are burned.

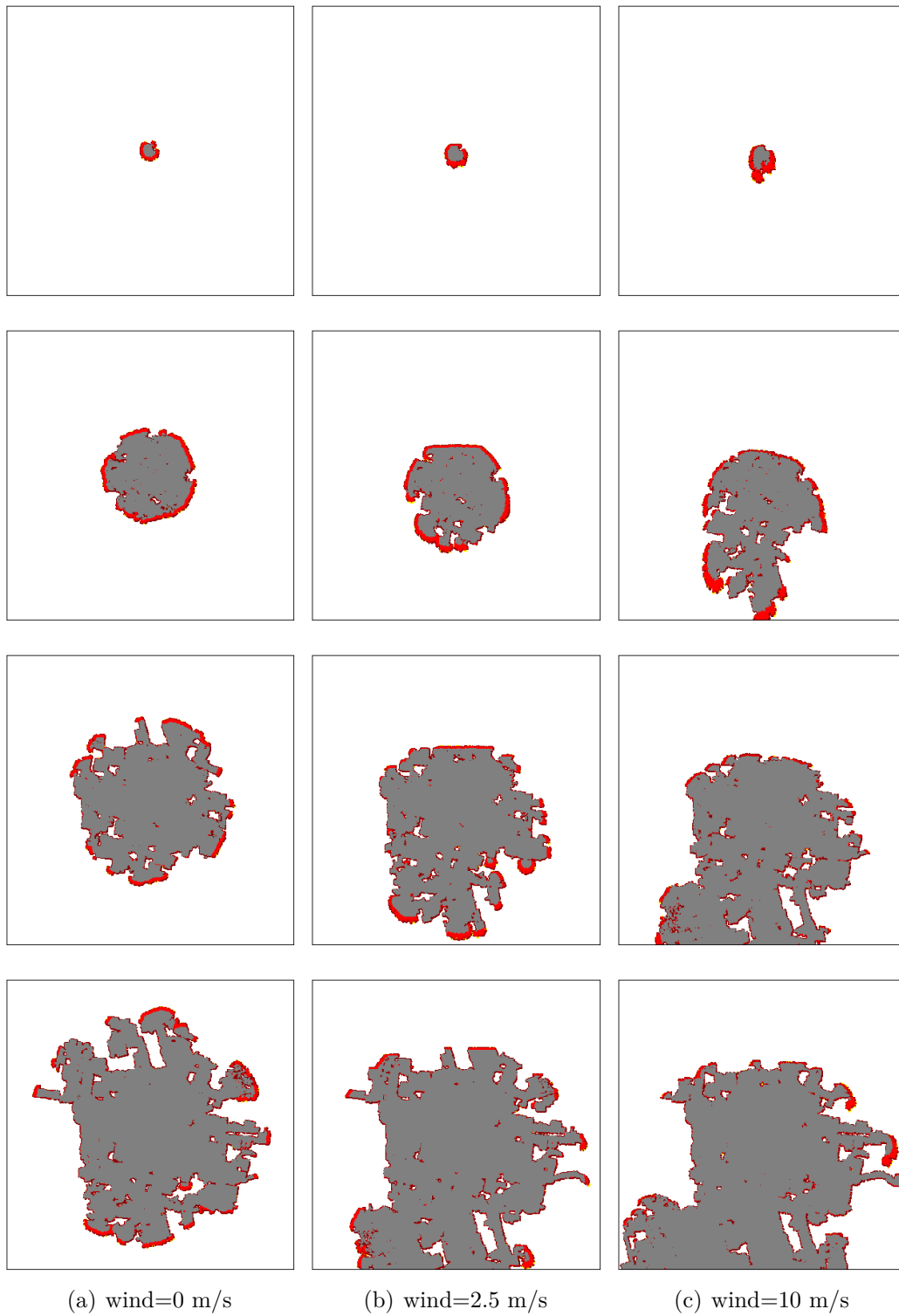


Figure 3.19 - Fire spread states at 2 day intervals in the “deforested landscape” study area with varying northerly wind speeds. Yellow cells are ignited, dark red are spreading, red are burning and grey are burned.

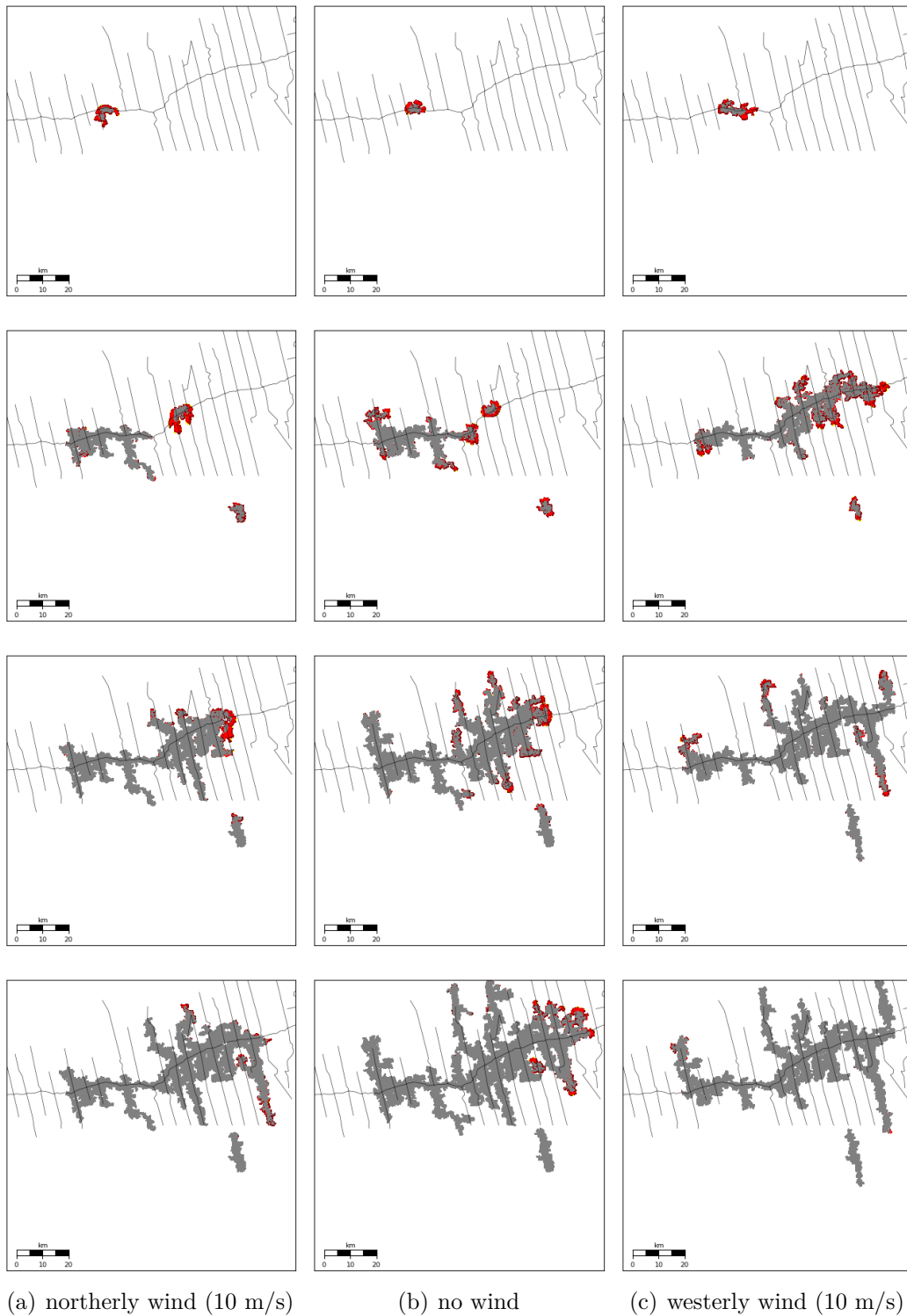


Figure 3.20 - Fire spread states at 3 day intervals (from top to bottom) in the “fishbone pattern” study area with varying wind direction. Yellow cells are ignited, dark red are spreading, red are burning and grey are burned.

3.3.3 Sensitivity to surface and air moisture

Figures 3.21 and 3.22 show the yearly-averaged values of *wsoia* (surface soil moisture), *totalit* (above ground litter carbon) and *vpds2* (VPD at 2m) that have been downscaled from the INLAND tiles to the high resolution maps. For each INLAND tile, the values are identical in all corresponding high-resolution pixels. In the case of the “highly deforested” area (Figure 3.21), soil moisture and surface litter are lower in deforested areas, while VPD is higher. We also see discontinuities in the moisture-related values at the borders between INLAND grid cells, showing that moisture is very sensitive to the input climate data, perhaps more so than actual land cover. These discontinuities could introduce artificial barriers in fire spread simulations and should be addressed with a blending algorithm. Discontinuities are less apparent in the “fishbone pattern” area (Figure 3.22), which is in a location that suffers less from drought. In this case the difference between forested and deforested areas is much more pronounced and fire behavior should also show marked differences.

VPD values fluctuate at various timescales: daily (due to changes in temperature, affecting relative humidity), seasonally (due mainly to changes in precipitation in the annual cycle), and inter-annually (due to climate variability). In areas with distinct wet/dry seasons VPD follows an annual cycle, with high values during the dry season, creating conditions more favorable for fire spread. Figures 3.23 and 3.24 show the annual cycle of moisture-related variables for the two study areas (using a single grid point for each). In both cases the left column shows values for a “normal” year (driven by CRU precipitation climatology) and the right column simulates a “dry” year (where input precipitation is halved). As in previous cases, the model was previously run for a 100-year spinup period with CRU-derived precipitation. Variables *xinprec* (monthly averaged precipitation from CRU) and *rain* (daily precipitation determined from INLAND’s weather generator) show a marked dry season, which is stronger in the “highly deforested” area (Figure 3.23). Seasonal changes in daily-averaged VPD (*vpds2*) and surface soil moisture (*wsoia*) are more visible in pasture (*vegtype* 18) than in forest (*vegtype* 1). In the first study area, VPD reaches higher levels during the dry season, but only once crosses the 750 Pa threshold (shown as a horizontal line) in the forested tile, suggesting that fire would not spread in normal years during the dry season. However, in the “dry” scenario, forest VPD is higher than 750 Pa for a few weeks. Note the sudden drop in VPD and peak in soil moisture in the middle of the dry season (in September), following a few precipitation events. In the case of the “fishbone pattern” area (Figure 3.24), changes in VPD and soil moisture in the forested tile is much less marked. Even in the “dry” year

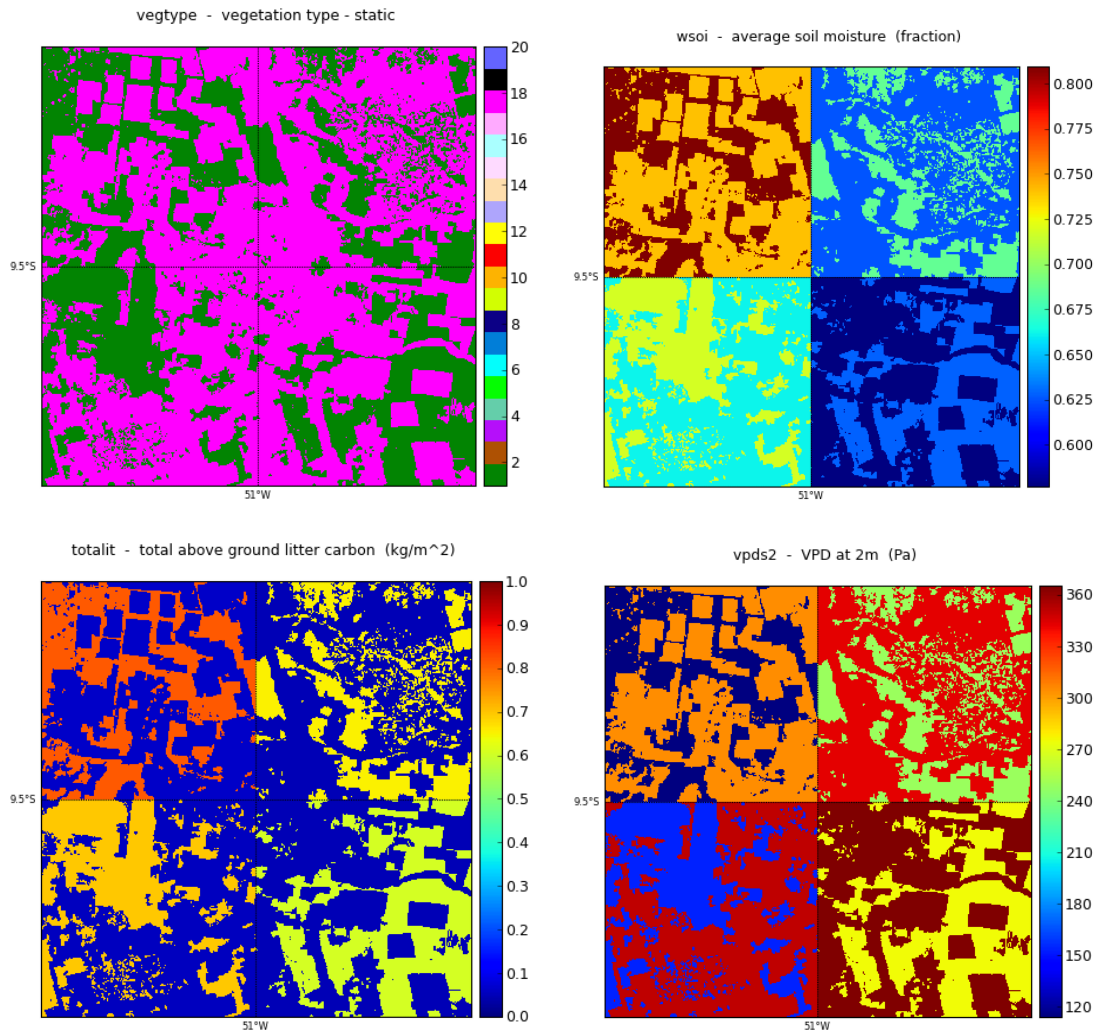


Figure 3.21 - Various fire-related variables downscaled from the INLAND model with tiles to the high-resolution land cover map, the “high deforested” area. Yellow cells are ignited, dark red are spreading, red are burning and grey are burned.

configuration, VPD stays well below 500 Pa, which would inhibit fire spread in the forest.

The 750 Pa VPD (at 2m) threshold condition for forest was incorporated into the fire spread model. To illustrate this, a number of simulations were done in the “highly deforested” domain, with an ignition on September 2 (in a period of high VPD) in a pasture area near the center of the domain. Fire spread states at 7 day intervals (5 days after ignition) are shown in Figure 3.25, for both the “normal year” and “dry year” precipitation inputs. In the normal case, fire spreads only to pasture areas, while in the dry scenario, fire slowly creeps into forested areas. Note that in the last date plotted (September 21), fire has stopped spreading in forested areas,

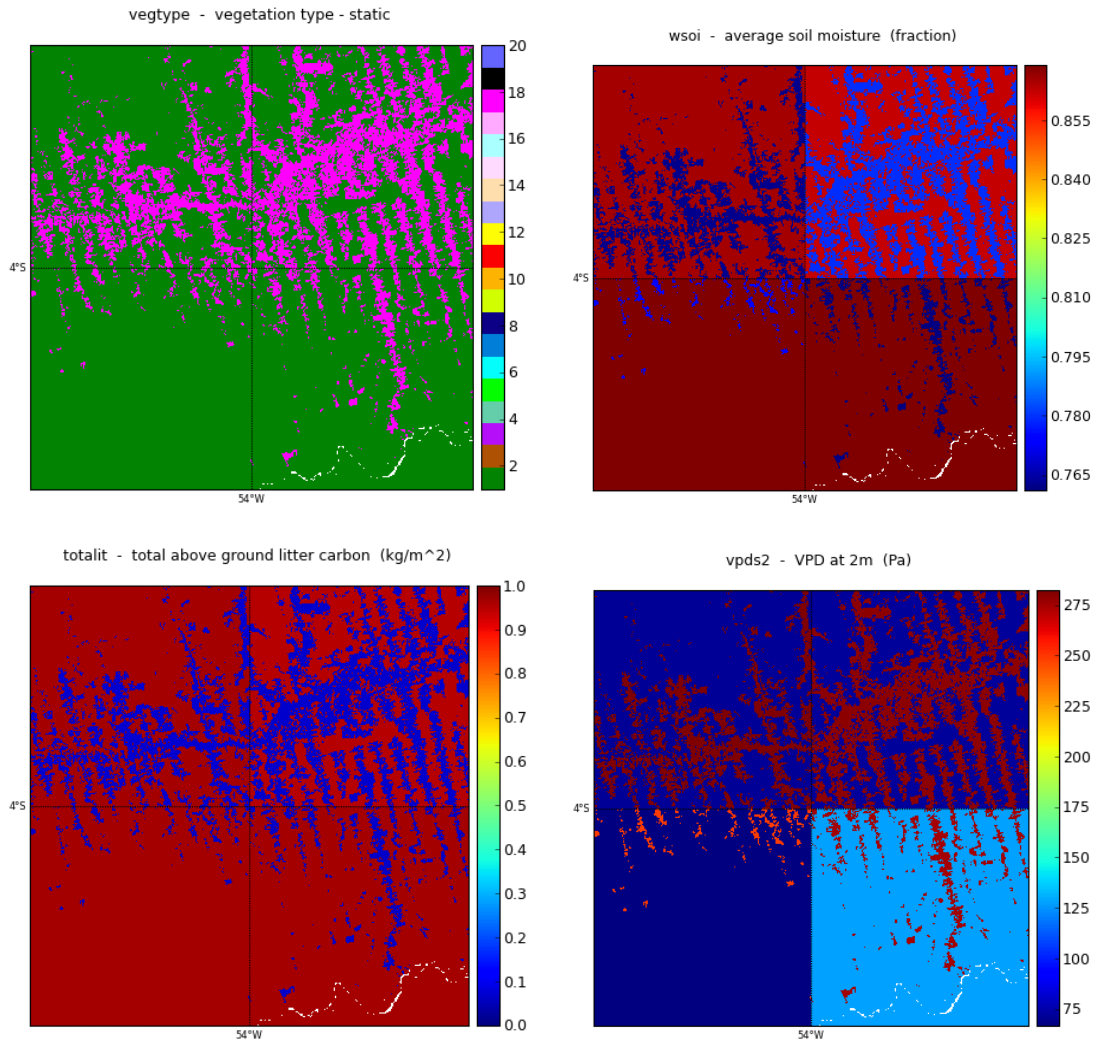


Figure 3.22 - As in Figure 3.21 but for the “fishbone pattern” area.

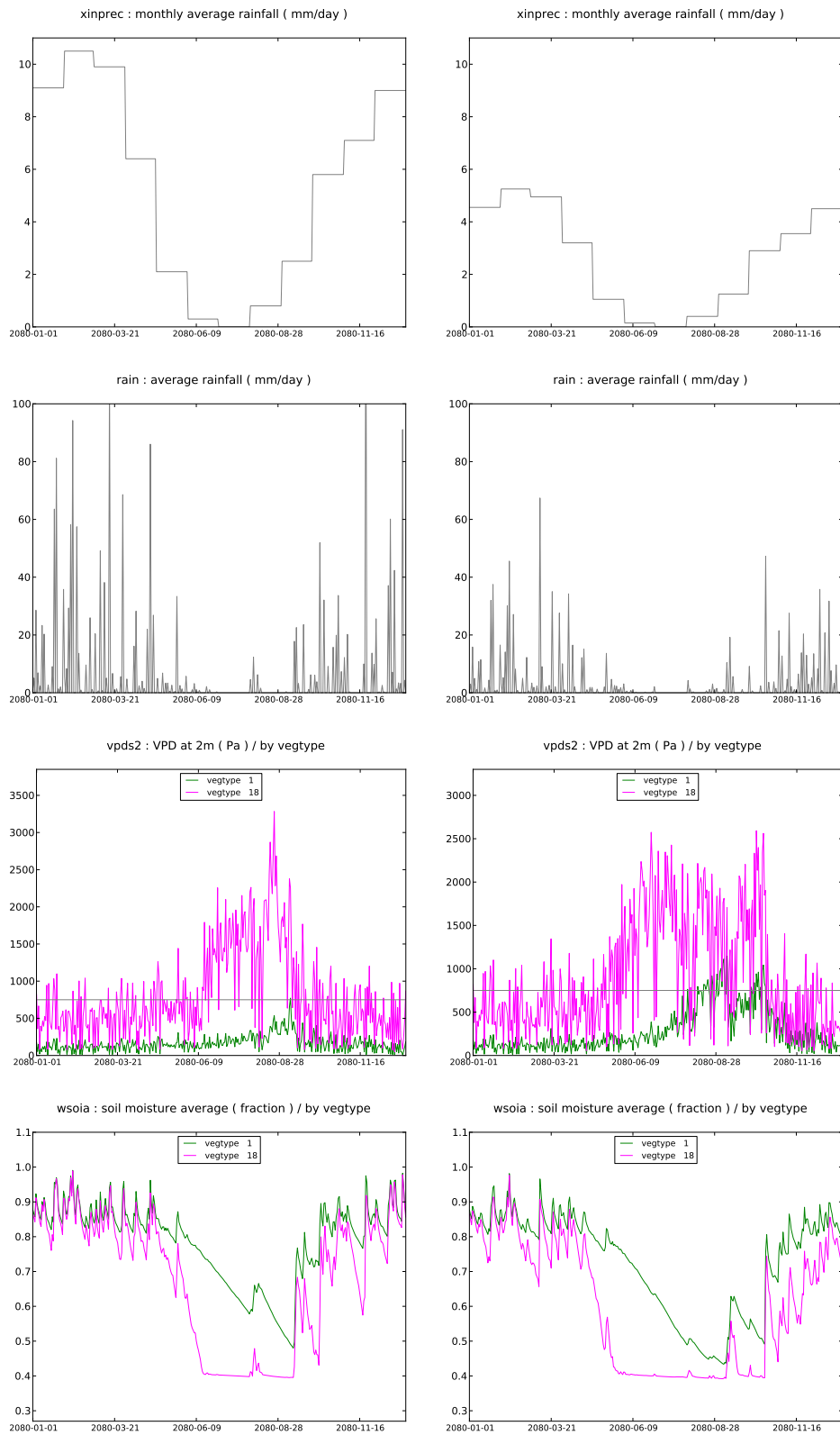
following the precipitation events which brought VPD below the 750 Pa threshold. This illustrates the capability of the model to terminate fire spread following changes in weather conditions.

3.4 Discussion

The sensitivity studies of the simple empirical fire spread model, coupled to the INLAND DGVM, show that it is able to create realistic patterns of fire spread under different land cover types (namely forest vs. pasture) and spatial deforestation structures (largely deforested vs. “fishbone” patterns). The model also creates very distinct fire spread spatial patterns when considering roads as deterministic fire breaks.

Finally the effects of the two main climatic drivers of fire spread and occurrence –wind and fuel moisture– were examined. It was shown that: variations in wind magnitude can be represented at the sub-canopy level; an ideal elliptic fire shape can be simulated in the presence of wind; and the effects of wind are much less important in dense forest than in open areas such as pasture. The most important element for representing the occurrence of fire spread (vs. the *rate* of spread) is fuel moisture, which can be approximated by sub-canopy VPD. While normal (climatological) conditions do not favor fire spread within tropical forests in the model, even during the dry season, these conditions can be met by inducing drought conditions.

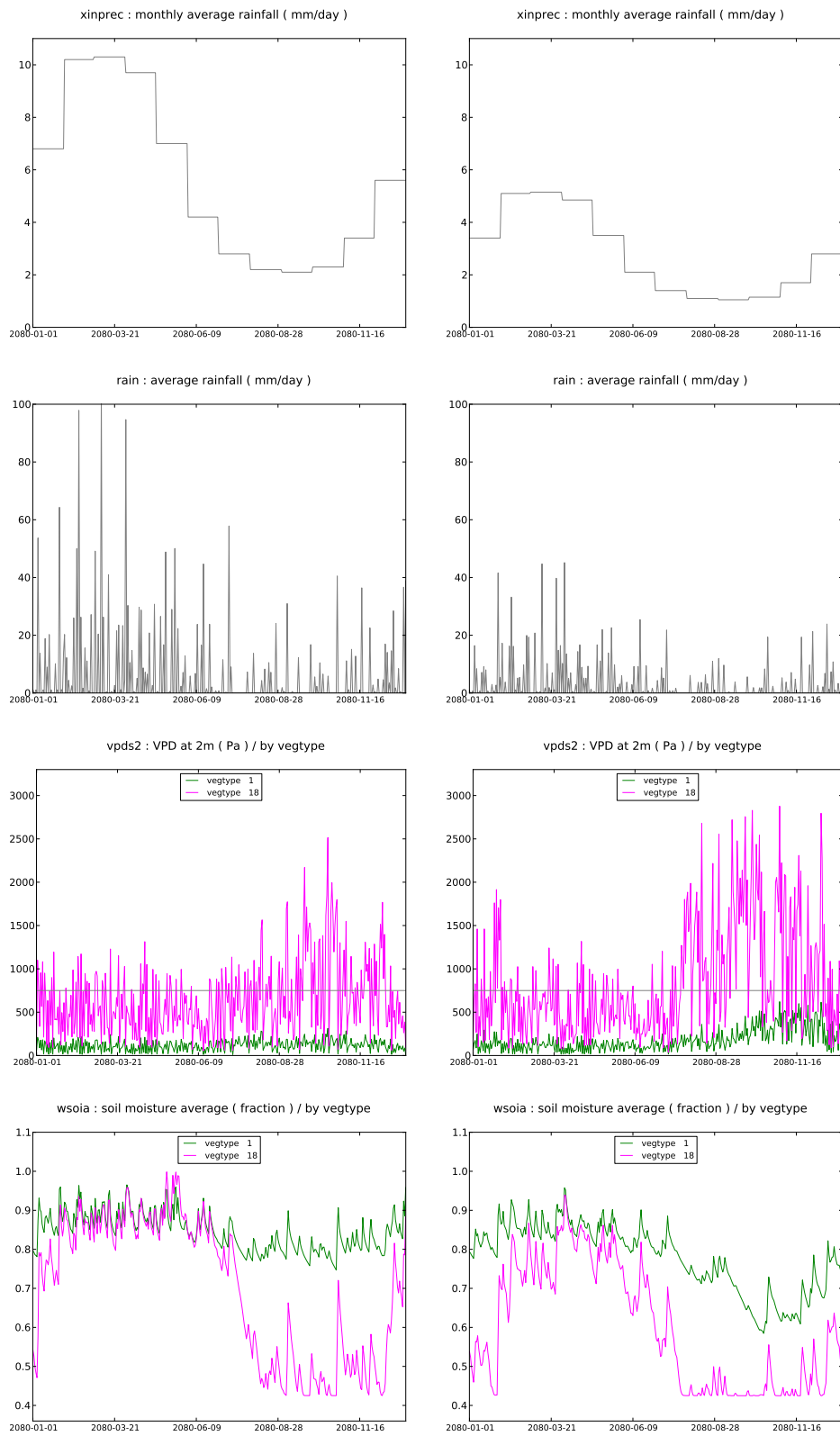
These results show the importance of using a land surface model that can represent the effect of varying land cover (forested vs. open areas) in order to represent sub-canopy wind and moisture conditions. They also highlight the importance of using *subgrid tiling* in a coarse-scale model, in order to represent subgrid-scale variations of important parameters (i.e. wind, moisture) related to fire occurrence and spread. The fire spread model thus presented, once properly calibrated, will contain the key elements needed to simulate fire occurrence and spread in the Brazilian tropics and study the effects of climatic variability.



(a) normal year

(b) dry year

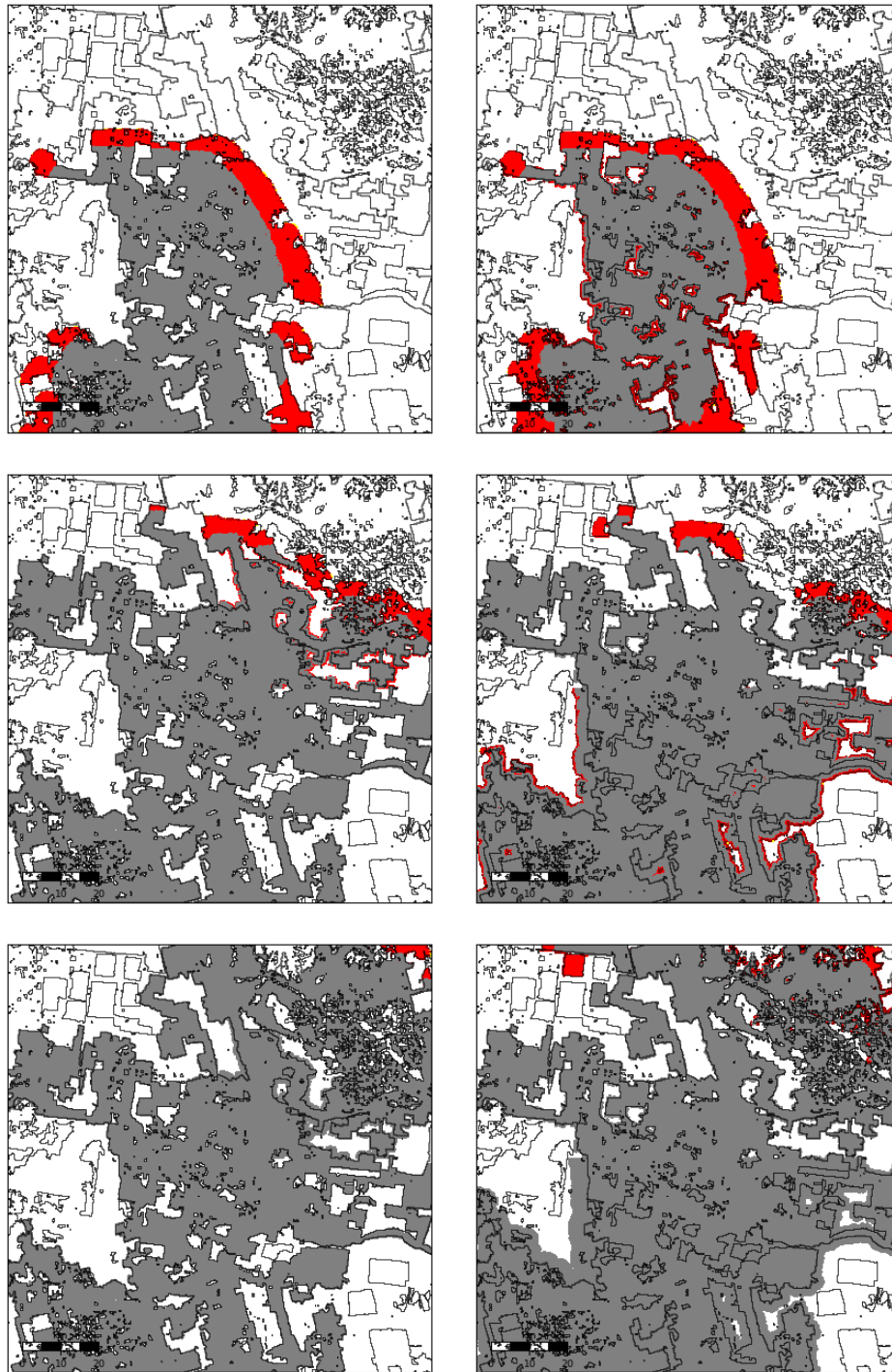
Figure 3.23 - Annual cycle of moisture-related variables in the “highly deforested” area, representing a “normal” and “dry” year.



(a) normal year

(b) dry year

Figure 3.24 - As in Figure 3.23, but for the “fishbone pattern” area.



(a) normal year

(b) dry year

Figure 3.25 - Fire spread states at 7 day intervals when 750 Pa VPD threshold is used for determining fire spread in forest. Contours identify the land use map (pasture vs. forest). Yellow cells are ignited, dark red are spreading, red are burning and grey are burned.

4 EVALUATION OF GLOBAL BURNED AREA PRODUCTS IN THE BRAZILIAN ARC OF DEFORESTATION

4.1 Introduction

Biomass burning of intentional, accidental or natural origin contributes significantly to atmospheric emissions of carbon dioxide and other trace gases, atmospheric pollution, and ecological disturbances. Projected changes in climate (e.g. warmer global temperatures, extremes in precipitation) suggest an increased frequency and severity of wildfires, especially when coupled to land use changes in the tropics (CARDOSO *et al.*, 2008). The global tropics are areas that currently suffer from the highest incidence of wildfires and, as they contain a large biomass pool, are a potentially high source of atmospheric emissions through biomass burning (BOWMAN *et al.*, 2009; COCHRANE, 2009). Tropical rainforests are rendered vulnerable to wildfires through deforestation, agricultural practices and ecological and climatic feedbacks (BARLOW; PERES, 2008). Tropical savannas (such as the cerrado of Brazil) are naturally subjected to wildfires but climate extremes and human practices are important factors for fire occurrence (BOWMAN *et al.*, 2009). Extreme droughts such as the 1997-1998 El Niño and the 2005 drought in the Amazon cause widespread vegetation burning (ARAGÃO *et al.*, 2007; COCHRANE, 2003). To understand the potential synergies between climate change, land use changes, climate extremes, ecological processes, and wildfires (COCHRANE; LAURANCE, 2008), researchers are increasingly turning to Dynamic Global Vegetation Models (DGVMs)—with a representation of fire processes included—for global studies (ARORA; BOER, 2005; SITCH *et al.*, 2003; THONICKE *et al.*, 2010).

Calibration and validation of such global fire models require reliable datasets on fire occurrence, on a global scale and for extended periods. A few suitable burned area products are available, especially those based on imagery from the Moderate Resolution Imaging Spectroradiometer (MODIS) satellite-based sensor platform. These include the MCD45A1 (ROY *et al.*, 2008) and MCD64A1 (GIGLIO *et al.*, 2009) products, which are available at their native resolution of 500m, and the Global Fire Emissions Database (GFED) (WERF *et al.*, 2010), at a coarser scale. Evaluation of these global products requires regional- and local-scale studies to compare them against known fire occurrence data. Whereas reliable, more ground-truthed data on burned area exist for mid-latitude areas such as the United States, Canada and Europe (e.g. the LANDFIRE program) (ROLLINS, 2009), there are few such databases available for the tropics. There has been some evaluation in selected tropical areas,

mostly in Africa (GIGLIO et al., 2009; ROY; BOSCHETTI, 2009).

This work aims to evaluate the performance of the MCD45A1, MCD64A1 and latest GFED burned area products in areas of the Brazilian “arc of deforestation” which lies at the ecotone of the Brazilian Amazon rainforest and the *cerrado* savanna. The goal is twofold: to evaluate the fine-scale structure and performance of the high-resolution MODIS products, and to evaluate the regional-scale performance of GFED and resampled data from the MODIS products. Our approach is to compare the global products with burned area maps generated from high-resolution products such as Landsat Thematic Mapper (TM) sensors. Our analyses focus on two scales: the native scale of the MODIS products (500m) which is suitable for local-scale studies and the native scale of the latest GFED product (0.25°), which is at the lower end of the scales used in DGVMs. Ideally, such a study would encompass a large sampling of temporal and spatial scales. As a first step we decided to study the 2010 dry season, a period during which biomass burning was anomalously high due to a severe drought in the Amazon (MARENGO et al., 2011) and *cerrado*. Due to spatial heterogeneity in forest composition and deforestation in the Brazilian “arc of deforestation”, we selected various sites with distinct and representative features, such as degree of deforestation, fragmentation type (e.g. “fishbone” vs. largely deforested).

4.2 Data

4.2.1 Landsat TM burned area maps

Individual Landsat scenes were selected based on a number of criteria, in order to represent the spatial variability in burned area amount and spatial structure in the area of interest – the Brazilian “arc of deforestation”. Our goal was to capture the following features: populated (and highly deforested) vs. remote areas, many vs. few burns, and pasture vs. deforestation burns. The area and selected scenes are shown in Figure 4.1. We decided to map the burn scars in two images from each scene, one taken near the beginning of the 2010 dry season and one near the end (except for scene 226/070, where we used four images). Overlapping the mapped burn scars from the two dates allowed us to determine which burn scars detected at the end of the dry season were not present at the beginning, indicating fires that must have happened between the dates of the two images. Data from the MODIS burned area products (see below) indicate that, on average, over 90% of burning in 2010 occurred between the dates chosen for each scene. However, the amount of time between images is large enough to allow for vegetation regrowth after fires, and as

such this method could result in some underestimation of dry-season burned area. Specific dates with low contamination by cloud and smoke, as well as high amounts of burn scars (for the last map) were chosen for analysis. The scenes and dates chosen are shown in Figure 4.1. Landsat imagery was obtained from INPE’s Image Catalog server (INPE - National Institute For Space Research, 2012) and geo-referenced with ortho-rectified imagery from the NASA GeoCover dataset, using the Universal Transverse Mercator coordinate system (UTM) with appropriate zone (as given in Table 4.1) and the WGS-84 datum. Atmospheric correction was not deemed necessary.

Table 4.1 - UTM zone, mapping method, and dates for both images from each scene of the products used in this study. Dates are given in MM/DD format for Landsat 5 imagery and Julian day of year for the MODIS products.

Landsat scene	UTM zone	Mapping method	First Date		Last Date	
			Landsat	MODIS	Landsat	MODIS
224_066	22S	LSMM	06/24	175	09/28	271
224_067	22S	visual	07/26	207	09/12	255
226_070	21S	visual	06/22	173	09/26	269
226_071	21S	visual	07/24	205	09/26	269
225_065	22S	LSMM	06/15	166	09/03	246
226_067	21S	LSMM	07/24	205	10/12	285
227_065	21S	LSMM	06/13	164	09/01	244
232_067	20S	LSMM	05/15	135	08/19	231

Scenes 224/067, 226/070 and 226/071 were mapped for a previous project using Landsat 5 Thematic Mapper (TM) Bands 3 (630–690 nm, red), 4 (760–900 nm, near infrared), and 5 (1550–1750 nm, short-wave infrared), and numerous active fire products (e.g. MODIS, NOAA, GOES, METEOSAT) from INPE’s active fire database (INPE - National Institute For Space Research, 2014), using SPRING software (CÂMARA et al., 1996). Landsat imagery was used to visually identify and digitize burn scars, with the guidance of active fire occurrences to assist in the interpretation. The remaining scenes were processed using the Linear Spectral Mixing Model (LSMM) technique (LIMA et al., 2012; SHIMABUKURO et al., 2009). We used Landsat bands 5, 4 and 3 with similarity=8 and area=25 parameters to generate the vegetation, soil, and shade components of the LSMM method. The ISOSEG algorithm was used on the shade component (with an acceptance threshold of 75%) to generate a burn scar map, which was visually inspected and corrected for false positives (such as water and relief shading).

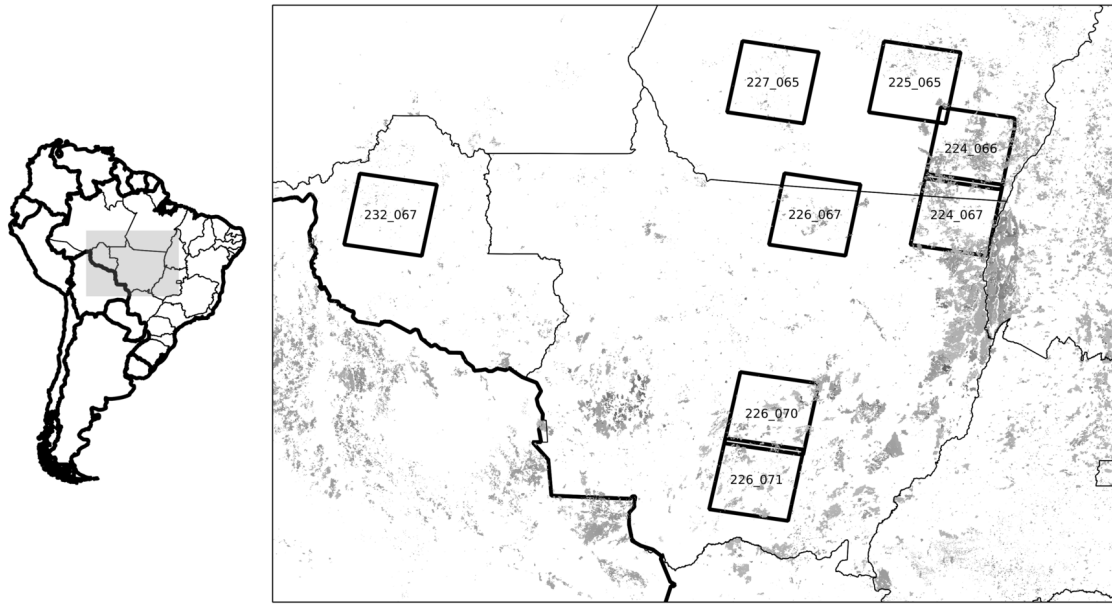


Figure 4.1 - Location of Landsat scenes used, overlaid with burned area from MCD45 during the 2010 dry season.

Geo-referenced imagery (R5G4B3 color composition in GeoTIFF format), as well as final burn scar maps (polygons in shapefile format) are available on request.

4.2.2 MODIS daily burned area products (500m) MCD45 and MCD64

The Collection 5 MODIS burned area product (MCD45A1, hereafter referred to as MCD45) is a global dataset estimating burned area at daily temporal resolution (with an average delay of one day due to the presence of clouds and smoke) and 500m spatial resolution (ROY *et al.*, 2008). The MCD45 algorithm identifies burned areas based on changes in reflectance following the removal of vegetation and deposition of ash and charcoal by burning. The MCD45 product has been evaluated in numerous global studies (ROY *et al.*, 2008) but few tropical areas (RIVERA-LOMBARDI, 2009; ROY; BOSCHETTI, 2009). In areas with dense vegetation, such as the Amazon, the MCD45 product under-estimates burned area mainly due to understory fires which cannot be detected through changes in reflectance and are frequently of smaller scale than the mapping algorithm. However, the algorithm fares better in open areas such as savannas and grasslands (ROY *et al.*, 2008). Rivera-Lombardi (2009) analyzed the performance of the MCD45 product in the Brazilian states of Acre and Rondônia and concluded that although agreement was not very good, it remained the best tool for the systematic estimation of burned areas at regional or larger scales in this region.

A different methodology (hereafter referred to as MCD64), developed by Giglio et al. (2009), combines 500m MODIS surface reflectance products and 1km MODIS active fire products to map burn scars. Compared to burned area maps derived from Landsat imagery, the MCD64 product is satisfactory except in areas of dense forest, and false positives have been identified in areas suffering from intense deforestation (GIGLIO et al., 2009).

Both MODIS burned area products have a resolution of approximately 500m in the MODIS sinusoidal projection and are distributed in Hierarchical Data Format (HDF) format with monthly resolution in $10^{\circ}\times 10^{\circ}$ tiles. MCD45 files are available from <ftp://e4ftl01.cr.usgs.gov/MOTA/MCD45A1.005/> and MCD64 files from <ftp://fire:burnt@fuoco.geog.umd.edu/db/MCD64A1/>. We obtained the 2010 monthly MODIS sinusoidal tiles covering the area of interest (h11v09, h11v10, h12v09, h12v10, h13v09 and h13v10). For each tile, individual HDF4 monthly tiles were converted to GeoTIFF format and aggregated into a single file containing burned area date for 2010. The Quality Assessment (QA) values were not considered (i.e. all pixels identified as burned were used). The various tiles were converted into a single mosaic. These operations were done using the GDAL Geospatial Data Abstraction Library (GDAL, 2013).

4.2.3 GFED4 daily burned area product (0.25°)

The Global Fire Emissions Database (GFED) is a global dataset of estimates of burned area and emissions from biomass burning (GIGLIO et al., 2010; GIGLIO et al., 2013; WERF et al., 2010). Burned area estimates from the fourth version of GFED (GFED4) consist of daily maps at 0.25° resolution covering the period 1995-2011. The GFED4 product uses active fire observations from the VIRS and ATSR sensors to estimate burned area before the MODIS period (1995-2000), and a method similar to that used in the MCD64 product during the MODIS period (2000-present) (GIGLIO et al., 2013). Burned area and emissions estimates from previous versions of GFED are used in most evaluations of the fire components of climate and earth system models (THONICKE et al., 2010).

The GFED4 burned area data were obtained from <ftp://fire:burnt@fuoco.geog.umd.edu/gfed4/>, in the form of global maps at 0.25° resolution in the HDF format. Individual daily maps of burned area for 2010 were combined into a single file in the NetCDF format that contained daily values of burned fraction (for ease of comparison with other products). For each of the Landsat scenes evaluated, the daily burned fraction values within the mapping period (see Figure 4.1) were added. These steps

were performed using GDAL (GDAL, 2013) and CDO (Climate Data Operators) software packages.

4.3 Methods

4.3.1 MODIS burned area products at native (500m) resolution

In order to remove the effects of differences in spatial resolution of the Landsat and MODIS burned area maps, all analyses were performed at the native MODIS resolution of 500m (more precisely, 462.5m). Landsat burned area polygons at their native 30m resolution were rasterized and resampled to 500m resolution, with a 500m pixel marked as “burned” only if at least 50% of the 30m pixels included in its boundaries were identified as burned. Landsat and MODIS burned data were filtered to include only pixels where the burn date was between the first and last Landsat images of each scene. Therefore, any burn scars identified in the MODIS products before/after the first/last Landsat map were discarded from the analysis. For each of the scenes analyzed, the MODIS mosaics were cropped and masked using the Landsat overlap polygons and re-projected to the same coordinate system and datum as the Landsat maps.

We used several techniques to compare the accuracy of the MODIS products at 500m to our Landsat-based maps. So-called “confusion matrices” or “contingency tables” are commonly used in assessments of spatial classification agreement, as they provide information on the agreement between a given classified map with a reference map (CONGALTON; GREEN, 1999). Here, we used confusion matrices to evaluate overall accuracy (OA, the fraction of correctly classified pixels) as well as omission and commission error of the burned class (OE and CE; the fraction of actual burned and unburned pixels, respectively, that were incorrectly classified). Estimated omission errors can be considered more reliable than commission errors in our analysis, since it is much more likely for our Landsat-based mapping method to miss an actual burn scar (e.g., due to vegetation regrowth before the second Landsat image for a scene) than for it to map a burn scar where no fire occurred. We also used several other metrics developed for the evaluation of spatial classifications, including the Cohen Kappa score (K). This is a traditional metric used in the evaluation of spatial classifications, with values < 0 indicating poor agreement, 0–0.20 slight, 0.21–0.40 fair, 0.41–0.60 moderate, 0.61–0.80 substantial, and 0.81–1 almost perfect agreement (LANDIS; KOCH, 1977). Kloc, and Khisto (or Kquantity) are related metrics that allow better discrimination between location and quantification errors, respectively (HAGEN, 2002; PONTIUS, 2000).

We calculated these metrics, as well as burned area fraction for the entire scene, for all scenes and both MODIS products. We also plotted maps of burned area, overlaying MODIS products and Landsat data in order to show areas of agreement and disagreement and visually evaluate the accuracy of MODIS burned area products. Calculations and plots were done using R (R Core Team, 2012) and GDAL software (GDAL, 2013).

4.3.2 MODIS and GFED4 at coarser resolutions (5km and 0.25°)

As there may be some differences in spatial structure due to different spatial resolutions of the Landsat maps and MODIS burned area products, we analyzed burned area estimates at a coarser resolution. Individual burned pixel maps at 500m resolution were resampled to burned fraction maps at 5 km resolution, where each pixel contains the fraction of underlying pixels marked as burned. From these maps, we computed scene-wide burned fraction (i.e. average across all cells in each scene) for comparison among products. In order to quantify the agreement in spatial structure between the MODIS products and Landsat maps, we calculated the spatial Pearson correlation of burned fraction in each scene, by pairwise comparison of burned fraction Landsat and MODIS pixels. While this does not measure agreement in the magnitude of burned fraction, it does indicate whether the detected burns are well situated spatially. For example, a negative correlation between two products would indicate that one product tends to find high burned fraction pixels where the other finds low burned fraction pixels and vice versa, even though the scene-wide average burned fraction might be identical.

We performed the analyses mentioned above at a 0.25° resolution as well, with MCD45 and MCD64 maps being resampled using the aforementioned procedure and GFED4 daily maps being used at their native resolution (0.25°).

4.4 Results

4.4.1 MODIS burned area products at native (500m) resolution

Area-averaged burned fraction by scene (at 500m resolution) of the Landsat, MCD45, and MCD64 products is shown in Figure 4.2. There is significant variability in burned fraction from scene to scene, and both MODIS products capture this variability, with Pearson correlation coefficients of 0.99 and 0.95 for MCD45 and MCD64, respectively (not shown). There is a tendency for the MODIS products to underestimate burned extent, and MCD64 seems to show larger differences (positive

or negative) than MCD45. Average values (over all scenes) give an overall view and an indication of relative performance of both products. Scene-wide burned fraction (from Table 4.2) is very similar between the Landsat and MODIS products (11% and 10% on average, respectively) and shows good agreement of both products in quantifying the amount of burned area, with a very small absolute error but a large average relative error (~30% underestimate).

Table 4.2 - Scene-wide burned fraction estimates from MCD45 and MCD64 products at native 500m resolution, compared with the resampled 500m Landsat burned area product, for each Landsat scene. Negative values of relative error indicate underestimates by the MODIS products. Also shown are average values across all scenes and for scenes with high Landsat-mapped burned fraction (“High BF”, defined as > 10%) and those with low burned fraction (“Low BF”).

Landsat scene	Burned Fraction (Relative Error)		
	Landsat	MCD45	MCD64
224_066	30%	27% (-9%)	31% (+5%)
224_067	17%	18% (+5%)	24% (+37%)
226_070	14%	12% (-17%)	9% (-39%)
226_071	14%	10% (-24%)	8% (-40%)
225_065	7%	4% (-49%)	3% (-54%)
226_067	6%	3% (-41%)	5% (-17%)
227_065	2%	1% (-50%)	1% (-47%)
232_067	2%	1% (-49%)	1% (-53%)
Average: All	11%	10% (-29%)	10% (-26%)
Average: High BF	19%	17% (-11%)	18% (-9%)
Average: Low BF	4%	2% (-47%)	2% (-43%)

Table 4.3 shows that Kappa is within the “moderately acceptable” range on average for both MODIS products, with a slight advantage for MCD45. Khisto is higher than Kloc for both MODIS products, indicating that they are better at estimating the amount of burned than its location, which is consistent with low absolute burned fraction errors. Overall Accuracy is high (90%) but this is expected because (a) there are only two classes (burned and not burned), and (b) the vast majority of pixels are not burned. Omission errors are mostly higher than commission errors (~50% and ~30%, respectively) for both products, although errors are slightly higher for MCD64.

Burned Fraction by scene

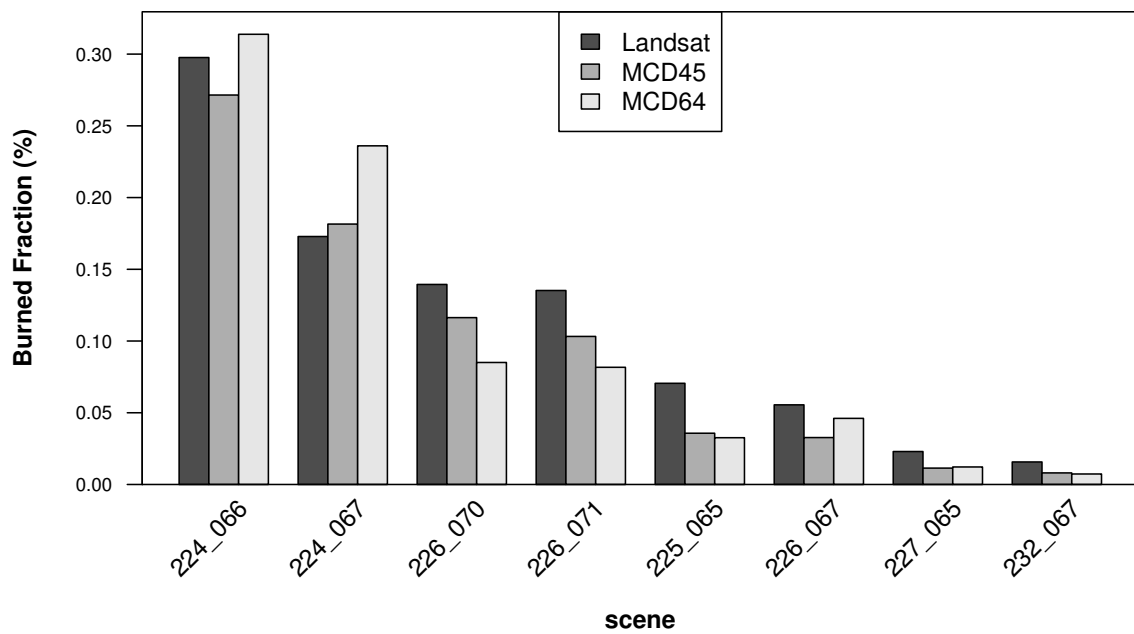


Figure 4.2 - Burned fraction by scene (at 500m resolution) of Landsat, MCD45 and MCD64 products.

Table 4.3 - As in Table 4.2, but for spatial performance instead of scene-wide burned fraction estimates.

Landsat scene	Kappa		Kloc		Khisto		Overall accuracy		Commission error		Omission error	
	MCD45	MCD64	MCD45	MCD64	MCD45	MCD64	MCD45	MCD64	MCD45	MCD64	MCD45	MCD64
224_066	0.61	0.39	0.65	0.41	0.94	0.96	84%	74%	24%	44%	31%	41%
224_067	0.72	0.64	0.74	0.79	0.97	0.81	92%	88%	25%	38%	21%	16%
226_070	0.61	0.47	0.68	0.64	0.90	0.74	91%	89%	28%	31%	39%	57%
226_071	0.69	0.60	0.81	0.83	0.85	0.73	93%	92%	16%	15%	36%	49%
225_065	0.54	0.49	0.82	0.79	0.66	0.62	95%	95%	16%	20%	58%	63%
226_067	0.30	0.39	0.40	0.43	0.73	0.90	94%	94%	56%	54%	74%	62%
227_065	0.52	0.53	0.78	0.77	0.66	0.69	98%	98%	21%	23%	61%	59%
232_067	0.51	0.45	0.76	0.71	0.68	0.63	99%	99%	24%	29%	61%	67%
Average: All	0.56	0.49	0.71	0.67	0.80	0.76	93%	91%	26%	32%	48%	52%
Average: High BF	0.66	0.53	0.72	0.67	0.91	0.81	90%	86%	23%	32%	32%	41%
Average: Low BF	0.47	0.46	0.69	0.67	0.68	0.71	97%	97%	29%	31%	63%	63%

The MODIS products appear to perform particularly poorly in scenes with little burning (burned fraction < 10%). If we consider only the scenes with Landsat-based burned fraction of at least 10% (224/066, 224/067, 226/070 and 226/071), accuracy as measured by most statistics (other than Kloc) improves markedly. Average relative errors in scene-wide burned fraction are much lower (a decrease of nearly 20% to an underestimate of ~%), average Kappa values are higher and even fall in the “acceptable” category for MCD45, and Khisto values show very good agreement in the quantity of pixels marked as burned.

4.4.2 MODIS and GFED4 at coarser resolutions (5km and 0.25°)

Scene-wide burned fraction and relative errors for the MODIS products resampled to 5km are virtually identical to the 500m data (Table 4.4). Spatial correlation values are rather high, especially for MCD45 (correlation > 0.8, except for scene 226/067). This means that even if individual 500m burned pixels may not correspond to pixels marked as burned by our Landsat mapping, at the 5km scale patterns of high and low burned fraction values are well captured by both MODIS products. This indicates a rather good agreement for the scenes with high burned fraction, with low relative errors, especially in the case of MCD45.

Table 4.4 - Performance of the 5km MODIS products relative to the Landsat product.

Landsat scene	Burned Fraction (Relative Error)			Spatial correlation	
	Landsat	MCD45	MCD64	MCD45	MCD64
224_066	29%	27% (-6%)	31% (+8%)	0.82	0.57
224_067	17%	18% (+5%)	23% (+35%)	0.95	0.89
226_070	13%	11% (-14%)	8% (-36%)	0.80	0.63
226_071	13%	10% (-23%)	8% (-39%)	0.88	0.79
225_065	7%	3% (-51%)	3% (-56%)	0.86	0.84
226_067	6%	3% (-48%)	4% (-25%)	0.55	0.71
227_065	2%	1% (-53%)	1% (-50%)	0.84	0.86
232_067	2%	1% (-53%)	1% (-58%)	0.84	0.83
Average: All	11%	9% (-30%)	10% (-28%)	0.82	0.77
Average: High BF	18%	17% (-10%)	18% (-8%)	0.86	0.72
Average: Low BF	4%	2% (-51%)	2% (-47%)	0.77	0.81

Table 4.5 presents the results of comparing the MODIS and GFED4 products to our Landsat product at the scale of 0.25°. As expected, area-averaged burned fraction and relative errors of the MODIS products are very close to those at 500m and

5km scales. Spatial correlation values are even higher at this coarse resolution (>0.9 and >0.8 for MCD45 and MCD64, respectively), due to a smoothing of local-scale differences between the Landsat and MODIS products at this scale. The values for GFED4 are virtually identical to those of MCD64 at 0.25° resolution, which is expected since GFED4 is based on MCD64 data. This is illustrated in Figure 4.4, which shows 0.25° maps of burned fraction from all products for a single scene. Noteworthy of the MCD64 and GFED4 products at this resolution is that while scenes with high burning have lower relative errors (near zero on average) than scenes with little burning, spatial correlation there tends to be worse, although still acceptable.

Table 4.5 - Burned fraction and spatial correlation of MODIS and GFED4 products at 0.25°

Landsat scene	Burned Fraction (Relative Error)			Spatial correlation			
	Landsat	MCD45	MCD64	GFED4	MCD45	MCD64	GFED4
224_066	31%	30% (-4%)	36% (+16%)	37% (+20%)	0.91	0.75	0.76
224_067	14%	15% (+8%)	21% (+56%)	21% (+52%)	0.98	0.98	0.98
226_070	15%	12% (-19%)	8% (-45%)	8% (-43%)	0.92	0.68	0.67
226_071	13%	10% (-24%)	9% (-37%)	9% (-34%)	0.92	0.83	0.83
225_065	8%	4% (-49%)	4% (-51%)	4% (-47%)	0.93	0.95	0.95
226_067	7%	4% (-42%)	6% (-15%)	6% (-12%)	0.73	0.91	0.91
227_065	3%	1% (-55%)	1% (-51%)	2% (-50%)	0.94	0.93	0.93
232_067	2%	1% (-53%)	1% (-57%)	1% (-58%)	0.92	0.94	0.94
Average: All	12%	10% (-30%)	11% (-23%)	11% (-22%)	0.91	0.87	0.87
Average: High BF	18%	17% (-10%)	18% (-2%)	19% (-1%)	0.93	0.81	0.81
Average: Low BF	5%	3% (-50%)	3% (-43%)	3% (-42%)	0.88	0.93	0.93

4.4.3 Spatial analysis

Figure 4.3 shows maps of scene 224/067 (with a burned fraction of 17% in the Landsat burned area product) in order to illustrate the performance of the MODIS and GFED4 products at various scales. Maps for other scenes are available in the Supplementary Material or on request. The top row shows burn scars at 500m resolution of MCD45 (left) and MCD64 (right) products; pixels where burns were identified in both Landsat and MODIS data are in red, those in Landsat only in green, and those in MODIS only in blue. The middle row shows the end-of-season Landsat 5 image (RGB composition of Bands 5, 4, and 3, obtained on 2010/09/12 ; left) and the 5km map of burned fraction from our Landsat product (right). The bottom row shows the 5km burned fraction maps for the MCD45 (left) and MCD64 (right) products. In the 500m burn scar maps, red areas showing agreement between Landsat and MODIS products predominate. However, there are a number of what appear to be understory fires (in the northwest quadrant) that were not mapped in the Landsat or MCD45 products. Such fires are notoriously hard to identify (MORTON et al., 2011), and may have been identified better from the Landsat imagery with the help of the LSMM method. Another area of disagreement is in the southeast quadrant (shown with a small arrow), where smoke and an active fire line show evidence of an ongoing fire that was partially mapped in the Landsat product. The burn scar mapped in the MCD64 product (but not in MCD45) is visible in the subsequent Landsat map of 09/28 (not shown) and is genuine, but the date attributed to the burn is too early. This explains some of the discrepancies between the products, as the date of burn attributed to the MODIS products may be offset from reality and thus could skew the evaluation.

The 5km burn fraction maps shown in Figure 4.3 (last 3 sub-figures) allow a focus on larger scale patterns rather than small scale “noise”. Particularly striking are the large burn patch to the northwest (where MCD64 shows higher burned fraction values), a V-shaped (inverted) burn pattern to the northeast, and significant burning in the southeast. These indicate that the MODIS products are well capable of capturing the spatial patterns of burn scars, with some limitations on the actual burn amount in some areas (as described above). With a focus on even larger scales, Figure 4.4 shows burned fraction at 0.25° resolution for MCD45, MCD64, Landsat and GFED4. First, we see that, as expected, MCD64 and GFED4 are nearly identical. Second, we see that the differences between both MODIS products are very small, consistent with a spatial correlation of 0.98 (Table 4.5). Third, the large relative errors in scene-averaged burned fraction of the MCD64 product are much less notable

visually than in the 500m and 5km maps, but are still present.

4.5 Discussion

In this study we evaluated the performance of two MODIS-based global burned area products in the Brazilian “arc of deforestation” during the dry season of 2010, a period with a high occurrence of fires in this region. We compared the MODIS products to burn scar maps produced from Landsat TM imagery at small (500m), intermediate (5km) and coarse (0.25°) spatial scales in 8 Landsat scenes. We found that the burned area products tend to under-estimate total burned area, but scene-averaged burned fraction is satisfactory in the scenes with high burned fraction. In scenes with low burned fraction, absolute error is small but relative errors are large.

At the native scale of the MODIS products (500m) errors in burn scar location are not ideal but are deemed acceptable, Kappa scores are better for MCD45 but burned fraction errors are less for MCD64, errors in omission are higher than errors in commission, and results are generally better for scenes with high burned fraction values. It is also noteworthy that errors in omission are likely more robust, since we are fairly confident that most burn scars identified in the Landsat maps are genuine. However, errors in commission may indicate that any of the MODIS products are correct and actual burn scars were not identified in our Landsat maps. This could be due to any of the following: (1) the long period between the Landsat maps used to generate the final burn scar maps (80 days on average, except for scene 226/070), (2) errors in the classification of the Landsat maps, particularly in forested areas subject to understory fires, and (3) errors in the date attributed to the burn scar in the MODIS products.

At coarser scales (5km and 0.25°), we find that spatial correlation is good and increases with scale, and is best for MCD45. Spatial patterns of high and low burned fraction are well represented, even if total scene-averaged burned fraction is not perfect. The MCD64 and GFED4 products perform slightly better in terms of total burn amount.

In light of these results, we conclude that, for this area and period of study (2010 in the Brazilian “arc of deforestation”), the MODIS burned area products are satisfactory at scales of 5km and above, therefore suitable for global studies. The MCD45 product has a slight advantage over MCD64, although if total burn area is of higher concern than spatial representation, the MCD64/GFED4 products are preferred. Also, as GFED products are readily available at coarse scale and also provide at-

mospheric emissions estimates, they are more accessible for global-scale climate research. We recommend extending this analysis over more extended periods of time, in order to evaluate the effects of climate variability on the performance of the MODIS global burned area products in this area. This is necessary in order to ascertain that the effects of climate extremes on burned area are captured in these burned area products, before using them to evaluate global climate model performance in the region.

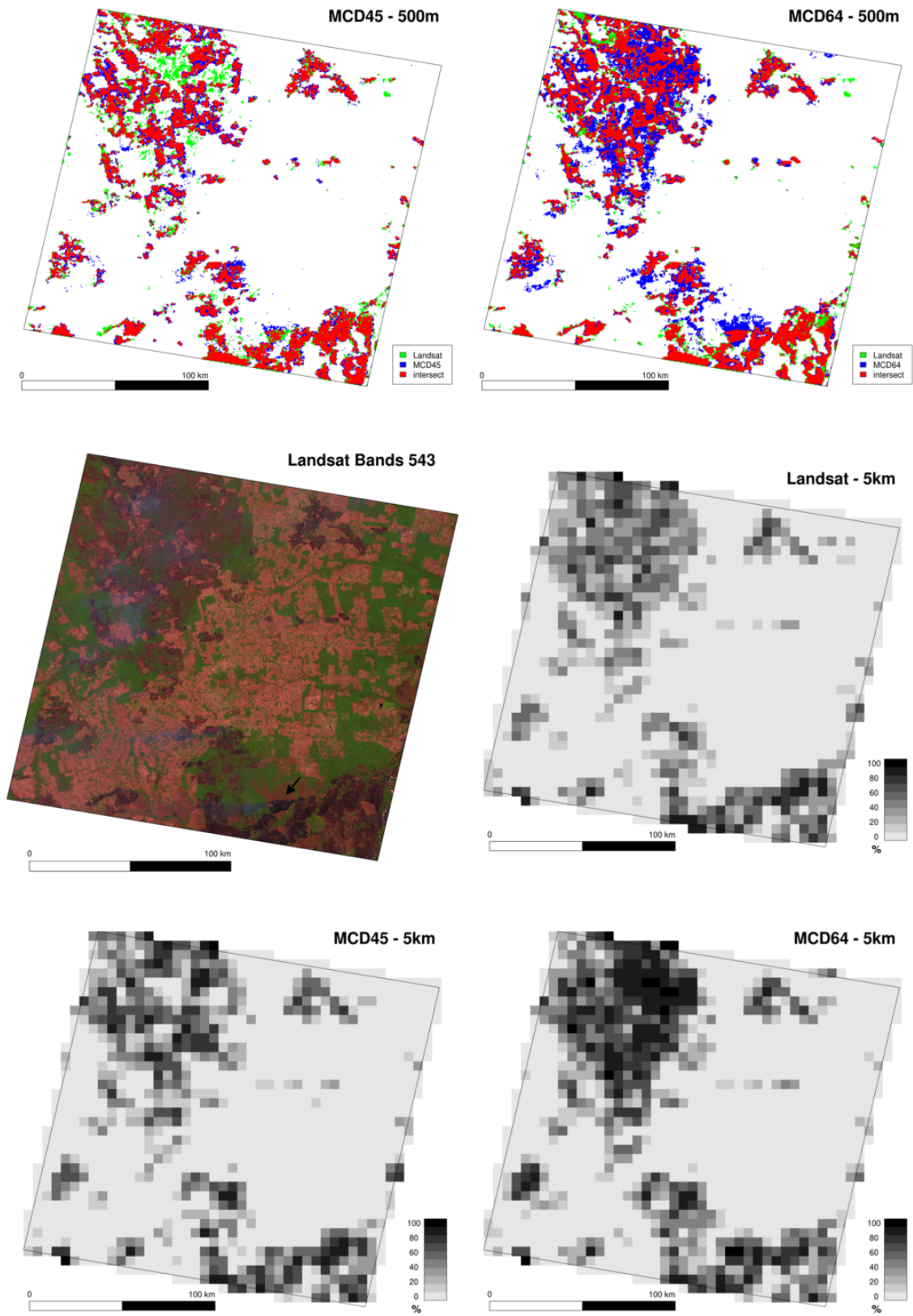


Figure 4.3 - 500m and 5km maps for scene 224/067.

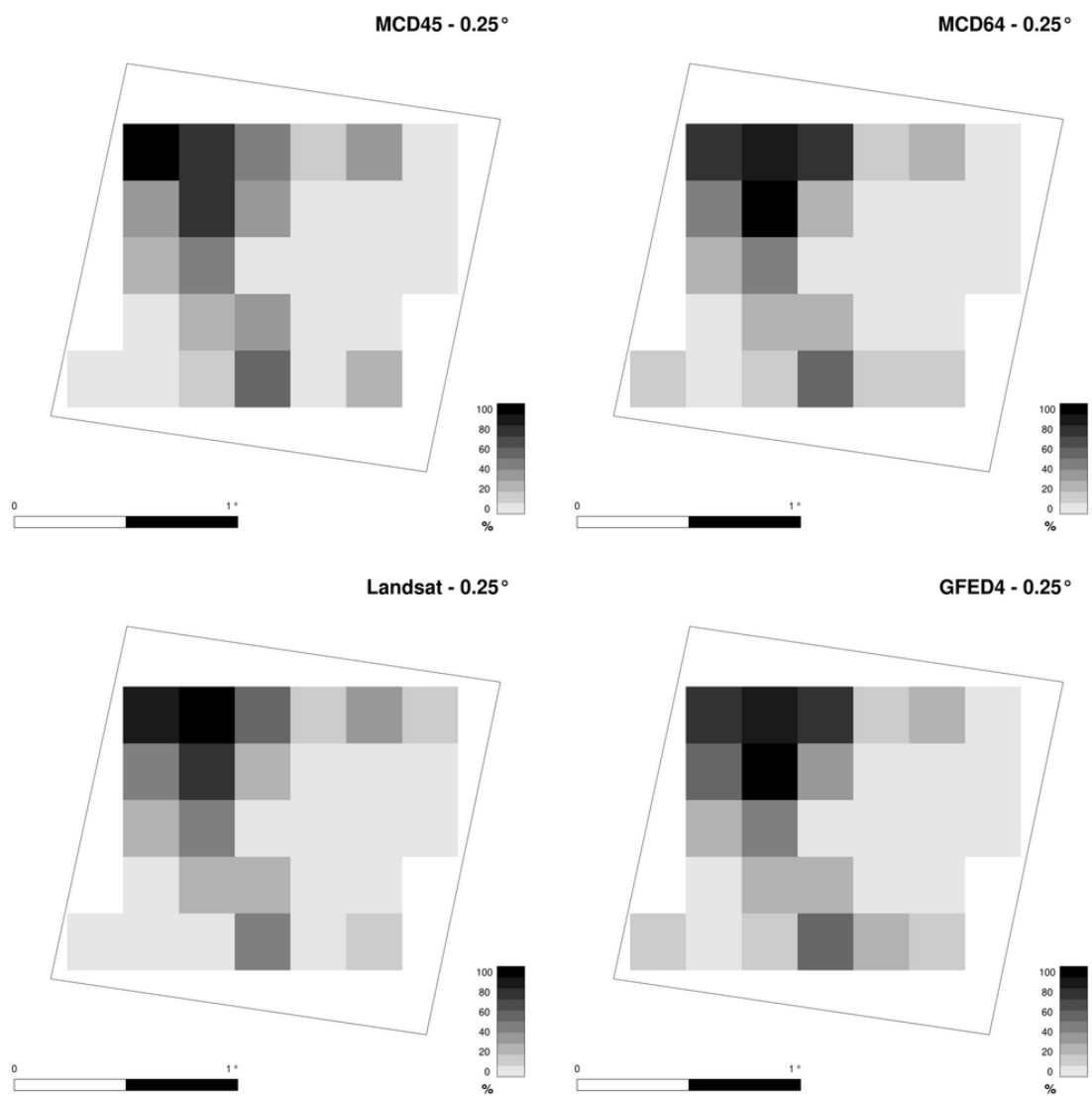


Figure 4.4 - Burned fraction maps at 0.25° resolution for all products, scene 224/067.

5 CONCLUSION

The primary goal of this work was to represent fire spread in a DGVM across fragmented landscapes in the Brazilian “arc of deforestation”. As DGVMs cannot, by design, represent any detailed spatial structure, a means was devised to overcome this limitation. The strategy employed was to implement *subgrid tiling* inside the INLAND DGVM and create a multi-scale framework to bridge the gap between the coarse scale of the DGVM and the fine-scale of the detailed landscape. This work has shown that representing fine scale details is possible, with much less computational cost than increasing model resolution. Further work is needed in order to parametrize the new land use types included inside the model (e.g. pasture, urban).

Fire spread across the landscape is simulated using a simple custom fire spread model coupled to the INLAND DGVM using this framework. Sensitivity studies have shown the potential of such an approach, which allows to explore different fire spread scenarios in different spatial configurations. It has been shown that the model is responsive to changes in parameters and is very sensitive to landscape structure and fragmentation. However, it must be improved in order to make use of the biophysical (e.g. soil moisture, VPD) and vegetation properties (e.g. litter, LAI) simulated by the DGVM. This work has investigated the down-scaling of a DGVM to the fine scale fire spread processes, further research and implementation are needed to up-scale fire spread to the coarse scale of DGVMs and ESMs.

Finally, this work has evaluated global burned area products in the Brazilian “arc of deforestation” during a year with high fire occurrence (2010). It was demonstrated that these products represent well the amount and broad spatial structure of burned area. While they are by no means perfect and not suitable for detailed local-scale studies, they are sufficiently reliable for climate-scale studies. It therefore seems reasonable to use them as calibration and validation tools for studies using the modeling framework developed in this work. However, in order to ascertain that these models also respond well to climatic variations, it would be advisable to study their reliability in other years with less fire occurrence.

The following topics are suggested to improve and make use of subgrid tiling and the multi-scale framework in INLAND:

- research pasture and other new land use *vegtype* parameterizations
- represent past and projected land use transitions as natural and deforested

tiles with varying tile fractions

- prepare and validate a global high-resolution land cover dataset
- improve the PROVEG dataset to make it suitable for local-scale studies

The following improvements and studies are suggested for the firespread module:

- improve the fire spread algorithm by using the 8-cell Moore neighborhood instead of the 5-cell von Neumann
- identify and calibrate the important biophysical parameters to drive the fire behavior module
- implement and calibrate a LUCC component to the ignitions module
- up-scale the fire spread processes to the DGVM
- perform climate-change studies to investigate the relationships between LUCC, climate and fire

And finally the following suggestions apply to burned area product validations:

- extend the study to other years in order to ascertain the reliability of the products in function of climate variability
- perform a similar study in the *cerrado* biome

REFERENCES

- ALBINI, F. A. **Estimating wildfire behavior and effects**. Ogden, UT, 1976. 92 p. (Gen. Tech. Rep., INT-GTR-30). Available from: <<http://www.treesearch.fs.fed.us/pubs/29574>>. Access in: 2014-04-11. 39, 41
- ALENCAR, A.; NEPSTAD, D.; DIAZ, M. C. V. Forest understory fire in the brazilian amazon in ENSO and non-ENSO years: Area burned and committed carbon emissions. **Earth Interactions**, v. 10, n. 6, p. 1–17, 2006. Available from: <<http://dx.doi.org/10.1175/EI150.1>>. Access in: 2014-06-25. 47
- ALENCAR, A. A. C.; SOLÓRZANO, L. A.; NEPSTAD, D. C. MODELING FOREST UNDERSTORY FIRES IN AN EASTERN AMAZONIAN LANDSCAPE. **Ecological Applications**, v. 14, n. sp4, p. 139–149, 2004. ISSN 1051-0761. Available from: <<http://dx.doi.org/10.1890/01-6029>>. Access in: 2010-12-02. 48
- ALMEIDA, C. A. d.; PINHEIRO, T. F.; BARBOSA, A. M.; ABREU, M. R. B. S. d.; LOBO, F. d. L.; SILVA, M.; GOMES, A. R.; SADECK, L. W. R.; MEDEIROS, L. T. B. d.; NEVES, M. F.; SILVA, L. d. C. T. d.; TAMASAUSKAS, P. F. L. F. **Metodologia para mapeamento de vegetação secundária na Amazônia Legal**. São José dos Campos, 2009. 32 p. Available from: <<http://urlib.net/8JMKD3MGP7W/36F3Q92>>. Access in: 2014-06-25. 25
- ALMEIDA, R. M. **Modelagem da propagação do fogo como ferramenta de auxílio à tomada de decisão no combate e prevenção de incêndios no Parque Nacional das Emas, GO**. PhD Thesis (Tese de Doutorado em Computação Aplicada) — Instituto Nacional de Pesquisas Espaciais, São José dos Campos, 2012. Available from: <<http://urlib.net/8JMKD3MGP7W/3CTKFU8>>. Access in: 2014-06-25. 48
- ANDERSON, D. H.; CATCHPOLE, E. A.; MESTRE, N. J. D.; PARKES, T. Modelling the spread of grass fires. **The Journal of the Australian Mathematical Society. Series B. Applied Mathematics**, v. 23, n. 04, p. 451–466, 1982. Available from: <<http://dx.doi.org/10.1017/S0334270000000394>>. Access in: 2014-06-25. 43
- ANDREWS, P. L. **BEHAVE**: fire behavior prediction and fuel modeling system-BURN subsystem, part 1. Ogden, UT, 1986. 130 p. (Gen. Tech. Rep.,

INT-194). Available from: <<http://www.treesearch.fs.fed.us/pubs/29612>>. Access in: 2014-04-11. 42

ARAGÃO, L. E. O. C.; MALHI, Y.; ROMAN-CUESTA, R. M.; SAATCHI, S.; ANDERSON, L. O.; SHIMABUKURO, Y. E. Spatial patterns and fire response of recent amazonian droughts. **Geophys. Res. Lett.**, v. 34, n. 7, p. L07701, 2007. ISSN 0094-8276. Available from: <<http://dx.doi.org/10.1029/2006GL028946>>. Access in: 2014-06-25. 2, 47, 77

ARINO, O.; BICHERON, P.; ACHARD, F.; LATHAM, J.; WITT, R.; WEBER, J.-L. The most detailed portrait of earth. **ESA Bulletin**, v. 136, p. 25–31, 2008. Available from: <<https://earth.esa.int/web/guest/-/globcover-the-most-detailed-portrait-of-earth-5910>>. Access in: 2014-06-25. 23

ARORA, V. K.; BOER, G. J. Fire as an interactive component of dynamic vegetation models. **J. Geophys. Res.**, v. 110, n. G2, 2005. ISSN 0148-0227. Available from: <<http://dx.doi.org/10.1029/2005JG000042>>. Access in: 2014-06-25. 10, 15, 77

BACHELET, D.; LENIHAN, J. M.; DALY, C.; NEILSON, R. P.; OJIMA, D. S.; PARTON, W. J. **MC1: a dynamic vegetation model for estimating the distribution of vegetation and associated ecosystem fluxes of carbon, nutrients, and water**. Portland, OR, 2001. 95 p. (Gen. Tech. Rep., PNW-GTR-508). Available from: <<http://www.treesearch.fs.fed.us/pubs/2923>>. Access in: 2014-06-25. 12

BALCH, J.; NEPSTAD, D.; CURRAN, L. Pattern and process: Fire-initiated grass invasion at amazon transitional forest edges. In: COCHRANE, M. A. (Ed.). **Tropical fire ecology**. Springer Berlin Heidelberg, 2009, (Springer Praxis Books). Available from: <http://dx.doi.org/10.1007/978-3-540-77381-8_17>. Access in: 2014-06-25. 47

BALCH, J. K.; NEPSTAD, D. C.; BRANDO, P. M.; CURRAN, L. M.; PORTELA, O.; CARVALHO, O. D.; LEFEBVRE, P. Negative fire feedback in a transitional forest of southeastern amazonia. **Global Change Biology**, v. 14, p. 2276–2287, 2008. Available from: <<http://dx.doi.org/10.1111/j.1365-2486.2008.01655.x>>. Access in: 2010-05-07. 47

BALCH, J. K.; NEPSTAD, D. C.; CURRAN, L. M.; BRANDO, P. M.; PORTELA, O.; GUILHERME, P.; REUNING-SCHERER, J. D.; JR., O. de C. Size, species, and fire behavior predict tree and liana mortality from experimental burns in the brazilian amazon. **Forest Ecology and Management**, v. 261, n. 1, p. 68–77, 2011. Available from: <<http://dx.doi.org/10.1016/j.foreco.2010.09.029>>. Access in: 2014-07-16. 47

BARLOW, J.; PERES, C. A. Fire-mediated dieback and compositional cascade in an amazonian forest. **Philosophical Transactions of the Royal Society B: Biological Sciences**, v. 363, n. 1498, p. 1787–1794, 2008. Available from: <<http://dx.doi.org/10.1098/rstb.2007.0013>>. Access in: 2014-06-25. 1, 47, 77

BARTHOLOMÉ, E.; BELWARD, A. S. GLC2000: a new approach to global land cover mapping from earth observation data. **International Journal of Remote Sensing**, v. 26, n. 9, p. 1959–1977, 2005. ISSN 0143-1161. Available from: <<http://dx.doi.org/10.1080/01431160412331291297>>. Access in: 2014-04-18. 23

BERJAK, S. G.; HEARNE, J. W. An improved cellular automaton model for simulating fire in a spatially heterogeneous savanna system. **Ecological Modelling**, v. 148, n. 2, p. 133–151, 2002. ISSN 0304-3800. Available from: <[http://dx.doi.org/10.1016/S0304-3800\(01\)00423-9](http://dx.doi.org/10.1016/S0304-3800(01)00423-9)>. Access in: 2014-06-25. 46, 54, 55

BONAN, G. B.; LEVIS, S.; KERGOAT, L.; OLESON, K. W. Landscapes as patches of plant functional types: An integrating concept for climate and ecosystem models. **Global Biogeochem. Cycles**, v. 16, 2002. Available from: <<http://dx.doi.org/10.1029/2000GB001360>>. Access in: 2014-06-25. 16

BOND, W. J.; KEELEY, J. E. Fire as a global 'herbivore': the ecology and evolution of flammable ecosystems. **Trends in Ecology & Evolution**, v. 20, n. 7, p. 387–394, jul. 2005. ISSN 0169-5347. Available from: <<http://www.sciencedirect.com/science/article/B6VJ1-4G39H6X-1/2/85762a1f2f3a5209a0aa94361bac12fc>>. Access in: 2014-06-25. 1, 2

BONTEMPS, S.; DEFOURNY, P.; BOGAERT, E. V.; ARINO, O.; KALOGIROU, V.; PEREZ, J. R. **GLOBCOVER 2009 products description and validation report**. [S.l.], 2011. Available from: <<http://due.esrin.esa.int/globcover/>>. Access in: 2014-06-25. 23

BOTTA, A.; RAMANKUTTY, N.; FOLEY, J. A. Long-term variations of climate and carbon fluxes over the amazon basin. **Geophysical Research Letters**, v. 29, p. 4 PP., 2002. Available from:

<<http://dx.doi.org/200210.1029/2001GL013607>>. Access in: 2010-05-15. 14

BOWMAN, D. M. J. S.; BALCH, J. K.; ARTAXO, P.; BOND, W. J.; CARLSON, J. M.; COCHRANE, M. A.; D'Antonio, C. M.; DeFries, R. S.; DOYLE, J. C.; HARRISON, S. P.; JOHNSTON, F. H.; KEELEY, J. E.; KRAWCHUK, M. A.; KULL, C. A.; MARSTON, J. B.; MORITZ, M. A.; PRENTICE, I. C.; ROOS, C. I.; SCOTT, A. C.; SWETNAM, T. W.; WERF, G. R. van der; PYNE, S. J. Fire in the earth system. **Science**, v. 324, n. 5926, p. 481–484, 2009. Available from:

<<http://dx.doi.org/10.1126/science.1163886>>. Access in: 2014-06-25. 77

BRANDO, P. M.; BALCH, J. K.; NEPSTAD, D. C.; MORTON, D. C.; PUTZ, F. E.; COE, M. T.; SILVÉRIO, D.; MACEDO, M. N.; DAVIDSON, E. A.; NÓBREGA, C. C.; ALENCAR, A.; SOARES-FILHO, B. S. Abrupt increases in amazonian tree mortality due to drought–fire interactions. **Proceedings of the National Academy of Sciences**, p. 201305499, 2014. Available from:

<<http://dx.doi.org/10.1073/pnas.1305499111>>. Access in: 2014-07-16. 1, 47

BRANDO, P. M.; NEPSTAD, D. C.; BALCH, J. K.; BOLKER, B.; CHRISTMAN, M. C.; COE, M.; PUTZ, F. E. Fire-induced tree mortality in a neotropical forest: the roles of bark traits, tree size, wood density and fire behavior. **Global Change Biology**, v. 18, n. 2, p. 630–641, 2012. Available from:

<<http://dx.doi.org/10.1111/j.1365-2486.2011.02533.x>>. Access in: 2014-07-16. 47

BURGAN, R. E. **1988 revisions to the 1978 national fire-danger rating system**. Asheville, NC, 1988. 144 p. (Res. Pap., SE-273). Available from:

<<http://www.treesearch.fs.fed.us/pubs/593>>. Access in: 2014-06-25. 42

CÂMARA, G.; SOUZA, R. C. M.; FREITAS, U. M.; GARRIDO, J. Spring: Integrating remote sensing and gis by object-oriented data modelling. **Computers & Graphics**, v. 20, n. 3, p. 395–403, 1996. ISSN 0097-8493. Available from:

<[http://dx.doi.org/10.1016/0097-8493\(96\)00008-8](http://dx.doi.org/10.1016/0097-8493(96)00008-8)>. Access in: 2014-02-19. 79

CARAPIÁ, V. **Predição do índice de risco de incêndio e modelagem computacional do comportamento do avanço da frente do fogo no Parque Nacional da Floresta da Tijuca**. PhD Thesis (PhD) — Universidade Federal do Rio de Janeiro, Rio de Janeiro, 2006. 48

CARDOSO, M.; NOBRE, C.; SAMPAIO, G.; HIROTA, M.; VALERIANO, D.; CÂMARA, G. Long-term potential for tropical-forest degradation due to deforestation and fires in the brazilian amazon. **Biologia**, v. 64, n. 3, p. 433–437, jun. 2009. Available from: <<http://dx.doi.org/10.2478/s11756-009-0076-9>>. Access in: 2014-06-25. 2

CARDOSO, M. F.; HURTT, G. C.; III, B. M.; NOBRE, C. A.; PRINS, E. M. Projecting future fire activity in amazonia. **Global Change Biology**, v. 9, n. 5, p. 656–669, 2003. Available from: <<http://dx.doi.org/10.1046/j.1365-2486.2003.00607.x>>. Access in: 2014-06-25. 11

CARDOSO, M. F.; NOBRE, C. A.; LAPOLA, D. M.; OYAMA, M. D.; SAMPAIO, G. Long-term potential for fires in estimates of the occurrence of savannas in the tropics. **Global Ecology and Biogeography**, v. 17, n. 2, p. 222–235, 2008. Available from: <<http://dx.doi.org/10.1111/j.1466-8238.2007.00356.x>>. Access in: 2014-06-25. 77

CARVALHO, J. A.; VERAS, C. A. G.; ALVARADO, E. C.; SANDBERG, D. V.; LEITE, S. J.; GIELOW, R.; RABELO, E. R. C.; SANTOS, J. C. Understorey fire propagation and tree mortality on adjacent areas to an amazonian deforestation fire. **Int. J. Wildland Fire**, v. 19, n. 6, p. 795–799, 2010. Available from: <<http://dx.doi.org/10.1071/WF08047>>. Access in: 2010-09-17. 47

CARVALHO, J. A. d.; VERAS, C. A. G.; ALAVARADO, E.; SANDBERG, D. V.; CARVALHO, E. R.; GIELOW, R.; SANTOS, J. C. Fire spread around a forest clearing site in the brazilian amazon region. In: INTERNATIONAL WILDLAND FIRE ECOLOGY AND FIRE MANAGEMENT CONGRESS, 2., 2003, Orlando. **Proceedings...** Orlando: AMS, 2003. 47

CASTRO, E. A. D.; KAUFFMAN, J. B. Ecosystem structure in the brazilian cerrado: A vegetation gradient of aboveground biomass, root mass and consumption by fire. **Journal of Tropical Ecology**, v. 14, n. 03, p. 263–283, 1998. Available from: <<http://dx.doi.org/10.1017/S0266467498000212>>. Access in: 2010-07-22. 48

CLARK, T.; COEN, J.; LATHAM, D. Description of a coupled atmosphere–fire model. **Int. J. Wildland Fire**, v. 13, n. 1, p. 49–63, 2004. Available from: <<http://dx.doi.org/10.1071/WF03043>>. Access in: 2010-11-30. 43

CLAUSSEN, M.; MYSAK, L.; WEAVER, A.; CRUCIFIX, M.; FICHEFET, T.; LOUTRE, M.-F.; WEBER, S.; ALCAMO, J.; ALEXEEV, V.; BERGER, A.; CALOV, R.; GANOPOLSKI, A.; GOOSSE, H.; LOHMANN, G.; LUNKEIT, F.; MOKHOV, I.; PETOUKHOV, V.; STONE, P.; WANG, Z. Earth system models of intermediate complexity: closing the gap in the spectrum of climate system models. **Climate Dynamics**, v. 18, n. 7, p. 579–586, 2002. Available from: <<http://dx.doi.org/10.1007/s00382-001-0200-1>>. Access in: 2010-05-16. 7

COCHRANE, M. (Ed.). **Tropical fire ecology: climate change, land use and ecosystem dynamics**. 1. ed. Springer, 2009. (Springer Praxis Books). ISBN 978-3-540-77381-8. Available from: <<http://www.springer.com/life+sciences/ecology/book/978-3-540-77380-1>>. Access in: 2010-07-04. 47, 48, 77

COCHRANE, M. A. Fire science for rainforests. **Nature**, v. 421, n. 6926, p. 913–919, 2003. ISSN 0028-0836. Available from: <<http://dx.doi.org/10.1038/nature01437>>. Access in: 2014-06-25. 1, 77

COCHRANE, M. A.; ALENCAR, A.; SCHULZE, M. D.; SOUZA, C. M.; NEPSTAD, D. C.; LEFEBVRE, P.; DAVIDSON, E. A. Positive feedbacks in the fire dynamic of closed canopy tropical forests. **Science**, v. 284, n. 5421, p. 1832–1835, 1999. Available from: <<http://dx.doi.org/10.1126/science.284.5421.1832>>. Access in: 2010-05-15. 47

COCHRANE, M. A.; LAURANCE, W. F. Synergisms among fire, land use, and climate change in the amazon. **AMBIO: A Journal of the Human Environment**, v. 37, n. 7, p. 522–527, 2008. ISSN 0044-7447. Available from: <<http://dx.doi.org/10.1579/0044-7447-37.7.522>>. Access in: 2014-06-25. 77

COE, M. T.; COSTA, M. H.; HOWARD, E. A. Simulating the surface waters of the amazon river basin: impacts of new river geomorphic and flow parameterizations. **Hydrological Processes**, v. 22, n. 14, p. 2542–2553, 2008. ISSN 1099-1085. Available from: <<http://dx.doi.org/10.1002/hyp.6850>>. Access in: 2014-04-16. 16

COE, M. T.; COSTA, M. H.; SOARES-FILHO, B. S. The influence of historical and potential future deforestation on the stream flow of the amazon river - land surface processes and atmospheric feedbacks. **Journal of Hydrology**, v. 369, n. 1-2, p. 165–174, 2009. ISSN 0022-1694. Available from:

<<http://dx.doi.org/10.1016/j.jhydrol.2009.02.043>>. Access in: 2014-06-25. 14

COEN, J. L.; CAMERON, M.; MICHALAKES, J.; PATTON, E. G.; RIGGAN, P. J.; YEDINAK, K. M. WRF-Fire: coupled weather–wildland fire modeling with the weather research and forecasting model. **Journal of Applied Meteorology and Climatology**, v. 52, n. 1, p. 16–38, 2012. ISSN 1558-8424. Available from: <<http://journals.ametsoc.org/doi/abs/10.1175/JAMC-D-12-023.1>>. Access in: 2014-04-24. 43

CONGALTON, R. G.; GREEN, K. **Assessing the accuracy of remotely sensed data: principles and practices**. New York: Lewis Publishers, 1999. 82

COSTA, M. H.; FOLEY, J. A. Combined effects of deforestation and doubled atmospheric CO₂ concentrations on the climate of amazonia. **J. Climate**, v. 13, n. 1, p. 18–34, 2000. ISSN 0894-8755. Available from: <[http://dx.doi.org/10.1175/1520-0442\(2000\)013<0018:CEODAD>2.0.CO;2](http://dx.doi.org/10.1175/1520-0442(2000)013<0018:CEODAD>2.0.CO;2)>. Access in: 2014-06-25. 14

COSTA, M. H.; NUNES, E. L.; SENNA, M. C. A.; IMBUZEIRO, H. M. A. Estado-da-arte da simulação da taxa de fixação de carbono de ecossistemas tropicais. **Revista Brasileira de Meteorologia**, v. 24, n. 2, p. 179–187, jun. 2009. ISSN 0102-7786. Available from: <<http://dx.doi.org/10.1590/S0102-77862009000200007>>. Access in: 2014-06-11. 15

COSTA, M. H.; PIRES, G. F. Effects of amazon and central brazil deforestation scenarios on the duration of the dry season in the arc of deforestation. **International Journal of Climatology**, v. 30, n. 13, p. 1970–1979, 2010. ISSN 1097-0088. Available from: <<http://dx.doi.org/10.1002/joc.2048>>. Access in: 2014-06-25. 14

COX, P. M. **Description of the TRIFFID dynamic global vegetation model**. London Road, Bracknell, Berks, RG122SY, UK, 2001. (Technical note, 24). 10

COX, P. M.; BETTS, R. A.; COLLINS, M.; HARRIS, P. P.; HUNTINGFORD, C.; JONES, C. D. Amazonian forest dieback under climate-carbon cycle projections for the 21st century. **Theoretical and Applied Climatology**, v. 78, n. 1, p. 137–156, jun. 2004. Available from: <<http://dx.doi.org/10.1007/s00704-004-0049-4>>. Access in: 2009-05-13. 1, 2

DEARDORFF, J. W. Efficient prediction of ground surface temperature and moisture, with inclusion of a layer of vegetation. **Journal of Geophysical Research**, v. 83, n. C4, p. 1889–1903, 1978. Available from: <<http://dx.doi.org/197810.1029/JC083iC04p01889>>. Access in: 2010-05-13. 8

DICKINSON, R. E. Modeling evapotranspiration for three-dimensional global climate models. In: HANSEN, J. E.; TAKAHASHI, T. (Ed.). **Geophysical Monograph Series**. Washington, D. C.: American Geophysical Union, 1984. v. 29, p. 58–72. ISBN 0-87590-404-1. Available from: <<http://dx.doi.org/10.1029/GM029p0058>>. Access in: 2014-04-11. 8

DICKINSON, R. E.; HENDERSON-SELLERS, A.; KENNEDY, P. J.; WILSON, M. F. **Biosphere-Atmosphere Transfer Scheme(BATS) for the NCAR community climate model**. [S.l.], 1986. Available from: <<http://dx.doi.org/10.5065/D6668B58>>. Access in: 2014-06-25. 8

DICKINSON, R. E.; SHAIKH, M.; BRYANT, R.; GRAUMLICH, L. Interactive canopies for a climate model. **Journal of Climate**, v. 11, n. 11, p. 2823–2836, 1998. Available from: <[http://dx.doi.org/10.1175/1520-0442\(1998\)011<2823:ICFACM>2.0.CO;2](http://dx.doi.org/10.1175/1520-0442(1998)011<2823:ICFACM>2.0.CO;2)>. Access in: 2014-06-25. 9

DORMAN, J. L.; SELLERS, P. J. A global climatology of albedo, roughness length and stomatal resistance for atmospheric general circulation models as represented by the simple biosphere model (SiB). **Journal of Applied Meteorology**, v. 28, n. 9, p. 833–855, 1989. Available from: <[http://dx.doi.org/10.1175/1520-0450\(1989\)028<0833:AGCOAR>2.0.CO;2](http://dx.doi.org/10.1175/1520-0450(1989)028<0833:AGCOAR>2.0.CO;2)>. Access in: 2014-07-17. 23

FARQUHAR, G. D.; CAEMMERER, S.; BERRY, J. A. A biochemical model of photosynthetic CO₂ assimilation in leaves of c₃ species. **Planta**, v. 149, n. 1, p. 78–90, 1980. Available from: <<http://dx.doi.org/10.1007/BF00386231>>. Access in: 2010-05-13. 9

FEARNSIDE, P. H. M. Deforestation in brazilian amazonia: History, rates, and consequences. **Conservation Biology**, v. 19, n. 3, p. 680–688, 2005. Available from: <<http://dx.doi.org/10.1111/j.1523-1739.2005.00697.x>>. Access in: 2014-06-25. 1

FERNANDES, G. D. D. A. **Simulação de incêndio florestal no Parque Estadual Serra do Rola-Moça, Minas Gerais, utilizando o FARSITE**.

Master Thesis (Mestrado) — Universidade Federal de Viçosa, Viçosa, Minas Gerais – Brasil, 2003. Available from:
<<http://www.bibliotecaflorestal.ufv.br/handle/123456789/2432>>. Access in: 2014-07-17. 49

FERREIRA, N. C.; FERREIRA, L. G.; HUETE, A. R.; FERREIRA, M. E. An operational deforestation mapping system using MODIS - data and spatial context analysis. **International Journal of Remote Sensing**, v. 28, n. 1, p. 47, 2007. ISSN 0143-1161. Available from:
<<http://www.informaworld.com/10.1080/01431160600835861>>. Access in: 2010-12-05. 24

FINNEY, M. Fire growth using minimum travel time methods. **Canadian Journal of Forest Research**, v. 32, p. 1420–1424, 2002. Available from:
<<http://dx.doi.org/10.1139/X02-068>>. Access in: 2014-06-25. 44, 45

FINNEY, M. A. **FARSITE**: fire area simulator—model development and evaluation. Ogden, UT, 2004. 47 p. (Res. Pap., RMRS-RP-4). Available from:
<<http://www.treearch.fs.fed.us/pubs/4617>>. Access in: 2014-06-25. 43, 44

FINNEY, M. A.; GRENFELL, I. C.; McHugh, C. W.; SELI, R. C.; TRETHERWEY, D.; STRATTON, R. D.; BRITTAIN, S. A method for ensemble wildland fire simulation. **Environmental Modeling & Assessment**, 2010. ISSN 1420-2026. Available from:
<<http://dx.doi.org/10.1007/s10666-010-9241-3>>. Access in: 2010-12-03. 45

FOLEY, J. A.; LEVIS, S.; PRENTICE, I. C.; POLLARD, D.; THOMPSON, S. L. Coupling dynamic models of climate and vegetation. **Global Change Biology**, v. 4, n. 5, p. 561–579, 1998. Available from:
<<http://dx.doi.org/10.1046/j.1365-2486.1998.t01-1-00168.x>>. Access in: 2009-06-04. 12

FOLEY, J. A.; PRENTICE, I. C.; RAMANKUTTY, N.; LEVIS, S.; POLLARD, D.; SITCH, S.; HAXELTINE, A. An integrated biosphere model of land surface processes, terrestrial carbon balance, and vegetation dynamics. **Global Biogeochem. Cycles**, v. 10, 1996. Available from:
<<http://dx.doi.org/10.1029/96GB02692>>. Access in: 2014-06-25. 10, 12

FORESTRY CANADA FIRE DANGER GROUP. **Development and structure of the Canadian Forest Fire Behavior Prediction System**. Ottawa, ON, 1992. 64 p. (Information Report, ST-X-3). Available from:

<<https://cfs.nrcan.gc.ca/publications?id=10068>>. Access in: 2014-06-25.
39

FRANÇA, H.; NETO, M. B. R.; SETZER, A. **O fogo no Parque Nacional das Emas.** [S.l.], 2007. 140 p. 49

FRIEDL, M. A.; SULLA-MENASHE, D.; TAN, B.; SCHNEIDER, A.; RAMANKUTTY, N.; SIBLEY, A.; HUANG, X. MODIS collection 5 global land cover: Algorithm refinements and characterization of new datasets. **Remote Sensing of Environment**, v. 114, n. 1, p. 168–182, jan. 2010. ISSN 0034-4257. Known issues:

http://daac.ornl.gov/MODIS/MODIS-menu/MCD12Q1_known_issues.html. Available from: <<http://dx.doi.org/10.1016/j.rse.2009.08.016>>. Access in: 2014-04-18. 23

FURLEY, P. A. The nature and diversity of neotropical savanna vegetation with particular reference to the brazilian cerrados. **Global Ecology and Biogeography**, v. 8, n. 3-4, p. 223–241, 1999. ISSN 1466-822X. Available from: <<http://dx.doi.org/10.1046/j.1466-822X.1999.00142.x>>. Access in: 2010-08-24. 2

GDAL. **GDAL - Geospatial Data Abstraction Library.** Open Source Geospatial Foundation, 2013. Available from: <<http://gdal.osgeo.org>>. Access in: 2014-06-25. 81, 82, 83

GIGLIO, L.; CSISZAR, I.; JUSTICE, C. O. Global distribution and seasonality of active fires as observed with the terra and aqua moderate resolution imaging spectroradiometer (MODIS) sensors. **Journal of Geophysical Research**, v. 111, p. G02016, jun. 2006. Available from: <<http://dx.doi.org/10.1029/2005JG000142>>. Access in: 2010-08-05. 5

GIGLIO, L.; LOBODA, T.; ROY, D. P.; QUAYLE, B.; JUSTICE, C. O. An active-fire based burned area mapping algorithm for the MODIS sensor. **Remote Sensing of Environment**, v. 113, n. 2, p. 408–420, 2009. ISSN 0034-4257. Available from: <<http://dx.doi.org/10.1016/j.rse.2008.10.006>>. Access in: 2010-09-29. 5, 77, 78, 81

GIGLIO, L.; RANDERSON, J. T.; WERF, G. R. van der. Analysis of daily, monthly, and annual burned area using the fourth-generation global fire emissions database (GFED4). **Journal of Geophysical Research: Biogeosciences**,

v. 118, n. 1, p. 317–328, 2013. ISSN 2169-8961. Available from:

<<http://dx.doi.org/10.1002/jgrg.20042>>. Access in: 2014-02-06. 6, 81

GIGLIO, L.; RANDERSON, J. T.; WERF, G. R. van der; KASIBHATLA, P. S.; COLLATZ, G. J.; MORTON, D. C.; DeFries, R. S. Assessing variability and long-term trends in burned area by merging multiple satellite fire products.

Biogeosciences, v. 7, n. 3, p. 1171–1186, 2010. ISSN 1726-4170. Available from:

<<http://dx.doi.org/10.5194/bg-7-1171-2010>>. Access in: 2010-09-16. 5, 81

GOCHIS, D. **Advancing Coupled Land-Atmosphere Prediction**. Boulder, CO: [s.n.], nov. 2004. Available from:

<<http://www.cuahsi.org/PageFiles/VisionPapers/Gochis-20041201.pdf>>.

Access in: 2014-06-25. 9

HAGEN, A. Multi-method assessment of map similarity. In: AGILE CONFERENCE ON GEOGRAPHIC INFORMATION SCIENCE, 5., 2002, Palma (Illes Balears). **Proceedings...** Palma: Universitat de les Illes Balears Palma, 2002. p. 171–182. 82

HANSEN, M. C.; DEFRIES, R. S.; TOWNSHEND, J. R. G.; SOHLBERG, R. Global land cover classification at 1 km spatial resolution using a classification tree approach. **International Journal of Remote Sensing**, v. 21, n. 6, p. 1331, 2000. ISSN 0143-1161. Available from:

<<http://www.informaworld.com/10.1080/014311600210209>>. Access in: 2010-06-07. 23

HANSEN, M. C.; STEHMAN, S. V.; POTAPOV, P. V.; LOVELAND, T. R.; TOWNSHEND, J. R. G.; DeFries, R. S.; PITTMAN, K. W.; ARUNARWATI, B.; STOLLE, F.; STEININGER, M. K.; CARROLL, M.; DiMicelli, C. Humid tropical forest clearing from 2000 to 2005 quantified by using multitemporal and multiresolution remotely sensed data. **Proceedings of the National Academy of Sciences**, v. 105, n. 27, p. 9439–9444, jun. 2008. ISSN 0027-8424. Available from:

<<http://www.pnas.org/content/early/2008/06/27/0804042105.abstract>>. Access in: 2010-05-12. 1

HARGROVE, W. W.; GARDNER, R. H.; TURNER, M. G.; ROMME, W. H.; DESPAIN, D. G. Simulating fire patterns in heterogeneous landscapes. **Ecological Modelling**, v. 135, n. 2-3, p. 243–263, 2000. ISSN 0304-3800. Available from:

<[http://dx.doi.org/10.1016/S0304-3800\(00\)00368-9](http://dx.doi.org/10.1016/S0304-3800(00)00368-9)>. Access in: 2014-06-25. 45, 46, 48, 52

HE, H. S. Forest landscape models: Definitions, characterization, and classification. **Forest Ecology and Management**, v. 254, n. 3, p. 484–498, 2008. ISSN 0378-1127. Available from: <<http://dx.doi.org/10.1016/j.foreco.2007.08.022>>. Access in: 2014-06-25. 12

HEINSCH, F. A.; ANDREWS, P. L. **BehavePlus fire modeling system, version 5.0: Design and Features**. Fort Collins, CO, 2010. 111 p. (Gen. Tech. Rep., RMRS-GTR-249). Available from: <<http://www.treesearch.fs.fed.us/pubs/36989>>. Access in: 2014-06-25. 42

HOFFMANN, W. A.; ORTHEN, B.; NASCIMENTO, P. K. V. d. Comparative fire ecology of tropical savanna and forest trees. **Functional Ecology**, v. 17, n. 6, p. 720–726, 2003. Available from: <<http://dx.doi.org/10.1111/j.1365-2435.2003.00796.x>>. Access in: 2010-04-30. 2

HOLDSWORTH, A. R.; UHL, C. FIRE IN AMAZONIAN SELECTIVELY LOGGED RAIN FOREST AND THE POTENTIAL FOR FIRE REDUCTION. **Ecological Applications**, v. 7, n. 2, p. 713–725, 1997. Available from: <[http://dx.doi.org/10.1890/1051-0761\(1997\)007\[0713:FIASLR\]2.0.CO;2](http://dx.doi.org/10.1890/1051-0761(1997)007[0713:FIASLR]2.0.CO;2)>. Access in: 2014-06-25. 47

IBGE. **Manual Técnico da Vegetação Brasileira**. Rio de Janeiro, 1992. 92 p. (Manuais técnicos em geociências, 1). 23

_____. **Projeto sistematização das informações sobre recursos naturais documentação técnica**. [S.l.], 2006. Available from: <ftp://geoftp.ibge.gov.br/mapeamento_sistematico/banco_dados_georeferenciado_recursos_naturais/>. Access in: 2014-06-25. 25

_____. **Manual técnico da vegetação brasileira**. Rio de Janeiro, 2012. 271 p. (Manuais técnicos em geociências, 1, 2a edição). Available from: <ftp://geoftp.ibge.gov.br/documentos/recursos_naturais/manuais_tecnicos/manual_tecnico_vegetacao_brasileira.pdf>. Access in: 2014-06-25. 23

INPE - National Institute For Space Research. **Portal for the monitoring of vegetation fires**. 2012. Available from: <<http://www.inpe.br/queimadas/>>. Access in: 2014-02-27. 79

_____. **Image Catalog**. 2014. Available from:

<<http://www.dgi.inpe.br/CDSR/>>. Access in: 2014-02-27. 79

KARAFYLLIDIS, I.; THANAILAKIS, A. A model for predicting forest fire spreading using cellular automata. **Ecological Modelling**, v. 99, n. 1, p. 87–97, 1997. ISSN 0304-3800. Available from:

<[http://dx.doi.org/10.1016/S0304-3800\(96\)01942-4](http://dx.doi.org/10.1016/S0304-3800(96)01942-4)>. Access in: 2014-06-25. 46

KAUFFMAN, J. B.; CUMMINGS, D. L.; WARD, D. E. Relationships of fire, biomass and nutrient dynamics along a vegetation gradient in the brazilian cerrado. **Journal of Ecology**, v. 82, n. 3, p. 519–531, 1994. ISSN 00220477. Available from: <<http://dx.doi.org/10.2307/2261261>>. Access in: 2014-06-25. 48

KEANE, R. E.; RYAN, K. C.; RUNNING, S. W. Simulating effects of fire on northern rocky mountain landscapes with the ecological process model FIRE-BGC. **Tree Physiol**, v. 16, n. 3, p. 319–331, 1996. Available from: <<http://dx.doi.org/10.1093/treephys/16.3.319>>. Access in: 2014-06-25. 12, 45

KUCHARIK, C. J. Evaluation of a process-based agro-ecosystem model (agro-IBIS) across the U.S. corn belt: Simulations of the interannual variability in maize yield. **Earth Interactions**, v. 7, n. 14, p. 1–33, 2003. ISSN 1087-3562, 1087-3562. Available from: <[http://dx.doi.org/10.1175/1087-3562\(2003\)007<0001:EOAPAM>2.0.CO;2](http://dx.doi.org/10.1175/1087-3562(2003)007<0001:EOAPAM>2.0.CO;2)>. Access in: 2014-04-10. 16

KUCHARIK, C. J.; FOLEY, J. A.; DELIRE, C.; FISHER, V. A.; COE, M. T.; LENTERS, J. D.; YOUNG-MOLLING, C.; RAMANKUTTY, N.; NORMAN, J. M.; GOWER, S. T. Testing the performance of a dynamic global ecosystem model: Water balance, carbon balance, and vegetation structure. **Global Biogeochem. Cycles**, v. 14, 2000. Available from: <<http://dx.doi.org/10.1029/1999GB001138>>. Access in: 2014-06-25. 12, 13

LANDIS, J. R.; KOCH, G. G. The measurement of observer agreement for categorical data. **Biometrics**, v. 33, n. 1, p. 159, 1977. ISSN 0006341X. Available from: <<http://dx.doi.org/10.2307/2529310>>. Access in: 2014-02-22. 82

LAPOLA, D. M.; OYAMA, M. D.; NOBRE, C. A. Exploring the range of climate biome projections for tropical south america: The role of CO2 fertilization and

- seasonality. **Global Biogeochem. Cycles**, v. 23, 2009. Available from: <<http://dx.doi.org/10.1029/2008GB003357>>. Access in: 2014-06-25. 10
- LAURANCE, W. F. Forest-climate interactions in fragmented tropical landscapes. **Philosophical Transactions of the Royal Society of London. Series B: Biological Sciences**, v. 359, n. 1443, p. 345–352, 2004. Available from: <<http://dx.doi.org/10.1098/rstb.2003.1430>>. Access in: 2010-05-07. 1, 3, 47
- LEHSTEN, V.; TANSEY, K.; BALZTER, H.; THONICKE, K.; SPESSA, A.; WEBER, U.; SMITH, B.; ARNETH, A. Estimating carbon emissions from african wildfires. **Biogeosciences**, v. 6, n. 3, p. 349–360, 2009. ISSN 1726-4170. Available from: <<http://dx.doi.org/10.5194/bg-6-349-2009>>. Access in: 2014-06-25. 10
- LENIHAN, J. M.; BACHELET, D.; NEILSON, R. P.; DRAPEK, R. Simulated response of conterminous united states ecosystems to climate change at different levels of fire suppression, CO2 emission rate, and growth response to CO2. **Global and Planetary Change**, v. 64, n. 1-2, p. 16–25, 2008. ISSN 0921-8181. Available from: <<http://dx.doi.org/10.1016/j.gloplacha.2008.01.006>>. Access in: 2014-06-25. 10
- LIMA, A.; SILVA, T. S. F.; ARAGÃO, L. E. O. e. C. d.; FEITAS, R. M. d.; ADAMI, M.; FORMAGGIO, A. R.; SHIMABUKURO, Y. E. Land use and land cover changes determine the spatial relationship between fire and deforestation in the brazilian amazon. **Applied Geography**, v. 34, p. 239–246, 2012. ISSN 0143-6228. Available from: <<http://dx.doi.org/10.1016/j.apgeog.2011.10.013>>. Access in: 2014-02-19. 79
- LINN, R.; WINTERKAMP, J.; COLMAN, J. J.; EDMINSTER, C.; BAILEY, J. D. Modeling interactions between fire and atmosphere in discrete element fuel beds. **Int. J. Wildland Fire**, v. 14, n. 1, p. 37–48, 2005. Available from: <<http://dx.doi.org/10.1071/WF04043>>. Access in: 2010-11-30. 43
- MALHI, Y.; ARAGAO, L. E. O. C.; GALBRAITH, D.; HUNTINGFORD, C.; FISHER, R.; ZELAZOWSKI, P.; SITCH, S.; McSweeney, C.; MEIR, P. Tipping elements in earth systems special feature: Exploring the likelihood and mechanism of a climate-change-induced dieback of the amazon rainforest. **Proceedings of the National Academy of Sciences**, v. 106, n. 49, p. 20610–20615, feb. 2009. ISSN 0027-8424. Available from: <<http://www.pnas.org/content/early/2009/02/12/0804619106.abstract>>. Access in: 2010-05-12. 1, 2

MANABE, S. CLIMATE AND THE OCEAN CIRCULATION : I. THE ATMOSPHERIC CIRCULATION AND THE HYDROLOGY OF THE EARTH'S SURFACE. **Monthly Weather Review**, v. 97, n. 11, p. 739–774, 1969. ISSN 0027-0644, 1520-0493. Available from:

<[http://dx.doi.org/10.1175/1520-0493\(1969\)097<0739:CATOC>2.3.CO;2](http://dx.doi.org/10.1175/1520-0493(1969)097<0739:CATOC>2.3.CO;2)>.

Access in: 2014-04-11. 8

MANDEL, J.; BEEZLEY, J. D.; KOCHANSKI, A. K. Coupled atmosphere-wildland fire modeling with WRF 3.3 and SFIRE 2011. **Geosci. Model Dev.**, v. 4, n. 3, p. 591–610, jul. 2011. ISSN 1991-9603. Available from: <<http://www.geosci-model-dev.net/4/591/2011/>>. Access in: 2014-04-02. 43

MARENGO, J. A.; NOBRE, C. A.; TOMASELLA, J.; OYAMA, M. D.; OLIVEIRA, G. Sampaio de; OLIVEIRA, R. de; CAMARGO, H.; ALVES, L. M.; BROWN, I. F. The drought of amazonia in 2005. **Journal of Climate**, v. 21, n. 3, p. 495–516, 2008. Available from:

<<http://dx.doi.org/10.1175/2007JCLI1600.1>>. Access in: 2009-05-15. 47

MARENGO, J. A.; TOMASELLA, J.; ALVES, L. M.; SOARES, W. R.; RODRIGUEZ, D. A. The drought of 2010 in the context of historical droughts in the amazon region. **Geophysical Research Letters**, v. 38, n. 12, p. n/a–n/a, 2011. ISSN 1944-8007. Available from:

<<http://dx.doi.org/10.1029/2011GL047436>>. Access in: 2014-02-28. 78

MBOW, C.; GOÏTA, K.; BÉNIÉ, G. B. Spectral indices and fire behavior simulation for fire risk assessment in savanna ecosystems. **Remote Sensing of Environment**, v. 91, n. 1, p. 1–13, 2004. ISSN 0034-4257. Available from: <<http://dx.doi.org/10.1016/j.rse.2003.10.019>>. Access in: 2014-06-25. 49

McArthur, A. G. **Weather and grassland fire behaviour**. Canberra: Forest Research Institute, Forestry and Timber Bureau, 1966. (Leaflet, 100). 39

_____. **Fire behaviour in Eucalypt forests**. Canberra: Forest Research Institute, Forestry and Timber Bureau, 1967. (Leaflet, 107). 39

MIRANDA, H. S.; BUSTAMANTE, M. M. C.; MIRANDA, A. C. The fire factor. In: OLIVEIRA, P. S.; MARQUIS, R. J. (Ed.). **The Cerrados of Brazil: ecology and natural history of a Neotropical savanna**. New York: Columbia University Press, 2002. p. 51–68. 48

MIRANDA, H. S.; SATO, M. N.; NETO, W. N.; AIRES, F. S. Fires in the cerrado, the brazilian savanna. In: COCHRANE, M. A. (Ed.). **Tropical fire**

ecology. Springer Berlin Heidelberg, 2009, (Springer Praxis Books). Available from: <http://dx.doi.org/10.1007/978-3-540-77381-8_15>. Access in: 2014-06-25. 2, 48

MIRANDA, H. S.; SILVA, E. P. R. e; MIRANDA, A. C. Comportamento do fogo em queimadas de campo sujo. In: MIRANDA, H. S; SAITO, C. H; DIAS, B. F. S. (Ed.). **Impactos de queimadas em áreas de cerrado e restinga: anais do simpósio impacto das queimadas sobre os ecossistemas e mudanças globais**. Brasília, DF: UNB, 1996. 3o Congresso de Ecologia do Brasil, 6 a 11 de outubro de 1996. 48

MISTRY, J.; BERARDI, A. Assessing fire potential in a brazilian savanna nature reserve. **Biotropica**, v. 37, n. 3, p. 439–451, 2005. Available from: <<http://dx.doi.org/10.1111/j.1744-7429.2005.00058.x>>. Access in: 2010-04-29. 2, 49

MOLOD, A.; SALMUN, H. A global assessment of the mosaic approach to modeling land surface heterogeneity. **J. Geophys. Res.**, v. 107, 2002. Available from: <<http://dx.doi.org/10.1029/2001JD000588>>. Access in: 2014-06-25. 16, 17

MORITZ, M. A.; MORAIS, M. E.; SUMMERELL, L. A.; CARLSON, J. M.; DOYLE, J. Wildfires, complexity, and highly optimized tolerance. **Proceedings of the National Academy of Sciences of the United States of America**, v. 102, n. 50, p. 17912–17917, 2005. ISSN 0027-8424, 1091-6490. Available from: <<http://dx.doi.org/10.1073/pnas.0508985102>>. Access in: 2014-03-31. 39, 40

MORTON, D. C.; DeFries, R. S.; NAGOL, J.; JR., C. M. S.; KASISCHKE, E. S.; HURTT, G. C.; DUBAYAH, R. Mapping canopy damage from understory fires in amazon forests using annual time series of landsat and MODIS data. **Remote Sensing of Environment**, v. 115, n. 7, p. 1706–1720, 2011. ISSN 0034-4257. Available from: <<http://dx.doi.org/10.1016/j.rse.2011.03.002>>. Access in: 2014-02-27. 47, 90

MOSS, R. H.; EDMONDS, J. A.; HIBBARD, K. A.; MANNING, M. R.; ROSE, S. K.; VUUREN, D. P. van; CARTER, T. R.; EMORI, S.; KAINUMA, M.; KRAM, T.; MEEHL, G. A.; MITCHELL, J. F. B.; NAKICENOVIC, N.; RIAHI, K.; SMITH, S. J.; STOUFFER, R. J.; THOMSON, A. M.; WEYANT, J. P.; WILBANKS, T. J. The next generation of scenarios for climate change research and assessment. **Nature**, v. 463, n. 7282, p. 747–756, 2010. ISSN 0028-0836.

Available from: <<http://dx.doi.org/10.1038/nature08823>>. Access in:
2010-05-16. 7

MRAZ, M.; ZIMIC, N.; VIRANT, J. Intelligent bush fire spread prediction using fuzzy cellular automata. **Journal of Intelligent and Fuzzy Systems**, v. 7, n. 2, p. 203–207, 1999. ISSN 1875-8967. Available from:
<<http://iospress.metapress.com/content/pauu49lmbuf7t1jj>>. Access in:
2014-06-25. 45

NEPSTAD, D.; SOARES-FILHO, B. S.; MERRY, F.; LIMA, A.; MOUTINHO, P.; CARTER, J.; BOWMAN, M.; CATTANEO, A.; RODRIGUES, H.; SCHWARTZMAN, S.; McGrath, D. G.; STICKLER, C. M.; LUBOWSKI, R.; PIRIS-CABEZAS, P.; RIVERO, S.; ALENCAR, A.; ALMEIDA, O.; STELLA, O. The end of deforestation in the brazilian amazon. **Science**, v. 326, n. 5958, p. 1350–1351, 2009. Available from:
<<http://dx.doi.org/10.1126/science.1182108>>. Access in: 2014-06-25. 1

NOBRE, C. A.; BORMA, L. D. S. ‘Tipping points’ for the amazon forest. **Current Opinion in Environmental Sustainability**, v. 1, n. 1, p. 28–36, 2009. ISSN 1877-3435. Available from:
<<http://dx.doi.org/10.1016/j.cosust.2009.07.003>>. Access in: 2014-06-25.
1

NOBRE, C. A.; SELLERS, P. J.; SHUKLA, J. Amazonian deforestation and regional climate change. **Journal of Climate**, v. 4, n. 10, p. 957–988, 1991. Available from:
<[http://dx.doi.org/10.1175/1520-0442\(1991\)004<0957:ADARCC>2.0.CO;2](http://dx.doi.org/10.1175/1520-0442(1991)004<0957:ADARCC>2.0.CO;2)>. Access in: 2014-06-25. 9

OLIVEIRA-FILHO, A. T.; RATTER, J. A. Vegetation physiognomies and woody flora. In: OLIVEIRA, P. S.; MARQUIS, R. J. (Ed.). **The Cerrados of Brazil: ecology and natural history of a Neotropical savanna**. New York: Columbia University Press, 2002. p. 91–120. 2

OLIVEIRA, G. S. d. **Conseqüências climáticas da substituição gradual da floresta tropical amazônica por pastagem degradada ou por plantação de soja**: um estudo de modelagem. PhD Thesis (Tese de Doutorado em Meteorologia) — Instituto Nacional de Pesquisas Espaciais, São José dos Campos, mar. 2008. Available from:
<<http://urlib.net/sid.inpe.br/mtc-m17@80/2008/02.28.17.17>>. Access in:
2014-07-17. 23

OpenMP architecture review board. **OpenMP application program interface version 3.1**. 2011. Available from:

<<http://www.openmp.org/mp-documents/OpenMP3.1.pdf>>. Access in: 2014-06-25. 21

OTTMAR, R. D.; SANDBERG, D. V.; RICCARDI, C. L.; PRICHARD, S. J. An overview of the fuel characteristic classification system - quantifying, classifying, and creating fuelbeds for resource planning. **Canadian Journal of Forest Research**, v. 37, n. 12, p. 2383–2393, 2007. ISSN 1208-6037. Available from:

<<http://dx.doi.org/10.1139/X07-077>>. Access in: 2010-07-28. 42

OTTMAR, R. D.; VIHANEK, R. E.; MIRANDA, H. S.; SATO, M. N.; ANDRADE, A. M. A. **Stereo photo series for quantifying cerrado fuels in central Brazil—volume I**. Portland, OR, 2001. Available from:

<<http://www.treesearch.fs.fed.us/pubs/5516>>. Access in: 2014-06-25. 43, 49

OYAMA, M. D.; NOBRE, C. A. A new climate-vegetation equilibrium state for tropical south america. **Geophys. Res. Lett.**, v. 30, n. 23, p. 2199, 2003. Available from: <<http://dx.doi.org/10.1029/2003GL018600>>. Access in: 2014-06-25. 10

PERES, C. A.; GARDNER, T. A.; BARLOW, J.; ZUANON, J.; MICHALSKI, F.; LEES, A. C.; VIEIRA, I. C.; MOREIRA, F. M.; FEELEY, K. J. Biodiversity conservation in human-modified amazonian forest landscapes. **Biological Conservation**, In Press, Corrected Proof, 2010. ISSN 0006-3207. Available from:

<<http://dx.doi.org/10.1016/j.biocon.2010.01.021>>. Access in: 2014-06-25. 1

PETERSON, S. H.; MORAIS, M. E.; CARLSON, J. M.; DENNISON, P. E.; ROBERTS, D. A.; MORITZ, M. A.; WEISE, D. R. **Using HFire for spatial modeling of fire in shrublands**. Albany, CA, 2009. 44 p. (Res. Pap., PSW-RP-259). Available from:

<<http://www.treesearch.fs.fed.us/pubs/31914>>. Access in: 2014-06-25. 46

PITMAN, A. J. The evolution of, and revolution in, land surface schemes designed for climate models. **International Journal of Climatology**, v. 23, n. 5, p. 479–510, 2003. Available from: <<http://dx.doi.org/10.1002/joc.893>>. Access in: 2014-06-25. 7, 8

POLLARD, D.; THOMPSON, S. L. Use of a land-surface-transfer scheme (LSX) in a global climate model: the response to doubling stomatal resistance. **Global and Planetary Change**, v. 10, n. 1–4, p. 129–161, 1995. ISSN 0921-8181.

Available from: <[http://dx.doi.org/10.1016/0921-8181\(94\)00023-7](http://dx.doi.org/10.1016/0921-8181(94)00023-7)>. Access in: 2014-04-10. 12

PONTIUS, G. Quantification error versus location error in comparison of categorical maps. **Photogrammetric Engineering and Remote Sensing**, v. 66, n. 8, p. 1011–1016, 2000. 82

R Core Team. **R: A language and environment for statistical computing**. Vienna, Austria: R Foundation for Statistical Computing, 2012. Available from: <<http://www.r-project.org/>>. Access in: 2014-06-25. 83

RAMANKUTTY, N.; FOLEY, J. A. Estimating historical changes in global land cover: Croplands from 1700 to 1992. **Global Biogeochem. Cycles**, v. 13, n. 4, 1999. Available from: <<http://dx.doi.org/10.1029/1999GB900046>>. Access in: 2014-06-25. 14

RAMOS-NETO, M. B.; PIVELLO, V. R. Lightning fires in a brazilian savanna national park: Rethinking management strategies. **Environmental Management**, v. 26, n. 6, p. 675–684, 2000. Available from: <<http://dx.doi.org/10.1007/s002670010124>>. Access in: 2010-04-30. 2, 11

RAY, D.; NEPSTAD, D.; BRANDO, P. Predicting moisture dynamics of fine understory fuels in a moist tropical rainforest system: results of a pilot study undertaken to identify proxy variables useful for rating fire danger. **New Phytologist**, v. 187, n. 3, p. 720–732, 2010. ISSN 1469-8137. Available from: <<http://dx.doi.org/10.1111/j.1469-8137.2010.03358.x>>. Access in: 2014-06-25. 47, 56

RAY, D.; NEPSTAD, D.; MOUTINHO, P. MICROMETEOROLOGICAL AND CANOPY CONTROLS OF FIRE SUSCEPTIBILITY IN a FORESTED AMAZON LANDSCAPE. **Ecological Applications**, v. 15, n. 5, p. 1664–1678, oct. 2005. ISSN 1051-0761. Available from: <<http://dx.doi.org/10.1890/05-0404>>. Access in: 2010-10-06. 47

RIBEIRO, J. F.; WALTER, B. M. T. Fitofisionomias do bioma cerrado. In: SANO, S. M.; ALMEIDA, S. P. (Ed.). **Cerrado: ambiente e flora**. Brasília: Embrapa Cerrados, 1998. 2

RIVERA-LOMBARDI, R. J. **Estimativa de áreas queimadas com produtos modis como subsídio à estimativa de emissões de gases de efeito estufa pela queima de biomassa na Amazônia e Cerrado Brasileiros**. PhD Thesis

(Tese de Doutorado em Sensoriamento Remoto) — Instituto Nacional de Pesquisas Espaciais, São José dos Campos, 2009. Available from:

<<http://urlib.net/8JMKD3MGP8W/3573AP5>>. Access in: 2014-06-25. 80

ROLLINS, M. G. LANDFIRE: a nationally consistent vegetation, wildland fire, and fuel assessment. **International Journal of Wildland Fire**, v. 18, n. 3, p. 235–249, 2009. Available from: <<http://dx.doi.org/10.1071/WF08088>>. Access in: 2014-02-26. 77

ROTHERMEL, R. C. **A mathematical model for predicting fire spread in wildland fuels**. Ogden, UT: U.S., 1972. 40 p. Available from:

<<http://www.treesearch.fs.fed.us/pubs/32533>>. Access in: 2014-06-25. 10, 39, 42

ROY, D.; BOSCHETTI, L. Southern africa validation of the MODIS, L3JRC, and GlobCarbon burned-area products. **IEEE Transactions on Geoscience and Remote Sensing**, v. 47, n. 4, p. 1032–1044, 2009. ISSN 0196-2892. Available from: <<http://dx.doi.org/10.1109/TGRS.2008.2009000>>. Access in: 2014-06-25. 78, 80

ROY, D.; BOSCHETTI, L.; JUSTICE, C.; JU, J. The collection 5 MODIS burned area product – global evaluation by comparison with the MODIS active fire product. **Remote Sensing of Environment**, v. 112, n. 9, p. 3690–3707, 2008. ISSN 0034-4257. Available from:

<<http://dx.doi.org/10.1016/j.rse.2008.05.013>>. Access in: 2014-06-25. 6, 47, 77, 80

SAGE. **Atlas of the Biosphere**. 2002. Available from:

<<http://www.sage.wisc.edu/atlas/maps.php?datasetid=25&includerelatedlinks=1&dataset=25>>. Access in: 2014-04-11. 14

_____. **SAGE Maps, Data, Models**. 2014. Available from:

<<http://www.sage.wisc.edu/mapsdatamodels.html>>. Access in: 2014-04-11. 14, 32

SANDBERG, D. V.; RICCARDI, C. L.; SCHAAF, M. D. Reformulation of rothermel’s wildland fire behaviour model for heterogeneous fuelbeds. **Canadian Journal of Forest Research**, v. 37, n. 12, p. 2438–2455, 2007. ISSN 1208-6037. Available from: <<http://dx.doi.org/10.1139/X07-094>>. Access in: 2010-11-30. 43

- SANO, E. E.; ROSA, R.; BRITO, J. L. S.; FERREIRA, L. G. Mapeamento semidetalhado do uso da terra do bioma cerrado. **Pesquisa Agropecuária Brasileira**, v. 43, p. 153–156, 2008. Available from: <<http://dx.doi.org/10.1590/S0100-204X2008000100020>>. Access in: 2014-06-25. 2
- SCHELLER, R.; DOMINGO, J.; STURTEVANT, B.; WILLIAMS, J.; RUDY, A.; GUSTAFSON, E.; MLADENOFF, D. Design, development, and application of LANDIS-II, a spatial landscape simulation model with flexible temporal and spatial resolution. **Ecological Modelling**, v. 201, n. 3-4, p. 409–419, 2007. Available from: <<http://dx.doi.org/10.1016/j.ecolmodel.2006.10.009>>. Access in: 2014-06-25. 12
- SCHELLER, R.; MLADENOFF, D. An ecological classification of forest landscape simulation models: tools and strategies for understanding broad-scale forested ecosystems. **Landscape Ecology**, v. 22, n. 4, p. 491–505, 2007. Available from: <<http://dx.doi.org/10.1007/s10980-006-9048-4>>. Access in: 2014-06-25. 11
- SCHROEDER, W.; PRINS, E.; GIGLIO, L.; CSISZAR, I.; SCHMIDT, C.; MORISETTE, J.; MORTON, D. Validation of GOES and MODIS active fire detection products using ASTER and ETM+ data. **Remote Sensing of Environment**, v. 112, n. 5, p. 2711–2726, may 2008. ISSN 0034-4257. Available from: <<http://www.sciencedirect.com/science/article/B6V6V-4S0B2RV-1/2/568f0767ed9b2528f27592df4341302f>>. Access in: 2010-12-03. 5
- SCOTT, J. H.; BURGAN, R. E. **Standard fire behavior fuel models: a comprehensive set for use with Rothermel's surface fire spread model**. Fort Collins, CO, 2005. 72 p. (Gen. Tech. Rep., RMRS-GTR-153). Available from: <<http://www.treearch.fs.fed.us/pubs/9521>>. Access in: 2014-04-11. 41, 49
- SELLERS, P.; MINTZ, Y.; SUD, Y.; DALCHER, A. A simple biosphere model (SIB) for use within general circulation models. **Journal of the Atmospheric Sciences**, v. 43, n. 6, p. 505–531, 1986. Available from: <[http://dx.doi.org/10.1175/1520-0469\(1986\)043<0505:ASBMFU>2.0.CO;2](http://dx.doi.org/10.1175/1520-0469(1986)043<0505:ASBMFU>2.0.CO;2)>. Access in: 2014-06-25. 8
- SENNA, M. C. A.; COSTA, M. H.; PIRES, G. F. Vegetation-atmosphere-soil nutrient feedbacks in the amazon for different deforestation scenarios. **Journal of Geophysical Research**, v. 114, 2009. Available from: <<http://dx.doi.org/2009J01029/2008JD010401>>. Access in: 2010-12-03. 14

SHEVLIKOVA, E.; PACALA, S. W.; MALYSHEV, S.; HURTT, G. C.; MILLY, P. C. D.; CASPERSEN, J. P.; SENTMAN, L. T.; FISK, J. P.; WIRTH, C.; CREVOISIER, C. Carbon cycling under 300 years of land use change: Importance of the secondary vegetation sink. **Global Biogeochem. Cycles**, v. 23, n. 2, p. GB2022, 2009. ISSN 0886-6236. Available from:

<<http://dx.doi.org/10.1029/2007GB003176>>. Access in: 2014-06-25. 16, 18, 21

SHIMABUKURO, Y. E.; DUARTE, V.; ARAI, E.; FREITAS, R. M.; LIMA, A.; VALERIANO, D. M.; BROWN, I. F.; MALDONADO, M. L. R. Fraction images derived from terra modis data for mapping burnt areas in brazilian amazonia.

International Journal of Remote Sensing, v. 30, n. 6, p. 1537–1546, 2009.

ISSN 0143-1161. Available from:

<<http://dx.doi.org/10.1080/01431160802509058>>. Access in: 2014-06-25. 79

SILVESTRINI, R. A. **Modelo probabilístico de ignição e propagação de fogo em áreas de floresta na Amazônia Brasileira**. Master Thesis

(Mestrado) — Universidade Federal de Minas Gerais Instituto de Geociências, Belo Horizonte, 2008. Available from: <<http://www.bibliotecadigital.ufmg.br/dspace/handle/1843/MPBB-7PYEWE>>.

Access in: 2014-07-17. 48

SILVESTRINI, R. A.; FILHO, B. S. S.; ALENCAR, A. A. C.; RODRIGUES, H. O.; ASSUNÇÃO, R. M.; MENDOZA, E. Modelo probabilístico de espalhamento de fogo: Aplicação para a região do xingu. In: EPIPHANIO, J. C. N.; GALVÃO, L. S. (Ed.). **Simpósio Brasileiro de Sensoriamento Remoto, 14. (SBSR)**. São José dos Campos: INPE, 2009. p. 5459–5466. ISBN 978-85-17-00044-7. Available from: <<http://urlib.net/3ERPFQRTBW/34RQDB8>>.

Access in: 2014-06-27. 48

SILVESTRINI, R. A.; SOARES-FILHO, B. S.; NEPSTAD, D.; COE, M.;

RODRIGUES, H.; ASSUNÇÃO, R. Simulating fire regimes in the amazon in response to climate change and deforestation. **Ecological Applications**, v. 21, n. 5, p. 1573–1590, jul. 2011. ISSN 1051-0761. Available from:

<<http://www.esajournals.org/doi/abs/10.1890/10-0827.1>>. Access in: 2011-07-21. 48

SITCH, S.; SMITH, B.; PRENTICE, I. C.; ARNETH, A.; BONDEAU, A.;

CRAMER, W.; KAPLAN, J. O.; LEVIS, S.; LUCHT, W.; SYKES, M. T.;

THONICKE, K.; VENEVSKY, S. Evaluation of ecosystem dynamics, plant geography and terrestrial carbon cycling in the LPJ dynamic global vegetation

model. **Global Change Biology**, v. 9, n. 2, p. 161–185, 2003. Available from: <<http://dx.doi.org/10.1046/j.1365-2486.2003.00569.x>>. Access in: 2014-06-25. 10, 77

SULLIVAN, A. L. Wildland surface fire spread modelling, 1990-2007. 1: Physical and quasi-physical models. **International Journal of Wildland Fire**, v. 18, n. 4, p. 349–368, 2009. Available from: <<http://dx.doi.org/10.1071/WF06143>>. Access in: 2014-06-25. 39

_____. Wildland surface fire spread modelling, 1990-2007. 2: Empirical and quasi-empirical models. **International Journal of Wildland Fire**, v. 18, n. 4, p. 369–386, 2009. Available from: <<http://dx.doi.org/10.1071/WF06142>>. Access in: 2014-06-25. 39, 43, 45

_____. Wildland surface fire spread modelling, 1990-2007. 3: Simulation and mathematical analogue models. **International Journal of Wildland Fire**, v. 18, n. 4, p. 387–403, 2009. Available from: <<http://dx.doi.org/10.1071/WF06144>>. Access in: 2014-06-25. 39

THONICKE, K.; SPESSA, A.; PRENTICE, I. C.; HARRISON, S. P.; DONG, L.; CARMONA-MORENO, C. The influence of vegetation, fire spread and fire behaviour on biomass burning and trace gas emissions: results from a process-based model. **Biogeosciences Discuss.**, v. 7, n. 1, p. 697–743, 2010. ISSN 1810-6277. Available from: <<http://dx.doi.org/10.5194/bgd-7-697-2010>>. Access in: 2014-06-25. 10, 77, 81

THONICKE, K.; VENEVSKY, S.; SITCH, S.; CRAMER, W. The role of fire disturbance for global vegetation dynamics: coupling fire into a dynamic global vegetation model. **Global Ecology & Biogeography**, v. 10, n. 6, p. 661–677, 2001. Available from: <<http://dx.doi.org/10.1046/j.1466-822X.2001.00175.x>>. Access in: 2014-06-25. 10

VAKALIS, D.; SARIMVEIS, H.; KIRANOUDIS, C. T.; ALEXANDRIDIS, A.; BAFAS, G. A GIS based operational system for wildland fire crisis management II. system architecture and case studies. **Applied Mathematical Modelling**, v. 28, n. 4, p. 411–425, 2004. ISSN 0307-904X. Available from: <<http://dx.doi.org/10.1016/j.apm.2003.10.006>>. Access in: 2014-06-25. 45

VENEVSKY, S.; THONICKE, K.; SITCH, S.; CRAMER, W. Simulating fire regimes in human-dominated ecosystems: Iberian peninsula case study. **Global**

Change Biology, v. 8, n. 10, p. 984–998, 2002. Available from:
<<http://dx.doi.org/10.1046/j.1365-2486.2002.00528.x>>. Access in:
2014-06-25. 10

VIEIRA, R. M. d. S. P.; ALVALÁ, R. C. d. S.; CUNHA, A. P. M. d. A.; SESTINI, M. F.; CARVALHO, V. C.; VALERIANO, D. d. M.; SILVA, J. d. S. V. d.; ABDON, M. d. M.; PONZONI, F. J.; SANO, E.; DAMBRÓS, L. A.; HASENACK, H.; FERRAZ-NETO, S.; BARBOSA, A. A. **Mapa de uso e cobertura da terra do território brasileiro para uso em modelagem climática e meteorológica**. São José dos Campos, 2013. 33 p. Available from:
<<http://urlib.net/8JMKD3MGP7W/3ECULQ5>>. Access in: 2014-06-25. 24

WEISE, D. R.; BIGING, G. S. Effects of wind velocity and slope on flame properties. **Can. J. For. Res.**, v. 26, p. 1849–1858, 1996. Available from:
<<http://www.treesearch.fs.fed.us/pubs/23271>>. Access in: 2014-05-09. 55

WERF, G. R. van der; RANDERSON, J. T.; GIGLIO, L.; COLLATZ, G. J.; MU, M.; KASIBHATLA, P. S.; MORTON, D. C.; DeFries, R. S.; JIN, Y.; LEEUWEN, T. T. van. Global fire emissions and the contribution of deforestation, savanna, forest, agricultural, and peat fires (1997–2009). **Atmospheric Chemistry and Physics Discussions**, v. 10, n. 6, p. 16153–16230, 2010. ISSN 1680-7375. Available from: <<http://dx.doi.org/10.5194/acpd-10-16153-2010>>. Access in: 2010-09-16. 6, 77, 81

WOLFRAM, S. Statistical mechanics of cellular automata. **Reviews of Modern Physics**, v. 55, n. 3, p. 601, 1983. Available from:
<<http://dx.doi.org/10.1103/RevModPhys.55.601>>. Access in: 2010-05-12. 45

XUE, Y.; SELLERS, P.; KINTER, J.; SHUKLA, J. A simplified biosphere model for global climate studies. **Journal of Climate**, v. 4, n. 3, p. 345–364, 1991. Available from:
<[http://dx.doi.org/10.1175/1520-0442\(1991\)004<0345:ASBMFG>2.0.CO;2](http://dx.doi.org/10.1175/1520-0442(1991)004<0345:ASBMFG>2.0.CO;2)>. 23

APPENDIX A - PUBLICATIONS RELATED TO THESIS

A.1 Evaluation of global burned area products in the Brazilian Arc of Deforestation

Authors: Etienne Tourigny, Sam Rabin, Andre Lima, Stephen Pacala, Carlos Nobre

corresponding author address: etienne.tourigny@cptec.inpe.br

submitted to *Remote Sensing of Environment*

keywords: burned area, arc of deforestation, Landsat, MODIS, Amazon

A.1.1 ABSTRACT

We present an evaluation of the performance of MODIS-based burned area products MCD45A1 and MCD64A1 in the Brazilian “arc of deforestation” region at various spatial scales. Compared to maps produced with imagery from the Landsat 5 Thematic Mapper (TM) sensors, the MODIS burned area products tend to slightly underestimate total burned area, with very small errors in scenes with large amounts of burned area. They are deemed acceptable in terms of spatial location at their native resolution of 500m. They perform better at coarser scales (5km and 0.25°), where the spatial variability of burned areas is particularly well represented. We conclude that these products are well suited for regional- and global-scale studies of burned area for the region and period analyzed. The MCD45 product is preferred for studies where spatial variability is important, whereas MCD64 represents total burned area better.

A.1.2 SUPPLEMENTARY MATERIAL

Supplementary Material

Evaluation of global burned area products in the Brazilian Arc of Deforestation.

Authors: Etienne Tourigny, Sam Rabin, Andre Lima, Stephen Pacala, Carlos Nobre
corresponding author address etienne.tourigny@cptec.inpe.br

Submitted to Remote Sensing of Environment

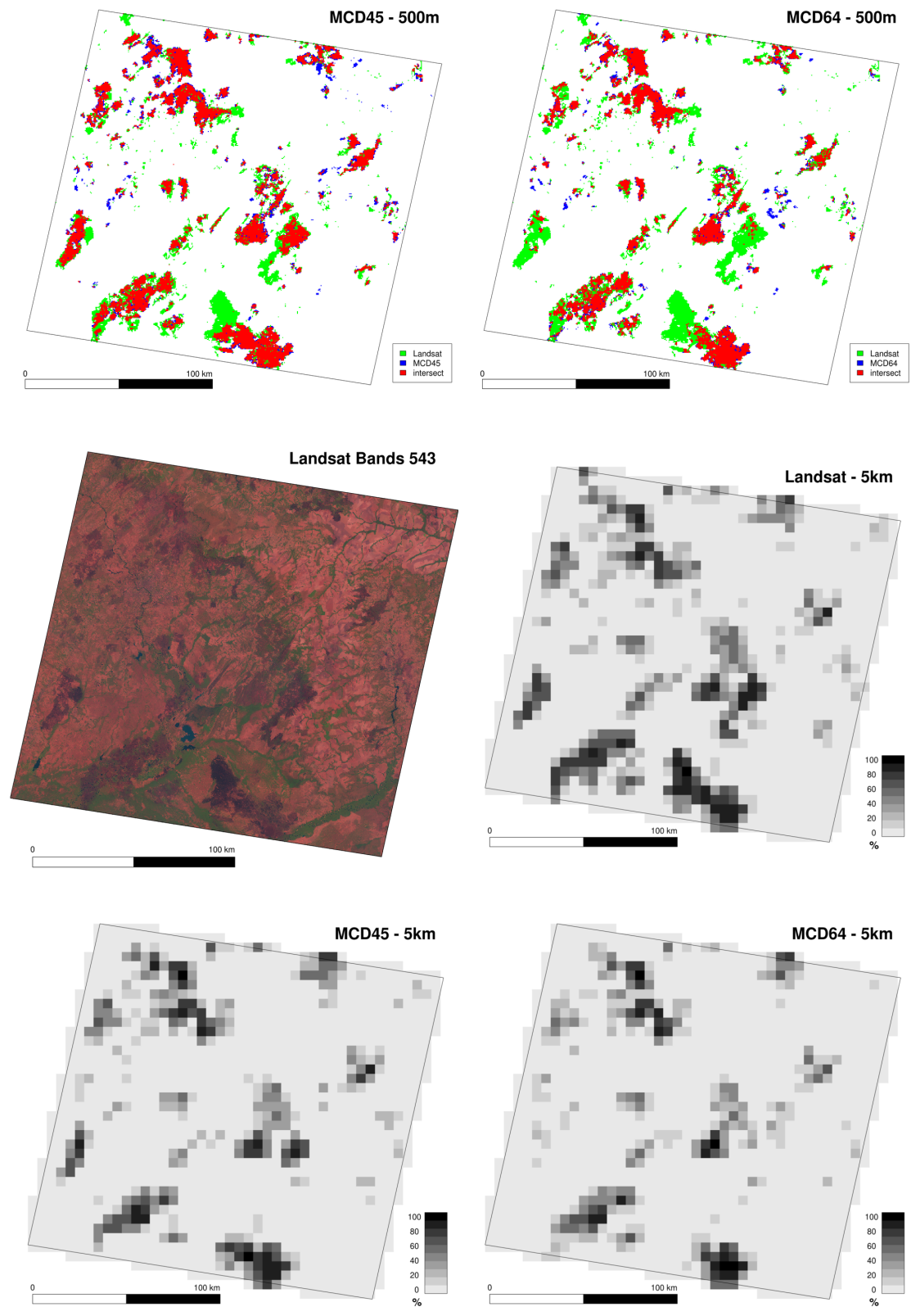


Figure S1 – As Figure 3 but for scene 226/071

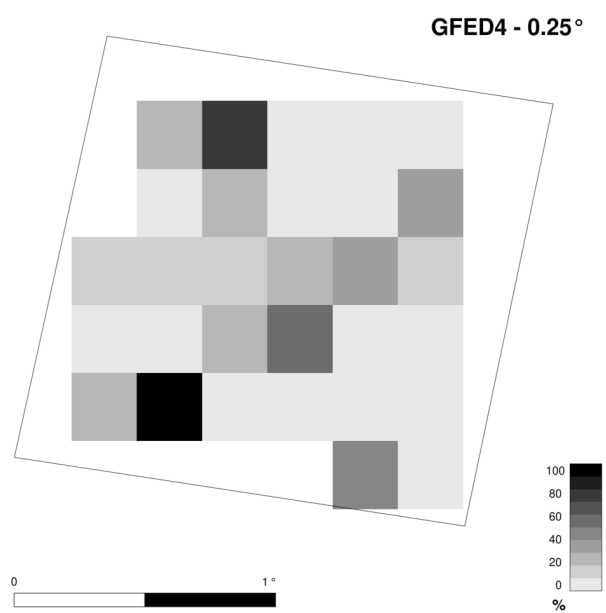
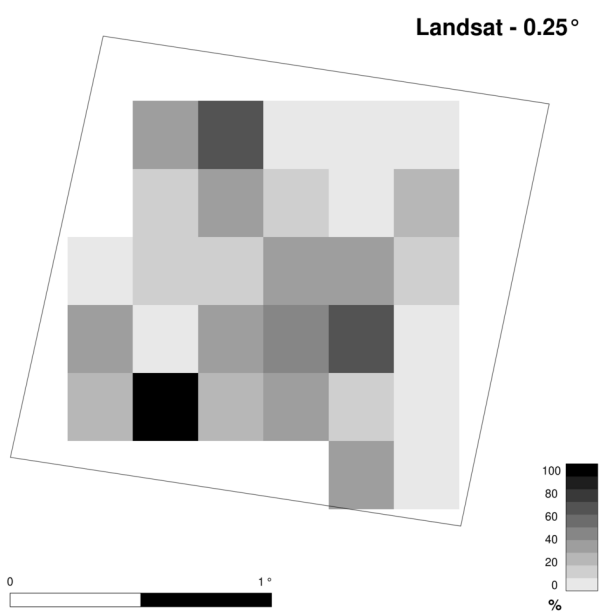
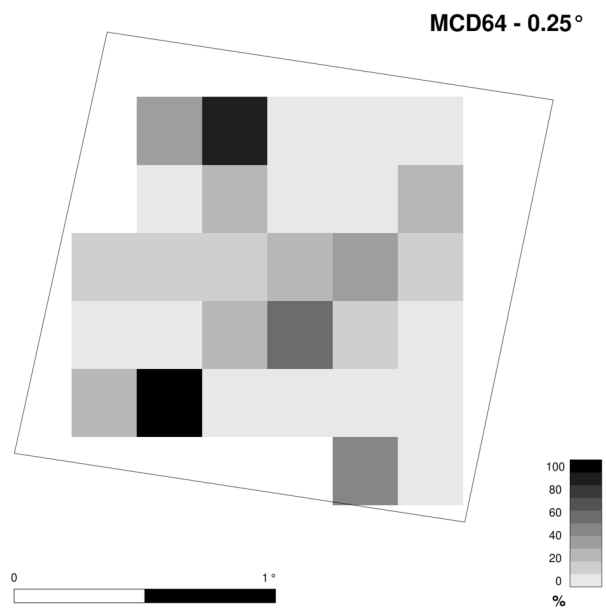
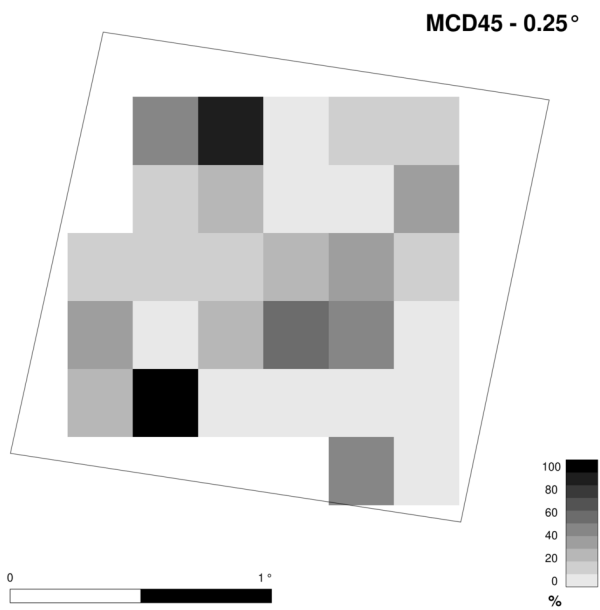


Figure S2 – As Figure 4 but for scene 226/071

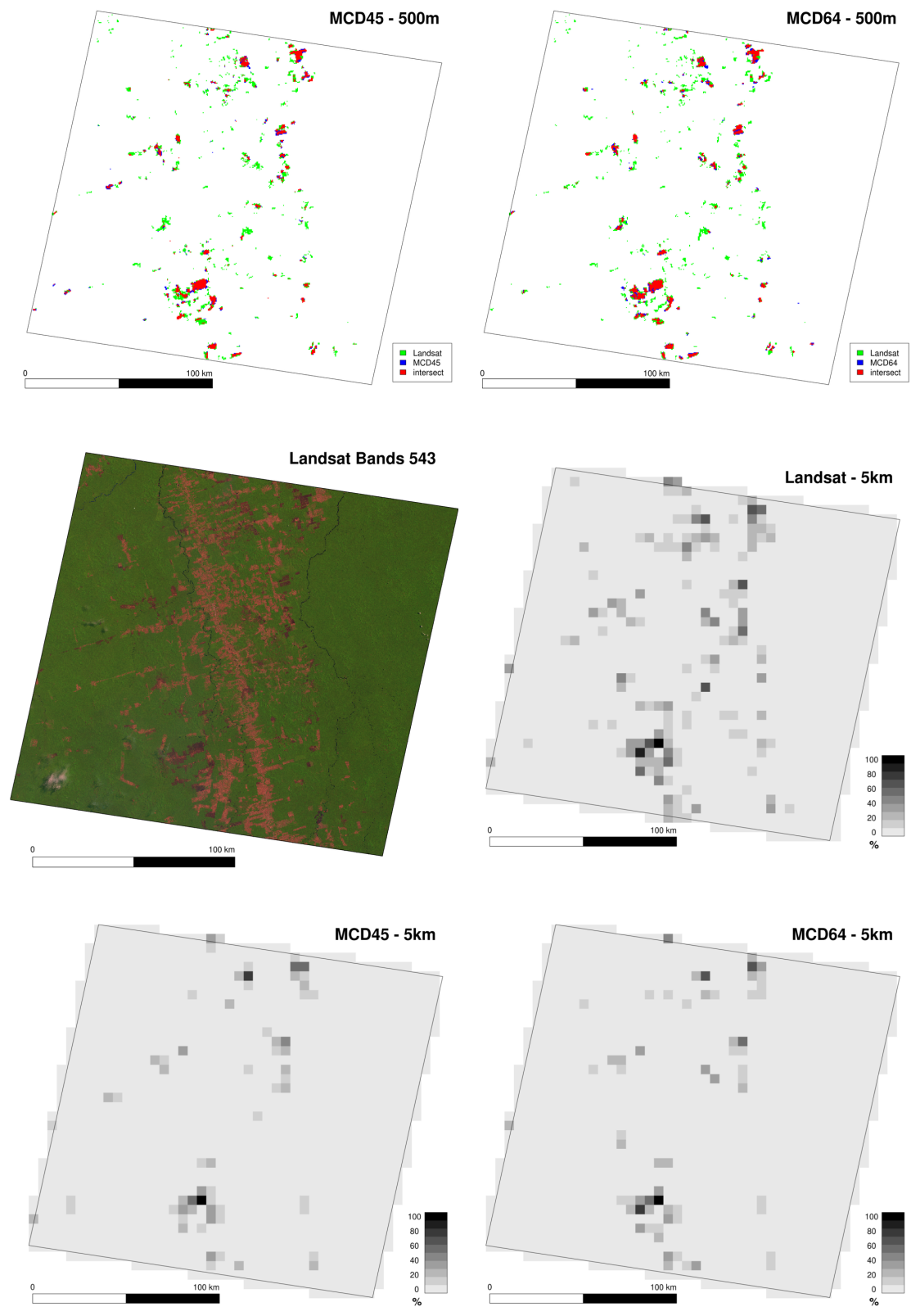


Figure S3 – As Figure 3 but for scene 227/065

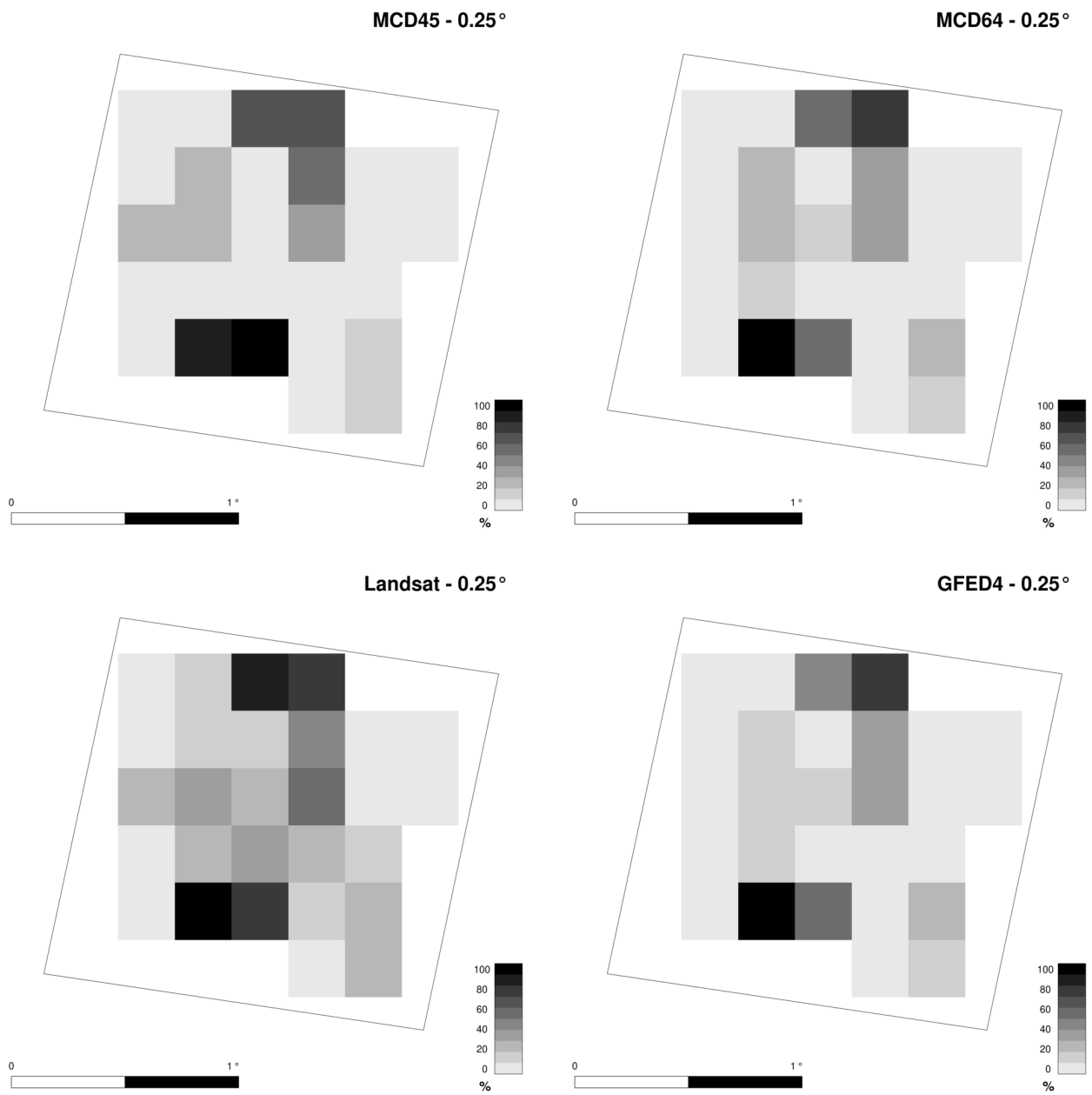


Figure S4 – As Figure 4 but for scene 227/065

A.2 Comparação de dados de área queimada obtidos por sensores remotos TM e MODIS no Parque Nacional Serra da Canastra, MG

Comparação de dados de área queimada obtidos por sensores remotos TM e MODIS no Parque Nacional Serra da Canastra, MG

Etienne Tourigny¹; Helena França²; Carlos Nobre³
¹ *Doutorando Meteorologia CPTEC/INPE*

(etienne.tourigny@cptec.inpe.br);

² *Prof. Dr. CECS/UFABC*; ³ *Prof. Dr. CCST/INPE*

Introdução e Objetivos

A vegetação de cerrado é frequentemente queimada para manejo de pastagem e abertura de frentes agrícolas, acarretando perda de *habitats* e emissão de gases para a atmosfera. Imagens de satélite de alta resolução, como as TM/Landsat são inadequadas para o mapeamento sistemático de queimadas devido à baixa frequência temporal (16 dias para o TM). O produto MCD45A1 do sensor MODIS, com 500 m de resolução espacial e alta frequência temporal (1 dia) fornece mapas de queimadas numa base mundial. Entretanto, esse produto necessita de validação para o cerrado brasileiro. O objetivo deste trabalho é comparar o mapeamento de queimadas dos produtos MODIS com aquele obtido por imagens TM/Landsat.

Material e Métodos

A área de estudo foi a porção regularizada do Parque Nacional da Serra da Canastra (PNSC), MG. Foram utilizadas 75 imagens TM/Landsat, bandas 3B, 4G, 5R, do período 2000 a 2010, órbita ponto 219/74 e 220/74. Essas imagens foram interpretadas visualmente em Sistema de Informações Geográficas, conforme método de [1], resultando em 10 mapas temáticos de queimadas. Cada mapa, considerado como “verdade terrestre”, correspondeu ao período 01/junho a 31/mayo do ano seguinte. Os dados MODIS MC45A1 [2] foram agregados em períodos compatíveis com os dados do TM para obtenção das estimativas anuais de área queimada. As áreas queimadas TM foram então comparadas com as do MODIS por regressão linear e cálculo de R^2 .

Resultados e Discussão

A Figura 1 mostra um exemplo de mapeamento obtido com os dois sensores no período de junho de 2007 a maio de 2008, evidenciando a similaridade espacial entre os mapas TM e MODIS. A Tabela 1 apresenta as estimativas anuais de área queimada no PNSC com ambos sensores. O Gráfico 1 mostra a regressão entre os totais anuais de área queimada entre TM e MODIS. O coeficiente de determinação

(R^2) obtido foi 0,934.



Figura 1. Mapas de área queimada em 2007-08 dos dados do Landsat (esquerda) e MODIS (direita).

Tabela 1. Área queimada TM e MODIS no PNSC.

Período	TM (km ²)	MODIS (km ²)
06/2000 a 05/2001	177,6	160,0
06/2001 a 05/2002	132,8	146,4
06/2002 a 05/2003	569,4	498,9
06/2003 a 05/2004	0,0	53,3
06/2004 a 05/2005	59,8	192,3
06/2005 a 05/2006	91,3	101,5
06/2006 a 05/2007	385,6	315,2
06/2007 a 05/2008	358,7	378,0
06/2008 a 05/2009	9,4	13,0
06/2009 a 05/2010	4,2	5,0
06/2010 a 12/2011	477,7	499,3

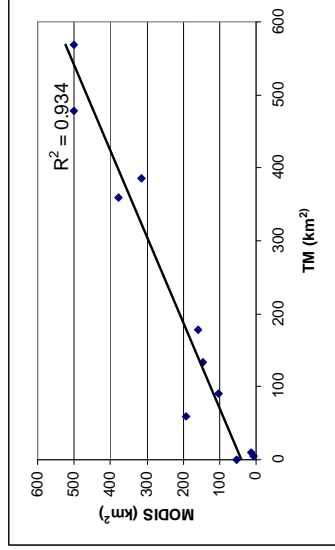


Gráfico 1. Comparação dos totais anuais de área queimada com dados TM e MODIS.

O alto R^2 possivelmente está relacionado às grandes dimensões das queimadas no PNSC, compatíveis com a resolução espacial grosseira (500 m) do MC45A1.

Conclusões

A estimativa de área obtida com os dados MC45A1 apresentou relação linear com a área calculada nos dados TM, apontando para a possibilidade de uso do MODIS para estimar área queimada no Cerrado. Entretanto, outras validações devem ser realizadas, sobretudo em áreas com queimadas de dimensões menores do que as do PNSC.

Referências Bibliográficas

- [1] FRANÇA, H.; RAMOS NETO, M. B.; SETZER, A. **O fogo no Parque Nacional das Emas**. Brasília, MMA, 2007.
- [2] ROY, D.; JIN, Y.; LEWIS, P.; JUSTICE, C. Prototyping a global algorithm for systematic fire-affected area mapping using MODIS time series data. **Remote Sensing of Environment**, 97, p. 137-162, 2005.

APPENDIX B - INLAND MODEL VARIABLES, DEFINITIONS AND SUPPORTING INFORMATION

B.1 Important variables

B.1.1 Variables that pertain to the simulation parameters

npoi1 The number of “real” model grid points

mlpt The number of tiles that each model grid point contains

npoi The actual number of model grid points ($npoi = mlpt * npoi1$)

B.1.2 Variables that pertain to each model grid point

vegtype The vegetation/surface type of the grid point at model initialization

vegtype0 The vegetation type determined by the vegetation dynamics module

tilefrac The fraction that each subgrid tile occupies in “real” grid point

landuse The fraction that each subgrid tile occupies in “real” grid point

plai The initial LAI of each PFT

B.2 Input files

B.2.1 PFT, *vegtype*, and *landusetype* parameters

```
#-----  
# PFTs (top to bottom)  
#-----  
c 1: tropical broadleaf evergreen trees  
c 2: tropical broadleaf drought-deciduous trees  
c 3: warm-temperate broadleaf evergreen trees  
c 4: temperate conifer evergreen trees  
c 5: temperate broadleaf cold-deciduous trees  
c 6: boreal conifer evergreen trees  
c 7: boreal broadleaf cold-deciduous trees
```

c 8: boreal conifer cold-deciduous trees
c 9: evergreen shrubs
c 10: cold-deciduous shrubs
c 11: warm (c4) grasses
c 12: cool (c3) grasses
c 13: soybeans
c 14: maize
c 15: wheat
c 16: sugarcane

#-----

Vegetation type classifications (used in subroutine iniveg)

#-----

c 1: tropical evergreen forest / woodland
c 2: tropical deciduous forest / woodland
c 3: temperate evergreen broadleaf forest / woodland
c 4: temperate evergreen conifer forest / woodland
c 5: temperate deciduous forest / woodland
c 6: boreal evergreen forest / woodland
c 7: boreal deciduous forest / woodland
c 8: mixed forest / woodland
c 9: savanna
c 10: grassland / steppe
c 11: dense shrubland
c 12: open shrubland
c 13: tundra
c 14: desert
c 15: polar desert / rock / ice
c 16: wetlands
c 17: cropland
c 18: pasture
c 19: urban

#-----

Variable name definitions (left to right)

#-----

plaievgr : initial total LAI of evergreen tree (upper canopy) PFTs
plaideci : initial total LAI of deciduous tree (upper canopy) PFTs
plaishrub : initial total LAI of shrub (lower canopy) PFTs
plaigrass : initial total LAI of grass (lower canopy) PFTs

```

# NOTE: These data are read in to array plai_init.
#       The original variable names could be dropped.
#-----
# plaievgr  plaideci plaishrub plaigrass      Veg Type
#-----
      5.00      1.00      0.25      0.25      !  1
      1.00      5.00      0.25      0.25      !  2
      4.00      1.00      0.25      0.25      !  3
      3.00      1.00      0.25      0.25      !  4
      1.00      3.00      0.25      0.25      !  5
      3.00      1.00      0.25      0.25      !  6
      1.00      3.00      0.25      0.25      !  7
      2.00      2.00      0.25      0.25      !  8
      0.50      1.00      0.50      2.00      !  9
      0.25      0.25      0.50      2.50      ! 10
      0.10      0.10      1.00      0.50      ! 11
      0.00      0.00      0.25      0.25      ! 12
      0.00      0.00      1.00      1.00      ! 13
      0.00      0.00      0.05      0.05      ! 14
      0.00      0.00      0.05      0.05      ! 15
      5.00      1.00      0.25      0.25      ! 16
      0.00      0.00      0.05      0.05      ! 17
      0.00      0.00      0.05      0.05      ! 18
      0.00      0.00      0.05      0.05      ! 19

#-----
# Land Use type classifications
#-----
c  1: natural
c  2: cropland
c  3: pasture
c  4: urban

B.2.2 Fire spread parameters

#-----
# Misc. definitions
#-----
# roads file (relative to datadir)
"hrmap/amz_roads.nc"

```

```

# ignitions file (relative to this dir) - set to empty if you want none
# max 1024 lines, max. of 80 chars. each like this
# 1980-01-01 12 -50.80 -9.50
"firespread_ignitions.txt"

#-----
# Variable name definitions (left to right)
#-----
# spreadrate : base rate of spread (m/s)
# spreadprob : base probability of fire spread from one cell to the next
#-----
# spreadrate spreadprob   Veg Type
#-----
0.003333333  0.005   ! 1   spreadrate 20cm/min based on litterature
0.003333333  0.005   ! 2
      0.1     0.75   ! 3
      0.1     0.75   ! 4
      0.1     0.75   ! 5
      0.1     0.75   ! 6
      0.1     0.75   ! 7
      0.1     0.75   ! 8
      0.5     0.75   ! 9
      0.1     0.75   ! 10
      0.1     0.75   ! 11
      0.1     0.75   ! 12
      0.1     0.75   ! 13
      0.1     0.75   ! 14
      0.1     0.75   ! 15
      0.1     0.75   ! 16
      0.1     0.75   ! 17
      0.2     0.75   ! 18
      0.0     0.75   ! 19

```

B.2.3 simulation and domain configuration files

```
! this is inland grid configuration file (namelist)
! change any parameters here, or comment/remove to use default values
!
&INLAND_GRID
!
! temporal parameters
irestart = 0 , ! irestart - 0: not a restart run 1: restart run (default 0)
iyrrestart = 9999 , ! iyrrestart - year to restart model (default 9999)
iyyear0 = 1980 , ! iyyear0 - initial year of simulation (don't change for restart) (default 1981)
nrun = 1 , ! nrun - number of years in this simulation (change for restart) (default 2)
iyrdaily = 9999 , ! iyrdaily - year to start reading daily data (ditto) (default 9999)
iyrmon = 9999 , ! iyrmon - year to start reading montly data (default 9999)
dtime = 3600 , ! dtime - time step in seconds (default 3600)
!
! simulation parameters
soilcspin = 0 , ! soilcspin - 0: no soil spinup, 1: acceleration procedure used (default 0)
isimveg = 1 , ! isimveg - 0: static veg, 1: dynamic veg, 2: dynamic veg-cold start (default 0)
isimfire = 0 , ! isimfire - 0: fixed fire (0.5% prob.), 1: dynamic fire, 2: CTEM fire method, 3: no fire [...]
isimco2 = 0 , ! isimco2 - 0: fixed co2, 1: ramped co2 (default 0)
co2init = 0.000350 , ! co2init - initial co2 concentration in mol/mol (real) (default 0.000350)
o2init = 0.209000 , ! o2init - initial o2 concentration in mol/mol (real) (default 0.209000)
isimland = 0 , ! 0: fixed land use, 1: dynamic land use
iyrloc = 9999 , ! year to start reading land transition data
nluc = 100 , ! number of years to read land transition data
isinfilt = 0 , ! isinfilt - Infiltration Function - 0: according to Darcy (1856); 1: according to Green-Ampt (1911)
isimrwu = 0 , ! isimrwu - Root water uptake module - 0: according to Foley et al., 1996; 1 according to Li et al. [...]
```

```

! output parameters
iyearout = 1      , ! iyearout - 0: no yearly output, 1: yearly output (default 1)
imonthout = 1    , ! imonthout - 0: no monthly output, 1: monthly output (default 1)
idailyout = 0    , ! idailyout - 0: no daily output, 1: daily output (default 0)
idiag = 0        , ! iddiag - 0: no diagnostic output, 1-10 # of files to output (default 0)
!
! crops simulation parameters
imetyear = 9999  , ! year to start using hourly met data
dmetryear = 1   , ! day to start using hourly met data (17 geovane)
imetend = 9999  , ! year to end reading in hourly met data
dmetend = 119   , ! day to end reading in hourly met data (39 geovane)
irrigate = 0    , ! 0: no irrigation 1: irrigation strategy used
isimagro = 0    , ! isimagro - 0: no agro crops, 1: unique crop defined by icroptype, 2: crops defined [...] cropsfile
icroptype = 16  , ! define crop type to use in all grid points - 13: soybean / 14: maize / 15: wheat / 16: sgc
iwheattype = 1 , ! 1: spring wheat 2: winter wheat - only used if icroptype = wheat
cropsfile = "crops_monfreda_05d.nc" , ! cropsfile - read crop data to produce crop veg map (use mlpt>1)
irotation = 0  , ! 0: none 1: winter wheat/fallow 2: 2 corn/soy 3: corn/soy/spring wheat 4: soy/winter wheat/corn
iholdsoiln = 1 , ! 0: doesn't save soil inorganic N from restart 1: save inorganic soil N
ffact = 1.0    , ! numeric multiplying factor applied to N fertilizer after 2000 (for all crops)
isoi1ay = 9    , ! soil layer for which nitrate leaching/drainage is output
elevin = 550   , ! site elevation (m)
thigh = 6      , ! tower input elevation (m)
!
! simulation domain - an entry with the same name and corresponding lon/lat values must be defined in inland-grid.domains
domain = "small12", ! domain name used to define lon/lat boundaries (default '')
!
! subgrid tile parameters - ignore if not using subgrid tiles
mlpt = 2      , ! mlpt - multiplicity of land points (subgrid tiles) (default 1, no tiles)

```

```

vegtypefile= "tiles/vegtype-deforest-50p.nc"      , ! file to read initial vegtype (and tileprop if mlpt>1) [...]
!hrmapfile = "hrmap/sam_INLAND_250m.nc"          , ! hrmapfile - read high-res data to produce initial veg map [...]
!
! Heterogeneous Parameterization
itauw = 0      , ! itauw - 0:reads 1 dimension tauwood0 from parms canopy; 1:reads 2 dimension from input HP maps [...]
ivmax = 0      , ! ivmax - 0:reads 1 dimension vmax_pft from parms canopy; 1:reads 2 dimension from input HP maps [...]
isla  = 0      , ! isla - 0:reads 1 dimension specia from parms canopy; 1:reads 2 dimension from input HP maps [...]
ica   = 0      , ! ica - 0:reads 1 dimension carbon allocation to wood, leaf and root from [...]
!
/

```

Domain configuration file:

```

default,    5.0   -15.0  -75.0  -55.0    ! default run (Amazon)
sam,       13.1   -55.0  -81.0  -35.25   ! South America
global,    90.0   -90.0 -180.0  180.0    ! global
br,        0      -35    -65    -35
toc,      -3.0   -12.0  -56.0  -42.0    ! Tocantins area
small1,   -7.75   -9.25 -50.25  -48.75   ! small test areas
small2,  -14.25 -14.74 -57.75  -57.25   ! 4 points
small3,  -14.25 -14.50 -57.75  -57.51   ! 1 point
sp1,     -18.75 -25.75 -53.75  -43.75   ! SP
sp2,     -23.75 -24.74 -46.75  -43.75   ! SP
amazlegal, 5.25   -17.75 -74.0   -44.1    ! legal Amazon
teste,    -18.75 -22.0  -53.75  -46.75
stop,     0.0    0.0    0.0    0.0
! here every line must be in the format
! name,    snorth ssouth swest  seast

```

B.2.4 climate and land surface input files

Table B.1 - climate and land surface input files

file	description	units
cld.mon.nc	monthly mean cloud cover	percent
deltat.mon.nc	diurnal temp range	degC
frostd.mon.nc	ground frost days	days/month
prec.mon.nc	monthly mean precipitation	mm/day
rh.mon.nc	monthly mean relative humidity	percent
temp.mon.nc	monthly mean temperature	degC
tmax.mon.nc	monthly maximum temperature	degC
tmin.mon.nc	monthly minimum temperature	degC
trange.mon.nc	monthly temperature range	degC
vapp.mon.nc	monthly mean vapor pressure	hPa
wdir.mon.nc	10 metre wind direction	degrees
wetd.mon.nc	monthly wet day frequency	days
wspd.mon.nc	monthly mean wind speed	m/s
vegtype.nc	cover types	none
topo.nc	topography	m
surta.nc	land/sea mask	mask
soita.clay.nc	soil clay percent	percent
soita.sand.nc	soil sand percent	percent

B.3 Output files

B.3.1 Output file variables

Table B.2 - yearly output file variables

variable	description	units
aet	average evapotranspiration	mm/year
anpptot	total above-ground npp	$kgm^{-2}year^{-1}$
awc	average volumetric water content	cm
caccount	end of year carbon correction	kg/m^2
co2mic	total microbe respiration carbon	kg/m^2
co2root	total root respiration carbon	kg/m^2
co2soi	total soil respiration carbon	kg/m^2
drainage	drainage	mm/year
fu	fractional cover of upper canopy	fraction
fl	fractional cover of lower canopy	fraction
neetot	total net ecosystem echange carbon	kg/m^2
nmintot	total nitrogen mineralization	kg/m^2
npptot	total npp	$kgm^{-2}year^{-1}$
rootbio	total live root biomass carbon	kg/m^2
srunoff	surface runoff	mm/year
totalit	total above ground litter carbon	kg/m^2
totlaiu	total lai for upper canopy	fraction
totlail	total lai for lower canopy	fraction
totbiou	total biomass for upper canopy	kg/m^2
totbiol	total biomass for lower canopy	kg/m^2
totfall	total litterfall	kg/m^2
totrlit	total below ground litter carbon	kg/m^2
totcsoi	total soil carbon w/o litter	kg/m^2
totcmic	total microbial carbon	kg/m^2
totanlit	total above ground litter nitrogen	kg/m^2
totrnlit	total below ground litter nitrogen	kg/m^2
totnsoi	total soil nitrogen w/o litter	kg/m^2
trunoff	total runoff	mm/year
tsoi	average soil temperature	degrees C
vwc	average volumetric water content	fraction
wisoi	average soil ice	fraction
wsoi	average soil moisture	fraction
landusetype	land use (1-4)	none
tilefrac	tile fraction	none
vegtype	vegetation type - static	none
vegtype0	vegetation type	none
biomass	biomass for each pft	kg/m^2
exist	existence for each pft	none
npp	npp of carbon for each pft	$kgm^{-2}year^{-1}$
plai	leaf area index for each pft	fraction

B.3.2 Example yearly output file

NetCDF definition of a yearly output file, containing 4D (longitude, latitude, tile, time) variables:

```
netcdf inland-yearly-1980 {
dimensions:
    longitude = 92 ;
    latitude = 137 ;
    pft = 16 ;
    tile = 4 ;
    time = UNLIMITED ; // (1 currently)
variables:
    double longitude(longitude) ;
        longitude:long_name = "longitude" ;
        longitude:units = "degrees_east" ;
    double latitude(latitude) ;
        latitude:long_name = "latitude" ;
        latitude:units = "degrees_north" ;
    double pft(pft) ;
        pft:long_name = "plant functional type" ;
        pft:units = "none" ;
        pft:axis = "E" ;
    double tile(tile) ;
        tile:long_name = "tile" ;
        tile:units = "none" ;
        tile:axis = "Z" ;
    double time(time) ;
        time:long_name = "time" ;
        time:units = "days since 1979-12-31" ;
    float npptot(time, tile, latitude, longitude) ;
        npptot:long_name = "total npp" ;
        npptot:units = "kg m-2 year-1" ;
        npptot:missing_value = 9.e+20f ;
    float anpptot(time, tile, latitude, longitude) ;
        anpptot:long_name = "total above-ground npp" ;
        anpptot:units = "kg m-2 year-1" ;
        anpptot:missing_value = 9.e+20f ;
```

```
[...]  
}
```

B.3.3 Example yearly PFT output file

NetCDF definition of a yearly PFT output file, containing 5D (longitude, latitude, pft, tile, time) variables:

```
netcdf inland-yearly-pft-1980 {  
dimensions:  
    longitude = 92 ;  
    latitude = 137 ;  
    pft = 16 ;  
    tile = 4 ;  
    time = UNLIMITED ; // (1 currently)  
variables:  
    double longitude(longitude) ;  
        longitude:long_name = "longitude" ;  
        longitude:units = "degrees_east" ;  
    double latitude(latitude) ;  
        latitude:long_name = "latitude" ;  
        latitude:units = "degrees_north" ;  
    double pft(pft) ;  
        pft:long_name = "plant functional type" ;  
        pft:units = "none" ;  
        pft:axis = "E" ;  
    double tile(tile) ;  
        tile:long_name = "tile" ;  
        tile:units = "none" ;  
        tile:axis = "Z" ;  
    double time(time) ;  
        time:long_name = "time" ;  
        time:units = "days since 1979-12-31" ;  
    byte exist(time, tile, pft, latitude, longitude) ;  
        exist:long_name = "existence for each pft" ;  
        exist:units = "none" ;  
        exist:missing_value = -127b ;  
    float plai(time, tile, pft, latitude, longitude) ;
```

```

    plai:long_name = "leaf area index for each pft" ;
    plai:units = "fraction" ;
    plai:missing_value = 9.e+20f ;
float biomass(time, tile, pft, latitude, longitude) ;
    biomass:long_name = "biomass for each pft" ;
    biomass:units = "kg/m^2" ;
    biomass:missing_value = 9.e+20f ;
float npp(time, tile, pft, latitude, longitude) ;
    npp:long_name = "npp of carbon for each pft" ;
    npp:units = "kg m-2 year-1" ;
    npp:missing_value = 9.e+20f ;
float burnpft(time, tile, pft, latitude, longitude) ;
    burnpft:long_name = "burned fraction for each pft" ;
    burnpft:units = "km^2" ;
    burnpft:missing_value = 9.e+20f ;
[...]
```

```

}
```

B.4 INLAND model diagrams

APPENDIX C - LAND COVER MAPS

Table C.1 - IGBP and INLAND land cover class equivalences

IGBP		INLAND	
ID	Name	ID	Name
0	Water	30	Water
1	Evergreen Needleleaf forest	4	Temperate Evergreen Conifer Forest
2	Evergreen Broadleaf forest	1	Tropical Evergreen Forest
3	Deciduous Needleleaf forest	5	Temperate Deciduous Forest
4	Deciduous Broadleaf forest	2	Tropical Deciduous Forest
5	Mixed forest	8	Mixed Forest / Woodland
6	Closed shrublands	11	Dense Shrubland
7	Open shrublands	12	Open Shrubland
8	Woody savannas	9	Savanna
9	Savannas	9	Savanna
10	Grasslands	10	Grassland / Steppe
11	Permanent wetlands	16	Wetlands
12	Croplands	17	Cropland
13	Urban and built-up	19	Urban
14	Cropland/Natural vegetation mosaic	17	Cropland
15	Snow and ice	15	Polar Desert / Rock / Ice
16	Barren or sparsely vegetated	14	Desert
254	Unclassified	127	Unclassified
255	Fill Value	127	Unclassified

Table C.2 - Mapping between PROVEG and INLAND land cover classes

PROVEG		INLAND	
ID	Name	ID	Name
0	Unclassified	127	Unclassified
1	Floresta Perene	1	Tropical Evergreen Forest
2	Floresta Decídua	2	Tropical Deciduous Forest
3	Floresta Mista	8	Mixed Forest / Woodland
6	Cerrado	9	Savanna
7	Arbustos/campo	10	Grassland / Steppe
8	Caatinga	11	Dense Shrubland
11	Solo Exposto	14	Desert
12	Agropecuária	18	Pasture
13	Água	30	Water
15	Area Urbana	19	Urban

Table C.3 - Mapping between IBGE1992 and INLAND land cover classes

IBGE1992		INLAND	
ID	Name	Formations	ID Name
D	Floresta Ombrófila Densa	Da, Db, Ds, Dm	1 Tropical Evergreen Forest
A	Floresta Ombrófila Aberta	Aa, Ab, As, Am	1
M	Floresta Ombrófila Mista	Ma, Mb, Ms, Mm	1
F	Floresta Estacional Semidecidual	Fa, Fb, Fs, Fm	2 Tropical Deciduous Forest
C	Floresta Estacional Decidual	Ca, Cb, Cs, Cm	2
L	Campinarana	Ld, La, Lb, Lg	9 Savanna
S	Savana	Sd, Sa, Sb, Sp, Sg, SP	9
T	Savana-Estépica	Td, Ta, Tp, Tg	11 Dense Shrubland
E	Estepe	Ea, Ep, Eg	11
P	Formação Pioneira	Pm, Pf, Pa	16 Wetlands
r	Refúgios Vegetacionais	rs, rm, rl, rsh	1 Tropical Evergreen Forest
Vs	Vegetação Secundária	Vs, Vsi	127 Unclassified
Ag	Agropecuária		18 Pasture
Ac	Agricultura		17 Cropland
Ap	Pecuária		18 Pasture
R	Reforestamento	R, Re	127 Unclassified
Iu	Influência urbana		19 Urban
Im	Degradadas por mineração		14 Desert
Ai	Indiscriminadas		14
Dun	Dunas		14
Afr	Afloramentos rochosos		14
agua	Água	agua, ag	30 Water
t	Ecótono	ONt	1 Tropical Evergreen Forest
t	Ecótono	NPt	2 Tropical Deciduous Forest
t	Ecótono	LOt, SNt, SOt, STt, STNt, SPt, SNC	9 Savanna
t	Ecótono	TNt, TPt	11 Dense Shrubland
NC	Unclassified	NC	127 Unclassified

Table C.4 - Mapping between TERRACCLASS and INLAND land cover classes

TERRACCLASS	INLAND	
	ID	Name
FLORESTA	127	Unclassified
FLORESTA_SOB_NUVEM	127	Unclassified
HIDROGRAFIA	30	Water
VEGETACAO_SECUNDARIA	20	Unclassified
NAO_FLORESTA	127	Unclassified
DEFLORESTAMENTO_2008	108	Pasture
AGRICULTURA_ANUAL	17	Cropland
AGROPECUARIA	18	Pasture
MOSAICO_DE_OCUPACOES	18	
PASTO_LIMPO	18	
PASTO_SUJO	18	
REGENERACAO_COM_PASTO	18	
PASTO_COM_SOLO_EXPOSTO	18	
MINERACAO	14	Desert
AREA_UrbanA	19	Urban
OUTROS	127	Unclassified
AREA_NAO_OBSERVADA	127	Unclassified
NC	127	Unclassified



Figure C.1 - GlobCover 2009 Land Cover Map

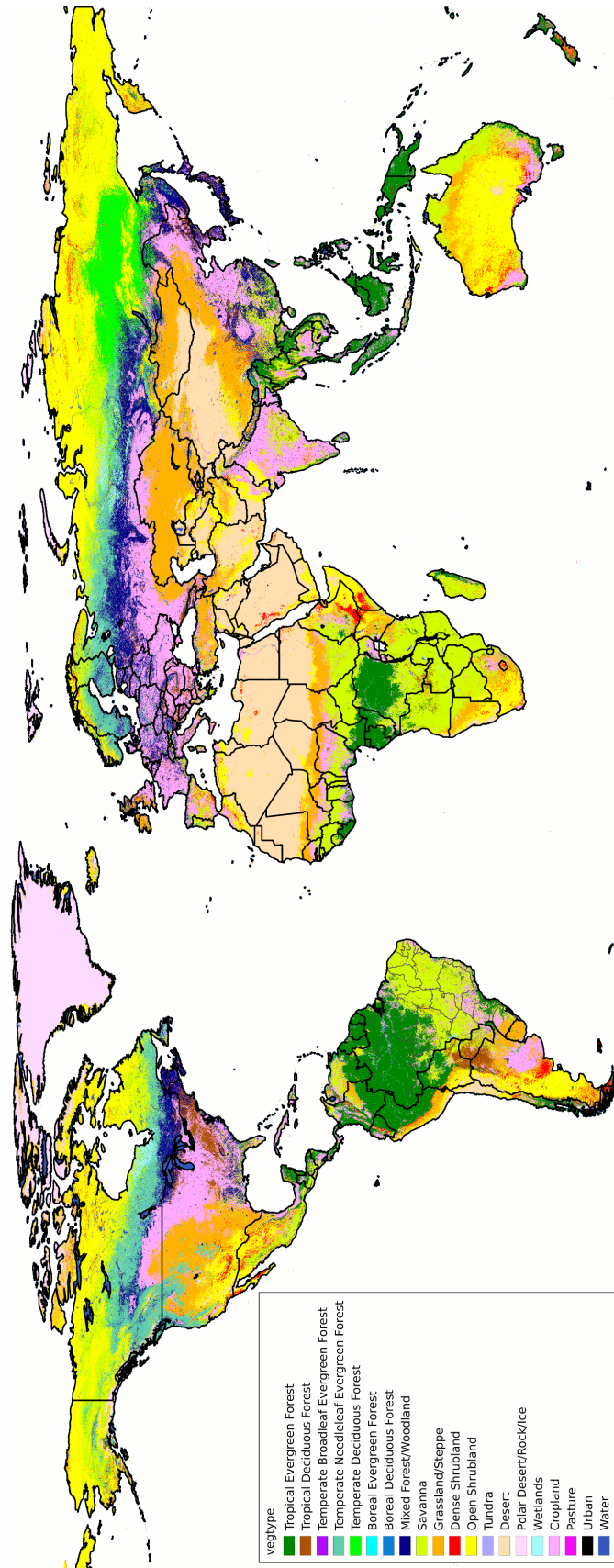


Figure C.2 - MCD12Q1 2009 Land Cover Map, using the INLAND classification (see Table C.1)

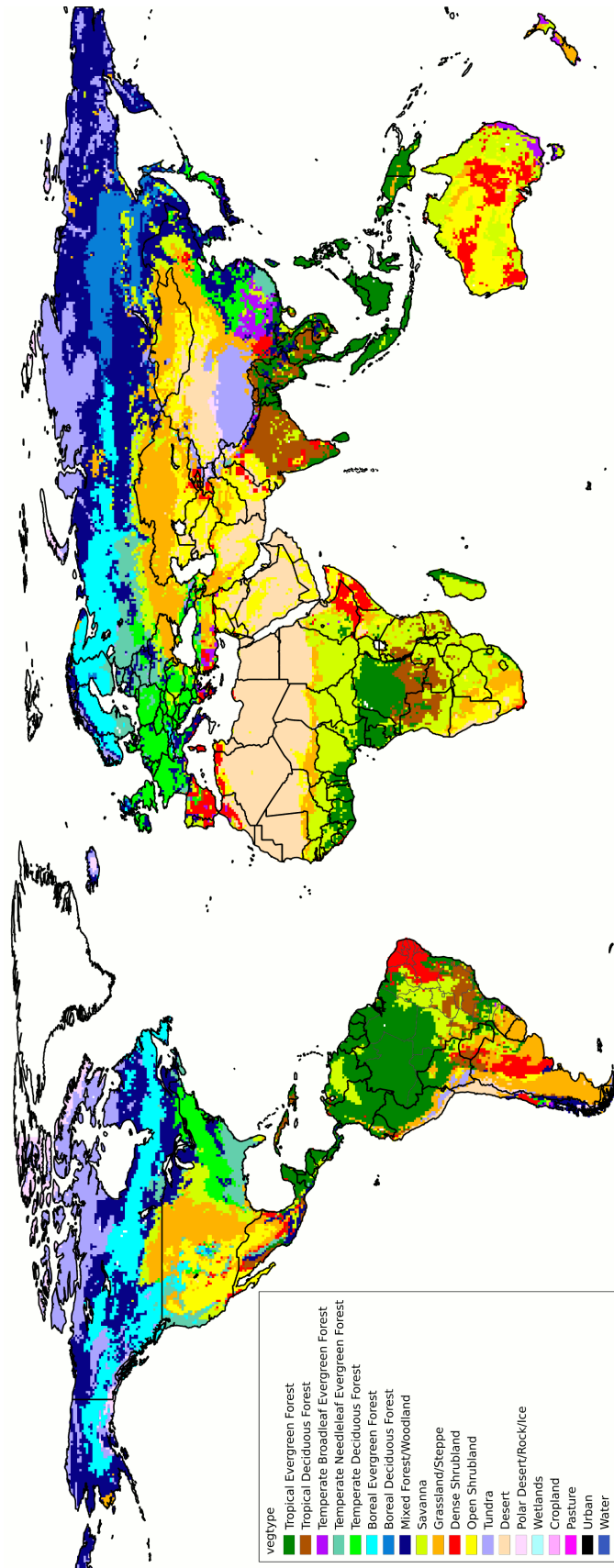


Figure C.3 - IBIS Land Cover Map, using the INLAND classification

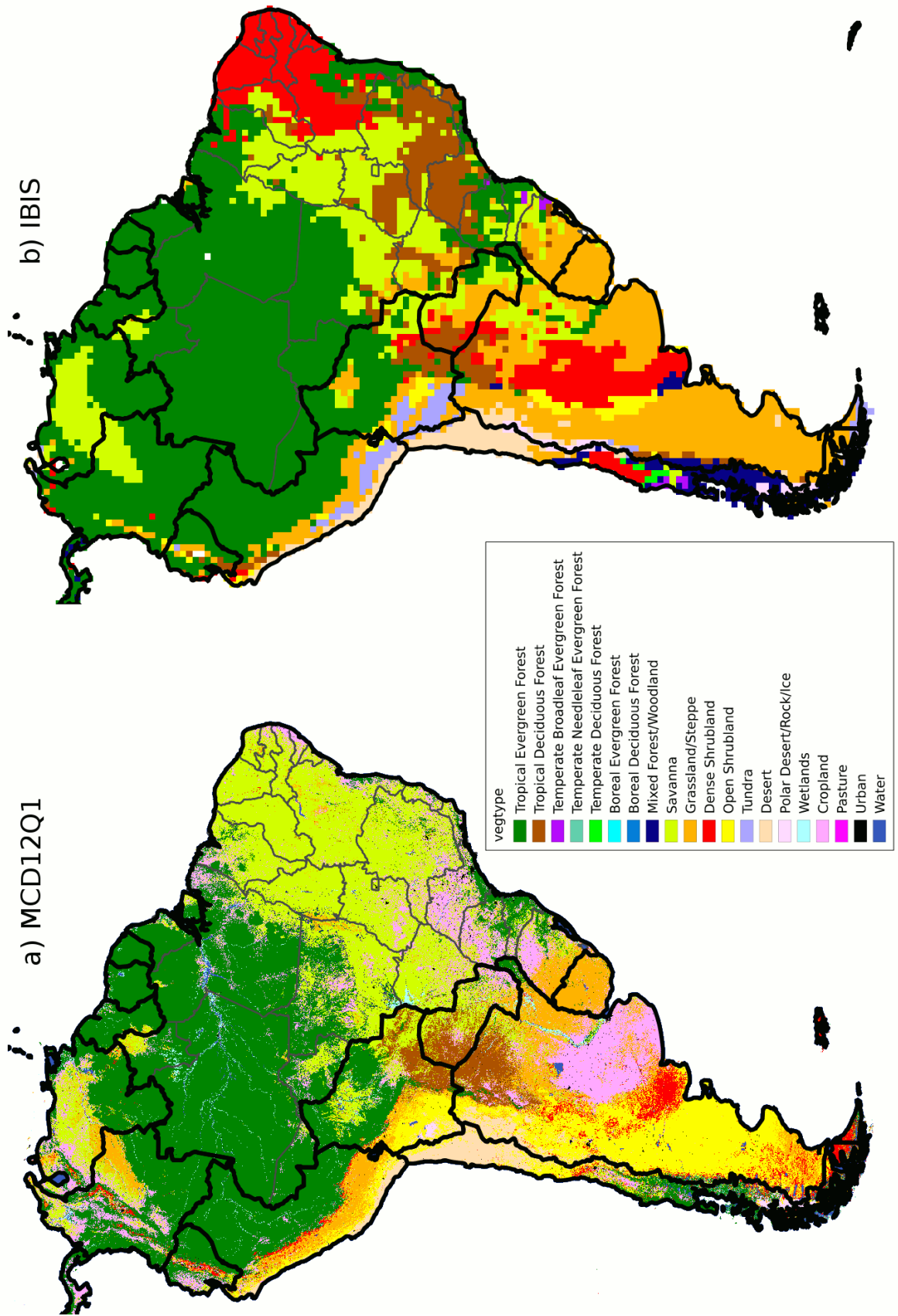
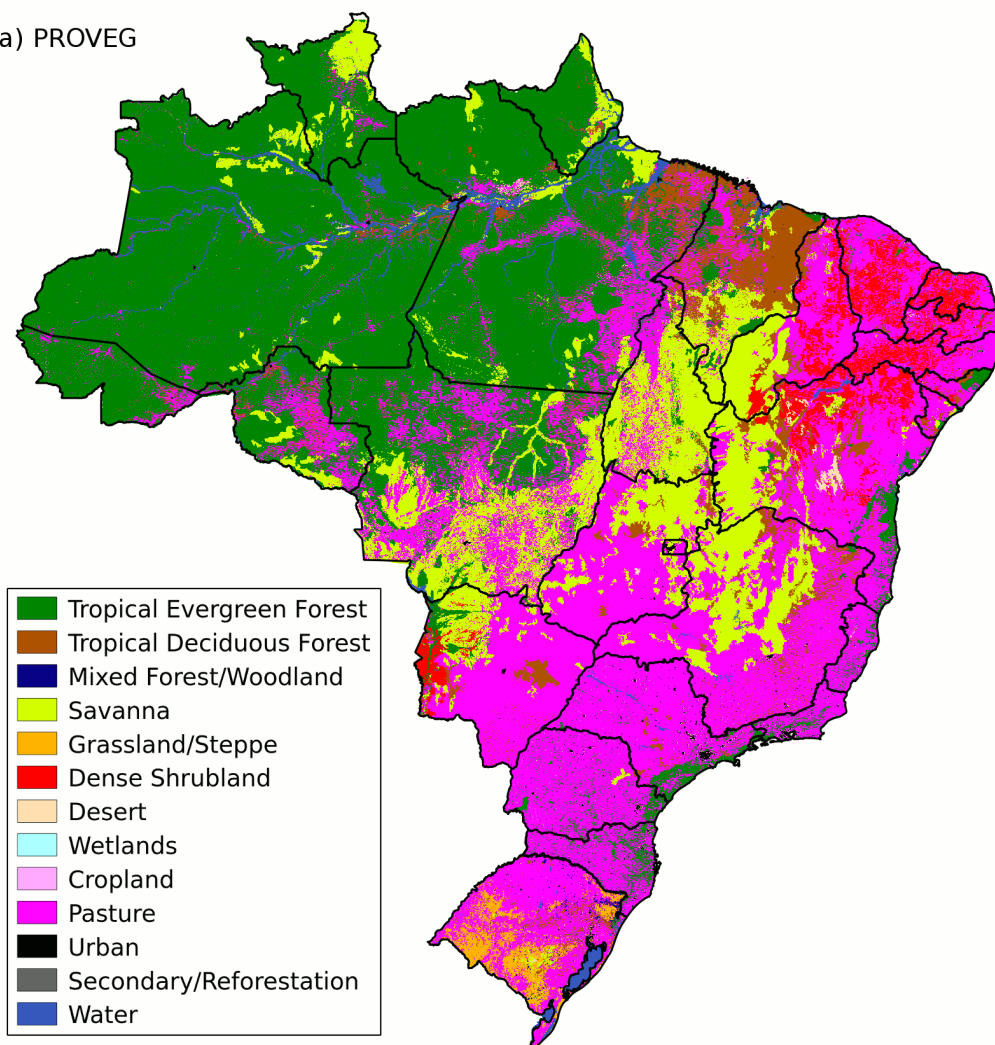


Figure C.4 - MCD12Q1 2009 and IBIS Land Cover Maps - South America only

a) PROVEG



b) IBGE / TERRACLASS

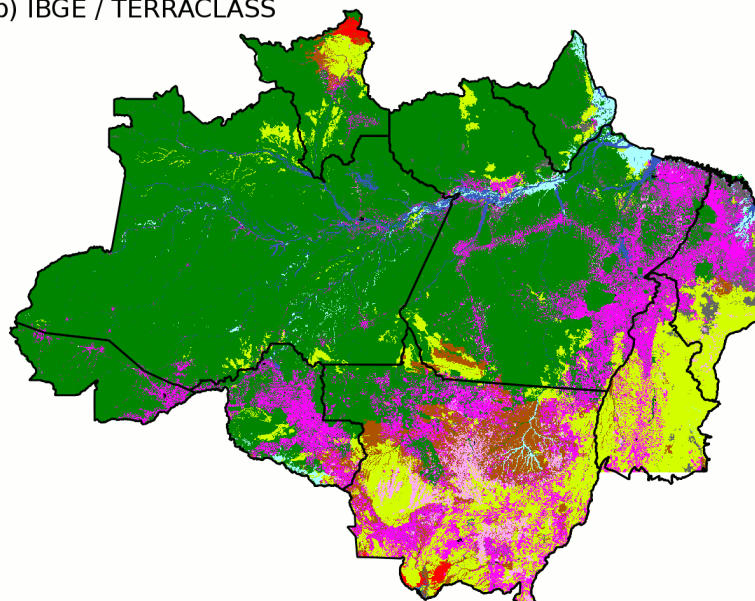


Figure C.5 - Land Cover Maps for Brazil, using the INLAND classification. a) PROVEG and b) IBGE2006/TERRACLASS.

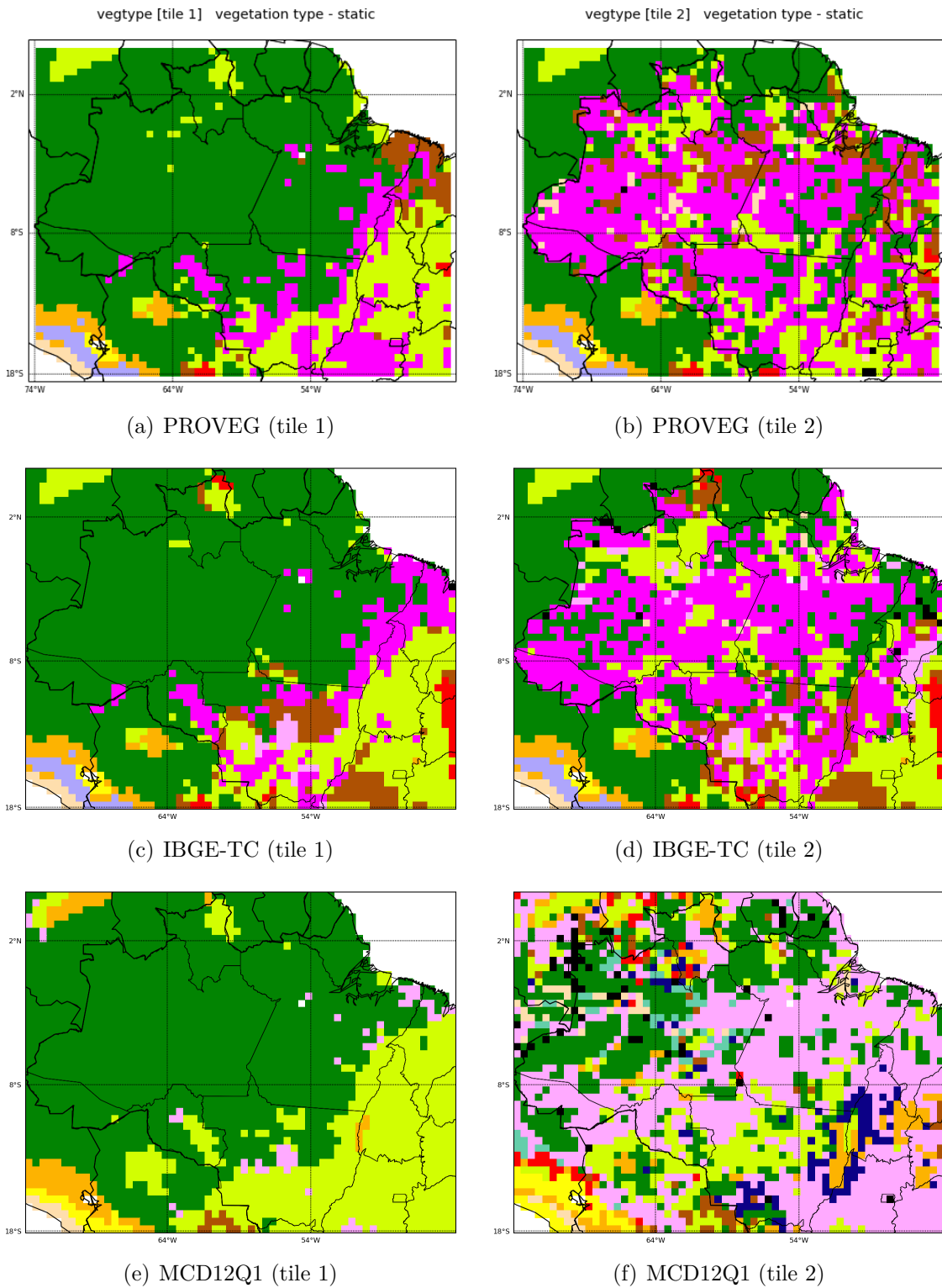


Figure C.6 - PROVEG, IBGE-TC and MCD12Q1 land cover maps, *vegtype* of tiles 1 and 2 of the Amazon region. Legend is the same as in Figure C.5.

PUBLICAÇÕES TÉCNICO-CIENTÍFICAS EDITADAS PELO INPE

Teses e Dissertações (TDI)

Teses e Dissertações apresentadas nos Cursos de Pós-Graduação do INPE.

Manuais Técnicos (MAN)

São publicações de caráter técnico que incluem normas, procedimentos, instruções e orientações.

Notas Técnico-Científicas (NTC)

Incluem resultados preliminares de pesquisa, descrição de equipamentos, descrição e ou documentação de programas de computador, descrição de sistemas e experimentos, apresentação de testes, dados, atlas, e documentação de projetos de engenharia.

Relatórios de Pesquisa (RPQ)

Reportam resultados ou progressos de pesquisas tanto de natureza técnica quanto científica, cujo nível seja compatível com o de uma publicação em periódico nacional ou internacional.

Propostas e Relatórios de Projetos (PRP)

São propostas de projetos técnico-científicos e relatórios de acompanhamento de projetos, atividades e convênios.

Publicações Didáticas (PUD)

Incluem apostilas, notas de aula e manuais didáticos.

Publicações Seriadas

São os seriados técnico-científicos: boletins, periódicos, anuários e anais de eventos (simpósios e congressos). Constam destas publicações o Internacional Standard Serial Number (ISSN), que é um código único e definitivo para identificação de títulos de seriados.

Programas de Computador (PDC)

São a seqüência de instruções ou códigos, expressos em uma linguagem de programação compilada ou interpretada, a ser executada por um computador para alcançar um determinado objetivo. Aceitam-se tanto programas fonte quanto os executáveis.

Pré-publicações (PRE)

Todos os artigos publicados em periódicos, anais e como capítulos de livros.